Description and control of decoherence in quantum bit systems

Henryk Peter Gregor Gutmann

München, Juni 2005

Description and control of decoherence in quantum bit systems

Henryk Peter Gregor Gutmann

Dissertation
an der Fakultät für Physik
der Ludwig–Maximilians–Universität
München

vorgelegt von
Henryk Peter Gregor Gutmann
aus Bonn

München, Juni 2005

Erstgutachter: PD Frank K. Wilhelm
Zweitgutachter: Prof. Dr. Axel Schenzle
Tag der mündlichen Prüfung: 03.08.2005

Contents

List of Publications **ix**
0.1 Introduction . . . 1
0.1.1 Outline of the thesis . . . 3

1 Derivation of Lindblad type master equations at finite temperatures **7**
1.1 Introduction . . . 7
1.2 Lindblad equation in the Bloch sphere representation . . . 10
1.2.1 Lindblad requirements and the concept of dynamical semigroups . . . 10
1.2.2 GKS formulation of the Lindblad equation . . . 12
1.2.3 Bloch-sphere formalism . . . 13
1.3 Born-Markov master equations . . . 14
1.3.1 Born approximation . . . 14
1.3.2 Markov approximations . . . 17
1.4 Spin-Boson Hamiltonian . . . 24
1.4.1 Thermodynamic limit and Ohmic bath . . . 25
1.5 Numerical results . . . 27
1.5.1 Naïve Markov approximation . . . 27
1.5.2 Davies-Łuczka approximation . . . 28
1.5.3 Bloch-Redfield approximation . . . 28
1.5.4 Celio-Loss approximation . . . 29
1.6 Quantitative comparison of the Born-Markovian approximations . . . 30
1.7 summary . . . 34

2 Qubit decoherence due to bistable fluctuators **35**
2.1 Qubit-bfl-bath model . . . 37
2.2 Bloch-Redfield master equation . . . 39
2.2.1 Bloch-Redfield tensor . . . 39
2.2.2 Qubit dephasing and relaxation rates . . . 40
2.2.3 Qubit decoherence spectra at fixed Ω_q for variable T . . . 41
2.2.4 Qubit decoherence spectra at fixed T for variable Ω_q . . . 43
2.2.5 $1/f$ noise . . . 46
2.3 Stochastic Schrödinger equation and random walk model . . . 48
2.3.1 Stochastic Hamiltonian . . . 49

2.3.2 Random walk model . . . 51
2.3.3 Symmetrical noise . . . 55
2.3.4 Bfl-noise at finite temperatures . . . 56
2.3.5 Criteria for an appropriate choice of bfl parameter . . . 59
2.3.6 Numerical and analytical results for temperature dependent bfl noise 61
2.3.7 Derivation of dephasing and relaxation rates . . . 64
2.4 Bfl-noise induced by an SET-measurement setup . . . 67
2.4.1 Flipping rates of the SET-electron . . . 68
2.5 Refocusing of bfl-noise by means of dynamical decoupling . . . 73
2.5.1 Refocusing (bang-bang) scheme . . . 74
2.5.2 Random walk model . . . 75
2.5.3 Pulse shapes . . . 78
2.5.4 Distributions of the random walks deviation . . . 79
2.5.5 Bang-bang control working as a high-pass filter . . . 80
2.5.6 Bang-bang refocusing of finite temperature bfl-noise . . . 82
2.5.7 Applicability of imperfect bang-bang pulses . . . 85
2.5.8 Numerical and analytical results . . . 87

3 Quantum phase diagram of a coupled qubit system 93
3.1 The 2-spins-3-bosonic-baths model . . . 93
3.2 The dressed double-spin Hamiltonian . . . 96
3.2.1 The Emery-Kivelson-transformation . . . 97
3.3 Scaling analysis and quantum phase diagram . . . 100
3.3.1 Scaling equations 1^{st} order . . . 100
3.3.2 Entanglement capability of the fixed point Hamiltonian . . . 102
3.4 Scaling equations 2^{nd} order . . . 105
3.4.1 Operator product expansion . . . 105

A Born master equation of the spin-Boson model 109
A.1 Derivation of the Born approximation correlation functions . . . 109

B Born-Markovian approximations of the Spin-Boson model 113
B.1 Naïve Markov approximation . . . 113
B.2 Bloch-Redfield approximation . . . 120
B.3 Davies-Łuczka approximation . . . 124
B.4 Lindblad approximation according Celio and Loss . . . 129

C Random walk analysis 131
C.1 Symmetrical random walk (driftless) . . . 131
C.1.1 Pure bfl-noise . . . 131
C.1.2 Bang-bang refocused random walk . . . 133

D Bosonic fields scaling formalism **135**
D.1 Derivation of the first order scaling equations 135
D.2 Derivation of the second order scaling equations 136
D.2.1 Calculation of the *operator product expansions* 137

Acknowledgements **154**

Deutsche Zusammenfassung **160**

List of Publications

Major parts of this thesis are discussed in the following publications

chapter 1

1. *Derivation of Lindblad type master equations by means of Born Markov approximations at finite temperature*
   Henryk Gutmann and Frank K. Wilhelm
   in preparation.

chapter 2

2. *Bang-bang refocusing of a qubit exposed to telegraph noise*
   Henryk Gutmann, F.K. Wilhelm, W.M. Kaminsky and S. Lloyd
   Quantum Information Processing **3**, 247 (2004).

3. *Compensation of decoherence from telegraph noise by means of an open loop quantum-control technique*
   Henryk Gutmann, W.M. Kaminsky, Seth Lloyd and Frank K. Wilhelm
   Physical Review A **71**, 020302 (2005).

4. *Dynamical decoupling of bistable fluctuator noise at finite temperature*
   Henryk Gutmann, A. Holzner, F.K. Wilhelm, W.M. Kaminsky and S. Lloyd
   in preparation.

5. *Random Walk description of backaction during quantum charge detection*
   Henryk Gutmann, A. Holzner and F.K. Wilhelm
   in preparation.

chapter 3

6. *Scaling analysis of a coupled two-spin system exposed to collective and localized noise*
   Henryk Gutmann, Gergely Zarand and Frank K. Wilhelm
   in preparation.

List of Figures

1.1 Davies-Łuczka permutation of the integration order 21
1.2 Qubit-bath model 24
1.3 GKS eigenvalues for the naïve Markovian and Davies-Łuczka approximation 28
1.4 GKS eigenvalues for the Bloch-Redfield and Celio-Loss approximation . . . 29
1.5 Evolution of the spin-Boson model in Born approximation 31
1.6 Evolution of the spin-Boson model in Markovian approximations 32
1.7 Fidelity and coherence decay of Born Markovian evolutions 33

2.1 Qubit-bistable fluctuator-heat bath model 37
2.2 Qubit relaxation rates at variable temperatures and Ω_{bfl} 41
2.3 Peak positions of the qubit-bfl resonance spectra of relaxation rates 42
2.4 Qubit relaxation rates at variable Ω_{bfl} and fixed temperature $T = 0.05K$. 43
2.5 Qubit relaxation rates at variable Ω_{bfl} and fixed temperature $T = 0.5K$ . . 44
2.6 Peak positions of the qubit-bfl resonance spectra of relaxation rates 45
2.7 Peak heights of the qubit-bfl resonance spectra of relaxation rates 45
2.8 $1/f$ type relaxation rate behaviour 46
2.9 Crossover 1/f to $1/f^2$ type relaxation rate behaviour 47
2.10 Telegraph noise due to bfl 49
2.11 Bfl induced random walk on the Bloch sphere 51
2.12 One-step random walk deviation due to bfl noise 52
2.13 Evolution of the bfl random walk deviation 56
2.14 Asymmetric bfl noise 58
2.15 Temperature dependence of bfl flipping times 61
2.16 Random walk evolutions of temperature dependent bfl noise 62
2.17 Random walk deviations of temperature dependent bfl noise 63
2.18 Dephasing on the Bloch sphere 64
2.19 Relaxation on the Bloch sphere 65
2.20 Physical setup of an SET-SCB measurement design 67
2.21 Level structure of an SET 69
2.22 Decoherence of SET induced bfl noise 70
2.23 Temperature dependence of flipping times of an SET 71
2.24 Dephasing and relaxation times due to SET noise 72
2.25 Bang-bang refocusing of bfl induced random walk 73

2.26 Detailed plot of bang-bang refocused bfl noise 74
2.27 One-step random walk deviation of bang-bang refocused bfl noise 76
2.28 Random walk evolution of bfl noise with and without bang-bang control . . 77
2.29 Two-step random walk distributions of sudden and smooth bang-bang pulses 78
2.30 Distributions of pure and bang-bang refocused bfl induced random walk . . 79
2.31 Bang-bang suppression factor 80
2.32 Temperature dependence of bang-bang refocused bfl noise (1) 82
2.33 Temperature dependence of bang-bang refocused bfl noise (2) 83
2.34 Suppression factors as function of bang-bang times 84
2.35 Suppression factors as function of temperature 85
2.36 Dephasing aberrations due to faulty bang-bang pulses 86
2.37 Relaxating aberrations due to faulty bang-bang pulses 88
2.38 Random walk deviations due to faulty bang-bang pulses 89
2.39 Random walk deviations due to faulty bang-bang refocused bfl noise 90

3.1 Figure of the 2-spin-3-Bosonic baths model 94
3.2 Physical realization of the 2-spin-3-Bosonic baths model 95
3.3 Quantum phase diagram by means of scaling analysis 1^{st} order 101

A.1 Exponential decay of the Born correlation functions 111

calvinandhobbes©2005.Watterson.reprinted-by-permission-of-universal-press-syndicate.allrights-reserved

0.1 Introduction

In the last decade quantum computing and information methods have become a field of interest of strong prominence for various experimental and theoretical disciplines [1, 2, 3, 4]. Besides its practical relevance for solving mathematically and computationally hard problems, in particular the breaking of current decryption techniques, this is founded in the unique combination of fundamental research of quantum mechanics with modern experimental methods. This renaissance of an original idea by Richard Feynman [5] in practise has led to many successful results in mesoscopic setups. Which includes *e.g.* the observation of interference phenomena in Rabi and Ramsey type experiments [6, 7], as well as continuous increase of decoherence times as a consequence of more effective shielding, cooling and *e.g.* cleaner fabrication of the mesoscopic setups, quantum information is stored and computed on. Also the feasibility of two-qubit gates have been experimentally proven in various realizations [8].

On the other hand theoretical developments have made the implementation of a quantum computing device more probable. In particular there is a threshold quality for quantum gates, *i.e.* a maximum error rate at the order of 10^{-4}, under which arbitrary long quantum computing should be feasible by means of appropriate error correction techniques [9, 2]. The application of encoding methods used to construct so-called decoherence free subspaces [10, 11], enlarges the confidence that quantum computing in principle could be implemented in spite of the omnipresent decoherence, which makes it such an expensive technical challenge. Last but not least, one should also quote alternative approaches as *e.g.* adiabatic quantum computation [12], which promises to provides beneficial results even in strongly correlated and quite non-coherent systems, at least for a particular class of mathematical problems.

David DiVincenzo has tabulated a catalogue of physical criteria, which in general should be fulfilled for experimental approaches to be promising candidates as future quantum computing devices [13]. This list of DiVincenzo criteria, lately extended by the concept of

"flying qubits" (the demand of the ability to exchange quantum information between different quantum computing devices, quasi the potentiality to build up networks of qubits), provides a guideline for any physical setup. It serves to decide, how close a physical setup is to a possible realization of quantum computation and to specify, where the remaining main problems lie. In accordance with this criteria, a US government panel recently laid out a "road-map"[14], where is listed, which of the DiVincenzo criteria have been or should be fulfilled in close future, regarding the various physical approaches. Of course, that report of actual and future status is updated from time to time.

There are different approaches for realizing quantum bits. At first should be mentioned the nuclear-magnetic resonance technique (NMR) [15] being the oldest and most developed method, which originally was invented for spin spectroscopy. Thereby different resonances of specified nuclear spins in appropriate designed molecules can be used as carrier of quantum information. As these spins couple only extremely weakly to the environment (which leads to extremely long decoherence times), one has to use huge ensembles (in typical macroscopic order of numbers $\simeq 10^{23}$) and apply very strong magnetic fields on the NMR probes. Nevertheless, the most powerful implementation, liquid state NMR, can be refined at room temperature and although NMR is working almost with thermal equilibrium states there have been invented numerous techniques to circumvent most NMR drawbacks. In particular by means of NMR technique the factorization of 15 [16] has been accomplished. Its non-scalability in larger sizes of qubit registers is probably a crucial reason for discarding NMR techniques for a future quantum computer.

Good results regarding decoherence times and experiences in manipulation of quantum bits as well have been achieved by quantum optics methods [17, 18]. The qubit is thereby defined as two levels of a particular atomic or molecular excitation process, respectively defined by two specific states of a photonic or microwave cavity. Rabi and Ramsey type experiments have proven compareably impressive decoherence times, as well as the capability to exchange of quantum information [7]. The method of ion traps and optical lattices are quite related to that field [19, 20]. Quantum information is stored in atomic or molecular energy levels as well and quantum manipulation and read-out are also performed by optical techniques, *e.g.* by means of laser pulses.

Probably the most promising approaches at least with respect to the yet unsolved problem of scalability provides the electric circuit implementations based on semi- and/or superconductor technology. On the one semi-conductor side there are quantum dot techniques where an appropriate confined restriction of two-dimensional electron gases leads to an artificial atomic level structure easy to manipulate electro-statically by corresponding gate voltages. These discrete level structures can be used to provides well-defined qubits, which can be manipulated electro-statically or by means of magnetic fields [21, 22]. On the other (superconducting) hand, Josephson junctions assembled in electric circuits provides us with mesoscopic effective two-level systems, which can be based on persistent currents (leading to so-called Josephson flux qubits) or on electron charges confined on

zero-dimensional islands (thus similar to quantum dot realizations) [23, 24, 25, 26, 27].

While different realizations have their characteristic advantages and drawbacks, the semi- and superconducting approaches probably provide the most promising candidates for real large-scaled quantum registers, as mesoscopic electrical circuit techniques are most obvious in regard of enlargening the corresponding quantum registers. Moreover, production techniques for computational electrical circuits have gained experiences in miniaturizing and perfecting their devices for almost half a century.

From the theoretical point of view it would be a desireable goal to derive a general formalism describing any kind of mesoscopic realization of qubit registers as well as the upon applied quantum gates including the miscellaneous influences of decoherence. There exist different approaches; at first master equations as kinetic equations of the density matrices presenting the (decohering) quantum states of the qubit registers. There are basically two ways of deriving them. Either by a phenomenological approach (which in particular is the usual way for deriving Lindblad type master equations). Or by applying perturbation theory, which is often a good choice if the environmental couplings were appropriately weak, as they define the perturbative parameter.

Quantum Langevin equations as for instance stochastic Schrödinger equations, can also provides a useful formalism. There the environmental noise is usually introduced by stochastic perturbation in the corresponding Schrödinger equations. For certain cases, there exist one-to-one mappings between master equations and corresponding stochastic Schrödinger equations, also denoted quantum state diffusion ([28] and references therein). For strongly coupled systems, where usual perturbation theory fails, are numerical techniques preferred ([29, 15, 30]). But these cases are not the most relevant for usual quantum bit realizations, as strong coupling to the environment normally means stronger decoherence and therefore less capability of storing and processing quantum information. One exception could be adiabatic quantum computing, where decoherence times do not necessarily play a crucial role.

Nevertheless, we will discuss a qualitative scheme of estimating effective quantum dynamics of a coupled two spin system exposed to arbitrary strong bath coupling. In particular we will find evidences for the presence of entanglement (*i.e.* the spatially non-locality of quantum information, which besides quantum coherence makes quantum computing devices so powerful).

0.1.1 Outline of the thesis

In our first chapter we will propose several attempts to derive Lindblad type master equations by use of perturbation theory on microscopic models. We quote an easily applicable criterion to decide whether a given Markovian master equation possesses the Lindblad form

or not. As exemplaric and highly relevant qubit decoherence model, we consider thereby the spin-Boson model with Ohmic heat bath spectral density. We conclude the first chapter with some quantitative comparisons of the fidelity between the various Markov approximations.

After the primarily formal discussion of master equations properties, presenting disturbances generated from Gaussian noise sources, *i.e.* where the central limit theorem applies, we will focus on a different class of noise sources, the so-called bistable fluctuators. These Nevertheless seems to be a very universal problem, in particular for condensed matter realizations. Thereby we will apply three different models.

Firstly, a microscopic description by use of the Bloch-Redfield equation, a special case of a Born-Markov technique. By this analysis we are able to estimate the decoherence for various choices of qubit, fluctuator and bath parameters. In particular, we receive an $1/f$-type behaviour for the low temperature regime for an ensemble of bistable fluctuators whose energy levels were homogenously distributed.

Secondly, we consider an effective single spin-fluctuator setup, where telegraph noise is involved and which can be described by an appropriate stochastic Schrödinger equation. By means of its numerical integration we receive insight in its decoherence evolution. For suitably chosen parameters (explicitly spoken: if the fluctuator evolves much slower than the qubit) we receive a random walk type behaviour. As a consequence we derive an appropriate random walk model in very good agreement predicting the noisy influenced evolution and thus provides us with analytical insights in the decoherence effects.

Furthermore, based on our analytical random walk picture, we propose a spin echo type dynamical decoupling technique in order to refocus the fluctuator induced decoherence. Numerical as well as analytical evaluations obtain a high pass filter effect of the so-called bang-bang control pulses; *i.e.* low-frequent noise will be suppressed most effectively. This is a promising result, as the particular perturbing $1/f$ noise is mostly harmful in its low-frequency spectrum.

As an additional application, we use the derived numerics to examine the fluctuator noise in a realistic setup of an single-charge box realization (SCB) of a qubit influenced by a weakly coupled single-electron transistor (SET) serving as a charge sensitive measurement device. We conclude this chapter with considerations of pulse imperfections of the bang-bang scheme and prove therewith the practical applicability of the bang-bang technique.

In the last chapter we examine a coupled two-spin system being exposed to two different types of bath influences, one collective and two localized, separate ones. We use a different technique in order to estimate the effective dynamics of the double-spin system in regard of the environmental coupling strengths. Thereby we in particular the strong environmental

coupling regime. The applied scaling technique provides us with a quantum phase diagram, where each phase represents qualitative different quantum dynamics in the corresponding scaling limit. By means of corresponding fixed point Hamiltonian we are also able to derive entanglement properties of these quantum phases. One main result of this analysis is, that even in the strong environmental coupling regimes, where most quantum dynamics is suppressed, there is still entanglement present or even arising due to the external influences.

Chapter 1

Derivation of Lindblad type master equations at finite temperatures

1.1 Introduction

The master equation as kinetic equation for reduced density matrices is one powerful method to describe dissipative and decoherent dynamics of open quantum systems. Therefore it is an essential tool for investigating mesoscopic systems, in particular systems proposed as quantum computing devices. Unfortunately generalized, non-Markovian master equations (mostly derived from a Liouville-Von Neumann equation in a closed system-environment model [31, 32, 28]) are in general not effectively solvable without further approximations, both analytically and numerically.

The most common methods apply in weak coupling limits, where perturbation theory (*e.g.* the Born approximation) is possible. In particular the limiting cases, when the correlation times of environmental memory effects to the reduced system turn out to be significantly shorter than the time-scales of typical unperturbed dynamical system, so-called Markovian limits are feasible.

From a mere mathematical point of view Lindblad and others [33, 34] have invented a particular class of Markovian master equations. Those were based on the concept of the *dynamical semigroups* [35], which is a generalization of the well-known unitary group for closed quantum evolutions. Hereby they have been mainly interested in the structural analogy of (semi)group-like behaviour of dissipative quantum systems to the unitary evolution groups of closed quantum dynamics. The discovery of the Lindblad master equation is therefore more a theorem of its structure and existence, while most practical examples for them have been stated in phenomenological ways. The Lindblad operators, which determine the so-called Lindblad master equation, are proved to satisfy all qualities of physically reasonable dissipative evolutions, nevertheless their practical derivation *e.g.* from Hamiltonian models is not obvious.

Thus this scheme represents a mere phenomenologic approach. As we are mainly interested in finding adequate kinetic equations for mesoscopic systems from corresponding microscopic Hamiltonian, we intend to explore a systematic approach to derive Lindblad type dynamical equations by perturbative methods.

The advantage of this special class of master equation is besides its practically simple solvability, that it preserves the mathematical properties of the density matrix. Beneath conserving the norm (physically spoken, the unity of the total amount of probability), they maintain the positivity of density matrices (*i.e.* no negative probability arises). Furthermore in the community of mathematical physics and quantum information theory many theorems and techniques were derived and based on this particular choice of equations of motion. To them belong prominent and important procedures like *e.g.* the existence of decoherence free subspaces [10, 11] as well as many active and passive error correction schemes for dissipative quantum computation (also called open quantum control [36, 37, 38] and quantum error correction codes [9]).

In the following chapter we will at first briefly review the essence of the Lindblad theorem without considering its non-trivial proof (the interested reader might be referred to my diploma thesis [28] and references therein). By use of related work [34] we will be able to formulate an operational criterion for diagnosing the complete positivity for any given Markovian master equation[1]. This feature constitutes the decisive point, whether a Markovian dynamics is of Lindblad type or not. For the sake of simplicity we will introduce this check of complete positivity on the particular case of one qubit, as we can use here the probably most intuitive description by means of the Bloch sphere representation. The one-qubit states can be represented by corresponding vectors in the Bloch sphere, pure states on its surface, mixed inside of it. Any Markovian master equation then can be translated in a 3-dimensional matrix form, avoiding the strenuousness of typical super-operator calculations. A generalization to larger qubit registers or even arbitrary (but finite dimensional) quantum systems would be straight-forward, even though producing a higher level of complexity in the corresponding calculations without obtaining deeper qualitative insights.

Having derived that tool for diagnosing Lindblad type of Markovian master equations, we will present one standard technique of deriving perturbative Master equations. In particular considering the Born approximation (*i.e.* the expansion in second order of the perturbative coupling), we encounter a quite generic structure of non-Markovian master

[1]The notation of complete positivity was introduced as a generalization of positivity of operators on density matrices (so-called super-operators). It means, that super-operators representing real dissipative quantum evolutions, should not only preserve the positivity of initially chosen density matrices, but also of any artificial expansion of them with arbitrary additional degrees of freedom. *I.e.* if one defines any larger Hilbert space, consisting of the originally considered subsystem as well as an isolated sideshow system, then applying the open quantum dynamics of the tensor-product of the origin super-operator with the corresponding additional evolution should also preserve positivity of the exptended density matrices.

equation, consisting of a (renormalized) unitary part (responsible for the effective coherent evolution) and an integro-differential dissipative part (producing decoherence effects). These kinetic equations are in general not obvious to solve. The integral part of those equations are usually of the form $\int_{t_0}^{t} \hat{\mathcal{K}}(t-s)\rho_{\mathrm{Sys}}(s)\,ds$, where $\hat{\mathcal{K}}$ represents the super-operator memory kernel. This encodes the environmental back-action on the actual system changes (at time t) in dependence of its history of former states $\rho_{\mathrm{Sys}}(s)$. The time scale, on which these feedback effects take place are defined by the environmental correlation functions being the inherent time-depending parts of that memory kernel. These correlations are determined on the one hand by the particular type of interaction between reduced system and environment, on the other hand they depend on the spectral function of the environment (*i.e.* a function which describes its density of modes). Moreover they crucially depend on the environmental temperature.

Up to now the high temperature limit was an at least encouraging criterion for receiving a sufficient Markovian behaviour. Intuitively spoken this is due to the rapidly vanishing bath correlations, once the noise becomes thermal. Unfortunately for protecting quantum bits most effectively from thermal noise as well as for their pure state initialization the experimental setups are cooled to minimal feasible temperatures. This requires in consequence a theoretical description of that systems for corresponding temperature regimes. Those may not satisfy Markovian criteria in the first view.

Preferable would be therefore Markovian descriptions, which are also valid in low-temperature regimes. Even more desirable, if they would fulfill all Lindblad requirements, such that coherence improvement or error correcting techniques based on Lindblad type considerations would be applicable. At least, if some kind of quantitative estimation of deviation from a corresponding Lindblad-approximation would be feasible, namely a theory of perturbation in time (non)-locality (in non-trivial, higher order terms of temporal convolution). Evidently this would be a beneficial tool to evaluate the use and applicability of Lindblad based correction and/or coherence-preserving techniques.

In the following chapter we will present different schemes of Markovian approximations by manipulating the environmental memory kernels and averaging out the integration part of the Born master equation in more or less elaborated ways. The resulting Markovian master equations will be translated in their corresponding Bloch sphere matrix form, in order to examine their status of complete positivity. As exemplaric test system of our one-qubit calculations we use the well-known spin-Boson model with an Ohmic spectral function for the Bosonic environment. This does not only keep our analytical calculations most descriptive, but it also seems to be an appropriate choice for many typical systems ([31, 39, 23, 40]).

We conclude our investigations with some critical remarks on the reliability of our Markovian Lindblad as well as non-Lindblad approximations. In particular we will perform quantitative comparisons in order to estimate their decoherence properties and their

mutually differences.

Some formal part of this work (in particular regarding the Bloch sphere reformulation of the GKS Lindblad equation) was done before by Dühmcke and Spohn [41], as well as Celio and Loss [42], and probably others unknown to me. While Spohn and Loss mainly have focused on high temperature limits, as well as symmetry aspects of the various Markovian approximations we mainly consider the intermediate and low temperature regime. Furthermore we also present some quantitative evaluation of the various Markovian approximations and comparisons between them.

1.2 Lindblad equation in the Bloch sphere representation

1.2.1 Lindblad requirements and the concept of dynamical semigroups

At first, we will provide a brief and intuitive description of the concept of dynamical semigroups, on which Lindblad constructed the particular class of Master equations. We do not want to deliver the most general, algebraic formulation, as we are rather interested in possible applications than in perfect mathematical rigor. The interested reader might be referred to the corresponding publications [33, 34] and references therein.

The *dynamical semigroup* is termed in context of dissipative evolutions on a physical system, whose states are usually described by corresponding density matrices[2]. These processes show the following characteristics. A *dynamical semigroup* is given by a time-indexed family of propagators, *i.e.* maps generating time evolution as follows

$$\Phi_t \quad : \quad \rho(t_0) \rightarrow \rho(t_0 + t) \ , \tag{1.1}$$

which map any initial state $\rho(t_0)$ onto its corresponding propagated state $\rho(t_0 + t)$. In analogy of the corresponding unitary evolution group of propagators this family should fulfill semi-group behaviour according the composition of two dissipative propagations

$$\Phi_t \circ \Phi_s \quad = \quad \Phi_{t+s} \ . \tag{1.2}$$

The limitation on a semi-group evidently is caused by the fact, that dissipative processes always tend to equilibrium or other stationary states. Therefore inverse propagations are

[2]Density matrices are rather chosen as state representation as wave functions, as relaxation effects inevitably create statistical mixtures. There are also alternative ways to describe open quantum systems; *e.g.* by using random variable indexed ensembles of wave functions, each representing a stochastically derived dissipative evolution of the system. Such descriptions can be useful, in particular in practise if using numerically Monte Carlo methods. For details see [28].

not feasible and thus corresponding propagators (backwards in time) does not exist, at least not practically computable ones.

Although this definition of dissipative propagators seems to be quite general, one has to be aware of the very strong Markovian requirement these kind of processes have to achieve. Evolutions generated by those kind of propagators are not only unaffected of earlier histories of the concerned initial states, but actually they are (due to eq. (1.2)) explicitly time-translational invariant, a feature clearly not satisfied by each realization of quantum decoherence.

The specifications Lindblad made on his class of dynamical semigroups are nevertheless very general; in fact, they only confirm, that the propagators Φ_t conserve the mathematical properties of the density matrices. Which there are its positivity (corresponding to non-negative probabilities), as well as its trace normalization (*i.e.* the total sum of probabilities equals one). As formerly mentioned, the preservation of positivity (which is positivity of the super-operators Φ_t as a linear map) is generalized to the term of complete positivity, which can be briefly paraphrased as positivity preservation of any composition of the origin density matrix space to the tensor product with an $n\times n$-dimensional complex matrix space, if the corresponding map will be adapted to

$$\Phi_t^{(n)} \equiv \Phi_t \otimes \mathbb{1}_n \ . \tag{1.3}$$

Following this concept of density matrix features preservation, time independence and locality given as *dynamical semigroup*, one receives a particular structure of the underlying master equations. Algebraicly spoken, the generators of the *dynamical semigroups* represents the so-called Lindblad (master) equations.

$$\begin{aligned} \frac{\partial\rho(t)}{\partial t} = \mathcal{L}[\rho(t)] &= -\frac{i}{\hbar}\left[\hat{H},\rho\right] + \frac{1}{2}\sum_j\left(\left[\hat{V}_j,\rho(t)\hat{V}_j^\dagger\right] + \left[\hat{V}_j\rho(t),\hat{V}_j^\dagger\right]\right) \\ &= \mathcal{L}_{\text{unitary}}[\rho(t)] + \mathcal{L}_{\text{diss}}[\rho(t)] \ , \end{aligned} \tag{1.4}$$

where $\mathcal{L}$ denotes the master equation representing super-operator, respectively the generator of the *dynamical semigroup* evolution. $\mathcal{L}_{\text{unitary}}$ represents the unitary part of the equation of motion induced by a Hermitian operator $\hat{H}$, representing a (renormalized) Hamiltonian. $\mathcal{L}_{\text{diss}}$ provides the dissipative evolution and is determined by a countable set of positive, bounded operators $\{\hat{V}_j\}$, the so-called Lindblad operators. As one of the lemmas from Lindblad famous papers tells us, this decomposition is not unique, as apparently any unitary part can be exchanged between $\mathcal{L}_{\text{unitary}}$ and $\mathcal{L}_{\text{diss}}$. This feature is of practical relevance for us, as we will furthermore pick out for any given Markovian master equation a particular choice of decomposition in unitary and dissipative part.

1.2.2 GKS formulation of the Lindblad equation

Here we present an alternative formulation of the Lindblad equation, given by Gorini, Kossakowski and Sudarshan [34] (GKS). Here an exemplaric basis of operators $\left\{\hat{B}_k\right\}$ is selected [3], such that by expanding the the set of Lindblad operators

$$\hat{V}_j \;=\; \sum_k v_{j,k}\hat{B}_k \tag{1.5}$$

with regard to this basis, one can rewrite the dissipative part (which we consider from now on as solely relevant) as follows

$$\mathcal{L}^{\mathrm{GKS}}_{\mathrm{diss}}[\rho(t)] \;=\; \frac{1}{2}\sum_{k,l}\gamma_{k,l}\left(\left[\hat{B}_k,\rho(t)\hat{B}_l^\dagger\right]+\left[\hat{B}_k\rho(t),\hat{B}_l^\dagger\right]\right)\;, \tag{1.6}$$

with

$$\gamma_{k,l} \;=\; \sum_j v_{j,k}v^*_{j,l}\;. \tag{1.7}$$

The Lindblad properties of $\hat{V}_j$ leads to positivity of the coefficient matrix $\gamma_{k,l}$ and vice versa [34, 28]. The only limitation of the GKS formulation is, that typically the initially chosen basis $\left\{\hat{B}_k\right\}$ of the operator space is finite dimensional. But as for most practical purposes physicists restrict their quantum subsystems on a finite number of degrees of freedom, this modification constitutes no serious restriction.

Furthermore we will investigate a (pseudo) spin system, such that the basis itself contents four elements. As most obvious and useful choice emerges the Pauli spin matrices plus the identity operator $\{\mathbb{1},\hat{\sigma}_x,\hat{\sigma}_y,\hat{\sigma}_z\}$. In this context, the GKS-like Lindblad equation reads as follows

$$\mathcal{L}^{\mathrm{GKS}}_{\mathrm{diss}}[\rho(t)] \;=\; \frac{1}{2}\sum_{j,k}c_{j,k}\left(\left[\hat{\sigma}_j,\rho(t)\hat{\sigma}_k^\dagger\right]+\left[\hat{\sigma}_j\rho(t),\hat{\sigma}_k^\dagger\right]\right)\;, \tag{1.8}$$

where we can evidently disregard terms involving $\mathbb{1}$, as the corresponding commutator terms disappear. Exploiting the isomorphy between $SU(2)$ and $SO(3)$ we can reduce our further analysis on the real-valued 3×3-dimensional coefficient matrices $c_{j,k}$.

[3] in particular this basis has to be an orthonormal system considering the standart pseudo-metric $\langle\hat{V},\hat{W}\rangle_{SP} = \mathrm{tr}\{\hat{V}\hat{W}^\dagger\}$ on the vector space $M_N(\mathbb{C})$ of N-dimensional operators, respectively complex-valued matrices. For m ore rigorous and detailed description see [28].

1.2.3 Bloch-sphere formalism

The essential advantage of the GKS Master equations is the simple feasibility of checking the crucial property of complete positivity. This attribute namely is equivalent to the positivity of the corresponding GKS coefficient matrix $c_{j,k}$. This is a criterion fa more easy to verify than evaluating every possible expansion of the system with arbitrary ancilla degrees of freedom. Now we only have to derive the corresponding coefficient matrix $c_{j,k}$ for a given Markovian master equation; and then, in order to check complete positivity, we only have to evaluate its eigenvalues.

Regarding our one-qubit test system, we can take advantage from the so-called Bloch sphere representation of a spin, where the usually 4-dimensional spin density matrix (given as complex 2×2-matrix) can be rewritten as a linear combination of the Pauli matrices as well as the identity operator.

$$\rho(t) \;=\; \sigma_x(t)\hat{\sigma}_x + \sigma_y(t)\hat{\sigma}_y + \sigma_z(t)\hat{\sigma}_z + \frac{\mathbb{1}}{2} \;, \tag{1.9}$$

where $\sigma_j(t)$ denotes the corresponding real-valued spin expectation value,

$$\sigma_j(t) \;=\; \mathrm{tr}\left\{\hat{\sigma}_j \rho(t)\right\} \;. \tag{1.10}$$

Hereby we can identify each qubit state, respectively its according density matrix with a 3-dimensional vector on (pure states) or inside (for mixed ones) the so-called Bloch-sphere

$$\rho(t) \;\leftrightarrow\; \vec{\sigma}(t) \;=\; \begin{pmatrix} \sigma_x(t) \\ \sigma_y(t) \\ \sigma_z(t) \end{pmatrix} \;. \tag{1.11}$$

If we now consider a Markovian (*i.e.* time local and independent) master equation

$$\frac{\partial \rho(t)}{\partial t} \;=\; \mathcal{M}\left[\rho(t)\right] \tag{1.12}$$

we can translate it into the corresponding Bloch vector form

$$\frac{\partial \vec{\sigma}(t)}{\partial t} \;=\; \hat{M}\vec{\sigma}(t) + \vec{I} \;, \tag{1.13}$$

with $\hat{M}$ a 3×3-matrix given by

$$\hat{M}_{j,k} \;=\; \langle \hat{\sigma}_k | \mathcal{M}\hat{\sigma}_j \rangle_{SP} \;=:\; \mathrm{tr}\left\{\hat{\sigma}_k^\dagger \mathcal{M}\hat{\sigma}_j\right\} \;. \tag{1.14}$$

$\langle ... | ... \rangle_{SP}$ denotes the standard scalar product of two matrices/operators; $\vec{I}$ is an inhomogenous term due to the static spin terms given by

$$\vec{I}_j \;=\; \langle \hat{\sigma}_j | \mathcal{M}\mathbb{1} \rangle_{SP} \;=:\; \mathrm{tr}\left\{\hat{\sigma}_j \mathcal{M}\right\} \;; \tag{1.15}$$

note also that $\hat{\sigma}_j^\dagger = \hat{\sigma}_j$.

This kind of matrix master equation now can canonically and uniquely be distinguished into a unitary and a dissipative parts, written as follows

$$\begin{aligned}\dot{\vec{\sigma}}(t) &= \underbrace{\begin{pmatrix} 0 & -h_x & h_y \\ h_x & 0 & -h_z \\ -h_y & h_z & 0 \end{pmatrix}}_{\text{anti-symmetric}} \vec{\sigma}(t) + \\ &+ \underbrace{\begin{pmatrix} \Gamma_{xx}-\Gamma_{yy}-\Gamma_{zz} & \Gamma_{xy} & \Gamma_{xz} \\ \Gamma_{xy} & \Gamma_{yy}-\Gamma_{xx}-\Gamma_{zz} & \Gamma_{yz} \\ \Gamma_{xz} & \Gamma_{yz} & \Gamma_{zz}-\Gamma_{xx}-\Gamma_{yy} \end{pmatrix}}_{\text{symmetric}} \vec{\sigma}(t) + \begin{pmatrix} I_{yz} \\ I_{xz} \\ I_{xy} \end{pmatrix} \quad .\end{aligned} \tag{1.16}$$

The anti-symmetric part corresponds to renormalization effects of the free Hamiltonian obtaining

$$\hat{H}_{\text{renormalized}} = \sum_j h_j \hat{\sigma}_j \ , \tag{1.17}$$

while the symmetric matrix term as well as the inhomogenous part induce dissipation. This decomposition in turn can be uniquely translated into a GKS-form, where the corresponding coefficient matrix is derived from the dissipative part of the matrix master equation by

$$c_{j,k} = \Gamma_{jk} - \frac{i}{2}\epsilon_{jkl} I_l \tag{1.18}$$

with ϵ_{jkl} the Levi-Civita symbol.

1.3 Born-Markov master equations

In the following chapter we will describe the standard method to microscopally derive generalized (*i.e.* time non-local) master equations by use of perturbation theory second order in the system-bath coupling. Hereby we regard the particular, but widely used case of an external, compareably large harmonic oscillator heat bath, which resides in its thermal equilibrium.

1.3.1 Born approximation

We start as follows; the total system Hamiltonian consists of three terms

$$\hat{H}_{\text{total}} = \hat{H}_{\text{Sys}} \otimes \mathbb{1}_{\text{B}} + \lambda \hat{H}_{\text{I}} + \mathbb{1}_{\text{Sys}} \otimes \hat{H}_{\text{B}} \tag{1.19}$$

the free unperturbed system Hamiltonian $\hat{H}_{\rm Sys}$, the pure bath Hamiltonian, which usually will be chosen to be a harmonic oscillator bath [4]

$$\hat{H}_{\rm B} \;=\; \sum_k \omega_k \left(\hat{a}_k^\dagger \hat{a}_k + \mathbb{1}_{\rm B}/2\right) \tag{1.20}$$

the at first discrete assumed set of modes can undergo a continuous limit (as in fact in the further calculations will be performed). The system-bath interactions will be described by $\hat{H}_{\rm I}$ and a perturbation prefactor $\lambda \ll 1$.

With this quite general total Hamiltonian we write down the closed quantum dynamics by use of the corresponding Liouville/von Neumann equation

$$\frac{\partial \rho_{\rm total}(t)}{\partial t} \;=\; -\frac{i}{\hbar}\left[\hat{H}_{\rm total}, \rho_{\rm total}(t)\right] \;. \tag{1.21}$$

If we change into the interaction picture, *i.e.* for states

$$\Psi(t) \;\rightarrow\; \tilde{\Psi}(t) \;=\; e^{+i\hat{H}_0 t/\hbar}\Psi(t) \tag{1.22}$$

and (density) operators

$$\hat{O}(t) \;\rightarrow\; \tilde{\hat{O}}(t) \;=\; e^{+i\hat{H}_0 t/\hbar}\hat{O}(t)e^{-i\hat{H}_0 t/\hbar} \;=\; e^{-\mathcal{L}_0 t}\hat{O}(t) \tag{1.23}$$

with

$$\mathcal{L}_0 \;:=\; -\frac{i}{\hbar}\left[\hat{H}_0, ..\right] \tag{1.24}$$

the free Liouvillian (generating unperturbed evolution), we receive as Liouville/von Neumann equation in the interaction representation

$$\frac{\partial \tilde{\rho}_{\rm total}(t)}{\partial t} \;=\; -\frac{i}{\hbar}\lambda\left[\tilde{\hat{H}}_{\rm I}(t), \tilde{\rho}_{\rm total}(t)\right] \;. \tag{1.25}$$

[4] This particular, but nevertheless quite variable choice of modeling the environment has proven to be very useful and suitable for numerous physical setups, also if the underlying particles are not Bosons, but Fermions as in many solid state applications [32, 39, 31, 23, 40]. There are situations, where this kind of description fails. In particular, if the noise origins exhibit clearly non Gaussian behaviour. This occurs in non-equilibrium, bounded and/or degenerated environments, where the central limit theorem does not apply. As an exemplaric case, telegraph noise induced by so-called *bistable fluctuators* is analyzed in chapter 2.

We perform a formal integration

$$\tilde{\rho}_{\text{total}}(t) \;=\; \tilde{\rho}_{\text{total}}(0) + \int_0^t \dot{\tilde{\rho}}_{\text{total}}(s)\, ds \;=\; \tilde{\rho}_{\text{total}}(0) - \frac{i}{\hbar}\lambda \int_0^t \left[\tilde{\hat{H}}_{\text{I}}(s), \tilde{\rho}_{\text{total}}(s)\right] ds \tag{1.26}$$

and insert this into eq. (1.21)

$$\frac{\partial \tilde{\rho}_{\text{total}}(t)}{\partial t} \;=\; -\frac{i}{\hbar}\lambda \left[\tilde{\hat{H}}_{\text{I}}(t), \tilde{\rho}_{\text{total}}(0)\right] - \frac{1}{\hbar^2}\lambda^2 \int_0^t \left[\tilde{\hat{H}}_{\text{I}}(t), [\tilde{\hat{H}}_{\text{I}}(s), \tilde{\rho}_{\text{total}}(s)]\right] ds \;, \tag{1.27}$$

which delivers a perturbative equation of second order in the coupling parameter λ. In order to derive a generic master equation (meaning equation of motion of the reduced density matrix), we now have to perform the usual tracing out of the bath degrees of freedom. For this task some additional assumptions have to be made.

At first, we require the external heat bath to be in its thermal equilibrium state according some environmental temperature T. Using $\beta = \frac{1}{k_B T}$ the state of the heat bath is given by the usual Boltzmann distributed density matrix

$$\rho_{\text{B}}(\beta) \;=\; \frac{e^{-\beta \hat{H}_{\text{B}}}}{\text{tr}\left\{e^{-\beta \hat{H}_{\text{B}}}\right\}} \;. \tag{1.28}$$

As long as the environment is much larger as the system, this should be an adequate assumption. Thermodynamically spoken, the heat bath provides an infinite energy reservoir at a fixed temperature.

Furthermore we assume, that the intitial state of the system and the bath were uncorrelated, *i.e.* their total density matrix factorizes

$$\rho_{\text{total}}(t=0) \;=\; \rho_{\text{Sys}}(0) \otimes \rho_{\text{B}}(\beta) \;. \tag{1.29}$$

This ansatz is the starting point of the Born approximation, as second order perturbation theory in λ. By regarding the second order Liouville/von Neumann equation 1.27 starting at $t = 0$ we recognize, that entangling terms between system and bath are exclusively produced by the integro-differential part of 1.27, such that they should arise only in second order of the interaction constant λ

$$\rho_{\text{total}}(s) \;=\; \rho_{\text{Sys}}(s) \otimes \rho_{\text{B}}(\beta) + \mathcal{O}\left(|\lambda|^2 \cdot s\right) \;. \tag{1.30}$$

Last, but probably the least limiting assumption is the choice of the form of the interaction Hamiltonian, given as sum over separable expressions

$$\hat{H}_{\text{I}} \;=\; \sum_j \hat{S}_j \otimes \hat{B}_j \;. \tag{1.31}$$

This should be no essential constraint, as one could consider for at least each analytical system-bath coupling its power series expansion in some suitable system-bath operator basis (*e.g.* called $\left\{\hat{s}_k \otimes \hat{b}_k\right\}$), such that we receive the adopted form by appropriate relabeling.

By means of these prerequisites we can carry out the reduction of the environmental degrees of freedom on eq.1.27 and obtain

$$\begin{aligned}
\frac{\partial\tilde{\rho}_{\mathrm{Sys}}(t)}{\partial t} &= \frac{-i\lambda}{\hbar}\,\mathrm{tr}_{\mathrm{B}}\left\{\left[\tilde{\hat{H}}_{\mathrm{I}}(t),\tilde{\rho}_{\mathrm{total}}(0)\right]\right\} + \frac{\lambda^2}{\hbar^2}\int_0^t \mathrm{tr}_{\mathrm{B}}\left\{\left[\tilde{\hat{H}}_{\mathrm{I}}(t),[\tilde{\hat{H}}_{\mathrm{I}}(s),\tilde{\rho}_{\mathrm{total}}(s)]\right]\right\}\,ds \\
&= \frac{-i\lambda}{\hbar}\sum_k \langle\hat{B}_k\rangle_\beta\left[\tilde{\hat{S}}_k(t),\tilde{\rho}_{\mathrm{Sys}}(0)\right] \\
&\quad -\frac{\lambda^2}{\hbar^2}\int_0^t\sum_{k,l}\Bigg(\mathcal{R}_{k,l}(t-s)\left[\tilde{\hat{S}}_k(t),\left[\tilde{\hat{S}}_l(s),\tilde{\rho}_{\mathrm{Sys}}(s)\right]\right] + \\
&\qquad\qquad +\mathcal{I}_{k,l}(t-s)\left[\tilde{\hat{S}}_k(t),\left[\tilde{\hat{S}}_l(s),\tilde{\rho}_{\mathrm{Sys}}(s)\right]_+\right]\Bigg)\,ds + \mathcal{O}\left(|\lambda|^2\right)\ ,
\end{aligned} \tag{1.32}$$

with $\left[\hat{A},\hat{B}\right]_+ = \hat{A}\hat{B}+\hat{B}\hat{A}$ the usual anti-commutator and

$$\begin{aligned}
\mathcal{R}_{k,l}(t-s) &= \mathrm{Re}\left(\langle\tilde{\hat{B}}_k(t)\tilde{\hat{B}}_l(s)\rangle_\beta\right) = \frac{1}{2}\langle[\tilde{\hat{B}}_k(t),\tilde{\hat{B}}_l(s)]_+\rangle_\beta \\
\mathcal{I}_{k,l}(t-s) &= \mathrm{Im}\left(\langle\tilde{\hat{B}}_k(t)\tilde{\hat{B}}_l(s)\rangle_\beta\right) = \frac{1}{2}\langle[\tilde{\hat{B}}_k(t),\tilde{\hat{B}}_l(s)]\rangle_\beta
\end{aligned} \tag{1.33}$$

the corresponding environmental correlation functions.

$$\langle\hat{A}\rangle_\beta = \mathrm{tr}_{\mathrm{B}}\left\{\rho_{\mathrm{B}}(\beta)\hat{A}\right\} \tag{1.34}$$

denotes hereby the thermal expectation value of $\hat{A}$ regarding the (inverse) equilibrium temperature $\beta = 1/k_BT$ of the bath (k_B the Boltzmann constant).

1.3.2 Markov approximations

The correlation functions (1.33) in the integro-differential part of the Born master equation (1.32) determine the time non-local behaviour of the bath backaction on the actual state changes $\dot{\rho}_{\mathrm{Sys}}(t)$ in dependence of the previous system evolution $\rho_{\mathrm{Sys}}(s)$ $(0<s<t)$. In super-operator language, this master equation has the structure of a general non-Markovian master equation

$$\frac{\partial\tilde{\rho}_{\mathrm{Sys}}(t)}{\partial t} = -\frac{i\lambda}{\hbar}\left[\langle\tilde{\hat{H}}_{\mathrm{I}}(t)\rangle_\beta,\tilde{\rho}_{\mathrm{Sys}}(0)\right] - \frac{\lambda^2}{\hbar^2}\int_0^t\tilde{\mathcal{K}}(t-s)\tilde{\rho}_{\mathrm{Sys}}(s)\,ds\ , \tag{1.35}$$

where $\tilde{\mathcal{K}}(t-s)$ plays the role of a memory kernel, which describes the environmental feedback on the system as function of intermediate time distance $(t-s)$. It is given as

$$\tilde{\mathcal{K}}(t-s) \;=\; \langle \tilde{\mathcal{L}}_{\rm I}(t)\tilde{\mathcal{L}}_{\rm I}(s)\rangle_\beta \tag{1.36}$$

with

$$\tilde{\mathcal{L}}_{\rm I}(t)\hat{X} \;=\; -\frac{i}{\hbar}\left[\tilde{\hat{H}}_{\rm I}(t),\hat{X}\right] \tag{1.37}$$

the Liouvillian given by the interaction part of the total Hamiltonian. Note besides, that $\mathcal{K}$ in general is a super-operator, thus its "left-multiplication" to a density matrix includes operations from both sides. In particular, we have emphasized with $\tilde{\mathcal{K}}$ its interaction picture version; $\mathcal{K}$ denotes the corresponding super-operator in Schrödinger representation, which is given as

$$\mathcal{K}(t-s) \;=\; e^{\mathcal{L}_0 t}\tilde{\mathcal{K}}(t-s)e^{-\mathcal{L}_0 s} \;; \tag{1.38}$$

this should not be confused with the usual interaction picture transformation for ordinary super-operators

$$\tilde{\mathcal{S}}(t) \;=\; e^{-\mathcal{L}_0 t}\mathcal{S}e^{+\mathcal{L}_0 t} \;, \tag{1.39}$$

as in particular the memory kernel back-transformation scheme (1.38) requires from the right side an s-dependent translation in order to be applied on states $\rho_{\rm Sys}(s)$, which are taken at the time s, not t.

In order to receive time local, so-called Markovian equation of motion, one has to dissolve the time-convolution and, naïvely spoken, to try to extract the former history density matrix $\rho_{\rm Sys}(s)$ out of the integration part. There are various approaches, how to execute such a kind of "time-average", which, alas, are not fully compatible. As one will recognize in our following derivations, all kind of Markovian approximations involve at some point a time-averaging process, also known as time coarsing technique. The essential distinctions of the various approaches lies in their more or less elaborated calculations. While we mainly focus our attention on the presence or absence of complete positivity, the aspect of qualitative as well as quantitative adequacy of these sorts of Markovian master equation in general remains an open question. This probably can in last consequence only be answered individually for concrete physical setups and practical applications by comparing resulting evolutions with experiments or numerically exact solutions.

Naïve approximation

The probably most easy way to convert the time non-local master equation (1.35) into a Markovian one, is done by the strict assumption that the typical environmental memory

time-scale δt proceed much faster than these of the dynamics of the free system. Such that the corresponding memory kernel expressed in mathematical terms behaves *e.g.* as

$$\mathcal{K}(\Delta t) \;\sim\; e^{-|\Delta t|/\delta t} \;. \tag{1.40}$$

With this premise, one can reduce the integro-differential part of eq. 1.35 to

$$\int_0^t \mathcal{K}(t-s)\tilde{\rho}_{\mathrm{Sys}}(s)\,ds \;\simeq\; \int_0^t \mathcal{K}(t-s)\,ds\rho_{\mathrm{Sys}}(t) \;=\; \mathcal{M}_0\rho_{\mathrm{Sys}}(t) \;, \tag{1.41}$$

where evidently

$$\mathcal{M}_0 \;=\; \int_0^t \mathcal{K}(t-s)\,ds \;=\; \int_0^t \mathcal{K}(s)\,ds \;\simeq\; \int_0^\infty \mathcal{K}(s)\,ds \tag{1.42}$$

is not explicitly time-dependent anymore, as long as one only considers sufficient large evolution times ($t \ll \delta t$), being on the relevant time scale for system processes anyway.

Bloch-Redfield approximation

A more adequate Markovian treatment of the Born approximation eq. (1.35), in particular for tow temperature regimes, is the so-called Bloch-Redfield approximation. This consists essentially of two steps. Firstly, an estimation of the problematic term $\tilde{\rho}_{\mathrm{Sys}}(s)$ in the integral part to $\tilde{\rho}_{\mathrm{Sys}}(t)$ has to be found. As dissipative processes are irreversible, the backward propagation in time is ill-defined (each initial state tend to the unique thermal equilibrium state; thus forward propagation is not an injective mapping). But in consistence with our perturbation theoretical approach, we can estimate $\tilde{\rho}_{\mathrm{Sys}}(t)$ in second order of λ as follows

$$\rho_{\mathrm{Sys}}(t) \;=\; e^{-i\hat{H}_0(t-s)/\hbar}\rho_{\mathrm{Sys}}(s)e^{+i\hat{H}_0(t-s)/\hbar} + \mathcal{O}\left(|\lambda|^2\right) \;=\; e^{+\mathcal{L}_0(t-s)}\rho_{\mathrm{Sys}}(s) \;, \tag{1.43}$$

as the deviations of the systems state evolutions from the free propagated ones were obviously implied by the integro-differential terms of (1.35), thus given as $\mathcal{O}\left(|\lambda|^2\right)$. By simple interchange we receive

$$\rho_{\mathrm{Sys}}(s) \;=\; e^{-\mathcal{L}_0(t-s)}\rho_{\mathrm{Sys}}(t) - \mathcal{O}\left(|\lambda|^2\right) \;. \tag{1.44}$$

So to say, we received a backward (free) propagation, with making an error of the order $\mathcal{O}\left(|\lambda|^2\right)$. As these corrections arise inside the integro-differential part, we can neglect them as effective terms of the order $\mathcal{O}\left(|\lambda|^4\right)$.

This leads to an effective memory equation of

$$\int_0^t \mathcal{K}(t-s)\rho_{\mathrm{Sys}}(s)\,ds \;=\; \int_0^t \mathcal{K}(t-s)e^{-\mathcal{L}_0(t-s)}\rho_{\mathrm{Sys}}(t)\,ds + \mathcal{O}\left(|\lambda|^4\right) \;. \tag{1.45}$$

such that the super-operator part remains in the time integral

$$\mathcal{M}_{\mathrm{BR}}(t) \;:=\; \int_0^t \mathcal{K}(t-s)e^{-\mathcal{L}_0(t-s)}\,ds \;=\; \int_0^t \mathcal{K}(s)e^{-\mathcal{L}_0 s}\,ds \;\simeq\; \int_0^\infty \mathcal{K}(s)e^{-\mathcal{L}_0 s}\,ds\;. \tag{1.46}$$

Thereby the last time-averaging step (which is the second step in the Bloch-Redfield approximation) is done analogously to eq. (1.42).

Davies-Łuczka-approximation

A different approach to a Markovian approximation is the concept proposed by J. Łuczka in [43], where he implement a time-average method previously developed by E.B. Davies [44, 45] on a spin-boson type model. Basically this time-coarsening procedure consists of two steps. At first, a still temporal dependent, but exact average of the memory kernel in its Schrödinger representation is performed. Secondly a simultaneous long-time/weak-coupling limit of the memory kernel using Davies' method is arranged . Hereby the decomposition of the free Liouvillian, respectively of its corresponding propagators in appropriate projector terms in this limit accomplishes the Markovian character.

The weak-coupling/long-time average limit according Davies proceed as follows[5]; we start with the non-Markovian Born equation (1.35) in interaction representation

$$\frac{\partial\tilde{\rho}_{\mathrm{Sys}}(t)}{\partial t} \;=\; \lambda\langle\tilde{\mathcal{L}}_{\mathrm{I}}(t)\rangle_\beta\rho_{\mathrm{Sys}}(0) + \lambda^2\int_0^t \tilde{\mathcal{K}}(t-s)\tilde{\rho}_{\mathrm{Sys}}(s)\,ds \tag{1.47}$$

with memory kernel given as in eq. (1.36).

As we are mainly interested in deriving an appropriate time averaging scheme for the integro-differential part, we will disregard in the following the influences of the initial conditions, *i.e.* the one linear in λ, which disappears in most applications anyway. First we consider under this circumstances the formal integral solution of (1.47)

$$\tilde{\rho}_{\mathrm{Sys}}(t) - \tilde{\rho}_{\mathrm{Sys}}(0) \;=\; \int_0^t \dot{\tilde{\rho}}_{\mathrm{Sys}}(u)\,du \;=\; \int_0^t\int_0^u \tilde{\mathcal{K}}(u-s)\tilde{\rho}_{\mathrm{Sys}}(s)\,ds\,du;$$

in order to integrate out pure environmental dynamics we transfer the memory kernel

[5] In fact, Davies derivation is much more rigorous and detailed in its mathematical description, in particular regarding appropriate continuity conditions. As we are mainly interested in the practical consequences of this average method, rather than its most general mathematical derivation, we encourage the interested reader to study his original works [44, 45].

$\tilde{\mathcal{K}}(u-s)$ into its Schrödinger representation

$$\begin{aligned} &= \int_0^t \int_0^u e^{-\mathcal{L}_0 u}\mathcal{K}(u-s)e^{\mathcal{L}_0 s}\tilde{\rho}_{\mathrm{Sys}}(s)\,ds\,du \\ &= \int_0^t e^{-\mathcal{L}_0 s}\left[\int_s^t e^{-\mathcal{L}_0(u-s)}\mathcal{K}(u-s)\,du\right]e^{\mathcal{L}_0 s}\tilde{\rho}_{\mathrm{Sys}}(s)\,ds \\ &= \int_0^t e^{-\mathcal{L}_0 s}\left[\int_0^{(t-s)} e^{-\mathcal{L}_0 v}\mathcal{K}(v)\,dv\right]e^{\mathcal{L}_0 s}\tilde{\rho}_{\mathrm{Sys}}(s)\,ds \\ &=: \int_0^t e^{-\mathcal{L}_0 s}\mathscr{K}(t-s)e^{\mathcal{L}_0 s}\tilde{\rho}_{\mathrm{Sys}}(s)\,ds\ , \end{aligned} \tag{1.48}$$

where we have exchanged the order of integrations as indicated in Fig. 1.1 and made a substitution $v := (u-s)$.

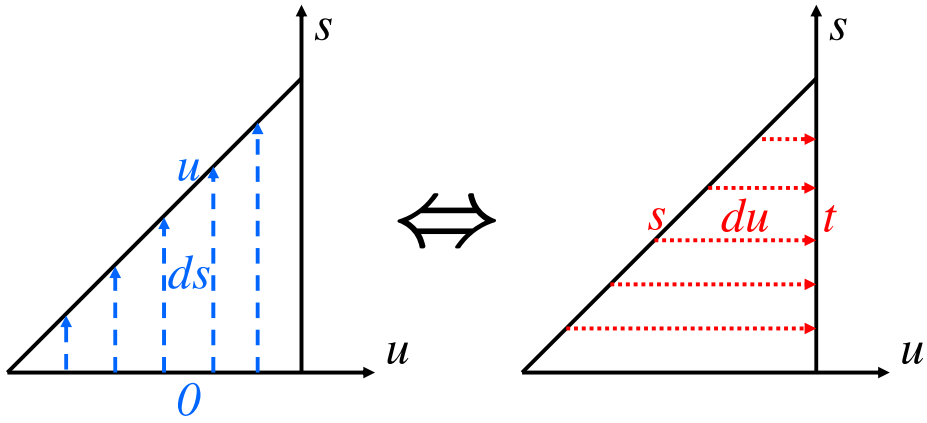

Figure 1.1: Schematic plot of the permutation of integration order, applied in equation (1.48). Hereby one has to keep in attention, how the integral boundaries change and adapt the integrands arguments congruently.

Now we introduce a scaling argument, whereat time and weak-coupling constant λ is played off against each other. With the notion $t \to t' := t/\lambda^2$ and $\rho_{\mathrm{Sys}}(t) \to \rho_\lambda(t') := \rho_{\mathrm{Sys}}(t'/\lambda^2)$ one receives

$$\tilde{\rho}_\lambda(t') \;=\; \rho_{\mathrm{Sys}}(0) + \int_0^{t'} e^{-\mathcal{L}_0 s/\lambda}\mathscr{K}_\lambda(t'-s)e^{+\mathcal{L}_0 s/\lambda}\tilde{\rho}_\lambda(s)\,ds\ , \tag{1.49}$$

with

$$\mathscr{K}_\lambda(t) \;=\; \int_0^{t/\lambda} e^{-\mathcal{L}_0\tau}\mathcal{K}(\tau)\,d\tau\ . \tag{1.50}$$

If we now consider the limit $\lambda \to 0$ with additional condition $t' = t/\lambda^2 = const.$ we receive as effective formal solution

$$\rho_0(t') \;=\; \rho_{\rm Sys}(0) + \int_0^{t'} \bar{\mathscr{K}}\,\rho_0(s)\,ds \;, \tag{1.51}$$

with

$$\bar{\mathscr{K}} \;=\; \sum_n \mathbb{P}_n \mathscr{K}_0 \mathbb{P}_n \tag{1.52}$$

the projector decomposition of

$$\mathscr{K}_0 \;=\; \int_0^{\infty} e^{-\mathcal{L}_0\tau}\mathcal{K}(\tau)\,d\tau \;, \tag{1.53}$$

the concatenated weak-coupling/long-time limit of the memory functional of the scaling solution (1.49). The set of projection operators $\{\mathbb{P}_n\}$, with respect to which the decomposition of $\mathcal{K}_0$ takes place, is given by the spectral decomposition of the free Liouvillian

$$\mathcal{L}_0 \;=\; \sum_j \hbar\omega_j \mathbb{P}_j \tag{1.54}$$

with ω_j the various frequencies of the unperturbed unitary evolution, and $\mathbb{P}_j$ the according projections of the free Liouvillian eigenstates (which evidently where given as density matrices), such that

$$\mathbb{P}_j\mathbb{P}_k \;=\; \delta_{jk}\mathbb{P}_j \tag{1.55}$$

δ_{jk} the usual Kronecker symbol.

The projector decomposition is justified iff the Liouvillian spectrum of its eigenvalues is not degenerate and thus

$$\begin{aligned}\int_0^{t/\lambda} e^{-\tilde{\mathcal{L}}_0 s/\lambda}\mathcal{S}(s)e^{+\tilde{\mathcal{L}}_0 s/\lambda}\,ds \;&=\; \int_0^{t/\lambda}\sum_{j,k} e^{-i\omega_j s/\lambda}\mathbb{P}_j\mathcal{S}(s)\mathbb{P}_k e^{+i\omega_k s/\lambda}\,ds \\ &\overset{\lambda\to 0}{=} \int_0^{t/\lambda}\sum_j \mathbb{P}_j\mathcal{S}(s)\mathbb{P}_j\,ds\end{aligned} \tag{1.56}$$

for any super-operator $\mathcal{S}$.

If we now consider the derivation of the integral solution (1.51) we receive as Markovian master equation in the weak-coupling/long-time limit

$$\frac{\partial\rho_0(t')}{\partial t'} \;=\; \bar{\mathscr{K}}\,\rho_0(t') \;, \tag{1.57}$$

and therefore as Davies-Łuczka Markov approximation

$$\mathcal{M}_{\mathrm{DL}} \;=\; \bar{\mathscr{K}} \;=\; \sum_n \mathbb{P}_n \left(\int_0^\infty e^{-\mathcal{L}_0 \tau} \mathcal{K}(\tau)\, d\tau \right) \mathbb{P}_n \;. \tag{1.58}$$

Markov approximation according to Celio and Loss

M. Celio and D. Loss [42] made a similar analysis of Markovian master equations derived in different ways for a spin-boson type system. Their observations with respect to (complete) positivity behaviour of these approximations were mainly founded on the symmetry aspects of the corresponding matrix formulation as well as on high temperature limits. Observing that the matrix representations of two different Markovian approximations exhibit complementary symmetry, they construct a symmetrized combination, namely the arithmetic average of them.

The corresponding Markovian memory kernel is calculated as follows; on the one hand they use the Bloch-Redfield type of master equation

$$\mathcal{M}_{\mathrm{CL},1} \;=\; -\frac{\lambda^2}{\hbar^2} \int_0^\infty \langle \mathcal{L}_{\mathrm{I}} e^{-\mathcal{L}_0 \tau} \mathcal{L}_{\mathrm{I}} \rangle_\beta e^{\mathcal{L}_S \tau}\, d\tau \;, \tag{1.59}$$

where

$$e^{-\mathcal{L}_S (t-s)} \rho_{\mathrm{Sys}}(t) \;=\; \rho_{\mathrm{Sys}}(s) + \mathcal{O}\left(\lambda^2\right) \tag{1.60}$$

denotes the free backward propagator of the system density matrices. Furthermore they introduce a version with opposite symmetry

$$\mathcal{M}_{\mathrm{CL},2} \;=\; -\frac{\lambda^2}{\hbar^2} \int_0^\infty e^{\mathcal{L}_S \tau} \langle \mathcal{L}_{\mathrm{I}} e^{-\mathcal{L}_0 \tau} \mathcal{L}_{\mathrm{I}} \rangle_\beta\, d\tau \;. \tag{1.61}$$

This might be justified by the idea, that the order in which a free (backward) propagation and a double bath-induced interaction with internal time difference τ takes place should make no difference, if the environmental backaction effects were real time-independent (*i.e.* Markovian in the strict sense of Lindblad).

The final and complete positive version by Celio and Loss is given as the arithmetic mean of $\mathcal{K}_{\mathrm{CL},1}$ and $\mathcal{K}_{\mathrm{CL},2}$

$$\mathcal{M}_{\mathrm{CL}} \;=\; \frac{1}{2}\left(\mathcal{M}_{\mathrm{CL},1} + \mathcal{M}_{\mathrm{CL},2}\right) \;=\; -\frac{\lambda^2}{2\hbar^2} \int_0^\infty \left(e^{\mathcal{L}_S \tau} \langle \mathcal{L}_{\mathrm{I}} e^{-\mathcal{L}_0 \tau} \mathcal{L}_{\mathrm{I}} \rangle_\beta + \langle \mathcal{L}_{\mathrm{I}} e^{-\mathcal{L}_0 \tau} \mathcal{L}_{\mathrm{I}} \rangle_\beta e^{\mathcal{L}_S \tau} \right) d\tau \;. \tag{1.62}$$

Detailed analysis (see Appendix B.4) indeed shows, that the corresponding Bloch sphere representation obtains a symmetric matrix form.

1.4 Spin-Boson Hamiltonian

In order to have an adequate but tangible testing object we consider the spin-Boson model as typical example to describe a single qubit exposed to a heat bath in thermal equilibrium. Consistently with our system-bath model (1.19) the corresponding spin-Boson Hamiltonian is formulated as follows

$$\hat{H}_{\mathrm{SB}} = \hat{H}_{\mathrm{S}} \otimes \mathbb{1}_{\mathrm{B}} + \lambda \hat{H}_{\mathrm{I}} + \mathbb{1}_{\mathrm{S}} \otimes \hat{H}_{\mathrm{B}} \tag{1.63}$$

with a generic (but time-independent) free qubit-Hamiltonian

$$\hat{H}_{\mathrm{S}} = \hbar \left(\epsilon \hat{\sigma}_z + \Delta \hat{\sigma}_x \right) \tag{1.64}$$

and an energy shifting coupling to the bosonic bath coordinates $\hat{x}_k = \left(\hat{a}_k^\dagger + \hat{a}_k \right)$ given as

$$\hat{H}_{\mathrm{I}} = \hbar \hat{\sigma}_z \sum_k g_k \hat{x}_k \ , \tag{1.65}$$

where g_k denotes a particular coupling strength of the k bath mode to the spin variable $\hat{\sigma}_z$.

In a pictorial way (which in fact is usually the practical way of designing a solid state qubit setup, *e.g.* by using semi- or super-conducting devices), the spin-Hamiltonian with its energy bias ϵ and its tunneling amplitude Δ can be interpreted as given by a double-well potential like in Fig. 1.2. The two $\hat{\sigma}_z$ Eigenstates were hereby represented by states located in the left and right minimum respectively.

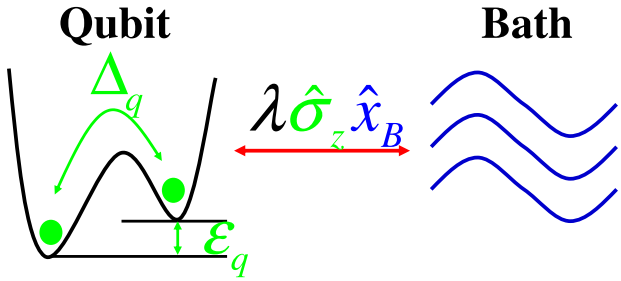

Figure 1.2: Schematic plot of an effective pseudo-spin system, given by the two lowest energy states, localized in the left and right minimum. The term $\epsilon \hat{\sigma}_z$ of the spin-Hamiltonian 1.63 correlates to the energy bias between both levels, $\Delta \hat{\sigma}_x$ describes the ability of quantum mechanical tunneling between them. The heat bath (indicated by the blue waves) is coupled to the qubit via a $\hat{\sigma}_z$-type interaction with coupling constant λ.

The bath Hamiltonian is given as usual

$$\hat{H}_{\mathrm{B}} = \sum_k \omega_k \left(\hat{a}_k^\dagger \hat{a}_k + \mathbb{1}_{\mathrm{B}}/2 \right) \ . \tag{1.66}$$

1.4.1 Thermodynamic limit and Ohmic bath

In order to calculate the bath correlation functions, and the corresponding memory kernel of the Born approximation, we have to specify the behaviour of the individual mode-dependent interaction strength g_k in $\hat{H}_{\rm I}$. Hereby we consider the thermodynamic limit of the bath, *i.e.* we change from a discrete to a continuous distribution of modes. The physical coupling behaviour of the bath therefor is given by its spectral function

$$J(\omega) \;=\; \sum_k g_k \delta(\omega - \omega_k) \tag{1.67}$$

which we here choose to be an Ohmic heat bath (*i.e.* linear in the frequency of the bath mode [31, 39])

$$J(\omega) \;=\; \lambda\omega \frac{\omega_c^2}{\omega_c^2 + \omega^2} \tag{1.68}$$

with an appropriate Drude-cutoff ω_c. This case corresponds to classical, velocity-dependent friction (thus Ohmic). The cutoff serves to avoid ultraviolet divergencies when evaluating the correlation functions (for detail see appendix B).

If we calculate the real and imaginary part of the interaction representation environmental correlation functions from eq. (1.32)

$$\begin{aligned} \mathcal{R}_{j,k}(t-s) &= \mathrm{Re}\left(\langle \tilde{\hat{x}}_j(t)\tilde{\hat{x}}_k(s)\rangle_\beta\right) \\ \mathcal{I}_{j,k}(t-s) &= \mathrm{Im}\left(\langle \tilde{\hat{x}}_j(t)\tilde{\hat{x}}_k(s)\rangle_\beta\right) \end{aligned} \tag{1.69}$$

we receive

$$\begin{aligned} \mathcal{R}_{j,k}(t-s) &= \mathrm{Re}\left(\mathrm{tr}\left\{\rho_{\rm B}(\beta) e^{+i/\hbar\hat{H}_{\rm B}t}\hat{x}_j e^{-i/\hbar\hat{H}_{\rm B}(t-s)}\hat{x}_k e^{-i/\hbar\hat{H}_{\rm B}s}\right\}\right) \\ &= \delta_{j,k}\cdot\mathrm{Re}\left(\mathrm{tr}\left\{\rho_{\rm B}(\beta)\left[e^{+i\omega_j t}\hat{a}_j^\dagger + e^{-i\omega_j t}\hat{a}_j\right]\left[e^{+i\omega_k s}\hat{a}_k^\dagger + e^{-i\omega_k s}\hat{a}_k\right]\right\}\right) \\ &= \delta_{j,k}\mathrm{Re}\left(\mathrm{tr}\left\{\rho_{\rm B}(\beta)\left[e^{+i\omega_k(t-s)}\hat{a}_j^\dagger\hat{a}_k + e^{-i\omega_k(t-s)}\hat{a}_j\hat{a}_k^\dagger\right]\right\}\right) \\ &= \delta_{j,k}\mathrm{Re}\left(\cos(\omega_j(t-s))\langle 2\hat{a}_j^\dagger\hat{a}_j + \mathbb{1}_{\rm B}\rangle_\beta - i\sin(\omega_j(t-s))\langle\mathbb{1}_{\rm B}\rangle_\beta\right) \\ &= \delta_{j,k}\mathrm{Re}\left(\cos(\omega_j(t-s))\coth\left(\frac{\omega_j\beta}{2}\right) - i\sin(\omega_j(t-s))\right) \\ &= \delta_{j,k}\cos(\omega_j(t-s))\coth\left(\frac{\omega_j\beta}{2}\right) \\ \mathcal{I}_{j,k}(t-s) &= \mathrm{Im}\left(\mathrm{tr}\left\{\rho_{\rm B}(\beta) e^{+i/\hbar\hat{H}_{\rm B}t}\hat{x}_j e^{-i/\hbar\hat{H}_{\rm B}(t-s)}\hat{x}_k e^{-i/\hbar\hat{H}_{\rm B}s}\right\}\right) \\ &= \delta_{j,k}\mathrm{Im}\left(\cos(\omega_j(t-s))\coth\left(\frac{\omega_j\beta}{2}\right) - i\sin(\omega_j(t-s))\right) \\ &= -\delta_{j,k}\sin(\omega_j(t-s)) \;, \end{aligned} \tag{1.70}$$

where we have used

$$\tilde{\hat{a}}_j^{(\dagger)}(t) \;=\; e^{\mp i\omega_j t} \tag{1.71}$$

and some other basic calculations, which in detail you can find *e.g.* in my diploma thesis [28].

In the thermodynamic limit this convert to frequency-depending functions

$$\begin{aligned}\mathcal{R}_\omega(t-s) &= \frac{J(\omega)}{\pi}\coth\left(\frac{\omega\beta}{2}\right)\cos(\omega(t-s)) \\ \mathcal{I}_\omega(t-s) &= -i\frac{J(\omega)}{\pi}\sin(\omega(t-s))\ .\end{aligned} \tag{1.72}$$

The corresponding double-sum inside the integro-differential part of 1.35 is thus replaced by a single frequency-integrations, such that in total the Born master equation of our Spin-Boson type model is according eq. (1.32) in its thermodynamic limit

$$\begin{aligned}\frac{\partial\tilde{\rho}_{\rm S}(t)}{\partial t} \;=\; -\frac{\lambda^2}{\hbar^2}\int_0^t\int_0^\infty \Big(&\mathcal{R}_\omega(t-s)\left[\tilde{\hat{\sigma}}_z(t),\left[\tilde{\hat{\sigma}}_z(s),\tilde{\rho}_{\rm Sys}(s)\right]\right] + \\ &+\mathcal{I}_\omega(t-s)\left[\tilde{\hat{\sigma}}_z(t),\left[\tilde{\hat{\sigma}}_z(s),\tilde{\rho}_{\rm Sys}(s)\right]_+\right]\Big)\,d\omega\,ds\ .\end{aligned} \tag{1.73}$$

For switching back into the Schrödinger picture we use the free Liouvillian (as the linear renormalization term disappeared due to $\langle\hat{x}\rangle_\beta = 0$) and apply the corresponding free propagators $e^{\mathcal{L}_0 t}$ from the left and $e^{-\mathcal{L}_0 s}$ from the right (respectively "inner") side of the super-operator integral kernel, receiving

$$\begin{aligned}\frac{\partial\rho_{\rm S}(t)}{\partial t} \;&=\; -\frac{i}{\hbar}\left[\hat{H}_{\rm S},\rho_{\rm S}(t)\right] - \\ &-\frac{\lambda^2}{\hbar^2}\int_0^t\int_0^\infty \mathcal{R}_\omega(t-s)e^{-i/\hbar\hat{H}_{\rm S}t}\left[\tilde{\hat{\sigma}}_z(t),\left[\tilde{\hat{\sigma}}_z(s),e^{i/\hbar\hat{H}_{\rm S}s}\tilde{\rho}_{\rm Sys}(s)e^{-i/\hbar\hat{H}_{\rm S}s}\right]\right]e^{i/\hbar\hat{H}_{\rm S}t} + \\ &\qquad +\mathcal{I}_\omega(t-s)e^{-i/\hbar\hat{H}_{\rm S}t}\left[\tilde{\hat{\sigma}}_z(t),\left[\tilde{\hat{\sigma}}_z(s),e^{i/\hbar\hat{H}_{\rm S}s}\tilde{\rho}_{\rm Sys}(s)e^{-i/\hbar\hat{H}_{\rm S}s}\right]_+\right]e^{i/\hbar\hat{H}_{\rm S}t}\,d\omega\,ds\ . \\ &=\; -\frac{i}{\hbar}\left[\hat{H}_{\rm S},\rho_{\rm S}(t)\right] - \\ &-\frac{\lambda^2}{\hbar^2}\int_0^t\int_0^\infty \Big(\mathcal{R}_\omega(t-s)\left[\hat{\sigma}_z,e^{-i/\hbar\hat{H}_{\rm S}(t-s)}\left[\hat{\sigma}_z,\rho_{\rm Sys}(s)\right]e^{i/\hbar\hat{H}_{\rm S}(t-s)}\right] + \\ &\qquad +\mathcal{I}_\omega(t-s)\left[\hat{\sigma}_z,e^{-i/\hbar\hat{H}_{\rm S}(t-s)}\left[\hat{\sigma}_z,\rho_{\rm Sys}(s)\right]_+e^{i/\hbar\hat{H}_{\rm S}(t-s)}\right]\Big)\,d\omega\,ds\ .\end{aligned} \tag{1.74}$$

1.5 Numerical results

By applying the formerly described Markovian approximations on the Born master equation (1.74) of the spin-Boson model we receive their matrix master equations in the Bloch-sphere picture (see 1.2.3). Translating them into the corresponding GKS matrix allows us to easily check, whether the particular Markovian process is of Lindblad type (*i.e.* complete positive) or not. As therefor eigenvalues (in particular the minimal one) of the coefficient matrices has to be determined for various temperatures, we perform this step by means of Maple®.

For the following analysis three different qubit situations were examined. At first the case of *pure dephasing*, where the spin Hamiltonian part is in parallel to its coupling to the bath, the corresponding parameters from eq. (1.64) set to $\epsilon = \Omega$ Hz and $\Delta = 0$. As second situation we consider the *pure relaxation* one, where the unperturbed spin axis is perpendicular to the noisy $\hat{\sigma}_z$ coupling (*i.e.* $\epsilon = 0$ and $\Delta = \Omega$ Hz). As *generic setup* we choose $\epsilon = \Omega/\sqrt{2}$ and $\Delta = \Omega/\sqrt{2}$, where we obviously expect to have dephasing and relaxation processes simultaneously. The spin-bath perturbation parameter is set to $\lambda = 0.1$, if not denoted otherwise. This arbitrary choice does not have any influence on the question of positivity as any coefficients in the matrix master equation, and consequently the GKS coefficients scales linearly with λ^2 and as we only check the algebraic signs of its eigenvalues, not their absolute values. The temperature will remain a free variable, which we mostly consider in the lower temperature regime, mostly below the total spin-energy $\Omega = \sqrt{\epsilon^2 + \Delta^2}$, as this is where we expect essential effects to happen.

1.5.1 Naïve Markov approximation

At first we investigate the most simple Markovian approach. After some tedious, but straightforward calculation (for details see Appendix B.1), we receive the corresponding GKS coefficient matrix. For that we usually have to symmetrize the derived Markovian master equation in matrix form, as generally also anti-symmetric terms arise, which represent renormalization effects on the unitary evolution, analogous to the Lamb shift.

By numerically determination of the minimal GKS eigenvalues at different temperatures we receive the results plotted in Fig. 1.3 [6]. Apparently, the naïve Markovian approximation does not satisfy complete positivity for any considered case in the whole temperature regime. Thus this approach does not deliver a Lindblad type evolution for the spin-Boson model in the parameter range under consideration.

[6] The experienced reader might object, that numerical treatment of a 3×3 matrix with float number entries, does in practise generate complex valued eigenvalues. But as the arising imaginary terms are in order of the preconveived calculational precision (number of digits), we manually disregard them.

1.5.2 Davies-Łuczka approximation

The situation for the Davies-Łuczka approximation also does not show satisfactory results (Fig. 1.3). Apparently the corresponding GKS coefficient matrix contents at least one negative eigenvalue for any spin Hamiltonian (dephasing, relaxation and generic case) in the whole temperature regime.

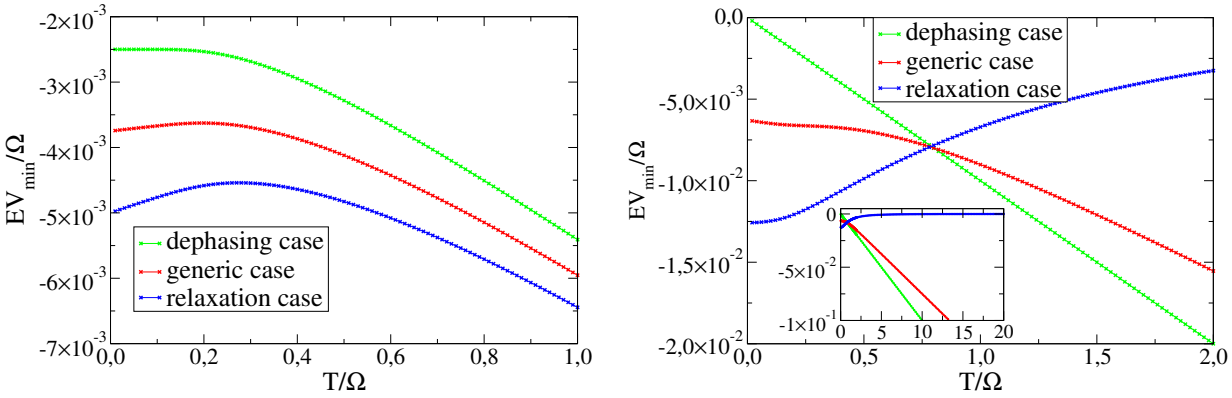

Figure 1.3: Minimal eigenvalues of the GKS coefficient matrix for the naïve (left plot), respectively Davies-Łuczka (right plot) Markovian approximation in dependence of the bath temperature. Three different spin-boson situations were considered: pure dephasing ($\epsilon = \Omega$, $\Delta = 0$), a generic one ($\epsilon = \Omega/\sqrt{2} = \Delta$) and pure relaxation ($\Delta = \Omega$, $\epsilon = 0$). Evidently positivity of the GKS matrix is received in none of these cases. Even in the higher temperature regime of the Davies-Łuczka approach (see insert). The spin-bath interaction parameter is given by $\lambda = 0.1$, the temperature is plotted in units of Ω.

1.5.3 Bloch-Redfield approximation

The numerical analysis of the according GKS-matrix shows positivity properties as described in Fig. 1.4, for detailed calculations see appendix B.2.

Apparently, complete positivity is obtained for the pure dephasing situation ($\epsilon = 10^{10}$ Hz and $\Delta = 0$) at any temperature. For the other cases a complete positivity is violated in the lower temperature regimes below about 60% for the generic situation, respectively 70% of the total energy Ω of the spin for the relaxation case. At least, there is complete positivity reachable by the Bloch-Redfield even for compareably moderate temperature regimes (*i.e.* long before $T \to \infty$).

1.5.4 Celio-Loss approximation

The results for the Markov-approximation according M. Celio and D. Loss [42] were similar to the Bloch-Redfield outcomes. As one can recognize from Fig. 1.4, the pure dephasing case is also complete positive from zero temperature on. The two further setups exhibits a transition from a negative GKS coefficient matrix at low temperatures to complete positivity at a temperature of about 50%, respectively 70% of the total spin energy Ω. In regard of complete positivity, the Celio-Loss proposal seems therefore to deliver slightly better results as the Bloch-Redfield approach.

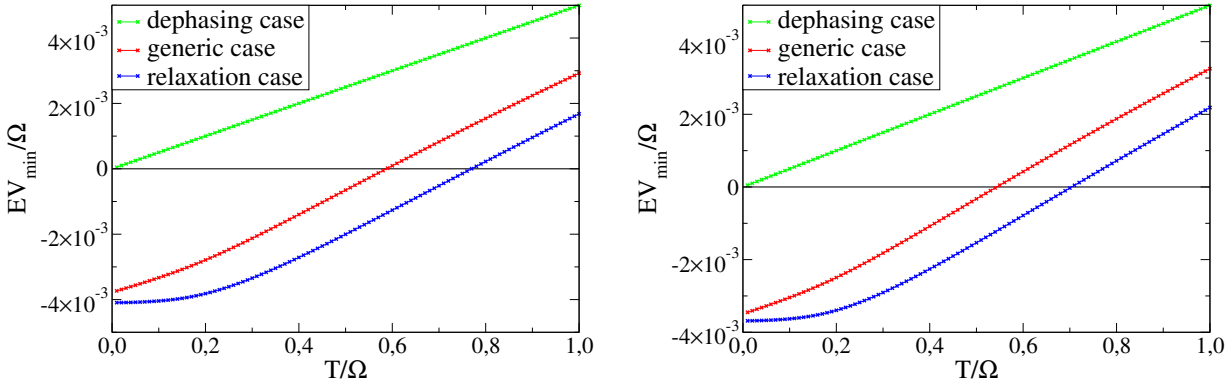

Figure 1.4: Minimal eigenvalues of the GKS coefficient matrix for the Bloch-Redfield (left figure) and the Celio-Loss approximation (right figure) as function of the bath temperature. The usual three different spin-boson setups were considered: pure dephasing ($\epsilon = \Omega$, $\Delta = 0$), a generic one ($\epsilon = \Omega/\sqrt{2} = \Delta$) and pure relaxation ($\Delta = \Omega$, $\epsilon = 0$). Positivity of the GKS matrix is received for all T only in the dephasing situations, while in the other situations a minimal threshold temperature in the order of 60% and 75%, respectively 55% and 70% of the total spin energy is required. Apparently the Celio-Loss approach reaches complete positivity already for slightly lower temperatures. The spin-bath interaction parameter is set to $\lambda = 0.1$, the temperature is plotted in units of Ω.

1.6 Quantitative comparison of the Born-Markovian approximations

Although an imprtant criterion for the quality of a master equation, completet positivity is not necessarty the best quantifier for the practical quality of an approximation. In order to get a quantitative rating, how accurate and useful a Markov approximation is one needs to have a standard of comparison. An obvious suggestion would be *e.g.* the numerical solution of the Born approximation (*i.e.* before any Markovian average takes place). A closer investigation of the memory kernel of the Born approximation of the spin-Boson model shows indeed, that a compareably simple numerical integration of the integro-differential master equation is feasible. This is due to the exponential decay of the memory kernel $\mathcal{K}(t-s) \approx e^{-|t-s|/\tau_{\rm corr}}$, such that one can restrict the integro-differential part of the non-Markovian master equation on several memory loss time scales $\tau_{\rm corr}$. Thus the numerical integration does not grow linearly with the evolution time, receiving the usual quadratic increase of computational time and memory ressources. For calculational details see appendix A. Nevertheless the results point out, that in our preferred parameter regime the Born approach itself is already positivity violating (see especially Fig. 1.5). Thus, it exposes as practically non-applicable, as our standard criterion of comparison. In particular, as the so-called mixed-state fidelity [2]

$$\mathcal{F}_{\rm mixed}(\rho_1,\rho_2) \;=\; {\rm tr}\left\{\sqrt{\sqrt{\rho_1}\rho_2\sqrt{\rho_1}}\right\} \;, \tag{1.75}$$

requires correct, *i.e.* positive density matrices as arguments (*e.g.* in Bloch sphere interpretation $|\vec{\sigma}|^2 \leq 1$).

We now consider the evolutions implied by the Born-Markovian approximations for an exemplaric setup of parameters. Firstly, we set the spin parameters to the usual generic values of $\epsilon = \Omega/\sqrt{2} = \Delta$. Furthermore we put the temperature to the moderate value of $T = \hbar\Omega/k_B$ with $\Omega = \sqrt{\epsilon^2+\Delta^2}$ the typical spin energy, as our positivity analysis promises a positivity preserving behaviour at least for the Bloch-Redfield and the Celio-Loss evolution (see plots 1.4). If we know choose as initial state the $\hat{\sigma}_y$ eigenstate $\sigma_y(t=0) = +1$ we receive the results plotted in Fig. 1.6. Apparent differences between the various approximations are visible. Hereby the Davies-Łuczka evolution exhibits the strongest deviations, in particular violating positivity of the according density matrix from the very beginning. Otherwise the Bloch-Redfield and the Celio-Loss approaches, which were based on analogous concepts of Markovian time-average, do expose very similar behaviour.

As a result of the preserved positivity for the naive, the Bloch-Redfield and the Celio-Loss approximations, we were able to compare their solutions ρ_{naive}, ρ_{BR} and ρ_{CL} by using the so-called mixed-state fidelity $\mathcal{F}_{\text{mixed}}$ eq. (1.75). This is a generalization of the usual fidelity measure, which is normally used for comparing dissipative evolution outcomes with idealized, pure states density matrices (*e.g.* to evaluate the quality of experimental or theoretically proposed quantum gates [46]).

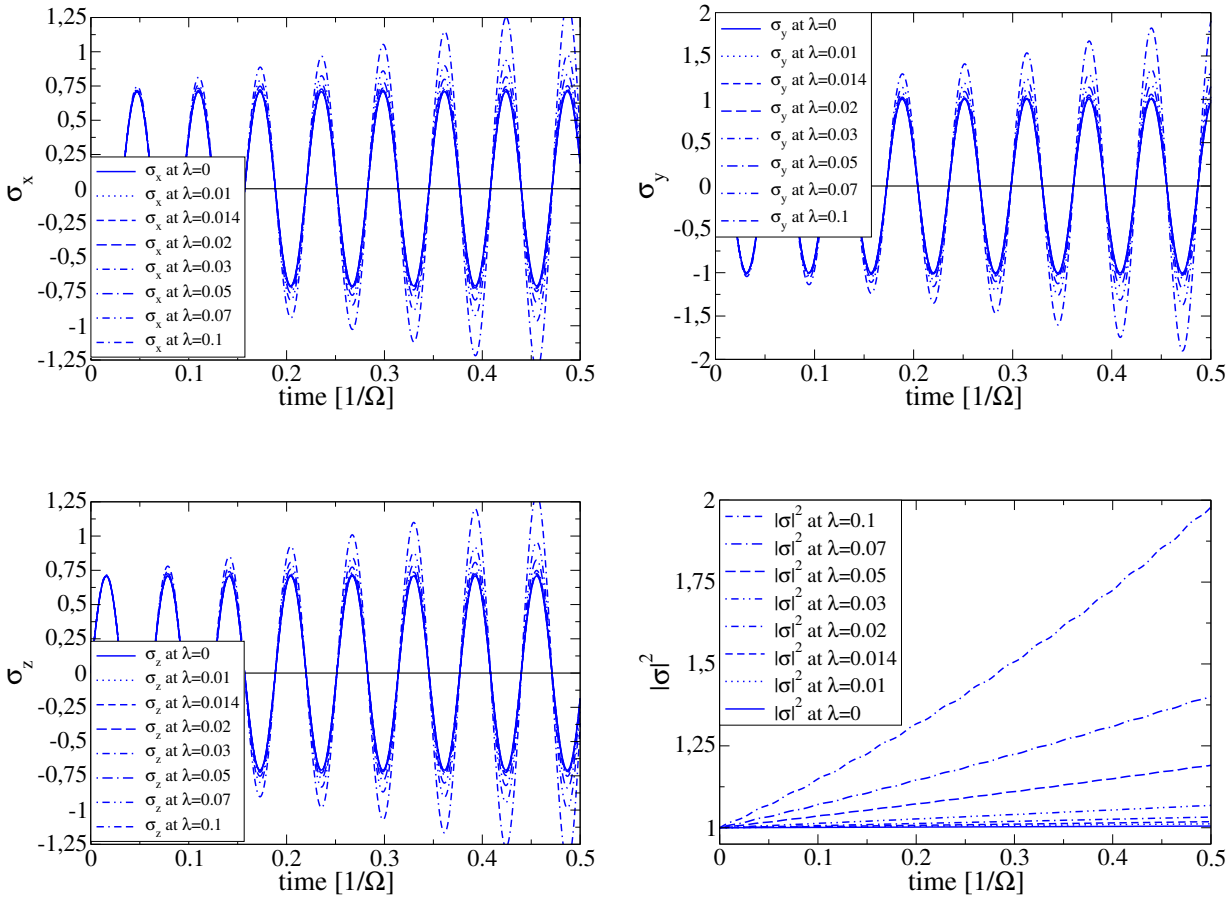

Figure 1.5: Numerically computated solution of the rigorous Born master equation. As initial state the $\sigma_y(t=0) = +1$ eigenstate is chosen, the spin parameter were taken for a generic situation, *i.e.* $\epsilon = \Omega/\sqrt{2} = \Delta$ with an intermediate temperature of $T = \hbar\Omega/k_B$. The spin-bath coupling is varied between $\lambda = 0$ and $\lambda = 0.01$. Evidently the positivity of the corresponding density matrix is absent at all couplings, as the absolute value of the according Bloch sphere vector exceeds unity.

At first, in order to estimate the strength of decoherence of the various Markovian approximations, we evaluate the loss of mixed-state fidelity between the different solutions and the free unitary evolution. As one can recognize from Fig. 1.7, corresponding to the analysis of the decay of the absolute spin-value (plot 1.6), the decrease of fidelity for the Bloch-Redfield and the Celio-Loss solutions were almost equal and approximatively doubly as fast as the naive Markovian decrement.

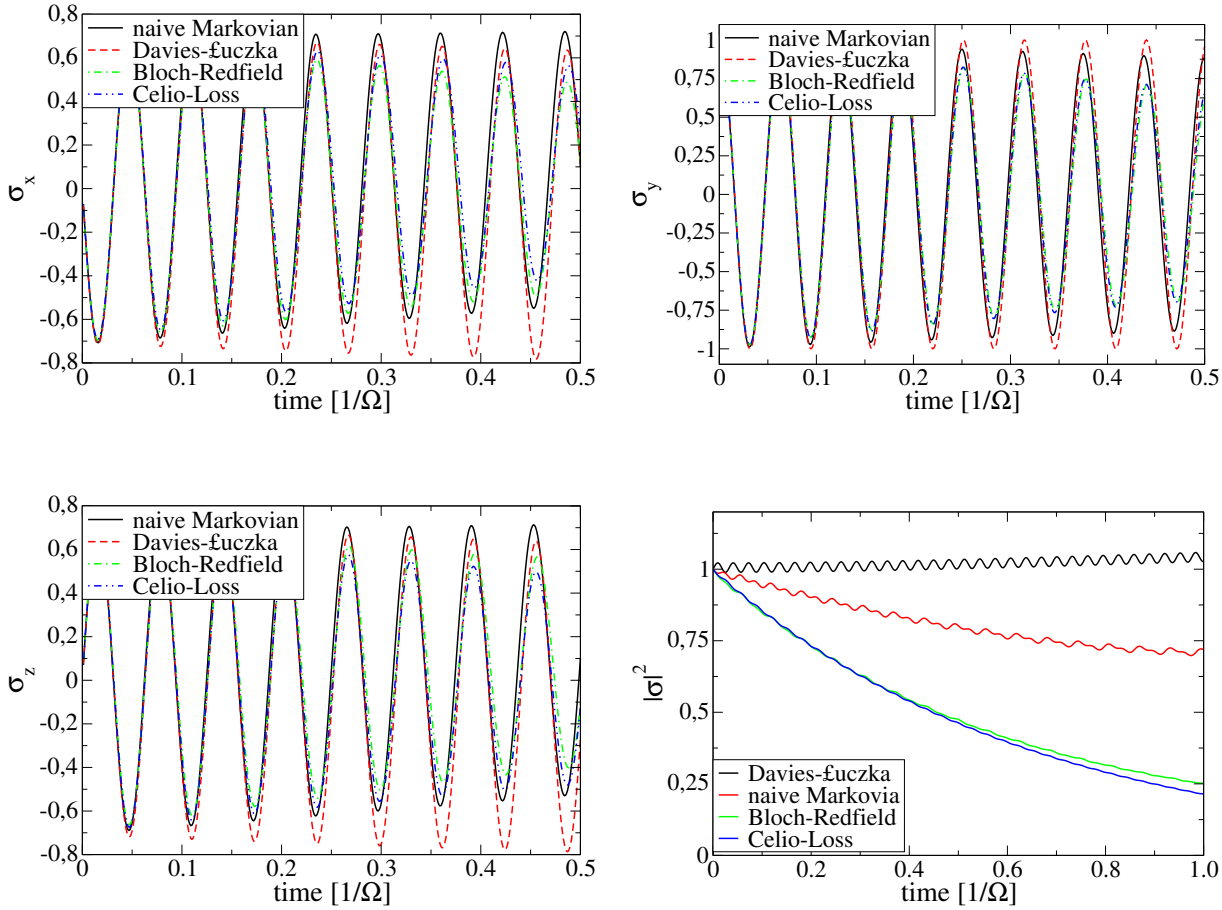

Figure 1.6: Spin evolutions of the Born-Markovian approximations. As initial state the $\sigma_y(t=0) = +1$ eigenstate is taken, the spin parameter were set to the usual generic values, *i.e.* $\epsilon = \Omega/\sqrt{2}$ Hz $= \Delta$ with a corresponding temperature of $T = \hbar\Omega/k_B$. The spin-bath coupling is chosen to $\lambda = 0.01$. Apparently the positivity of the corresponding density matrices is preserved in the considered time regime for all approaches with exception of the Davies-Łuczka case, where the absolute value of the according Bloch sphere vector exceeds unity. Typical values are $\Omega = 10^{10}$ Hz and corresponding $T = 0.07K$

If we derive the mutual mixed state fidelity of the three Markovian schemes, we observe a consistent phenomenon (see Fig. 1.7. The measure of identity between the Bloch-Redfield and the Celio-Loss solution remains on a compareably high level (larger 99%), while the deviation from the naïve Markovian approximation increases roughly with half the absolute decoherence rate.

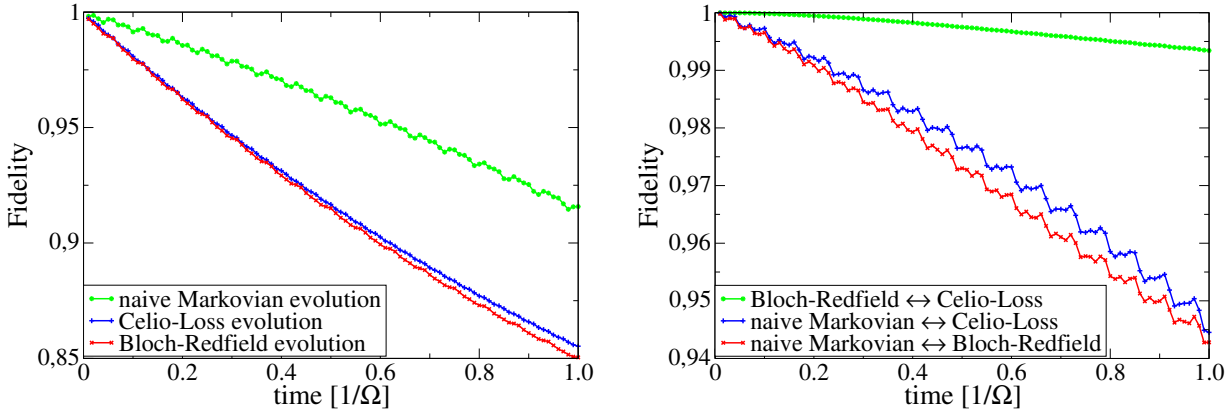

Figure 1.7: Fidelity decay of the Born-Markovian solutions regarding the free unitary evolution (left plot), as well as mutually compared (right plot). Evidently, the Celio-Loss and the Bloch-Redfield approach experiences approximatively the same amount of fidelity loss in regard of the free evolution, while the naive Markovian approximation exhibits decoherence of only about half the decaying rate. The mutual comparison of the Born-Markovian solutions indicates, that the Celio-Loss and the Bloch-Redfield approaches retain congruence on a much longer time scale, then they do in regard of the naive Markovian approximation.

Lacking a standard of comparison (a reliable, as well as positivity presaerving solution of the spin-Boson model) yet, we can only estimate, that Bloch-Redfield and Celio-Loss as more elaborated average schemes promises to be the more accurate methods of deriving Markovian evolutions. Probably higher order perturbation theory (*e.g.* up to λ^4) might be a promising way out.

1.7 summary

We have described in the former chapter an easy to verify criterion of complete positivity for arbitrary, but finite-dimensional Markovian master equations. By using the advantage of the isomorphy between the formal $SU(2)$ topology of the two-state density matrices and their $SO(3)$ representation in the Bloch sphere picture, we easily received finite-temperature results of Born-Markov approximations for the spin-Boson model with an Ohmic heat bath. For two of the approaches, we literally obtained only negative results. While two other outcomes (namely the Bloch-Redfield and the Celio-Loss approach) showed complete positivity even for compareal low temperatures (from about $T = 0.5\Omega$ with Ω the energy scale of the free system). In the last section we made quantitative analysis by means of the so-called mixed state fidelity. As this requires positive density matrices as arguments, we could not make comparisons with solutions of the pure Born approximations, we received received numerically by means of the exponential decay of the corresponding memory kernel. Instead we compared the three solutions, positive on intermediate time scales, mutually as well as with the free, unitary solution, as a kind of decoherence measure.

Chapter 2

Qubit decoherence due to bistable fluctuators

"I've got the poison, I've got the remedy,
I've got the pulsating, rhythmical remedy!"

The prodigy "poison"

The probably most promising candidates for providing quantum computational devices are solid state realizations of qubits, in particular with respect to the practically challenging request of scalability (*i.e.* the feasibility of producing larger scaled quantum bit registers, probably just by attaching several quantum bit copies to each other). Nevertheless, the numerous degrees of freedom, which are present in any condensed matter setup, provide various channels of decoherence and are the main obstacles of producing steadily working quantum computing devices. The most obvious noise sources are hereby usually Boson-type fluctuations, *e.g.* disturbances due to electro-magnetic noise (via non-perfect control lines or even due to electro-magnetic radiation). As such kind of noise origins are mainly produced by macroscopic systems, like thermal heat baths or electronic Fermi seas, they can often be regarded as Bosonic environments. That means they can be described by Bosonic bath spin (or several spin) models, analogous to the Born and Born Markovian treatment discussed in the previous chapter 1. This universal way of description is justified by to the availability of the central limit theorem [47], which applies if the environmental excitations and backaction with respect to the spin system do average out their original dynamics and thus leads to Gaussian distributed fluctuations in the bath. This even holds, if the elementary objects of the bath do follow Fermi-statistics (*e.g.* electronic leads), but their excitations show Bosonic character.

In practice, such noise sources are usually prevented or at least reduced by effective cooling or shielding techniques. Of course, as long as one is interested in strong interactions on and between various qubits, one always has to compromise between isolation of the qubits from external influences and most effective control of them. But there are

also situations, where the assumption of a Bosonic environment, composed of energetically unbounded, mutually independent noise sources, does not apply. In particular, if the environmental excitations turn out to have only a finite number of energy levels, or even more drastically, if they exhibit to be two-level systems itself. Experimentally indicated examples of such two- or few-level noise origins are *e.g.* background charges, trapped in non-perfect substrate of the physical qubit setup, or analogously (for flux sensitive qubit) trapped fluxes in superconducting devices [48, 49, 6, 50]. Those were assumed of being responsible for telegraph noise behaviour. Furthermore, if appearing in ensembles with stochastically independent distibutions of eigenfrequencies, such kind of noise sources are very probable candidates for 1/f-noise generation [51, 52, 53, 54].

In such cases, the noise influence can neither be described as Bosonic bath, nor can they easily be avoided by usual isolating techniques. Therefore one has to apply different methods for modeling this sort of decoherence. One particular, but nevertheless relevant case of such so-called two-state fluctuators, has been intensely discussed [55, 56]. One appropriate microscopic approach is a coupled qubit-fluctuator-oscillator bath system (as depicted in Fig. 2.1), where the fluctuator decoheres the qubit. It acts as a noise filter mediating the dissipation of the external heat bath. Even though this seems to be a quite generic approach of describing the decoherence induced by such limited-dimensional noise sources (in the limit of negligible direct qubit heat bath interaction), the further treatment of this three-component system is not obvious. Various attempts with more or less clear results have been performed [55, 56, 53, 54]. In order to mention two of them, one can on the one hand treat the coupled qubit-fluctuator part as a reduced quantum system exposed to the Bosonic heat bath, whose influences can be averaged out by the usual Born or Born-Markov approach (compare chapter 1). Finally one just has to trace out the fluctuator degrees of freedom, in order to receive the effective dynamics of the qubit. In fact, we will use this technique for our first microscopic investigation of the dependence of the impact of decoherence on fluctuator-energy and environmental temperature.

A different method would be treating the coupled fluctuator-bath system as an effective noise environment for the qubit. Analytically, there is no standard approach, how to derive quantum kinetic equations of a subsystem dissipatively influenced by an open quantum system (here the bath-influenced fluctuator) as one knows it for the usual master equations. But it proves to be successful, to consider the limiting case, where the two-state fluctuator is much stronger coupled to the external heat bath, than to the qubit. This should be a typical situation if the noise influences on the qubit due to fluctuators is not too intense. In this limit one can model the effective fluctuator-bath environment by a semi-classical noise source, appearing like a telegraph noise signal, which agrees with corresponding experimental evidences [48] and theoretical predictions [57]. We furthermore will denote the noise origins in this particular limit bistable fluctuators, as they apparently fluctuate between their two states driven by the external heat bath, but itself behave unperturbed by the qubit. In this description the noise influences on the qubit can fully be parametrized by three variables. At first the interaction strength between qubit and

bistable fluctuator, as well as the typical flipping time scales of the bistable fluctuator (the mean average time between two flips) and its asymmetry (the ratio between the average flipping times from a bfl state "up" to "down" and vice versa).

As we will describe in chapter 2.3 this setup can easily be described, on the one hand by numerical integration of the corresponding stochastic Schrödinger equation. On the other hand, we will provide an analytical random walk model, which correspond perfectly with the numerical results, if a particular time scale regime is reached.

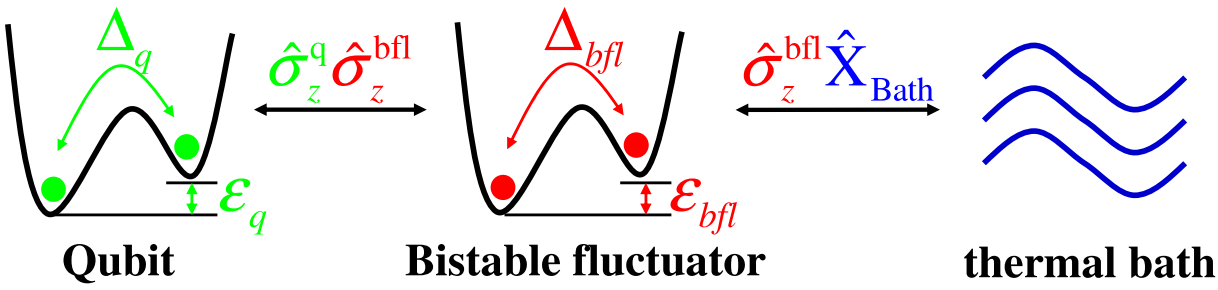

Figure 2.1: Schematical plot of a typical microscopic bistable-fluctuator model. The dynamics of the qubit and the bfl are defined by their energy bias ϵ_{q}, respectively ϵ_{bfl}, as well by their tunnel matrix elements Δ_{q}, respectively Δ_{bfl}. The noise generating couplings are assumed to be depending on $\hat{\sigma}_z$, for the qubit-fluctuator interaction as well as for the heat bath influences on the bfl.

2.1 Qubit-bfl-bath model

For the microscopic analysis we introduce the Hamiltonian of a single qubit **q** coupled weakly to a single bistable fluctuator **bfl**, which itself is driven to incoherent fluctuations by an external heat bath **B** (see Fig. 2.1). Here we assume, that the qubit itself is not directly coupled to any environmental degrees of freedom other than the bfl (which is justified, if the qubit is sufficiently isolated from thermal as well as electromagnetic noise). Our restriction on a one-qubit-one-fluctuator model is chosen for the sake of conceptual simplicity, as we are mainly interested in qubit relaxation and dephasing rates in dependence of fluctuator parameters as well as environmental temperature. The extension to several qubits and/or fluctuators is in principle straightforward, albeit its numerical and analytical treatment rapidly grows in complexity, as we will discuss in detail later. Moreover, experimental evidents indicates the presence of only a small number of fluctuators [48, 6, 50], as samples become smaller and cleaner.

The microscopic Hamiltonian reads as follows

$$\hat{H}_{\mathrm{tot}} = \hat{H}_q + \hat{H}_{\mathrm{q,bfl}} + \hat{H}_{\mathrm{bfl}} + \hat{H}_{\mathrm{bfl,B}} + \hat{H}_B \ , \tag{2.1}$$

where

$$\hat{H}_q = \hbar\left(\epsilon_q \hat{\sigma}_z^q + \Delta_q \hat{\sigma}_x^q\right) \tag{2.2}$$

$$\hat{H}_{\mathrm{bfl}} = \hbar\left(\epsilon_{\mathrm{bfl}} \hat{\sigma}_z^{\mathrm{bfl}} + \Delta_{\mathrm{bfl}} \hat{\sigma}_x^{\mathrm{bfl}}\right) \tag{2.3}$$

and

$$\hat{H}_B = \hbar \sum_j \omega_j \hat{a}_j^\dagger \hat{a}_j \tag{2.4}$$

denotes the qubit-, the bfl- and the bath-Hamiltonian respectively, while

$$\hat{H}_{\mathrm{q,bfl}} = \hbar\alpha \hat{\sigma}_z^q \otimes \hat{\sigma}_z^{\mathrm{bfl}} \tag{2.5}$$

$$\hat{H}_{\mathrm{bfl,B}} = \hbar\lambda \sum_j \hat{\sigma}_z^q \otimes \hat{X}_j^B = \hbar\lambda \sum_j \hat{\sigma}_z^q \otimes \left(\hat{a}_j^\dagger + \hat{a}_j\right) \tag{2.6}$$

represents the interactions between qubit and bfl, respectively between bfl and heat bath.

The main pre-requisite for the bfl to behave as bistable and fluctuating two-level system is the appropriate stronger coupling of the bfl to the external heat bath compared to the qubit, *i.e.* $\alpha \gg \lambda$. Otherwise we would expect merely a dynamics close to a quantum double pendulum, which is not experimentally indicated. In order to apply perturbation theory in the bfl-bath coupling, we furthermore require $\lambda \ll 1$.

We define the free Hamiltonian part of the reduced system (**qubit⊕bfl**) as follows

$$\hat{H}_0 = \hat{H}_q + \hat{H}_{\mathrm{q,bfl}} + \hat{H}_{\mathrm{bfl}} + \hat{H}_B \ , \tag{2.7}$$

and consider the interaction between fluctuator and bath as interaction Hamiltonian

$$\hat{H}_{\mathrm{int}} = \hat{H}_{\mathrm{bfl,B}} \ . \tag{2.8}$$

2.2 Bloch-Redfield master equation

As we have extensively discussed the technical steps in order to receive a Born-Markov master equation of Bloch-Redfield type in the former chapter 1, we only quote here explicitly the resulting Bloch-Redfield tensor, which is based on the corresponding Golden rule rates [31, 58].

2.2.1 Bloch-Redfield tensor

Written explicitly the Bloch-Redfield equation takes the form

$$\dot{\rho}_{mn}(t) = -i\omega_{nm}\rho_{nm}(t) - \sum_{k,l} R_{nmkl}\rho_{kl}(t), \tag{2.9}$$

where

$$\rho_{mn}(t) = \langle m|\rho_{\rm red}(t)|n\rangle \tag{2.10}$$

are the entries of the reduced density matrix according the eigenbasis of the reduced system Hamiltonian $H_{\rm red} = H_q + H_{\rm q,bfl} + H_{\rm bfl}$. The frequencies are defined by the corresponding energies E_j

$$\omega_{nm} = \frac{E_n - E_m}{\hbar} \ . \tag{2.11}$$

The Redfield relaxation tensor

$$R_{nmkl} = \delta_{lm}\sum_r \Gamma^{(+)}_{nrrk} + \delta_{nk}\sum_r \Gamma^{(-)}_{lrrm} - \Gamma^{(+)}_{lmnk} - \Gamma^{(-)}_{lmnk} \tag{2.12}$$

is given by the corresponding Golden rule rates ([31, 58])

$$\Gamma^{(+)}_{lmnk} = \frac{1}{\hbar^2}\int_0^\infty dt e^{-i\omega_{nk}t}\langle \tilde{\hat{H}}_{{\rm int},lm}(t)\tilde{\hat{H}}_{{\rm int},nk}(0)\rangle_\beta, \tag{2.13}$$

$$\Gamma^{(-)}_{lmnk} = \frac{1}{\hbar^2}\int_0^\infty dt e^{-i\omega_{lm}t}\langle \tilde{\hat{H}}_{{\rm int},lm}(0)\tilde{\hat{H}}_{{\rm int},nk}(t)\rangle_\beta. \tag{2.14}$$

with $\tilde{\hat{H}}_{{\rm int},lm}(t) = \langle l|\tilde{\hat{H}}_{\rm int}(t)|m\rangle$ the interaction Hamiltonian matrix elements in the interaction picture with respect to the eigenbasis of the reduced Hamiltonian.

2.2.2 Qubit dephasing and relaxation rates

In order to apply perturbation theory we set the coupling factor between the bfl and the bath to $\lambda = 0.1$. A strong coupling scheme will be presented in the next chapter. As the coupling between qubit and bfl should be weak compared to the fluctuator-bath interaction (to avoid beating effects), we assume $\alpha = 0.01\Omega_q$, with $\Omega_q = \sqrt{\epsilon_q^2 + \Delta_q^2}$ denotes the energy scale of the qubit. We will furthermore consider comparable energies of the bfl and the qubit, as we expect the strongest relaxation and dephasing effects on the qubit in the regime $\Omega_q \simeq \Omega_{\text{bfl}}$, so to say, if the qubit and bfl were in resonance to each other.

Choosing these parameters we can calculate by means of Maple® the dephasing and relaxation rates of the qubit in dependence of the qubit- (ϵ_q,Δ_q), the bfl- (ϵ_{bfl}, Δ_{bfl}) and the bath-parameter (temperature T). Hereby we study different questions. First, how the decoherence on the qubit dependis on the bfl-energy scale. We expect resonant behaviour, most probably with two peaks in the corresponding resonance spectra due to the hybridization of the two qubit levels with the two of the bfl. In other words, the loss of phase and energy is most effective, if the energy separations are equal. Secondly, we want to examine, how this behaviour depends on the environmental temperature. Naively, we expect a widening of the resonance peaks with increasing T, as thermal broadening of the bfl energy levels should arise. In consequence the peak heights should decrease, thus the corresponding rates, as the resonances get less sharp. In a more detailed analysis we also expect the resonance peak positions to move with changing T, as the renormalized energies of the bfl should also be attached. Complementary to that scheme we also want to discuss the resonance behaviour of the qubit decoherence, if the environmental temperature is fixed, but the qubit energy is variable, as this would be the most feasible case for experimental investigations.

Our numerical analysis will be performed as follows; in dependence of the qubit-, bfl- and bath-parameters the minimal dephasing and relaxation rate of the qubit will be evaluated from the numerically derived negative eigenvalues of the Redfield tensor (*i.e.* including the renormalized reduced Hamiltonian). We restrict ourself on the minimal decay rates, as we expect the corresponding eigenstates of the decohering system to be the most relevant, as longest visible ones.

2.2.3 Qubit decoherence spectra at fixed Ω_q for variable T

For the qubit parameters we assume (in correspondence with experimental data) energies in the order of $\Omega_q \simeq 10^{10}$ Hz corresponding to a temperature energy scale of about $0.07K$[1]. For the sake of simplicity we choose a symmetric, but still quite generic situation for the qubit $\epsilon_q = \Delta_q$. As all results are received from numerical routines, generalization to arbitrary qubit Hamiltonian are straightforward. For the bfl we will choose parameters in the regime between $0\Omega_q$ and $2\Omega_q$ in order to receive "resonance spectra" of the qubit dephasing and relaxation rates versus the qubit-bfl energy ratio $\Omega_{\text{bfl}}/\Omega_q$. Thereby we will assume a fixed ratio between bfl tunneling term and energy bias of $\Delta_{\text{bfl}}/\epsilon_{\text{bfl}} = 0.1$.

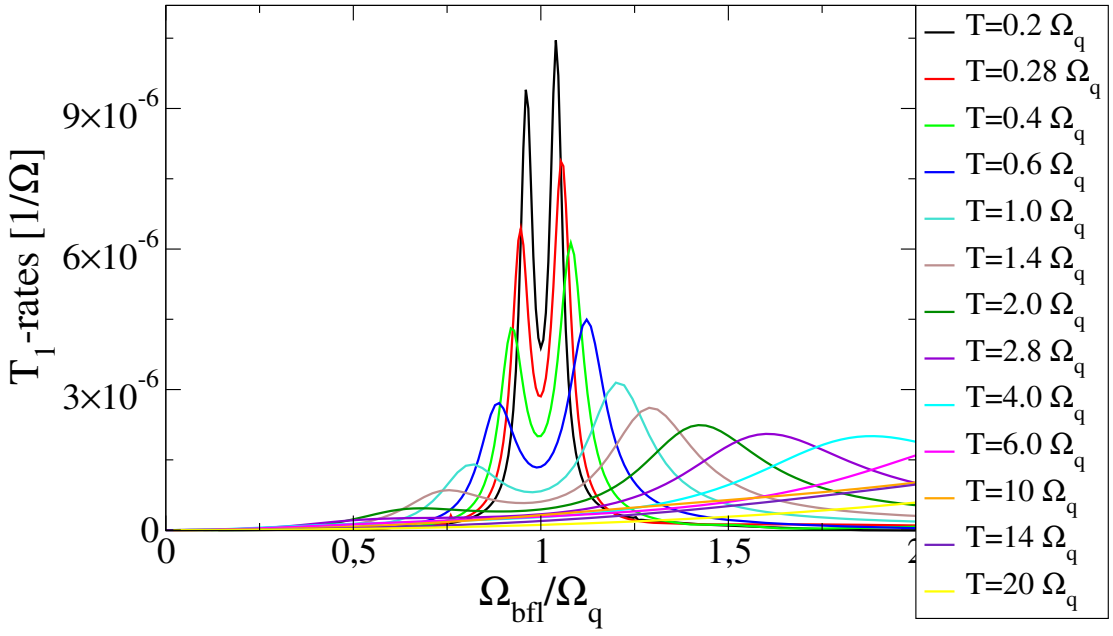

Figure 2.2: Plots of resonance spectra of the relaxation rate of a bfl-influenced qubit. The bfl-energy Ω_{bfl} is tuned from 0 to $2\Omega_q$, with a fixed qubit energy of $\Omega_q = 0.05K$. Each spectrum is received at different environmental temperature, which changing between $T = 0.2\Omega_q$ and $T = 20\Omega_q$.

At first, we produce a series of decoherence "resonance spectra" for a fixed qubit energy (exemplarically chosen to $\Omega_q = 0.05K$ and at different environmental temperatures

[1]Note beside, that we are using exclusively angular frequencies, which are directly connected to corresponding energies via $E_j = \hbar\omega_j$. The frequency notation preferably used in experimental publications convert to this energetic ones by a factor of 2π, meaning our 10 GHz corresponds to approx. 1.6 GHz in experimental language.

between 0.2 and $20\Omega_q$.

One evidently can see the expected double peak resonance structure, which is roughly centered at $\Omega_{\text{bfl}} = \Omega_q$. With increasing temperature, the height of the peaks decreases, while their width is accordingly increasing. The positions of the resonance peaks deviate linearly as function of temperature from the point $\Omega_{\text{bfl}}/\Omega_q = 1$ (see Fig. 2.3).

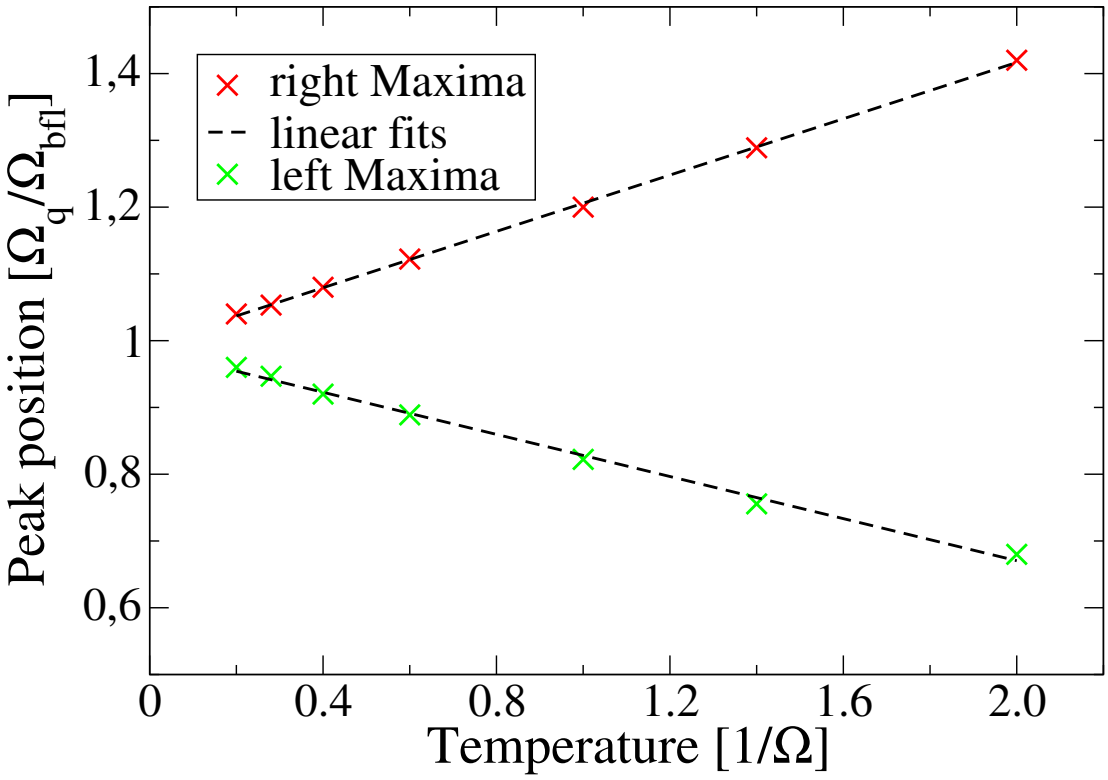

Figure 2.3: Positions of the left and right peaks of the resonance spectra at usual qubit energy $\Omega_q = 0.05K$ and their linear fit. Only peaks at lower temperatures, between $T = 0.2\Omega_q$ and $T = 2\Omega_q$, are considered in order to receive most reliable resolution of their position.

2.2.4 Qubit decoherence spectra at fixed T for variable Ω_q

Corresponding to typical experimental situations we now keep the temperature fixed at exemplaric values of $T = 0.05K$ and $T = 0.5K$, while we tune the qubit energies between $0.2T$ and $20T$, respectively $0.06T$ and $2T$ (see Fig. 2.4 and 2.5).

In the low temperature plot one can see an analogous picture to the variable temperature figure; instead of increasing peak widths and distances with growing temperatures, one receives similar behaviour at decreasing qubit energy Ω_q. Decreasing Ω_q at fixed T shows compareable behaviour as increasing temperature at fixed qubit energy. Also the functional dependence of the peaks distances are inverse proportional to Ω_q, analogous to its linearity in the variable temperature situation (see Fig. 2.6).

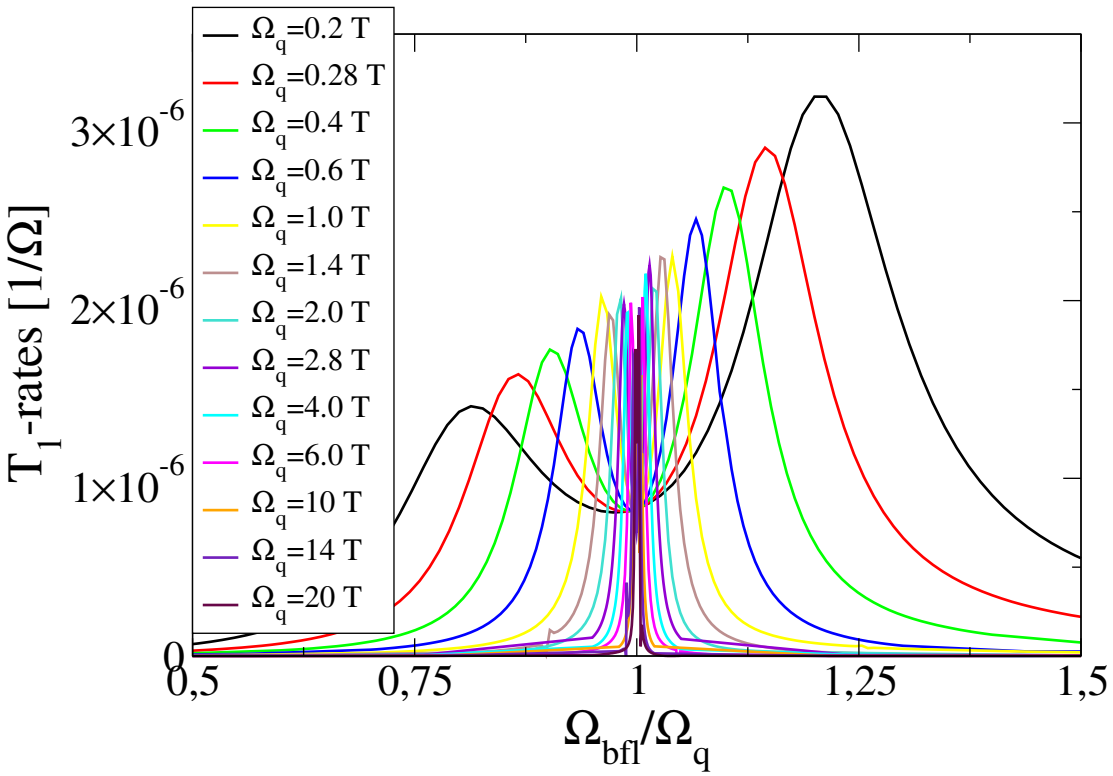

Figure 2.4: Plots of resonance spectra of the relaxation rate of a bfl-influenced qubit. The bfl-energy Ω_{bfl} is tuned from 0 to $2\Omega_q$, for each qubit energy Ω_q, which varies between $0.2T$ and $20T$, with $T = 0.05K$ the fixed environmental temperature.

There is still the difference, that although the peak width increases with decreasing Ω_q, the right peak experiences an almost linear increase in amplitude with growing ratio T/Ω_q (see Fig. 2.7). This could be explained as combination of two different phenomena. At first, the increase of peak width and distances results as consequence of an increasing energy scale ratio T/Ω_q. The bigger that ratio is, in consequence the bigger the environmental temperature compared to the bfl energy scale is, the more separated the hybridization states become as result of the stronger renormalization of the bfl. Furthermore in units of Ω_q the thermal broadening increases. On the other hand, decreasing qubit energy does lead to a linearily growing decoherence (thus relaxation rate, which at least seems to be right in the right peak case), as the environment with its increasing energy scale T becomes more capable for dissipating the reduced systems energy. This is in particularly confirmed by our further examination.

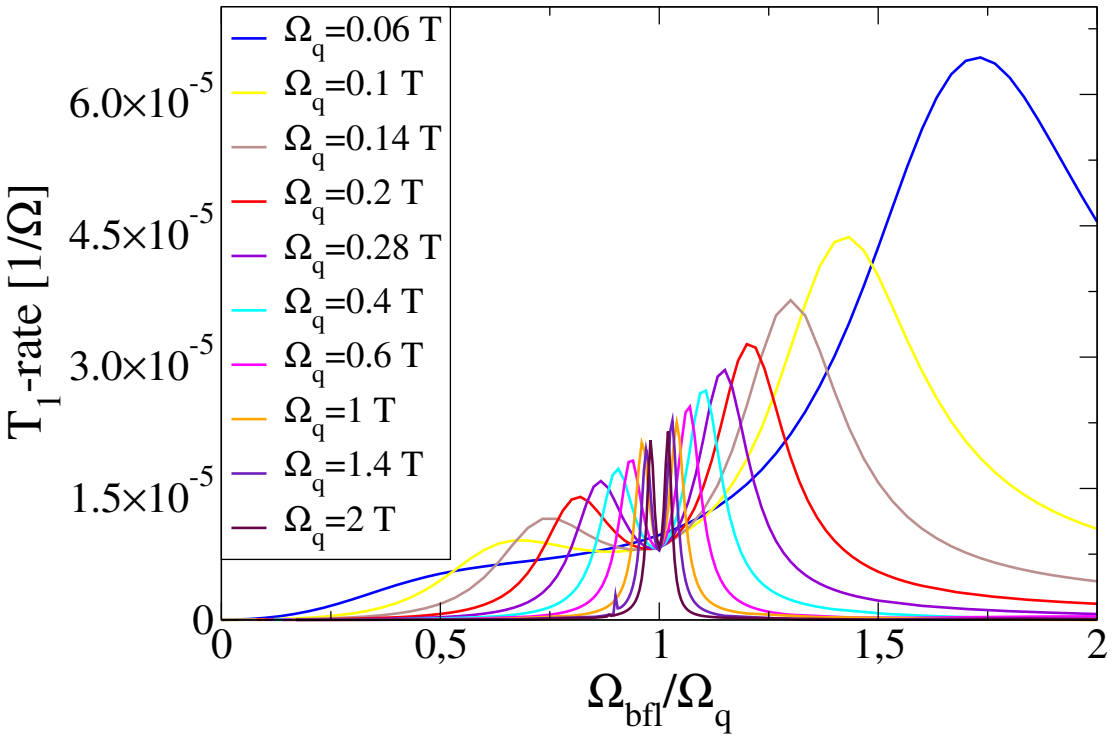

Figure 2.5: Plots of resonance spectra of the relaxation rate of a bfl-influenced qubit. The bfl-energy Ω_{bfl} is tuned from 0 to $2\Omega_q$, for each qubit energy Ω_q, which has values between $0.06T$ and $2T$ at an environmental temperature of $T = 0.5K$.

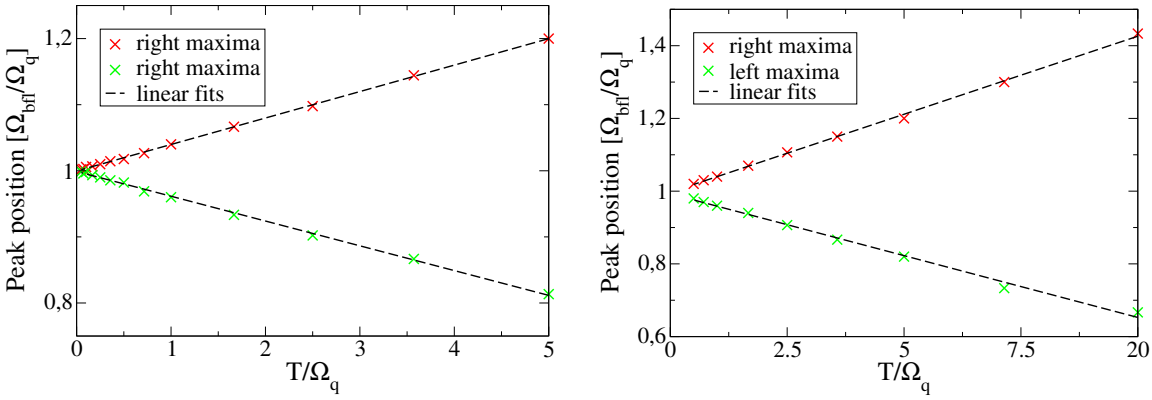

Figure 2.6: Positions of the left and right peaks of the resonance spectra versus their inverse qubit energies T/Ω_q at temperatures of $T = 0.05K$ (left plot) and $T = 0.5K$ (right plot) respectively. Linear fits shows an increase of the peak distances proportional to T/Ω_q.

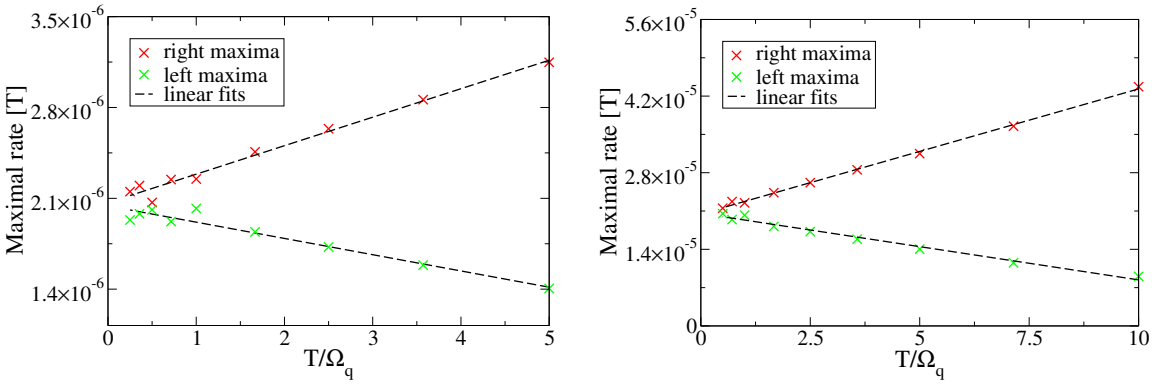

Figure 2.7: Heights of the left and right peaks of the resonance spectra versus their inverse qubit energies T/Ω_q at temperatures of $T = 0.05K$ (left plot) and $T = 0.5K$ (right plot) respectively. Linear fits shows an increase of the right peaks values, respectively a decrease of the left ones, proportional to T/Ω_q.

2.2.5 $1/f$ noise

We assume, that in a realistic physical setup, the energies of the bfl's are homogenously distributed, and that their dissipative influence on our "probe" qubit were statistically independent. This corresponds to the attributes of a $1/f$-generating ensemble of bistable fluctuators [51]. Thus we calculate the total dissipative influence on our qubit by integrating the bfl induced relaxation rates for a given qubit energy Ω_q and bath temperature T over all bfl energies, *i.e.*

$$\Gamma_q^{\text{total}} = \int_0^{\infty} d\Omega_{\text{bfl}} \Gamma_q(\Omega_{\text{bfl}}) \simeq \int_0^{10\Omega_q} d\Omega_{\text{bfl}} \Gamma_q(\Omega_{\text{bfl}}) \ . \tag{2.15}$$

For practical reasons we restrict the upper limit of our numerical integration on the reasonable value of $10\Omega_q$.

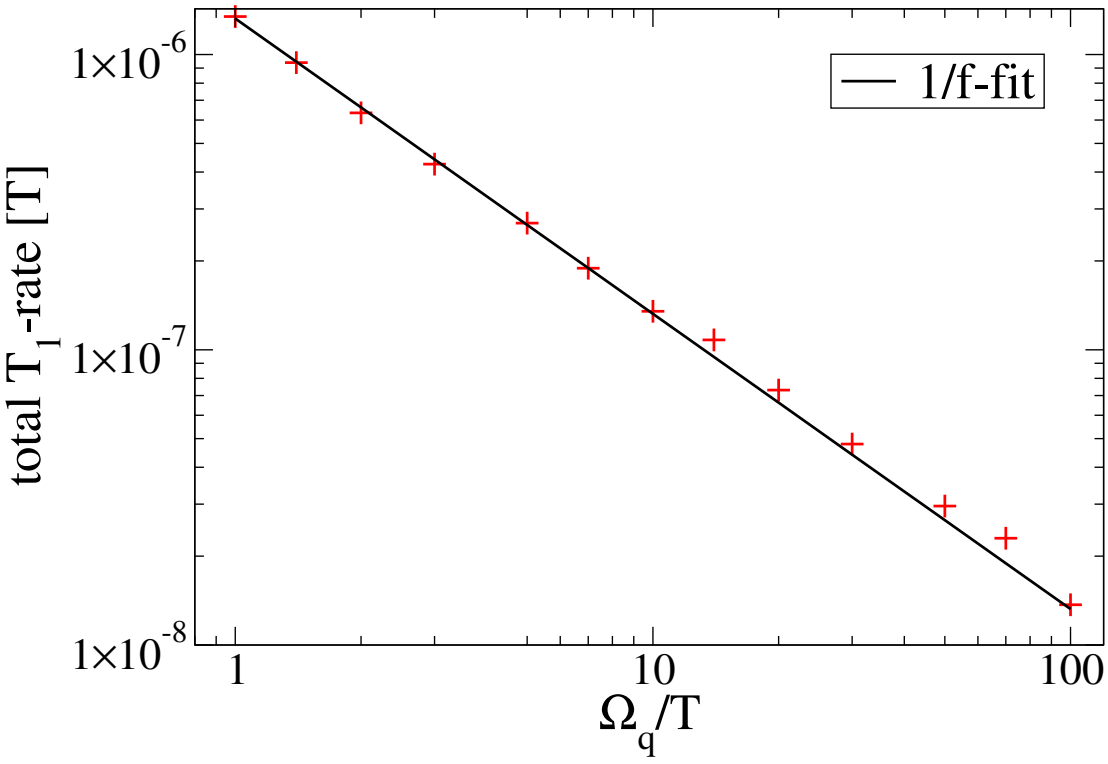

Figure 2.8: $1/f$-dependence of the total relaxation rate evaluated numerically by means of formula (2.15) at environmental temperature $T = 0.05K$.

As one can see from Fig.2.8 we receive in good accuracy an $1/f$ type behaviour of the total relaxation rate in dependence of the qubit energy Ω_q, as expected in [51]. If we consider the higher temperature regime $T = 0.5K$ (see Fig. 2.9) we recognize an increase of the total decoherence stronger than $1/f$ in the low-qubit-energy/relative-high-temperature limit, with a crossover at about $\Omega_q \simeq 0.5T$.

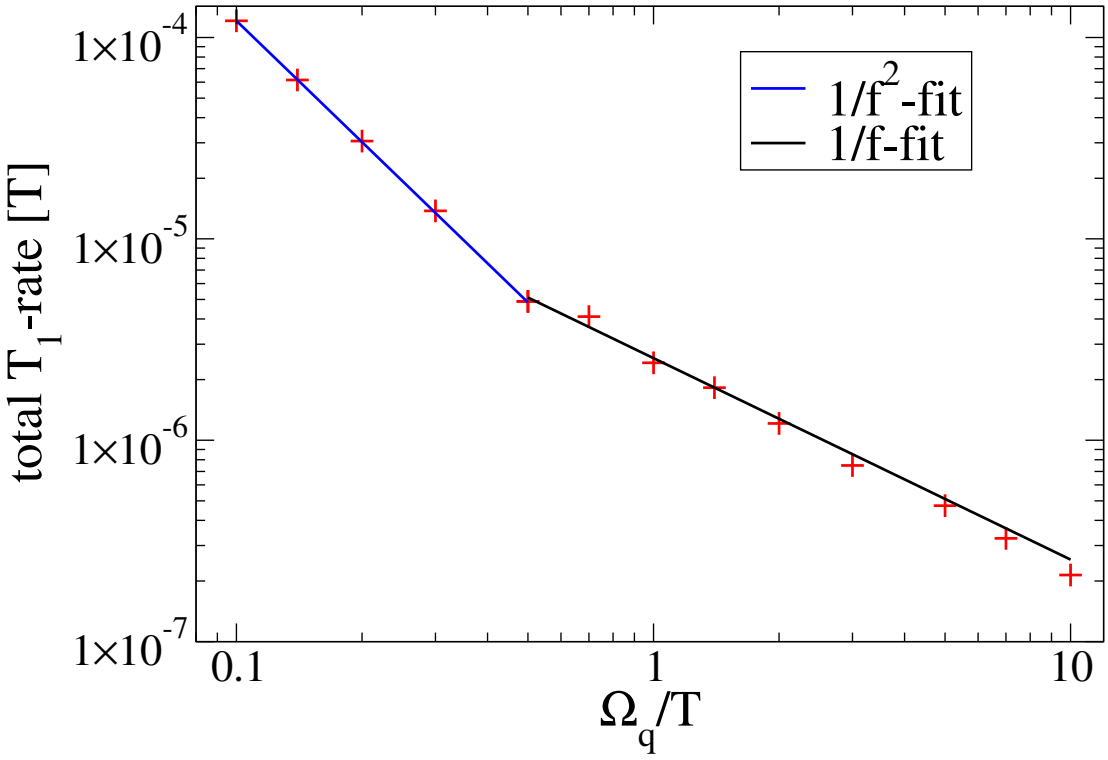

Figure 2.9: Total relaxation rates numerically evaluated according formula (2.15) at environmental temperature $T = 0.5K$. Besides the $1/f$-behaviour at higher Ω_q, one clearly recognizes a crossover to $1/f^2$-dependence in the low qubit energy regime (*i.e.* $\Omega_q \leq 0.5T$).

2.3 Stochastic Schrödinger equation and random walk model

In the first part we have presented a perturbative approach to describe the decoherence induced by a single fluctuator on a probe qubit. Therefore we have required weak coupling strength between the external degrees of freedom and the bfl, as well as thermal equilibrium for the environment. This leads to the Bloch-Redfield approximation and the corresponding results for different values and regimes of qubit frequency Ω_q compared to the external energy scale, the temperature T.

Now we will explicate an alternative way to describe and evaluate the decoherence induced by bistable fluctuators on a single qubit, which in particular permits also to investigate the strong coupling regime between environment and bfl (resulting in fastly flipping fluctuators). As an overall requirement the coupling between qubit and fluctuator should be weak (in order to treat the noise inducing two-level system as bfl, *i.e.* its states evolving independently of the qubit).

Our following examinations will be based on the concept of stochastical Schrödinger equations, as somewhat complementaric description to the typically used Fokker-Planck type kinetic equations [59, 60, 28]. The master equation as usual equation of motion for density matrices, as representants of a dissipative quantum system, will be replaced by a set of time-dependent Schrödinger equations

$$\frac{d}{dt}|\Psi(t)\rangle = -\frac{i}{\hbar}\hat{H}_\xi(t)|\Psi(t)\rangle \tag{2.16}$$

$$= -\frac{i}{\hbar}\left(\hat{H}_0 + \hat{H}_\xi^{\text{noisy}}(t)\right)|\Psi(t)\rangle \ , \tag{2.17}$$

each including and indexed by a random variable as noise term.

Starting from an arbitrary initial state $|\Psi(t_0)\rangle$, each single Schrödinger equations integration represents a possible evolution of the decohering system

$$|\Psi_\xi(t)\rangle = T_+ \exp\left(\int_{t_0}^{t} ds\hat{H}_\xi(s)\right)|\Psi(t_0)\rangle, \tag{2.18}$$

with T_+ the usual time-ordering operator (*i.e.* increasing time arguments from right to the left).

The typical determination of expectation values of any observable $\hat{O}$ of the dissipative system

$$\langle\hat{O}(t)\rangle = \text{tr}\{\hat{O}\rho(t)\} \tag{2.19}$$

will be replaced by a statistical mean of each of its $|\Psi_\xi\rangle$ expectation values

$$\langle \hat{O}(t) \rangle \;=\; \frac{1}{\#} \sum_\xi \langle \hat{O}(t) \rangle_\xi \;=\; \frac{1}{\#} \sum_\xi \langle \Psi_\xi(t) | \hat{O} | \Psi_\xi(t) \rangle, \tag{2.20}$$

where # denotes the number of members of the statistical ensemble of random variables. Of course, to represent a real dissipative evolution, the number of random variables has to tend to infinity, which is evidently not feasible in practical calculations. But as long as the time regime of the considered dissipative evolution is limited, sufficient numbers of representative trajectories can easily be reached; this is the case for our situation if choosing ensemble sizes of # between 10^3 and 10^6 (depending on the length of the evolution time).

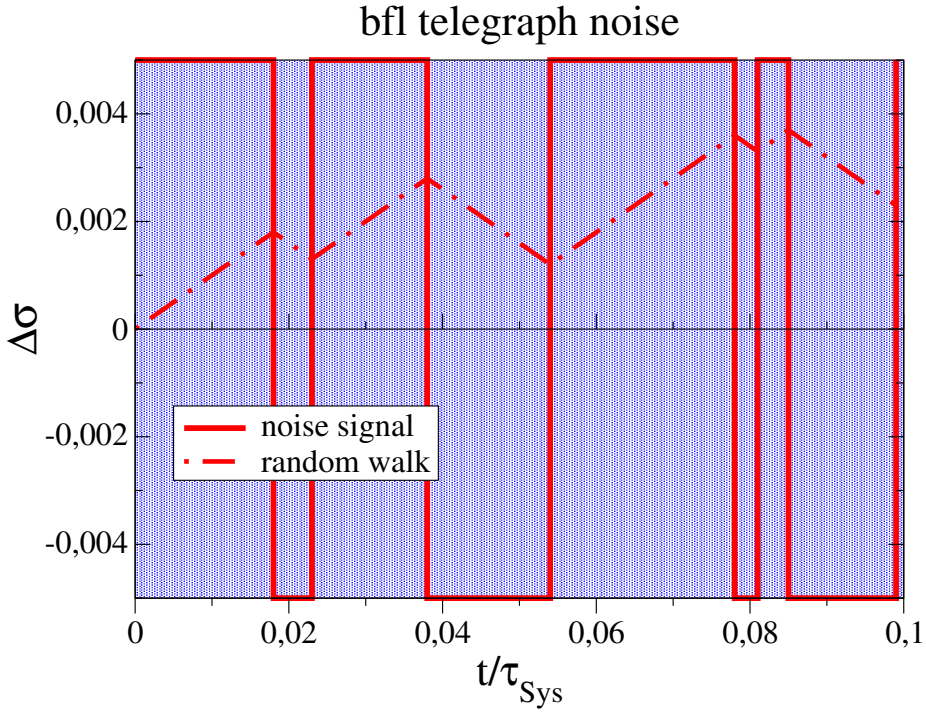

Figure 2.10: Schematic plot of a typical Poissonian bfl noise signal and its resulting random walk behaviour (in the limit of small deviations). The bfl parameters are chosen here as $\alpha = 0.1\Omega_q$ and $\tau_{\mathrm{bfl}} = 0.01\tau_{\mathrm{Sys}}$, with $\tau_{\mathrm{Sys}} = \pi/\Omega_q$ the free evolution period of the qubit.

2.3.1 Stochastic Hamiltonian

The reduced system Hamiltonian in our stochastic description will be analogous to the microscopic model Hamiltonian (see 2.2,2.5)

$$\hat{H}_q^{\mathrm{stoch}}(t) \;=\; \hat{H}_{\mathrm{q}} + \hat{H}_{\mathrm{noise}}(t) \tag{2.21}$$

with usual free qubit term

$$\hat{H}_{\mathrm{q}} \;=\; \hbar\,(\epsilon_{\mathrm{q}}\hat{\sigma}_{\mathrm{z}}^{\mathrm{q}} + \Delta_{\mathrm{q}}\hat{\sigma}_{\mathrm{x}}^{\mathrm{q}}) \tag{2.22}$$

and a random variable term, describing the influence of the telegrapf noise

$$H_{\mathrm{noise}}(t) \;=\; \hbar\alpha\;\hat{\sigma}_{\mathrm{z}}^{\mathrm{q}}\;\xi_{\mathrm{bfl}}(t). \tag{2.23}$$

The random variable $\xi_{\mathrm{bfl}}(t)$ might be interpreted as presenting as function of time the actual randomly switching state of the bfl in its $\hat{\sigma}_z$ basis. A typical example would be the noise signal with Poissonian distributed sxitching events (depicted in Fig.2.10).

For technical convenience we first model that semi-classical noise signal as a symmetrical Poissonian telegraph noise, which is only parametrized by the typical time scale τ_{bfl} between two successive bfl flips. This symmetrized ansatz corresponds to a relative high temperature limit of the bfl (which does not necessarily means high temperature for the qubit energy scale), which we will later generalize to a non-symmetrical telegraph noise for finite temperatures following the detailed balance condition.

As suitably designed picture of one qubit states we change in the so-called Bloch sphere representation, where each state $|\Psi(t)\rangle$ of a qubit is identified with a corresponding point $\vec{\sigma}(t)$ on the Bloch sphere; thus the integration solution of any arbitrary state can be calculated analogous to eq. (2.18)

$$\vec{\sigma}(t) \;=\; T_+ \exp\left(-i/\hbar \int_{t_0}^{t} H_{\mathrm{q}}^{\mathrm{eff}}(s)\,ds\right)\vec{\sigma}(t_0). \tag{2.24}$$

An exemplaric solution would look as plotted in Fig.2.11.

Here one can clearly recognize a random walk type behaviour of the qubit trajectory. This is valid, as long as the qubit fluctuator coupling is sufficient weak to persist the picture of "small deviations" from the free qubit evolution. The size of the corresponding deviation apparently scales with the noisy coupling strength as well as with the typical bfl flipping time scale τ_{bfl} (at least as long as one can treat the area of one-step deviations as almost flat, which we will furthermore call "Euclidean regime"). Such that as a first rule of thumb we estimate for the mean abberration of N bfl flip random walk steps

$$\Delta\sigma_{\mathrm{bfl}}(N) \;\sim\; \alpha\tau_{\mathrm{bfl}}\sqrt{N} \tag{2.25}$$

satisfying the typical random walk deviation behaviour, increasing with the square-root of step numbers. In this Euclidean regime we will now calculate the exact prefactor of that deviations by appropriate random walk models.

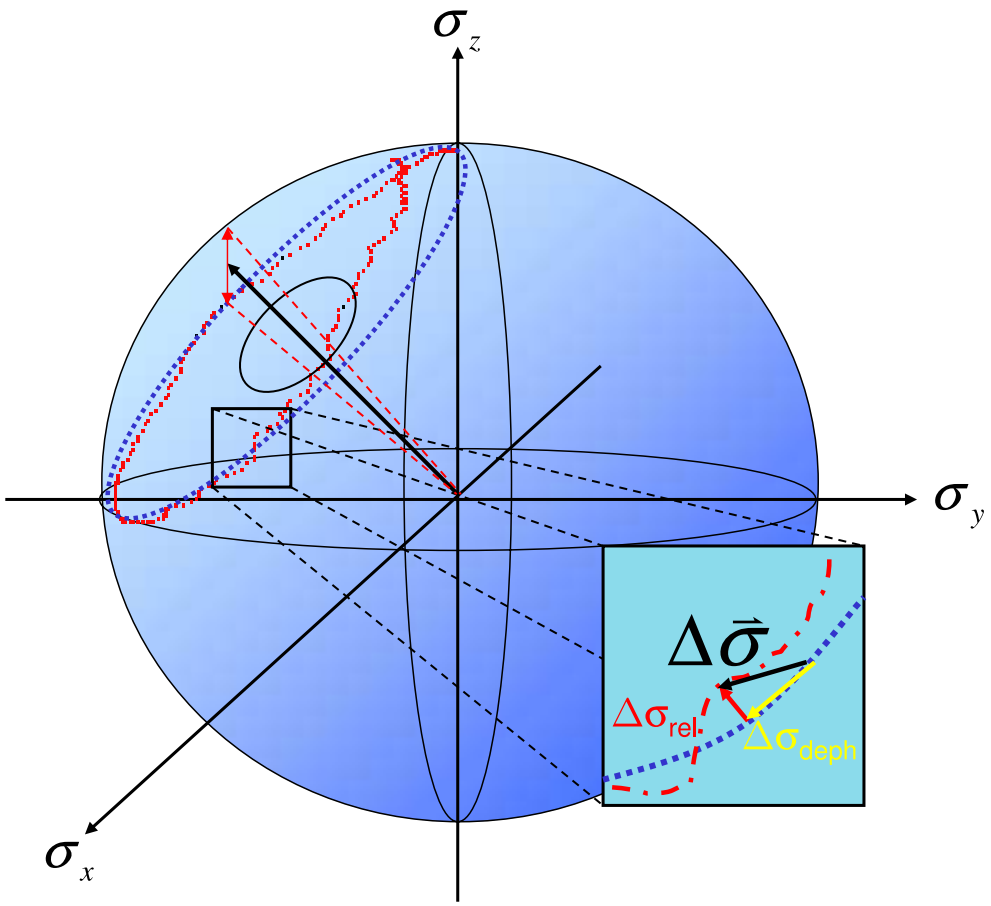

Figure 2.11: Schematic plot of a noisy qubit evolution generated by Poissonian telegraph noise. The resulting random walk (dot-dashed line) on the Bloch sphere is comprised both of deviations $\Delta\sigma_{\mathrm{deph}}$ in parallel to the free precession trajectory (dotted line), which correspond to dephasing, and deviations $\Delta\sigma_{\mathrm{rel}}$ perpendicular to it, corresponding to relaxation/excitation effects.

2.3.2 Random walk model

We now develop an analytical random walk model for our system. The random walk on the Bloch sphere is in general two-dimensional, containing parallel and perpendicular deviations to the free evolution trajectory (see Fig.2.11). In the following we restrict our analysis to the intermediate-time regime, *i.e.* long enough to encounter sufficient many random walk steps, but the qubit not yet totally decohered. Considering the later derived rule of thumb (2.72), this corresponds to the regime $t \geq 10^2 \tau_{\mathrm{bfl}}$ and $t \ll \frac{1}{\alpha^2 \tau_{\mathrm{bfl}}}$.

In order to evaluate the impact of that random walk accurately, we have to understand both, the distributions of one-step deviations, as well as their average size of each step, qualitatively and quantitatively. We first start with the calculation of the one-step mean

deviation, which consists of the mentioned parallel part (inducing dephasing) and the perpendicular one (responsible for energy relaxation/excitation of the qubit).

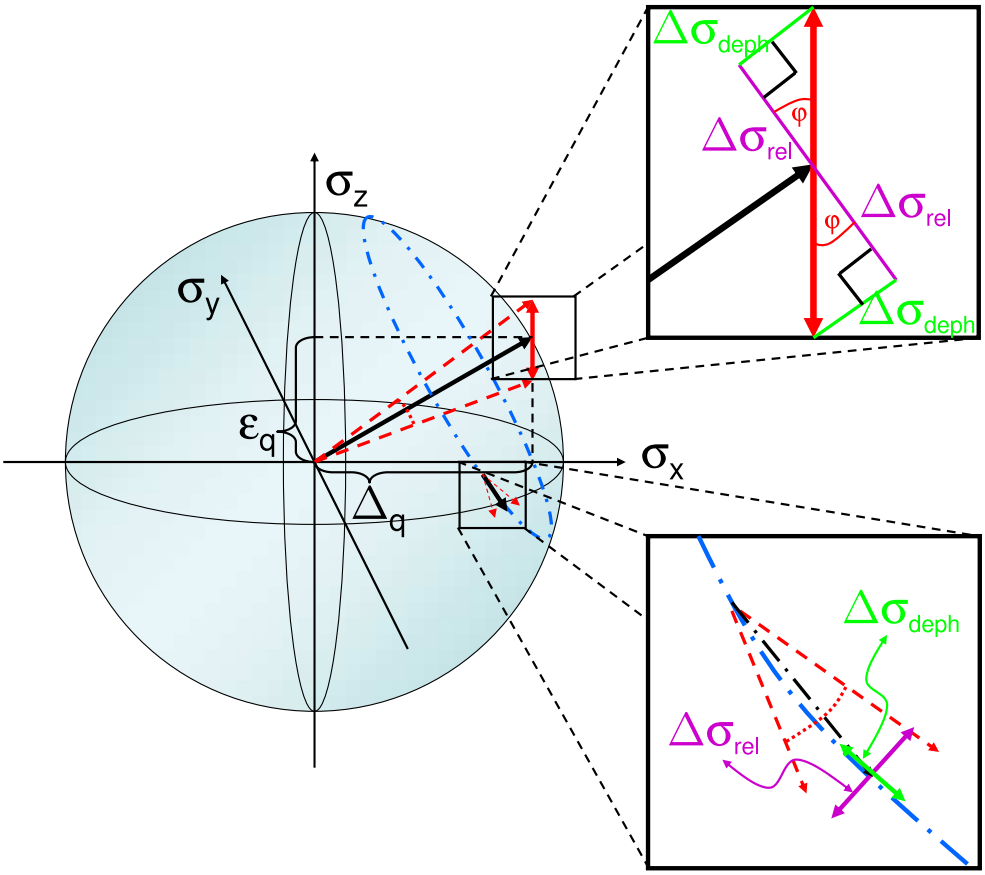

Figure 2.12: Plot of a typical one-step deviation from the unperturbed qubit trajectory with generic values for ϵ_q and Δ_q. The fractions of the bfl fluctuations in $\hat{\sigma}_z$-direction have to be distinguished with respect to their effect on the qubit: those that yield dephasing deviations (*i.e.* parallel to the free precession trajectory) that are proportional to $\sin\phi$ versus relaxation/excitation deviations (perpendicular), which are proportional to $\cos\Phi \sin\eta$. Both parts are additionally domineered by a factor of $\cos\phi$ due the diminished radius of the trajectory starting from the initial state $\sigma_z = +1$. The impact of the relaxation/excitation generating part is furthermore depending on $\sin\chi$, the azimuth angle of the qubits present position.

The dephasing part of the random walk is induced by differences of the bfl influenced precession periods $\tau_{\rm per}^{\pm}$ to the free evolution duration $\tau_{\rm per} = \pi/\Omega_q$. This leads to the parallel one-step abberration

$$\Delta\vec{\sigma}_{\rm deph}^{\rm bfl} \;=\; 2\pi\cos\Phi\left(\frac{1}{\tau_{\rm per}^{\pm}} - \frac{1}{\tau_{\rm per}}\right) \;=\; \pm 2\frac{\Delta_q\epsilon_q}{\Delta_q^2+\epsilon_q^2}\alpha\tau_{\rm bfl} \tag{2.26}$$

where the prefactor $\cos\Phi = \frac{\Delta_q}{\sqrt{\Delta_q^2+\epsilon_q^2}}$ takes the effective trajectory radius into account.

For the relaxation/excitation effect of the noise, one has to use the projection of the perturbation, which is orthogonal to the free axis (see Fig. 2.12); this leads to a factor $\sin\eta = \frac{\alpha\Delta_q}{\Delta_q^2+\epsilon_q^2}$. Furthermore this type of deviation also depends on the actual position of the spin on the Bloch sphere, *e.g.* there is no relaxation when the state is at one of the poles. Averaged in root-mean-square (rms) fashion over a full azimuthal cycle this leads hereby to a mean factor $1/\sqrt{2}$. Moreover, the impact of relaxation/excitation is scaled down by an additional factor of $\cos\Phi = \frac{\Delta_q}{\sqrt{\Delta_q^2+\epsilon_q^2}}$, this time corresponding to the projection of the Bloch vector onto the precession axis, accordingly decreasing the deviation angle. In total, using $\tau_{\rm per}^{\pm} \simeq \tau_{\rm per}$ in first order of α, we receive

$$\Delta\vec{\sigma}_{\rm rel}^{\rm bfl} \;=\; 2\pi\cos\Phi\sin\eta\frac{1}{\sqrt{2}}\cos\Phi\frac{\tau_{\rm bfl}}{\tau_{\rm per}^{\pm}} \simeq \sqrt{2}\frac{\Delta_q^3}{(\Delta_q^2+\epsilon_q^2)^{3/2}}\alpha\tau_{\rm bfl} \tag{2.27}$$

As the influences of dephasing and relaxation/excitation influences each other during several precession periods, we do not handle them separately, but adds them up to

$$\begin{aligned}\Delta\vec{\sigma}_{\rm total}^{\rm bfl} \;&=\; \sqrt{\Delta\vec{\sigma}_{\rm deph}^{\rm bfl\,2} + \Delta\vec{\sigma}_{\rm rel}^{\rm bfl\,2}} \;=\; \sqrt{4\frac{\Delta_q^2\epsilon_q^2}{(\Delta_q^2+\epsilon_q^2)^2} + 2\frac{\Delta_q^6}{(\Delta_q^2+\epsilon_q^2)^3}}\alpha\tau_{\rm bfl} \\ &=\; \frac{1}{(\Delta_q^2+\epsilon_q^2)^{3/2}}\sqrt{4(\Delta_q^2+\epsilon_q^2)\Delta_q^2\epsilon_q^2 + 2\Delta_q^6}\alpha\tau_{\rm bfl}.\end{aligned} \tag{2.28}$$

Although our rms-treatment does not distinguish the different types of decoherence, which there are dephasing and relaxation/excitation, corresponding to phase and bit-flip errors respectively, this is no crucial drawback, as this merely lies in the nature of our generic situation (where both kind of errors influence each other). In principle, one is feasible to estimate both sorts of dissipation individually.

By using standart random walk techniques we will now focus on the evolution of the bfl random walk in the intermediate time regime. For this we replace the somewhat fluctuating number of random walk steps for a given time Δt of noisy evolution by its expectation value $N_{\rm bfl} = \Delta t/\tau_{\rm bfl}$. This allows to use the number of random walk steps as time parameter. This simplification does not introduce significant errors, as the relative number variation for

ΔT scales as $\frac{\sqrt{\Delta t/\tau_{\rm bfl}}}{\Delta t/\tau_{\rm bfl}} = \Delta t/\tau_{\rm bfl} \to 0$ in our preferred intermediate-time limit. We encounter two different one-step-distributions, depending on whether the numeration of the step is an odd or even (corresponding to an up or down state of the bfl). For definiteness, we assume the bfl is initially in its up state, which is of no influence on the long time limit as the memory to the initial state is already erased. The step-size distribution of the bfl model in our small deviation regime is given from Poisson statistics

$$\Phi^{\rm bfl}_{\rm odd/even}(x) = \frac{e^{\mp x/\gamma}\theta(\pm x)}{\gamma} \tag{2.29}$$

with $\gamma = \frac{\sqrt{5}}{2}\alpha\tau_{\rm bfl}$ the typical one-step deviation as calculated in eq. (2.28). $\theta(x)$ denotes the Heaviside step function. We neglect correlations between transverse and perpendicular deviations as we expect them to average out in the long-time limit.

Using these one-step probability distributions, we are able to calculate by means of the convolution theorem the distributions for $2N_{\rm bfl}$-step random walks. Specifically, they are the inverse Fourier transforms of the $N_{\rm bfl}$-fold products of the Fourier transforms of the two-step distribution [61]. We receive (for details see Appendix C).

$$\begin{aligned}\Phi^{\rm bfl}_{\rm 2N_{bfl}}(x) &= \mathscr{F}^{-1}\left[\left(\mathscr{F}\left[\Phi^{\rm bfl}_2\right]\right)^{N_{\rm bfl}}\right] \\ &= \int_{-\pi}^{\pi}\frac{dk}{2\pi\gamma^{2N_{\rm bfl}}}e^{-ikx}\left(\frac{1}{1-2\cos(k)e^{-1/\gamma}+e^{-2/\gamma}}\right)^{N_{\rm bfl}}\end{aligned} \tag{2.30}$$

with $\mathscr{F}$ and $\mathscr{F}^{-1}$ denoting the discrete Fourier transformation and its inverse, respectively.

Detailed numerical analysis shows already for random walk step-numbers on the order of 10, that the resulting distributions are almost Gaussian. Their standard deviations can be derived analytically by use of standard random walks techniques from the $2N_{\rm bfl}$-step distributions in the k-space (see Appendix C.1.1). We find for their variances in real space representation

$$\Delta\sigma_{\rm bfl}(N_{\rm bfl}) = \sqrt{N_{\rm bfl}}\gamma = \sqrt{N_{\rm bfl}}\frac{\sqrt{5}}{2}\alpha\tau_{\rm bfl}. \tag{2.31}$$

$$\tag{2.32}$$

2.3.3 Symmetrical noise

We now want to compare numerical integrations of the stochastical Schrödinger equation (2.24) with the corresponding analytical random walk results (2.31). Therefor we choose the usual values for the qubit parameters, $\epsilon_q = \Delta_q = 1/\sqrt{2}10^{10}$ Hz, *i.e.* $\Omega_q = 10^{10}$ Hz $\simeq 0.07K$. The bfl noise is specified by its qubit-bfl coupling strength (here $\alpha = 0.1\Omega_q$) and the (symmetrical) average flipping time $\tau_{\mathrm{bfl}} = 0.01\tau_{\mathrm{Sys}}$. Hereby we choose $\tau_{\mathrm{Sys}} = \pi/\Omega_q$ the qubit free evolution period as natural time unit. A microscopic derivation of the flipping times, in particular a generalization to asymmetric noise, will be provided in a following paragraph.

Using these parameters we can numerically integrate the noisy evolution up to times of $1000\tau_{\mathrm{Sys}}$ and $\# = 10^3$ realizations. Simulations using larger sets of realizations have shown, that convergence of the statistically averaged results is already sufficiently advanced at this number of trajectories. As measure of the progressing qubit decoherence we calculate the rms deviations of this numerically received ensemble at given time points

$$\Delta\vec{\sigma}_{\mathrm{rms}}(t) = \sqrt{\frac{1}{N}\sum_{j=1}^{N}\left(\vec{\sigma}_j^{\mathrm{q}}(t) - \vec{\sigma}_{\mathrm{noisy},j}^{\mathrm{q}}(t)\right)^2}, \tag{2.33}$$

where $\vec{\sigma}_0^{\mathrm{q}}(t)$ denotes the free qubit evolution on the Bloch sphere, while $\vec{\sigma}_{\mathrm{noisy},j}^{\mathrm{q}}(t)$ describes the j^{th} noisy trajectory.

Using that definition, our numerical simulations generates the dissipative evolution of the qubit as shown as crosses in Fig.2.13. In the short time limit ($t \leq \tau_{\mathrm{Sys}}$) one clearly recognizes an approximately linear increase of the Bloch sphere deviation $\Delta\vec{\sigma}_{\mathrm{rms}}$. This is due to the few numbers of bfl flips, which have not led to a statistical average, typically for random walk behaviour. Lateron, when the random walk regime is reached, the total amplitude of the deviation grows as square-root of time, respectively number of steps. This crossover happens approximatively at $t \simeq \tau_{\mathrm{Sys}}$, where the slope of the abberration changes to the expected $t^{1/2}$ type. The numerically derived evolution apparently coincide perfectly with our analytical results (given as triangles in Fig. 2.13). We do not consider times longer than $t = 1000\tau_{\mathrm{Sys}}$, as here for the chosen parameters total decoherence of the qubit is reached (as $\Delta\vec{\sigma}_{\mathrm{rms}}$ is in the order of the Bloch sphere radius $r_{\mathrm{BS}} = 1$). A detailed examination of transverse and perpendicular deviations does not show significant differences.

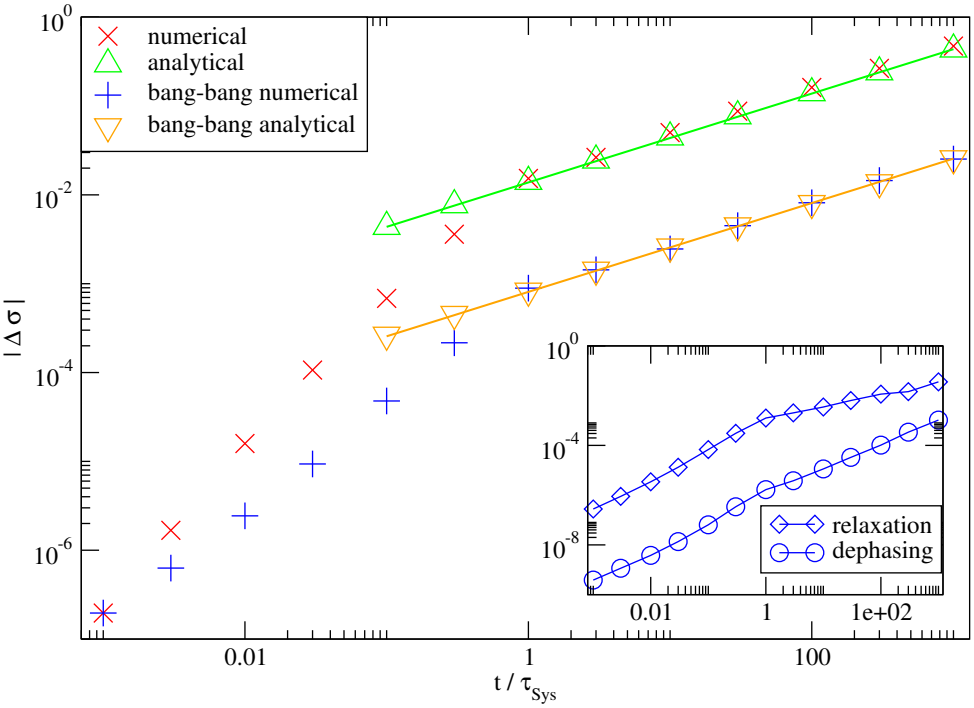

Figure 2.13: Temporal evolution of the rms deviations for bfl-induced random walks. As coupling constant is chosen $\alpha = 0.1$ and the bfl flipping time scale $\tau_{\text{bfl}} = 10^{-2}\tau_{\text{Sys}}$. The straight lines are square-root fits of the analytical derived random walk model variances (plotted as triangles).

2.3.4 Bfl-noise at finite temperatures

For simulating bfl-noise on the qubit by use of its stochastic Schrödinger equation and analyzing it by appropriate random walk models we have so far chosen simplified conditions (symmetrical telegraph noise, no temperature dependence). Usually the situation of equal flipping times for the "up" and the "down" state of the bfl would correspond to a high temperature regime of the bfl (not necessarily also for the qubit, as their energy scales might differ), which evidently is not always the case. Thus it is crucial to investigate, how an asymmetrical bfl-noise signal, following the detailed balance conditions, affects the qubit.

Therefore we adapt the well-known formula of spontaneous and induced relaxation as well as induced excitation, in order to derive an expression for the average bfl up and down flipping times $\tau_{\text{bfl}}^{\uparrow,\downarrow}$ [62]. By using the terms of the microscopic bfl-description (2.3), with

an ohmic heath bath (1.68) at temperature T, we receive for the flipping rates

$$(\tau_{\rm bfl}^{\uparrow})^{-1} = \frac{\Delta_{\rm bfl}^2}{\Omega_{\rm bfl}^2} J(\Omega_{\rm bfl})(1+n_\beta(\Omega_{\rm bfl})) \tag{2.34}$$

$$(\tau_{\rm bfl}^{\downarrow})^{-1} = \frac{\Delta_{\rm bfl}^2}{\Omega_{\rm bfl}^2} J(\Omega_{\rm bfl}) n_\beta(\Omega_{\rm bfl}), \tag{2.35}$$

with $\beta = 1/k_B T$ the inverse temperature, and

$$n_\beta(\omega) = \frac{1}{e^{\omega\beta}-1} \tag{2.36}$$

the Bose distribution, defining emission/absorption probabilities from the Bosonic bath. One clearly recognizes, that in the case of finite temperatures the rate $(\tau_{\rm bfl}^{\uparrow})^{-1}$ of down-flipping the bfl from its "up"-state to its "down"-state is in general larger than the up-flipping rate $(\tau_{\rm bfl}^{\downarrow})^{-1}$.

After some algebra and omitting the Drude-cutoff in the ohmic bath spectra $J(\omega)$ (which is no crucial as long as $\Omega_{\rm bfl} \ll \Omega_c$) we receive

$$\tau_{\rm bfl}^{\uparrow,\downarrow} = 2e^{\mp\Omega_{\rm bfl}\beta/2}\sinh(\Omega_{\rm bfl}\beta/2)\frac{\Omega_{\rm bfl}}{\lambda{\Delta_{\rm bfl}}^2} \tag{2.37}$$

which evidently fulfills the detailed balance condition [31]

$$\frac{\tau_{\rm bfl}^{\uparrow}}{\tau_{\rm bfl}^{\downarrow}} = e^{-\Omega_{\rm bfl}\beta} \ . \tag{2.38}$$

For different values of flipping rates $(\tau_{\rm bfl}^{\uparrow,\downarrow})^{-1}$ from "up" to "down" and vice versa we can analogously estimate a rule of thumb for the one-, as well as for the double-flip impact. As one can recognize from Fig. 2.14 we receive a collective drift effect on the qubit of the order

$$\epsilon_q \mapsto \epsilon_q^{\rm eff} = \epsilon_q + \alpha\frac{\tau_{\rm bfl}^{\uparrow} - \tau_{\rm bfl}^{\downarrow}}{\tau_{\rm bfl}^{\uparrow} + \tau_{\rm bfl}^{\downarrow}} \tag{2.39}$$

due to the relative longer residence of the bfl in its lower state.

According the fluctuations of the asymmetric Random walk one has to estimate the size of the upper and lower rectangles in Fig. 2.14 in regard of the effective drift line. This is the symmetry line, at which the rectangular areas coincide. Some basic geometric consideration leads to

$$\Delta\sigma_{\rm bfl,asymm}(N) \sim \alpha\left(2\frac{\tau_{\rm bfl}^{\uparrow}\tau_{\rm bfl}^{\downarrow}}{\tau_{\rm bfl}^{\uparrow} + \tau_{\rm bfl}^{\downarrow}}\right)\sqrt{N} \tag{2.40}$$

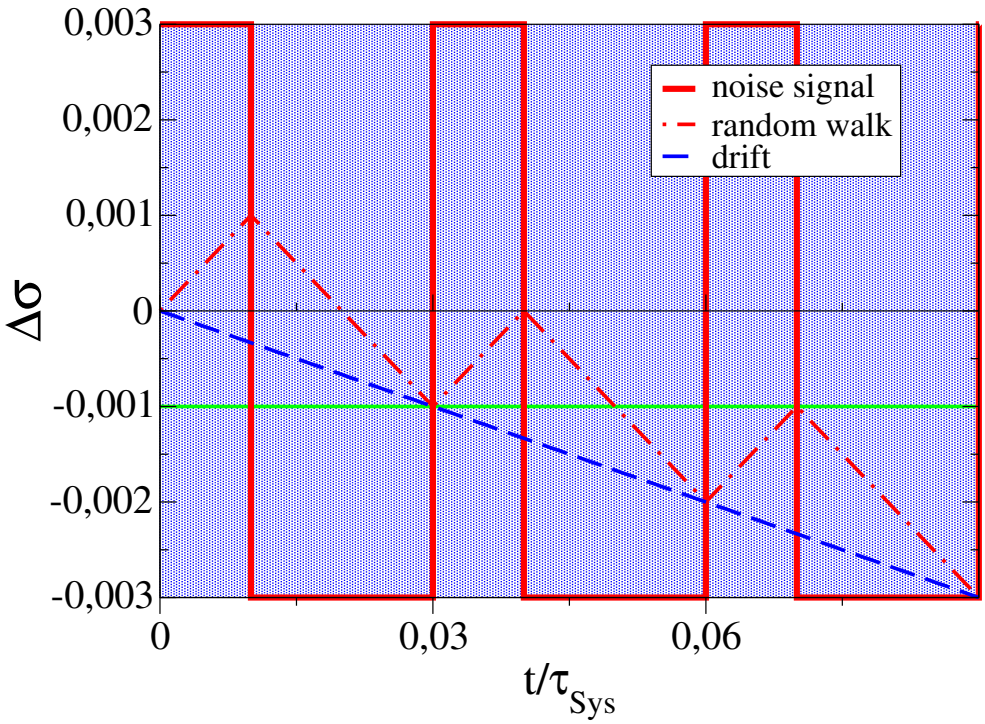

Figure 2.14: Simplified plot of a Poissonian bfl-noise signal with different flipping times set to $\tau_{\rm bfl}^{\uparrow} = 10^{-2}\tau_{\rm Sys}$ and $\tau_{\rm bfl}^{\downarrow} = 210^{-2}\tau_{\rm Sys}$ (corresponding to a temperature-energy relation of $\Omega_{\rm bfl}\beta = \ln(2) \simeq 0.693$). The green base line indicates the part of the bfl flips, which takes part in an effective drift of the qubit (it is chosen to equalize the rectangle areas of the bfl noise signal up- and downwards, corresponding to the impact of fluctuations). The flips are ideally positioned on their expectation times in order to emphasize the connection to their drift and fluctuation effects.

with N here describing the number of double-flips/steps.

By introducing an effective flipping time scale of the bfl

$$\tau_{\rm bfl}^{\rm eff} \equiv 2\frac{\tau_{\rm bfl}^{\uparrow}\tau_{\rm bfl}^{\downarrow}}{\tau_{\rm bfl}^{\uparrow} + \tau_{\rm bfl}^{\downarrow}} \tag{2.41}$$

one receives by usual analytical derivation for the corresponding random walk deviation (see appendix C) an analogous prefactor $\gamma_{\rm eff}$ (compare with eq. 2.31)

$$\Delta\sigma_{\rm bfl}^{\rm asymm}(N_{\rm eff}) = \sqrt{N_{\rm eff}}\gamma_{\rm eff} = \sqrt{N_{\rm eff}}\frac{\sqrt{5}}{2}\alpha\tau_{\rm bfl}^{\rm eff}, \tag{2.42}$$

$N_{\rm eff}$ denoting the effective number of steps, i.e. the number of double-flips.

With defining an average flipping time $\tau_{\rm bfl}^{mean} = \frac{(\tau_{\rm bfl}^{\uparrow}+\tau_{\rm bfl}^{\downarrow})}{2}$ we receive for the asymmtetric random walk deviation as function of time

$$\begin{aligned}\Delta\sigma_{\rm bfl}^{\rm asymm}(t) &= \sqrt{\frac{t}{\tau_{\rm bfl}^{mean}}}\gamma_{\rm eff} = \sqrt{\frac{10t}{(\tau_{\rm bfl}^{\uparrow}+\tau_{\rm bfl}^{\downarrow})^3}}\alpha\tau_{\rm bfl}^{\uparrow}\tau_{\rm bfl}^{\downarrow} \\ &= \sqrt{10t}\frac{4\sinh^2(\Omega_{\rm bfl}\beta/2)\frac{\omega_{\rm bfl}^2}{\lambda^2\Delta_{\rm bfl}^4}}{\left[4\cosh(\Omega_{\rm bfl}\beta/2)\sinh(\Omega_{\rm bfl}\beta/2)\frac{\Omega_{\rm bfl}}{\lambda\Delta_{\rm bfl}^2}\right]^{3/2}}\alpha \\ &= \sqrt{5t}\frac{[\cosh(\Omega_{\rm bfl}\beta)-1]}{\sinh^{3/2}(\Omega_{\rm bfl}\beta)}\sqrt{\frac{\Omega_{\rm bfl}}{\lambda\Delta^2}}\alpha \end{aligned} \tag{2.43}$$

2.3.5 Criteria for an appropriate choice of bfl parameter

For the random walk dscription to be an appropriate model of temperature dependent bfl-noise as semi-classical noise source, we have to develop some criteria to be fulfilled by the choice of the noise parameters ($\Omega_{\rm bfl}, \alpha, \lambda, \beta$, respectively T).

1) Symmetry

In order to observe a crossover from asymmetric to symmetric bfl noise in the usual temperature regime of $T \leq 1K$, we require an upper bound of the bfl-energy of

$$e^{\Omega_{\rm bfl}\beta_{\rm max}} \simeq 1 \quad \Leftrightarrow \quad \Omega_{\rm bfl}\beta_{\rm max} \leq 0.1 \quad \Rightarrow \quad \Omega_{\rm bfl} \leq 10^{10}{\rm Hz}. \tag{2.44}$$

2) Random walk frequency

For receiving a random walk type diffusion, *i.e.* a sufficient number of steps/flips during one free evolution period of the qubit, we assume

$$\tau_{\rm bfl}^{\uparrow,\downarrow} \ll \tau_{\rm Sys}. \tag{2.45}$$

3) Weak decoherence

To avoid total decoherence of the qubit during the first few random walk steps, we have to restrict the average one-step deviation to

$$\Delta\vec{\sigma}_{1step} \;\leq\; 0.01. \tag{2.46}$$

From these criteria we can develop as follows appropriate values of the fore-mentioned parameters.

In order to minimize the bfl times (2.37), respectively (2.45), we choose the maximum value of $\Omega_{\rm bfl} = 10^{10}$ Hz. Still assuming a fixed ratio of $\Delta_{\rm bfl}/\Omega_{\rm bfl} = 0.1$ we therefor get for the bfl parameters $\Delta_{\rm bfl} = \epsilon_{\rm bfl} = 10^{10}/\sqrt{2}$ Hz. If we apply the expression 2.37 we obtain in the formerly investigated low temperatur regime ($T \simeq 0.01K$)

$$\tau_{\rm bfl}^{\downarrow} \;=\; \frac{10^{-8}}{\lambda n_{\rm min}} \;\simeq\; \frac{10^{-5}}{\lambda} \tag{2.47}$$

$$\tau_{\rm bfl}^{\uparrow} \;=\; \frac{10^{-8}}{\lambda(1+n_{\rm min})} \;\simeq\; \frac{10^{-8}}{\lambda} \tag{2.48}$$

with $n_{\rm min} = n_{\beta_{\rm min}}(\Omega_{\rm bfl}) \simeq e^{\Omega_{\rm bfl}\beta_{\rm min}} \simeq e^{-7} \simeq 10^{-3}$.

Furthermore, regarding (2.40), the single-step, respectively double-flip deviation can in the particular harmful regime ($T = 0.01k$) be estimated to

$$\Delta\vec{\sigma}_{1step} \;\simeq\; \alpha\left(2\frac{\tau_{\rm bfl}^{\uparrow}\tau_{\rm bfl}^{\downarrow}}{\tau_{\rm bfl}^{\uparrow}+\tau_{\rm bfl}^{\downarrow}}\right) \;\simeq 2\;\alpha\tau_{\rm bfl}^{\uparrow} \;\simeq\; 2\alpha\frac{10^{-8}}{\lambda} \tag{2.49}$$

as $\tau_{\rm bfl}^{\uparrow} + \tau_{\rm bfl}^{\downarrow} \simeq \tau_{\rm bfl}^{\downarrow}$ at this temperature. With $\alpha = 0.01\Omega_q = 10^8$ Hz and following eq. (2.46) we receive as lower bound on the bath-fluctuator coupling

$$\lambda \geq 10^{-6}\alpha = 10^2 \;, \tag{2.50}$$

such that our random walk analysis clearly considers the strong coupling limit between fluctuator and external bath. This is in contrast to our former perturbative approach, where we were restricted to small couplings $\lambda \ll 1$.

2.3.6 Numerical and analytical results for temperature dependent bfl noise

For the numerical simulations, respectively random walk analysis we consider a temperature range from $T_{\min} = 0.01K$ to $T_{\max} = 1K$, which corresponds to about $0.1\Omega_q$, respectively $10\Omega_q$, with $\Omega_q = \sqrt{2}10^{10}$Hz $\simeq 0.1\text{K}k_B$ the qubit energy scale for generical chosen parameters $\Delta_q = \epsilon_q = 10^{10}$ Hz. As typical system time scale we consider the free qubit evolution period $\tau_{\text{Sys}} = \pi/\Omega_q \simeq 2.22110^{-10}$s. For the bistable fluctuator we assume the following parameters $\Delta_{\text{bfl}} = \frac{1}{\sqrt{1.01}}10^9$ Hz, $\epsilon_{\text{bfl}} = 10\Delta_{\text{bfl}} = 1/\sqrt{1.011}10^{10}$ Hz (such that $\Omega_{\text{bfl}} = 10^{10}$ Hz), receiving a energy scale compareable with Ω_q. For receiving an appropriate frequently random walk behaviour we choose $\lambda = 10^2$ for lower, and $\lambda = 10^3$ for higher frequent bfl noise.

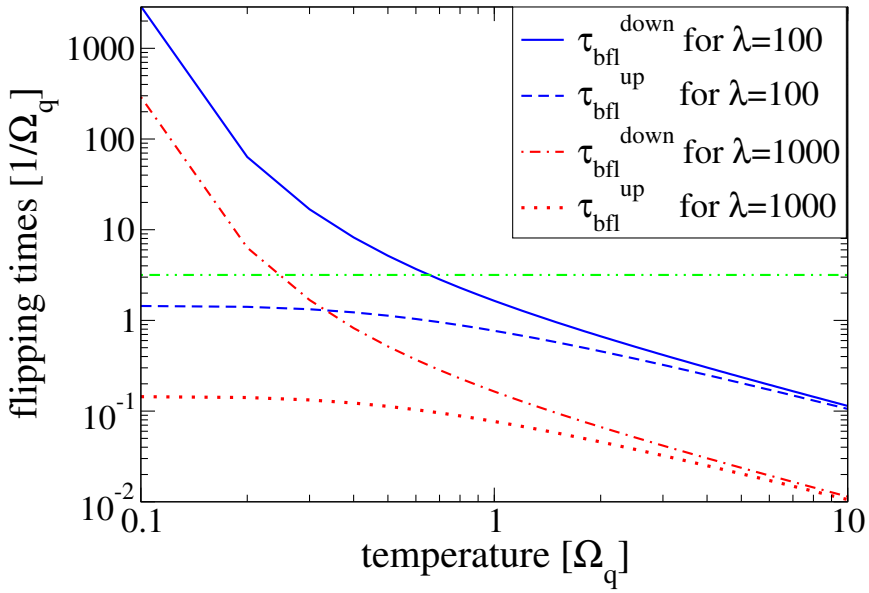

Figure 2.15: Plot of temperature dependent flipping times $\tau_{\text{bfl}}^{\downarrow,\uparrow}$ according eq.2.37 for "slower" (*i.e.* with $\lambda = 100$) and "faster" bfls ($\lambda = 1000$). The dash-double-dotted constant line describes the free evolution period of the influenced qubit and roughly gives an estimation, where the random walk approximation is expected to fail (at about $0.25\Omega_q$, respectively $0.7\Omega_q$).

At this selection of parameters we receive slower bfl flip times ($\lambda = 10^3$) regarding eq. (2.37) at the maximum temperature $T_{\max} = 1K$ of

$$\tau_{\text{bfl}}^{\uparrow}(T_{\max}) \simeq 7.391 \cdot 10^{-12}\text{s} \qquad \tau_{\text{bfl}}^{\downarrow}(T_{\max}) \simeq 8.017 \cdot 10^{-12}\text{s} \tag{2.51}$$

and in the lower temperature case ($T_{\min} = 0.01K$) of

$$\tau_{\text{bfl}}^{\uparrow}(T_{\min}) \simeq 1.010 \cdot 10^{-10}\text{s} \qquad \tau_{\text{bfl}}^{\downarrow}(T_{\min}) \simeq 2.096 \cdot 10^{-7}\text{s}. \tag{2.52}$$

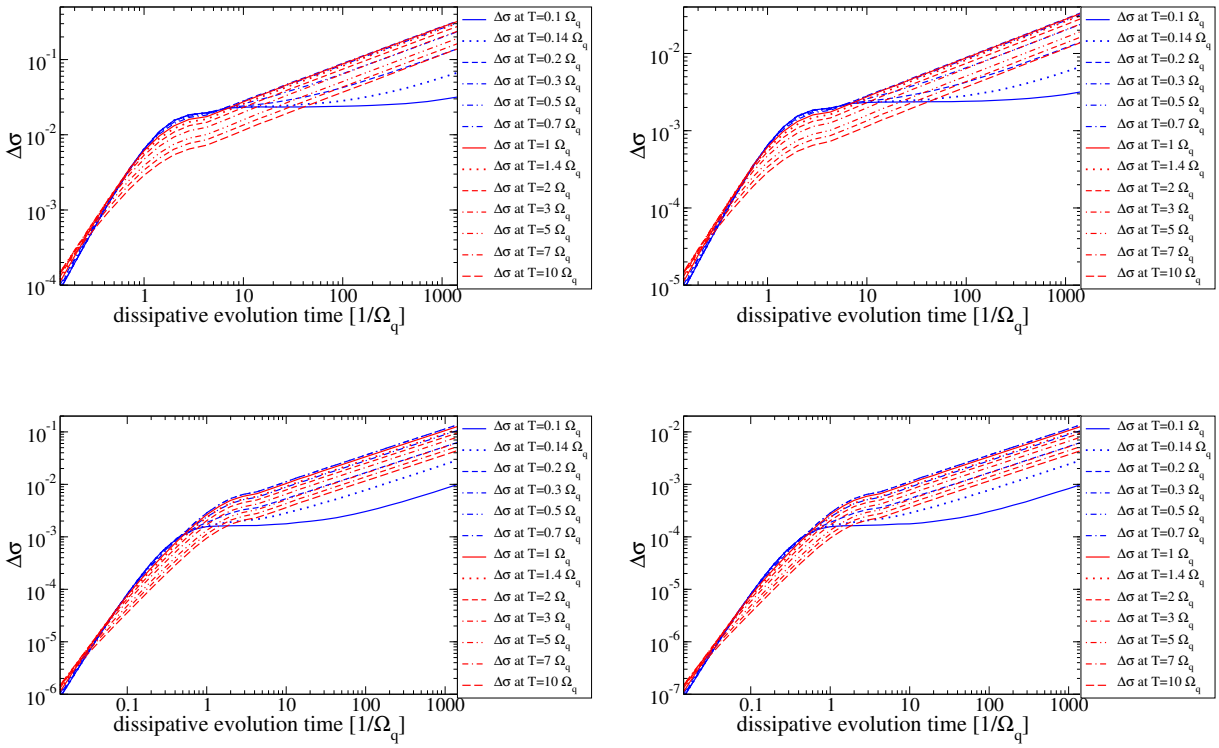

Figure 2.16: Time evolution of the rms deviations for temperature-dependent bfl-induced random walks, evaluated for temperatures between $T_{\min} = 0.1\Omega_q$ and $T_{\max} = 10\Omega_q$. The coupling constant to the qubit is chosen as $\alpha = 0.01$ for the left plots and $\alpha = 0.001$ for the right ones; the bfl flipping rates are given by eq. 2.37 with bfl parameters $\Delta_{\text{bfl}} = \epsilon_{\text{bfl}} = 10^{10}$ Hz, and $\lambda = 10^2$ for the figures above, $\lambda 10^3$ for the lower ones.

The times were ten times smaller times for the faster bfl case ($\lambda = 10^3$). Compared with the free qubit evolution period (Fig. 2.15) we expect a reasonably random walk type behaviour in our examined medium to high temperature regime (between 0.5 and 10 Ω_q). Evidently in the high temperature regime, the random walk symmetry 2.44 and frequency condition 2.45 were accurately fulfilled. As one can see from the numerical results in Fig. 2.16, proper random walk behaviour for the low temperature case emerges much later (on the scale of several bfl exciting flip times $\tau^{\downarrow}_{\text{bfl}}(T_{\min})$) as theoretically expected. Hereby we numerically evaluate the time evolution for noisy evolution times t between 10^{-12} and 10^{-7}s, *i.e.* up to approx. $500\tau_{\text{Sys}}$.

In Plot 2.17 we compare in detail the numerically derived mean deviations for various temperatures at different times ($t \in \{10^{-9}\text{s}, 10^{-8}\text{s}, 10^{-7}\text{s}\}$) with the corresponding expression 2.43 from the effective random walk model. For the case of sufficient frequently flipping ($\lambda = 10^3$) we clearly recognize an excellent agreement of numerical and analytical results. In the slow bfl case ($\lambda = 10^3$) the analytically predicted deviations were approx. 30 % overestimated (although the functional T-dependence is quite accurate). We trace this

overestimation back to the fact, that slower bfl random walk leads to down-averaged step-sizes, in particular when the single r.w. steps are in the order of the free precession period or even several times larger.

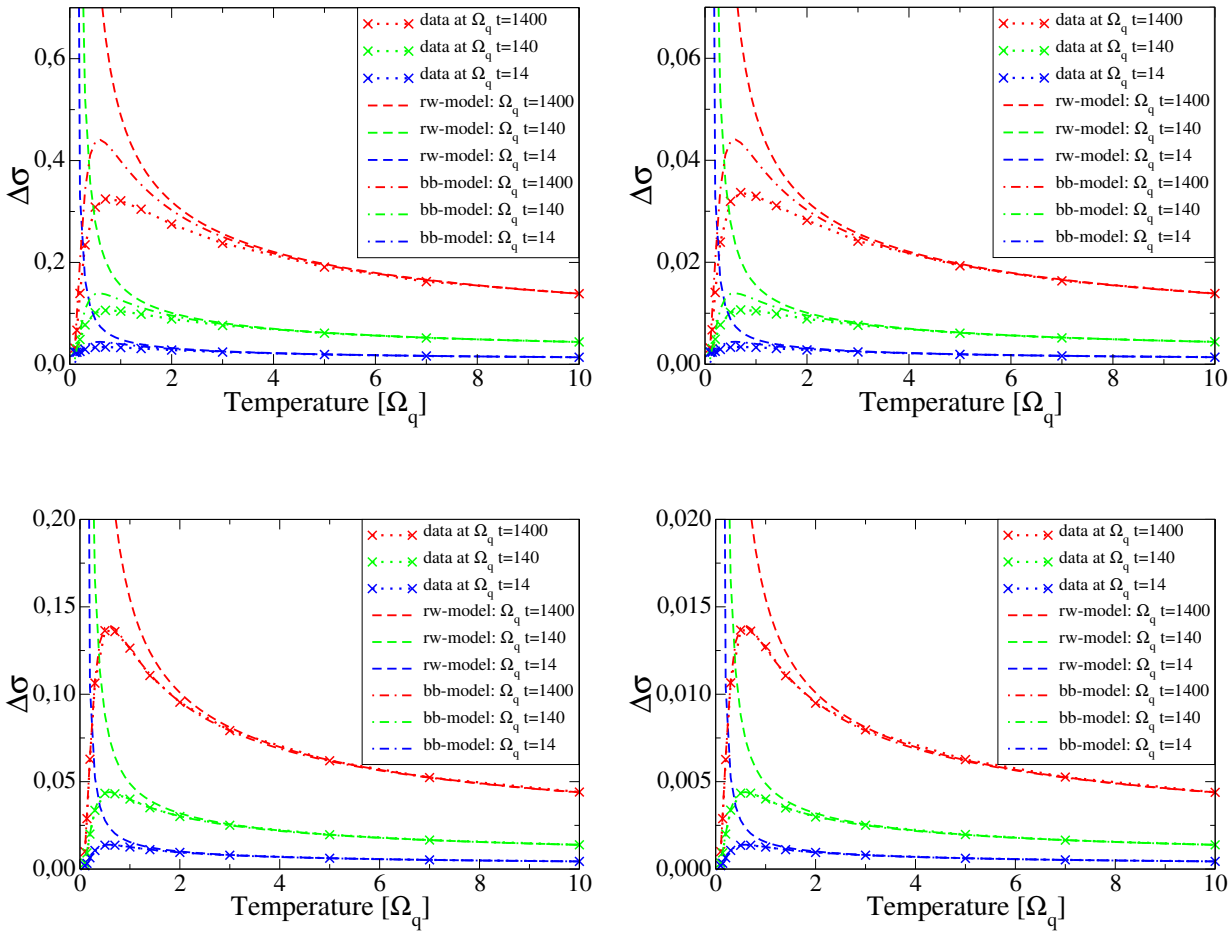

Figure 2.17: Comparison of the numerically and analytically derived rms deviations for asymmetric bfl-induced random walks. The numerical data were extracted for different times ($t = 10^{-7} - 10^{-9}$s) from Fig. 2.16 at various temperatures between $T_{\min} = 0.1\Omega_q$ and $T_{\max} = 10\Omega_q$. The coupling constant between qubit and bfl is chosen between $\alpha = 0.1\Omega_q$ (left plots) and $\alpha = 0.01\Omega_q$ (right ones), the bfl flipping rates are taken from eq. 2.37 by means of $\Delta_{\text{bfl}} = \epsilon_{\text{bfl}} = 10^{10}$ Hz, with $\lambda = 10^2$ for "slower" (figures on top) and $\lambda = 10^3$ for "faster" bfl flipping (bottom figures).

2.3.7 Derivation of dephasing and relaxation rates

Up to now we have presented a numerical as well as an analytical method to derive rms mean deviations of quasi-Gaussian distributions as measure of bfl-induced decoherence. These provides a compareably clear intuition of how coherent information stored on a qubit get lost. Of course, dissipating processes were not usually characterized and quantified by the size of some spatial abberration decohering states experiences, in this case in the Bloch sphere representation. Traditionally the typical time-scales, on which coherence decay take place, were the usual measures of decoherence. Thereby one distinguishes between the lost of phase knowledge of the qubit (dephasing) and the energy decay of the qubit (relaxation). Illustratively spoken, dephasing correspond to the spiral shaped decay of the qubit position on the Bloch sphere in perpendicular to the (effective) energy quantization axis (see Fig.2.19). While relaxation consists of the movement of the spin vector along this (renormalized) energy axis in order to reach its thermal equilibrium. Typically both kind of processes happens on different time-scales, denoted as dephasing time τ_{deph} and relaxation time τ_{rel} respectively.

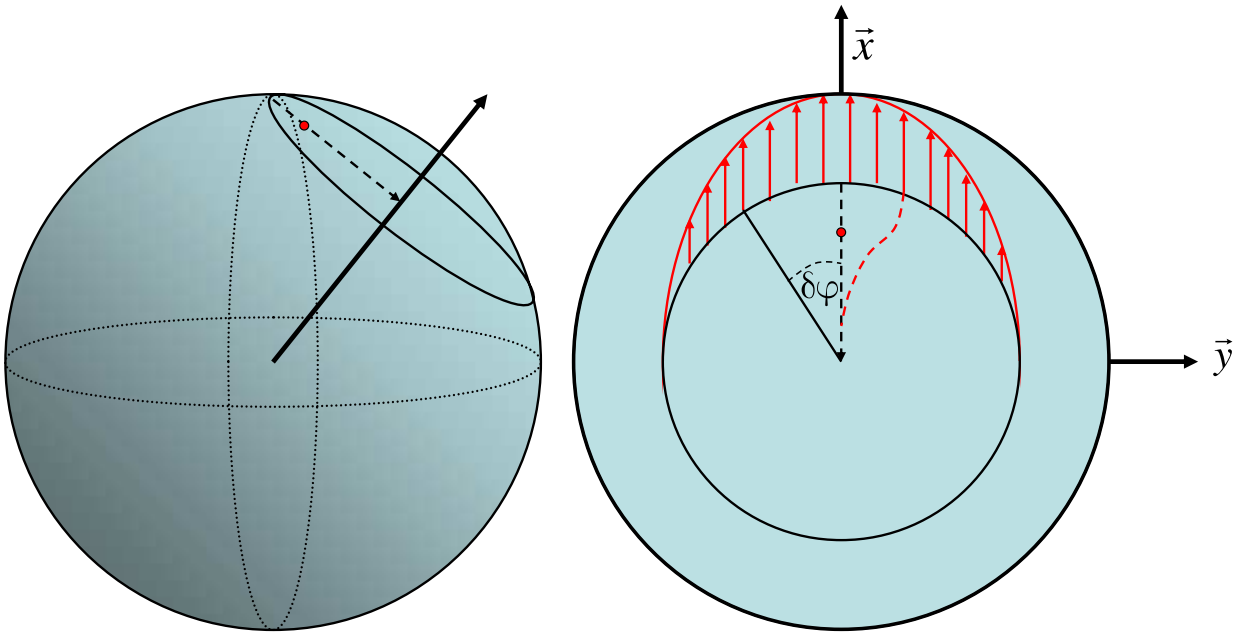

Figure 2.18: Schematic plot of the dephasing course of a qubit position on a Bloch sphere due to stochastical spreading along the free evolution trajectory. The Gaussian-shaped distribution (red line on the right plot) indicates the probability distribution on the cricle of free evolution and in average leads to dissipation towards the energy quantization axis. In consequence we obtain the red dotted position.

To translate our mean deviations into according time scales, we have to comprehend, how the time evolution of an initial pure qubit state to a Gaussian probability distribution on the Bloch sphere temporally proceed, leading to corresponding dephasing and relaxation. From Fig.2.19 one can see, that the random walk diffusion in parallel to the evolution trajectory integrates out to a corresponding point moving in direction to the quantization axis. Assuming a Gaussian shape for the dephasing distribution we obtain (given in polar coordinates as follows)

$$\Phi_{\mathrm{deph}}(\phi) \quad = \quad \frac{1}{\sqrt{2\pi}\delta\phi} e^{-\frac{\phi^2}{2\delta\phi^2}}, \tag{2.53}$$

with $\delta\phi$ the corresponding mean deviation.

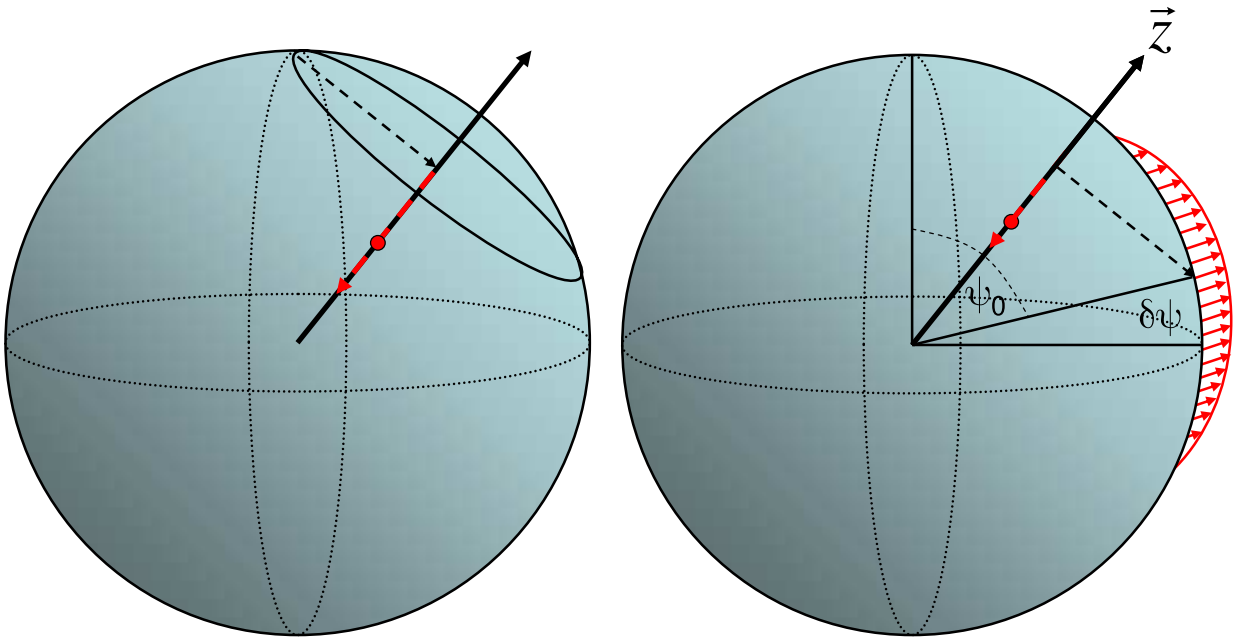

Figure 2.19: Schematic plot of the relaxation process of a qubit position on a Bloch sphere due to stochastical spreading perpendicular to the free evolution trajectory. The Gaussian-shaped distribution (red indicated) yields an according probability curve on the quantization axis leading to the mean point (red dot), approaching the qubit equilibrium state.

If we assume the symmetry axis in regard to the random walk distribution as x-direction and the other one as y-axis (see plot 2.19), we receive by integration of the probability function regarding its symmetry zero result for the y-part and for the x-value as follows

$$\begin{aligned} \bar{x}(\delta\phi) &= \int_{-\pi}^{\pi} d\phi \Phi_{\text{deph}}(\phi) \cos\phi \\ &= e^{-\delta\phi^2} \ . \end{aligned} \tag{2.54}$$

Evidently by assuming a random walk type increase of the Gaussian angle distribution

$$\delta\phi(t) = \delta\phi_0 \sqrt{t} \tag{2.55}$$

we receive for the x-line decay (i.e. dephasing) the following time dependence

$$\bar{x}(t) = e^{-t/\tau_{\text{deph}}} \tag{2.56}$$

with

$$\tau_{\text{deph}} = 1/{\delta\phi_0}^2 \ . \tag{2.57}$$

$$\tag{2.58}$$

We analogously proceed for a given relaxating Gaussian distribution

$$\Phi_{\text{rel}}(\psi) = \frac{1}{\sqrt{2\pi}\delta\psi} e^{-\frac{(\psi-\psi_0)^2}{2\delta\psi^2}} \ , \tag{2.59}$$

where in general $\Phi^{\text{rel}}_{\text{Gaussian}}(\psi)$ is distributed symmetrical around an offset angle ψ_0, given by the initial energy $\cos\psi_0$ of the qubit. Denoting the quantization axis with z, we receive for its expectation value

$$\begin{aligned} \bar{z}(\delta\psi) &= \int_{-\pi}^{\pi} d\psi \Phi_{\text{rel}}(\psi) \cos\psi \\ &= \cos\psi_0 e^{-\delta\psi^2} \ . \end{aligned} \tag{2.60}$$

Such that the time evolution of $\bar{z}$ is given as

$$\bar{z}(t) = \cos\psi_0 e^{-t/\tau_{\text{rel}}} \tag{2.61}$$

with

$$\tau_{\text{rel}} = 1/{\delta\psi_0}^2 \ . \tag{2.62}$$

2.4 Bfl-noise induced by an SET-measurement setup

After having analyzed different phenomena of bfl noise on a single qubit from a conceptual point of view, we now consider a physical example: the back-action of the charge fluctuations of a single-electron transistor (SET), capacitively coupled to an single-charge box (SCB), which represents a qubit. We assume, that the SET, which is designed to admit single shot-measurements of the charge-qubit due to the sensivity of its applied current with regard to the states of the SCB is currently switched off (*i.e.* only weakly coupled to the SCB). The single-electron transistor, which is able to measure microscopic charges accurately, serves in its measurement activation as a highly sensitive indicator of the qubits charge state. During its off-state, the fluctuations of the SET between inhabiting zero and one additional electron (see level picture 2.21) corresponds to the flips of the bfl. The main difference here is, that the flips and their frequency are depending not solely on external temperature, but in particular also from the electrostatic characteristics of the circuit (as will be discussed in detail later).

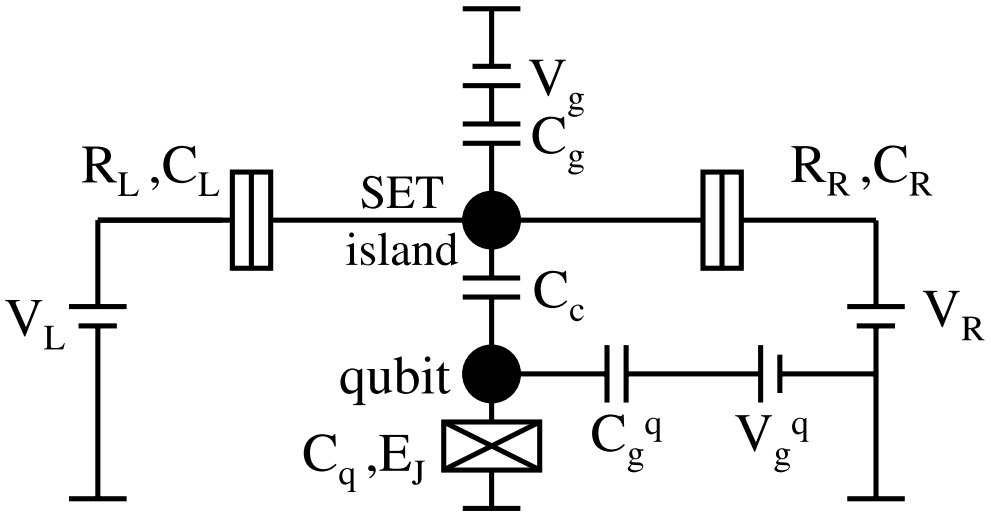

Figure 2.20: Electronic circuit of an SET-SCB-setup, where the single-charge box represents an charge qubit, which energy parameters can be tuned by changing of the corresponding gate voltage V_g^q. The SET serves in its on-state as a highly sensitive measurement device of the qubits charge by its currence dependence due to the coupling capacity C_c. At its offline phase (*i.e.* no SET-current when$|V_R - V_L| < \Delta E_C$) it behaves as a bistable fluctuator, which excited state correspond to an additional electron on the island (see 2.21).

2.4.1 Flipping rates of the SET-electron

The SET consists of a small island, coupled to two leads by thin insulating layers (typically generated by oxidation), such that the dominating energy scale is given by the single electron charging energy

$$E_{\mathrm{C}} = \frac{e^2}{2C_{\mathrm{total}}} \tag{2.63}$$

where the total capacitance of the SET is given as

$$C_{\mathrm{total}} = C_L + C_q + C_R + C_c \tag{2.64}$$

and usually is in the order of $C_{\mathrm{total}} \simeq 10^{-15}F$, corresponding to a temperature scale of $T_{\mathrm{SET}} = E_{C_{\mathrm{total}}}/k_B \simeq 10K$. For our situation of low temperatures ($T \leq T_{\mathrm{SET}}$) we only have to take into account the two SET-states, where zero or only one additional electron are on the island (compared to the equilibrium number of electrons in respect to the external gate voltages). Analogously to our bfl considerations we will denote the energetically higher state of an extra charge with $|1\rangle$ and lower state with $|0\rangle$. The fluctuations between these two states arise due to four different possibilities of tunneling processes. At first, starting from an extra electron state, the SET can relax by tunneling out of this electron to the left or to the right lead. As extensively discussed in the work by G. Schön [63], the corresponding tunneling rates were given as follows

$$\Gamma_{L\leftarrow I} = \frac{1}{e^2 R_L} \frac{\delta E_L}{1 - \exp[-\delta E_L/k_B T]} \tag{2.65}$$

for an electron departing the island to the left lead and

$$\Gamma_{I\rightarrow R} = \frac{1}{e^2 R_R} \frac{\delta E_R}{1 - \exp[-\delta E_R/k_B T]} \tag{2.66}$$

leaving to the right one. On the other hand, the zero electron state can be excited by tunneling of an additional electron on the SET-island from the left lead

$$\Gamma_{L\rightarrow I} = \frac{1}{e^2 R_L} \frac{\delta E_L}{\exp[\delta E_L/k_B T] - 1} \tag{2.67}$$

as well as from the right one

$$\Gamma_{I\leftarrow R} = \frac{1}{e^2 R_R} \frac{\delta E_R}{\exp[\delta E_R/k_B T] - 1} \ . \tag{2.68}$$

Thereby

$$\delta E_{L/R} \;=\; \Delta E_C - eV_{L/R} \tag{2.69}$$

denotes the energy gain/loss by attaching or detaching an extra electron from the corresponding lead (see level diagram in Fig. 2.21). The relative position of the relevant level $|1\rangle$ will be encoded by an asymmetry variable n_{asymm}, which can vary between $+0.5$ and -0.5, corresponding to coincidence of the island level with the left or the right lead energy level respectively ($n_{\text{asymm}} = 0$ denotes the symmetric situation).

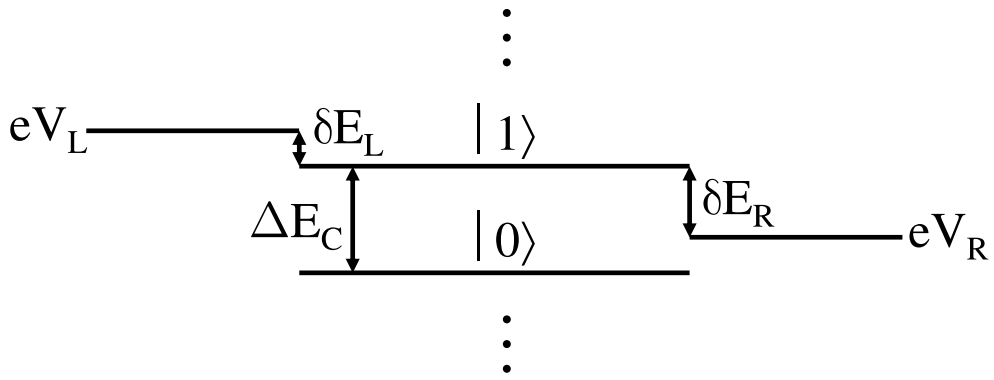

Figure 2.21: Schematic plots of a typical SET level-structure with appended left and right lead gate voltages $V_{L/R}$. If $V_{L/R}$, V_G and the environmental temperature is appropriately chosen, only two SET charge states were significantly contributing (denoted here as $|0\rangle$ and $|1\rangle$).

Similar to the work by Johansson et al. [64, 65] we choose as typical values for the SET characterizing parameters a charging energy of $\Delta E_C = 1.25K \cdot k_B$ and symmetric tunneling resistances $R_L = R_R = 22k\Omega$. For the SCB we assume corresponding to Schoelkopf et al. [66] an energy bias of the qubit of $\epsilon_{\text{q}} = 0.5K \cdot k_B$ and a tunneling strength of $\Delta_{\text{q}} = 0.25K \cdot k_B$. The coupling between SET and SCB is set to $0.1\Omega_{\text{q}} \simeq 0.0559K \cdot k_B$.

By means of these physical specifications we were able to simulate numerically the energy and phase representing observables of that qubit system in dependence of external temperature as well as of the voltage biases of the SET. As effective energy measure we consider $\hat{\sigma}^q_{z,\text{eff}}$, the renormalized energy axis, for studying the dephasing we exemplarically choose $\hat{\sigma}^q_y$. As one can recognize from Fig.2.22, we observe dephasing on a faster time scale (of about $\tau_{\text{deph}} = 10^{-8}$ s) compared to the relaxating one (approximately $\tau_{\text{rel}} = 10^{-7}$ s).

If we consider the corresponding flipping times of the SET (plot 2.23 as function of temperature and compare these with the free qubit evolution period $\Omega_{\text{q}}^{-1} \simeq 1.37110^{-10}$, we expect an appropriate random walk behaviour of the decoherence effects at least at

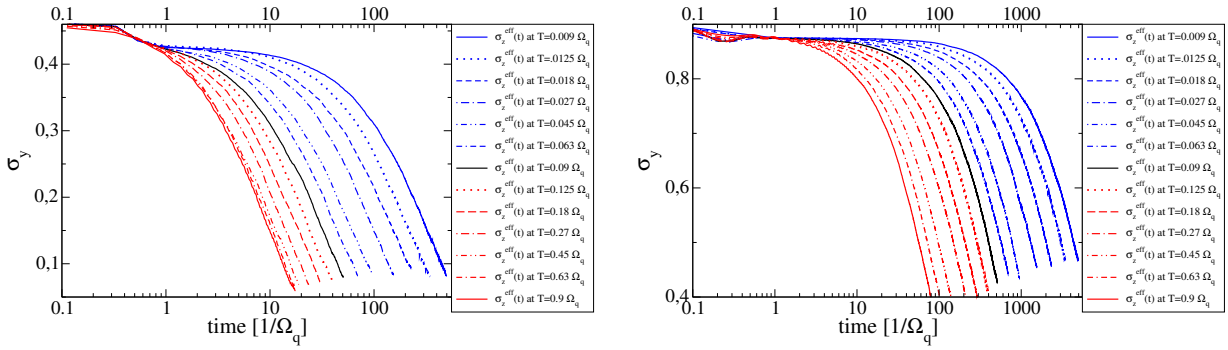

Figure 2.22: σ_y and σ_z^{eff} evolution of a qubit exposed to SET-induced bfl noise at various temperatures. The σ_y decay represents dephasing, σ_z^{eff} relaxation effects of the qubit. The physical parameters of the qubit were set to $\epsilon_{\text{q}} = 1Kk_B$ and $\Delta_{\text{q}} = 0.5Kk_B$. The SET characteristics were given as $\Delta E_C = 2.5Kk_B$, $R_L = R_R = 22k\Omega$, $V_{L/R} = \Delta E_C/2$, as well as an asymmetry factor of $n_{\text{asymm}} = 0.25$. The temperatures vary approximatively between $0.01\Omega_q$ and $1\Omega_q$.

temperatures larger than the typical qubit energy $\Omega_{\text{q}} = \sqrt{\epsilon_q^2 + \Delta_q^2} \simeq 0.559Kk_B$.

By applying appropriate exponential fits of the numerical data

$$\hat{\sigma}^q_{z,\text{eff}}(t) \;\simeq\; \hat{\sigma}^q_{z,\text{eff}}(0)e^{-t/\tau_{\text{rel}}} \;, \tag{2.70}$$

respectively

$$\hat{\sigma}^q_{y}(t) \;\simeq\; \hat{\sigma}^q_{y}(0)e^{-t/\tau_{\text{deph}}} \;, \tag{2.71}$$

we obtain the following decaying times (Fig. 2.24). Apparently, we receive a good agreement between the numerical data and analytical results, derived by means of expressions (2.42) and (2.26), respectively (2.27).

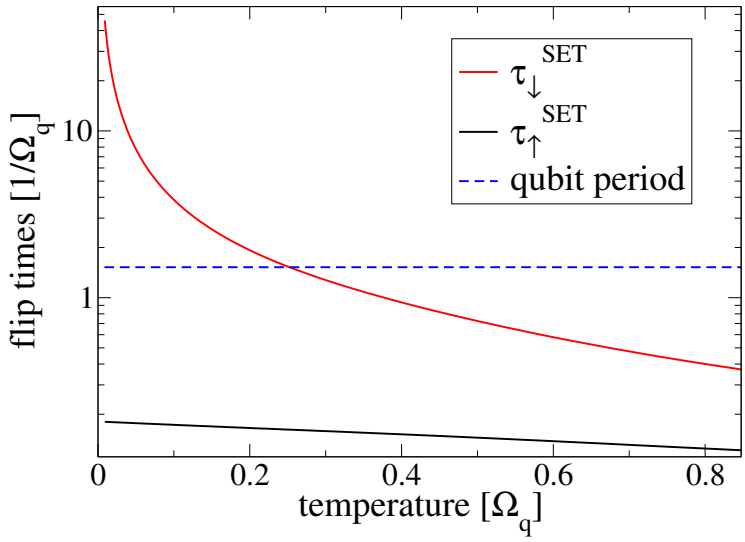

Figure 2.23: Flipping times of an SET. $\tau_\uparrow$ denotes the average residence time of an additional electron on the SET island, while $\tau_\downarrow$ is the average time of its absence. The dashed line describes the free volution period of the qubit; it serves as a guideline for random walk like behaviour, which we expect to appear in the higher temperature regime (approx. $T \geq 0.3K$). The SET parameters were chosen as $\Delta E_C = 2.5Kk_B$, $R_L = R_R = 22k\Omega$ and a voltage bias of $V_{L/R} = \Delta E_C$ with an asymmetry of $n_{\text{asymm}} = 0.25$. The temperatures vary approximatively between $0.01\Omega_q$ and $1\Omega_q$..

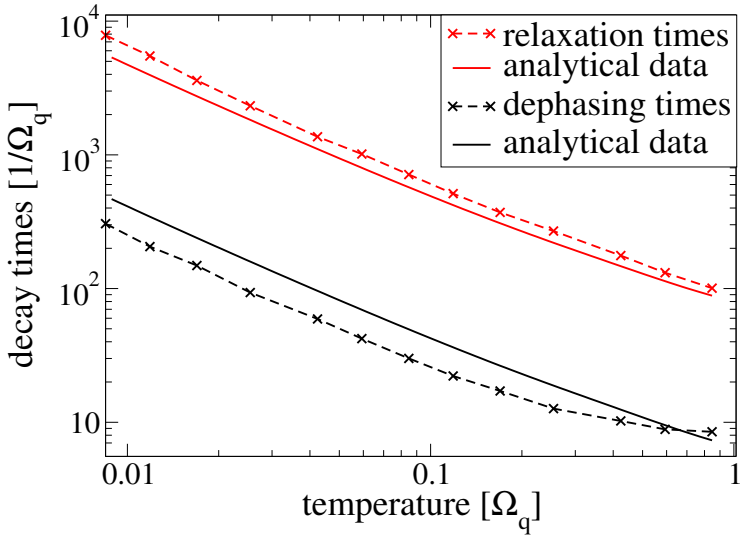

Figure 2.24: Temperature dependence plot of the relaxation, respectively dephasing times of a qubit exposed to SET induced bfl-noise. Numerically fitted values are compared with corresponding analytical random walk results. Evidently the analytical prognosticated behaviour of $\tau_{\mathrm{rel/deph}} \simeq \mu T^{-x}$ is satisfied in good accuracy by the numerical data. The physical parameters of the qubit were given by $\epsilon_{\mathrm{q}} = 1Kk_B$ and $\Delta_{\mathrm{q}} = 0.5Kk_B$. The SET parameters were $\Delta E_C = 2.5Kk_B$, $R_L = R_R = 22k\Omega$, $V_{L/R} = \Delta E_C$ and an asymmetry of n_{asymm}. The temperatures vary approximatively between $0.01\Omega_q$ and $1\Omega_q$.

2.5 Refocusing of bfl-noise by means of dynamical decoupling

In the first part of this chapter we have extensively discussed different approaches to describe decoherence originated by defects and impurities in the bulk material, which qubit setups were build of. Now we want to propose a general scheme, by means of which this sort of decoherence might be suppressed or at least diminished to a tolerable amount. Hereby we use the general concept of dynamical decoupling. This works different to active correction techniques, where at first errors has to be diagnosed, in order to correct them by individual rearrangement of the qubit afterwards. Neither does it consist in encoding logical qubits into several physical one, which might be protected from decoherence by using higher symmetries of the noisy system. Dynamical decoupling (also called open loop quantum control) denotes procedures, in which the qubit is influenced during its noisy evolution by external control pulses in order to keep its actual state as protected as possible from the uncontrolled noise degrees of freedom [36, 37, 38].

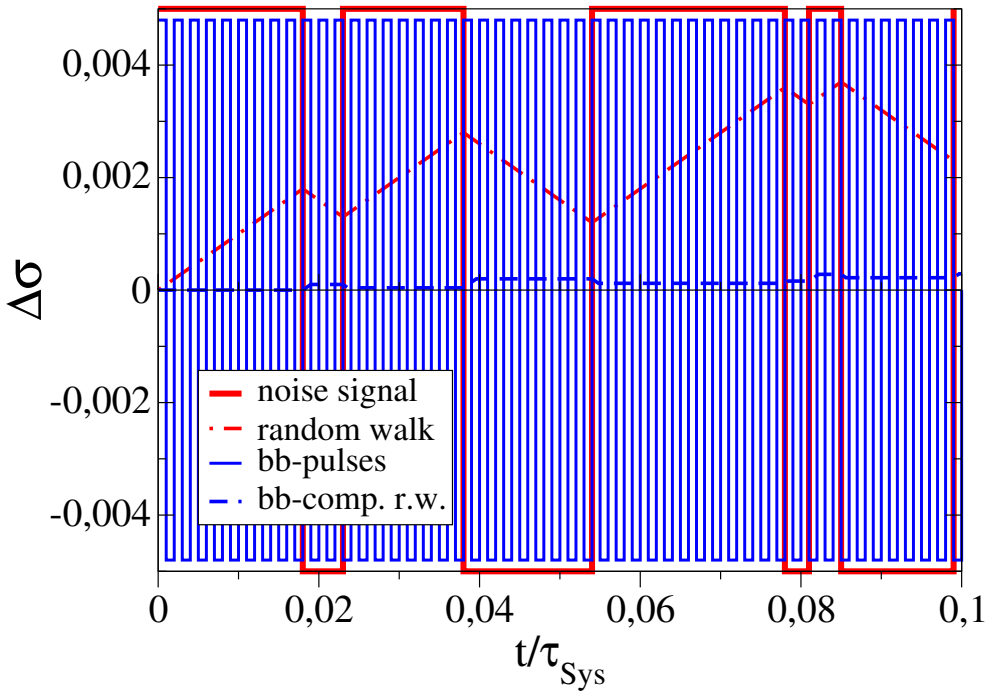

Figure 2.25: Schematic plot of a typical Poissonian bfl noise signal with its resulting random walk behavior without (red line) and with (blue line) bang-bang refocusing. The bfl parameters are given here as usual $\alpha = 0.1\Omega_q$ and $\tau_{\mathrm{bfl}} = 10^{-2}\tau_{\mathrm{Sys}}$, while the bang-bang period is chosen to $\tau_{\mathrm{bb}} = 10^{-3}\tau_{\mathrm{Sys}} \ll \tau_{\mathrm{bfl}}$.

2.5.1 Refocusing (bang-bang) scheme

The refocusing pulse sequence we suggest, also called bang-bang due to its rapidly and iteratively applied pulse sequences, is based on the same concept as the well-known Carr-Purcell-Gill-Meiboom echo technique first used in NMR [67] (an extension of the more familiar spin-echo method). The technique consist of averaging out of quasi-static deviations from the free Hamiltonian, generated by comparabely slow fluctuations of the bfl. As indicated in Fig. 2.25 rapidly flips of the qubit $\hat{\sigma}_z^q$-spin refocus the main fraction of the pure bfl-deviations,*i.e.* every integer numbers of bang-bang periods represents a spin-echo circle, as long as no bfl flip takes place. Only for unperturbed bang-bang periods (without bfl flips), this average scheme works perfectly. If a bfl flip occurs during one bang-bang cycle, there would arise remaining decoherence effects. Those spin-flips could be executed *e.g.* by using infinitesimally short π-pulses in $\hat{\sigma}_x^q$-direction, applied on well-defined equally separated times (with iteration period $\tau_{\rm bb} \ll \tau_{\rm bfl}$).

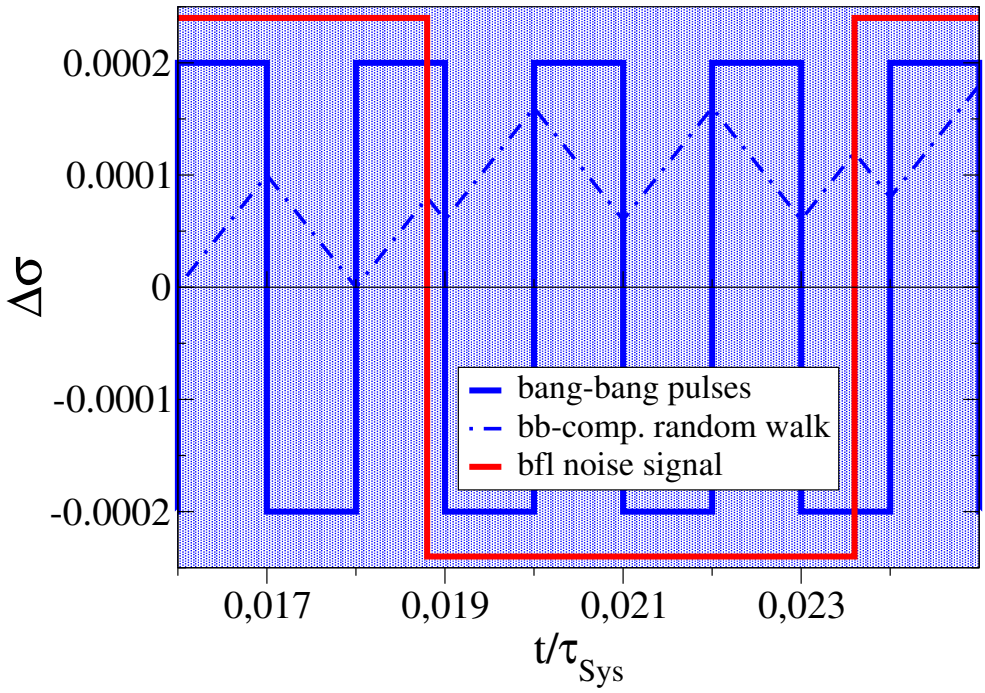

Figure 2.26: Detailed plot of the bang-bang refocused random walk (blue dot-dashed line) in dependence of the bfl flip positions (red line). As zoom extract from Fig.2.25 the same physical parameters were given, *i.e.* $\alpha = 0.1\Omega_q$, $\tau_{\rm bfl} = 10^{-2}\tau_{\rm Sys}$ and $\tau_{\rm bb} = 10^{-3}\tau_{\rm Sys}$.

These spin-flips would lead to correspondingly fast sign-flipping of the noise term in the Hamiltonian 2.5, thus to an averaging out of its decohering effect with respect to 2.24, as each two bang-bang periods would refocus the $\hat{H}_{\mathrm{q,bfl}}$-induced deviations. Virtually the bang-bang pulses would reduce the bfl mean influence time τ_{bfl} during each inter-flip duration to a reduced time separation of τ_{bb}. Heuristically one would expect a decrease of the decoherence impact in the order of $\tau_{\mathrm{bb}}/\tau_{\mathrm{bfl}}$. As the frequency of the reduced random walk steps stays constant, we would expect as rule of thumb of the bang-bang refocused random walk deviations

$$\Delta\sigma_{\mathrm{bb}}(N) \quad \sim \quad \alpha\tau_{\mathrm{bb}}\sqrt{N} \ . \tag{2.72}$$

For technical convenience, we will assume the π-pulses to be of infinitesimal duration. This is no crucial simplification, as detailed analysis of finite-length pulses below will confirm. As one easily recognize, the bang-bang pulses will not only suppress the noisy σ_z^q-term of the total Hamiltonian 2.23, but also any static σ_z^q-part of the qubit Hamiltonian 2.22. Theoretically this would reduce our feasible coherent qubit operations on only one remaining degree of freedom, which is the same as the bang-bang pulses, as thereby commutation of pulses and static terms would permit them. But this restriction on feasible qubit dynamicss can be circumvented, if one implements appropriate pulse sequences in σ_x^q and σ_y^q-direction. When chosing the σ_z^q-refocusing driving simultaneously to the intended dynamics, corresponding gate pulses are admitted [38].

2.5.2 Random walk model

In analogy to our random walk analysis of the pure bfl noise, we develop a detailed model of the bang-bang refocused random walk. From there we obtain an accurate analytical expression for the remaining decoherence in its intermediate time regime. To evaluate a qualitative picture of the one-step deviations during bang-bang compensation, one has to consider, that the bfl flip produces maximum abberration, if the symmetry of a bang-bang double-period is maximally broken. This is the case if the bfl flip coincides with the second bang-bang pulse (in the middle of one double-period). As one can see from Fig.2.27 the usual pure σ_x^q-evolution would then receive in the second part of the bang-bang period not a refocusing driving, but a deviation in the same direction. Thus, we obtain for this a maximal one-step deviation of $2\alpha\tau_{\mathrm{bb}}$. However, this abberation is scaled down by a factor of $1/\sqrt{2}$, as its impact is depending on the longitudinal angle χ of the spin present Bloch sphere position, by a factor of $\sin\chi$. This is as the σ_z^q-component of the noisy evolution does not influence the qubit if it is near the $\sigma_z^q = \pm 1$-states, and its effect in- and decreases in between correspondingly. As we are mainly interested in mean aberrations for the regime of several random walk steps, we simply average the maximal one-step deviation in typical rms manner to

$$\left\langle \Delta\sigma_{\mathrm{max}}^{\mathrm{bb}} \right\rangle \quad = \quad \sqrt{\frac{1}{2\pi}\int_0^{2\pi} \sin^2\chi 4\alpha^2\tau_{\mathrm{bb}}^2 \, d\chi} \quad = \quad \sqrt{2}\alpha\tau_{\mathrm{bb}}. \tag{2.73}$$

Evidently this variance only contributes to relaxation, dephasing is strongly suppressed (see also Fig.2.28).

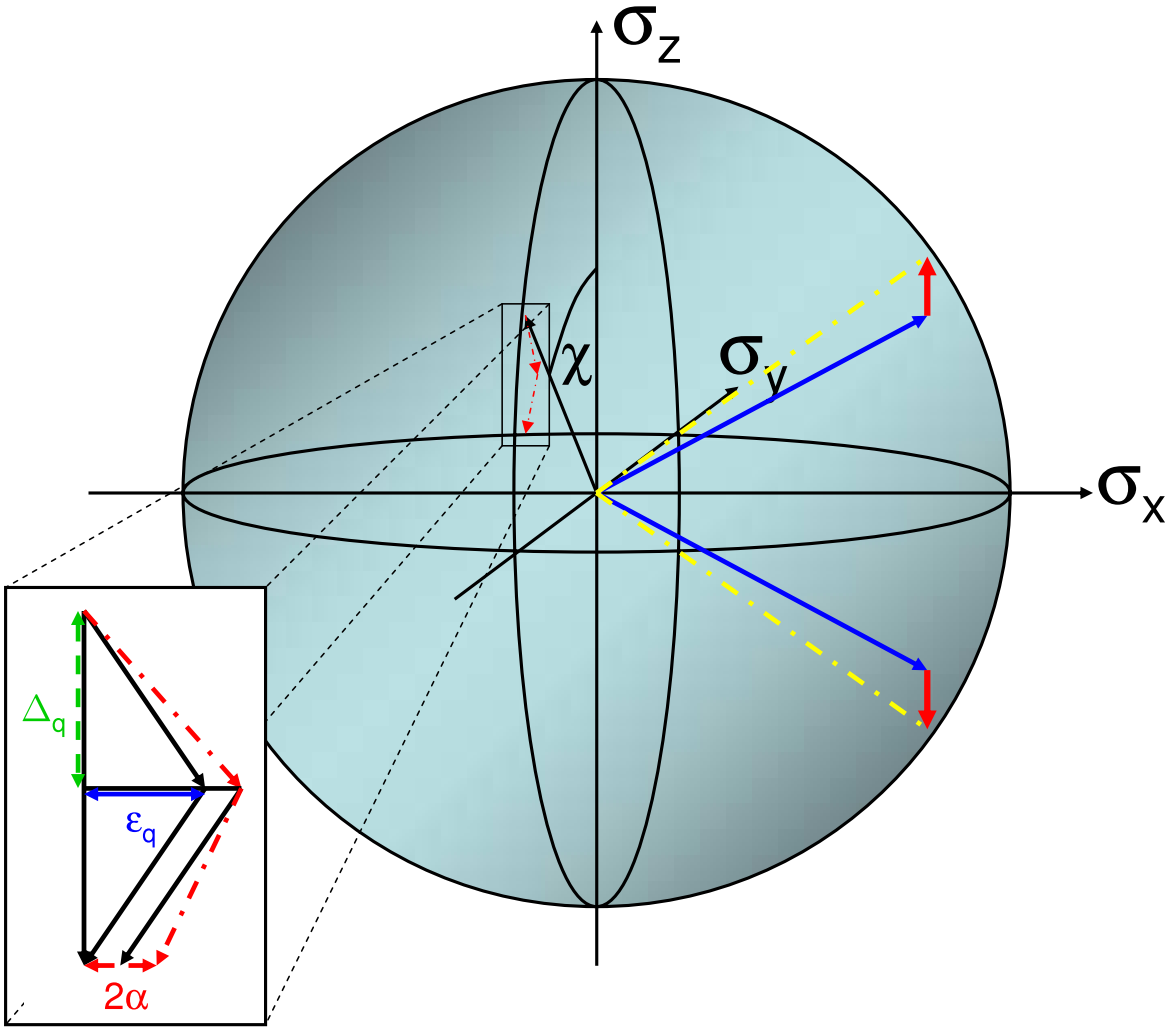

Figure 2.27: Sketch of a maximal one-step deviation during a bang-bang modulated cycle, which appears if the bfl state flips precisely at the intermediate bang-bang pulse time. The dephasing part of deviation evidently averages out, while a relaxating aberrance arise proportional to the noise-coupling constant α, as well as to $\sin\chi$ with χ the actual longitudinal angle of the spin position (measured from $\sigma_z^q = +1$).

With this maximum one-bfl-flip deviation we can now formulate a corresponding one-step random walk distribution. Thereby we have to mention, that in contrast to our former Poissonian distribution 2.29, the size of the random walk step is given by the actual position of the bfl flip in the bang-bang double-period. The maximum effect is obtained, if the flip is exactly in the middle of such a double-period (*i.e.* when the second bang-bang pulse apply) and correspondingly linearly rescaled otherwise (until zero impact, if the flip is directly at the begin or end of such a double-period). As we consider $\tau_{\mathrm{bb}} \ll \tau_{\mathrm{bfl}}$, the position of bfl flips

in concerned double-periods appears total randomly, *i.e.* equally distributed, we receive for the one-step random walk distribution of the bang-bang refocused system

$$\Phi^{\mathrm{bb}}_{\mathrm{odd/even}}(x) \quad = \quad \frac{\theta(\pm x)\theta\left(\gamma_{\mathrm{bb}} \mp x\right)}{\gamma_{\mathrm{bb}}}. \tag{2.74}$$

with $\theta(x)$ the Heaviside-function. $\gamma - \mathrm{bb} = \sqrt{2}\alpha\tau_{\mathrm{bb}}$ corresponds to the maximum abberration regarding 2.73. The difference between odd and even case is analogous to the up and down states of the former pure bfl situation. It represents left and right deviation from the effective trajectory of a noiseless evolution with bang-bang pulses.

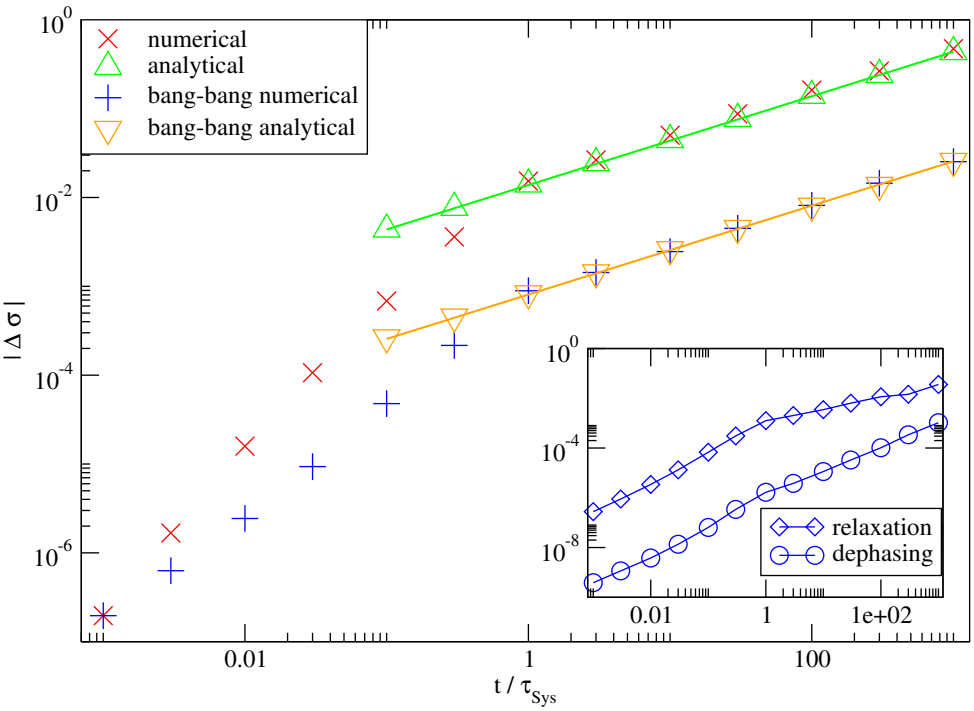

Figure 2.28: Time evolution of the rms deviations for bfl-induced random walks with and without bang-bang control. The coupling constant is given as $\alpha = 0.1$ and the mean flipping time scale is $\tau_{\mathrm{bfl}} = 10^{-2}\tau_{\mathrm{Sys}}$. The separation between two bang-bang pulses amount $\tau_{\mathrm{bb}} = 10^{-3}\tau_{\mathrm{Sys}}$. The straight lines are square-root fits of the analytical derived random walk model variances (plotted as triangles). Inset: Components of the deviations from the free precession trajectory that are parallel to it (dephasing) and perpendicular to it (relaxation/excitation) with bang-bang control.

Analogous to the former situation, we can also express the $2N_{\rm bfl}$ random walk distribution by means of the convolution theorem

$$\begin{aligned}\Phi^{\rm bb}_{2{\rm N_{bfl}}}(x) &= \mathscr{F}^{-1}\left[\left(\mathscr{F}\left[\Phi^{\rm bb}_2\right]\right)^{N_{\rm bfl}}\right] \\ &= \int_{-\pi}^{\pi}\frac{dk}{2\pi\gamma^{2N_{\rm bfl}}}e^{-ikx}\left(\frac{[1-\cos((\gamma+1)k)]}{[1-\cos(k)]}\right)^{N_{\rm bfl}} \end{aligned} \tag{2.75}$$

with $\mathscr{F}$ and $\mathscr{F}^{-1}$ denoting the discrete Fourier transformation and its inverse, respectively.

Applying the saddle point approximation again we obtain for the Gaussian mean deviation

$$\Delta\sigma_{\rm bb}(N_{\rm bfl}) = \sqrt{N_{\rm bfl}}\frac{\gamma_{\rm bb}}{2} = \sqrt{N_{\rm bfl}}\frac{1}{\sqrt{2}}\alpha\tau_{\rm bb}\ . \tag{2.76}$$

Which appearantly fits very accurately with the corresponding numerical simulations (see Fig.2.28).

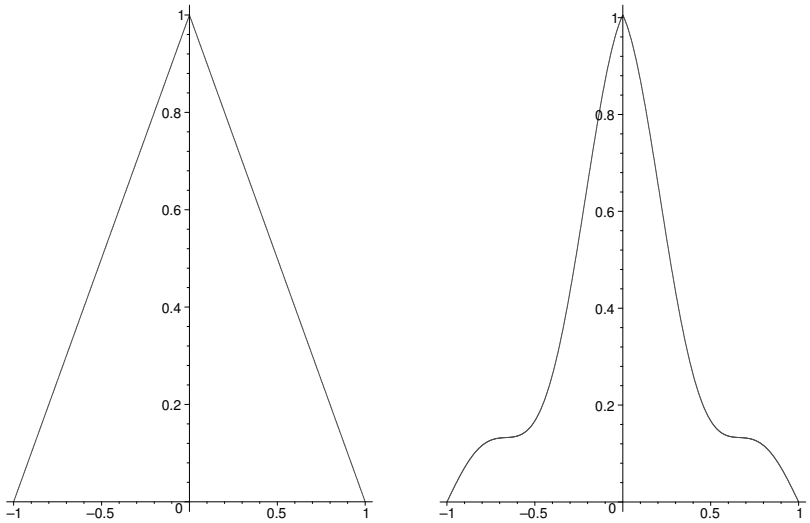

Figure 2.29: Comparison of two-step distributions for the random walks with bang-bang control with pulse shapes that are taken to be δ-functions (left) versus a continuous sine wave $\sin(\frac{\pi}{\tau_{bb}}t)$ (right). For clarity, the y-axis is rescaled to the maximum values of the distributions, while the x-axis is given in units of $\gamma_{\rm bb}$.

2.5.3 Pulse shapes

At first sight, treating bang-bang pulses as δ-function impulses appears to be an extraordinarily strong assumption. This in particular as in a practical implementations, the large

bandwidth associated with very short pulses would most probably excite other noise sources or even higher levels of pseudo-spin realizations of the qubit. However, this δ-function impulse approximation is chosen for technical simplification, in particular in our numerical simulation. In fact, regarding the other extreme of a wide, continuous pulse of the form $\sin(\frac{\pi}{\tau_{bb}}t)$, this would also refocus our bfl-noise over the course of its periods. Comparing the two-step distributions arising from δ-function impulses with the ones from continuous sine waves, one recognizes for the δ-function case

$$\Phi_2^{\text{inf}}(x) \quad = \quad \frac{|\gamma - x|}{\gamma}\theta(\gamma - x)\theta(\gamma + x) \tag{2.77}$$

and for the continuous sine wave case

$$\Phi_2^{\text{cont}}(x) \quad = \quad \left\{\left[\frac{\pi}{2\gamma} + \frac{\pi}{4\gamma}\cos\left(2\pi\frac{x}{\gamma}\right)\right]\left(1 - \frac{x}{\gamma}\right) + \frac{3}{16\gamma}\sin\left(2\pi\frac{x}{\gamma}\right)\right\}\theta(\gamma - x)\theta(\gamma + x) \ . \tag{2.78}$$

These distributions are depicted in Fig. 2.29. Evidently the distribution arising in the continuous realization by sine waves is even narrower (and therefore indicates more effective noise refocusing) than the δ-function case.

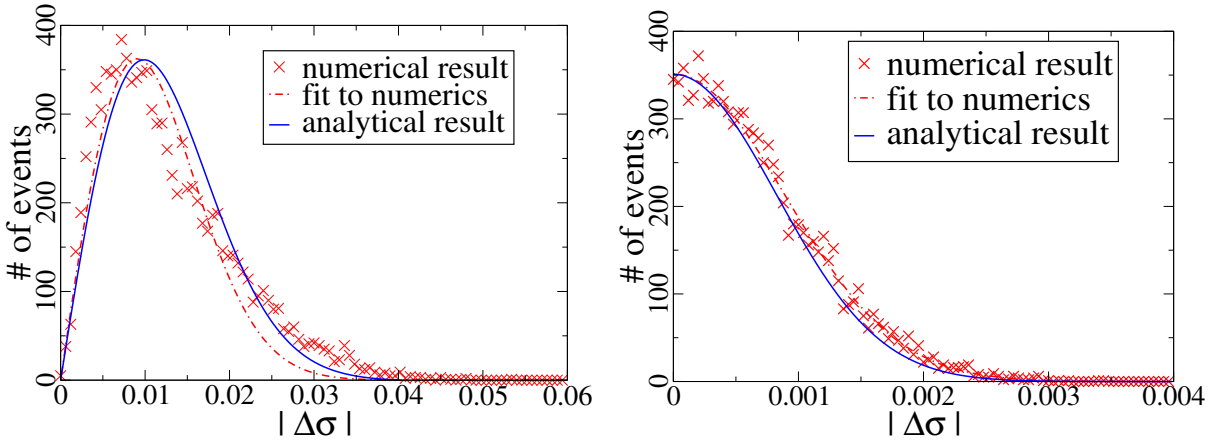

Figure 2.30: Histograms of the deviation from free qubit evolution both without bang-bang control (left) and with bang-bang control (right). Numerical data were collected over 10^4 realizations at a fixed time $t_0 = \tau_{\text{Sys}}$. $\tau_{\text{bfl}} = 0.01\tau_{\text{Sys}}$ and thus $N_{\text{bfl}} = \tau_{\text{Sys}}/\tau_{\text{bfl}} = 100$ steps.

2.5.4 Distributions of the random walks deviation

Beyond predicting the variances of the random walks, our analysis also allows evaluation of their full probability distributions. We compare them to numerical evaluations with and without bang-bang compensation by use of simulations with 10^4 realizations at an

evolution time $t_0 = \tau_{\mathrm{Sys}}$. The numerical histograms of the deviations with their respective one- and two-dimensional Gaussian fits are shown in Fig. 2.30.

We observe that not only the distribution obtained with bang-bang control is much narrower than the distribution for pure bfl noise, but also that its shape is qualitatively different. The maximum of the bang-bang controlled distribution is at zero error. In contrast, the uncontrolled distribution has its maximum at a finite error $|\Delta\sigma|_{\max} \approx 0.01$, and it has zero probability of zero error. This reflects the one-dimensional nature of the bang-bang controlled random walk on the Bloch sphere in contrast to the generic two-dimensional expansion of the pure bfl random walk.

2.5.5 Bang-bang control working as a high-pass filter

In order to measure the degree of noise suppression due to bang-bang control, we define a suppression ratio $\mathcal{S}_{t_0}$ as follows for a given evolution time t_0

$$\mathcal{S}_{t_0}(\tau_{\mathrm{bfl}}/\tau_{\mathrm{bb}}) \equiv \frac{\Delta\vec{\sigma}^{\mathrm{bfl}}_{\mathrm{rms}}(t_0)}{\Delta\vec{\sigma}^{\mathrm{bb}}_{\mathrm{rms}}(t_0)}. \tag{2.79}$$

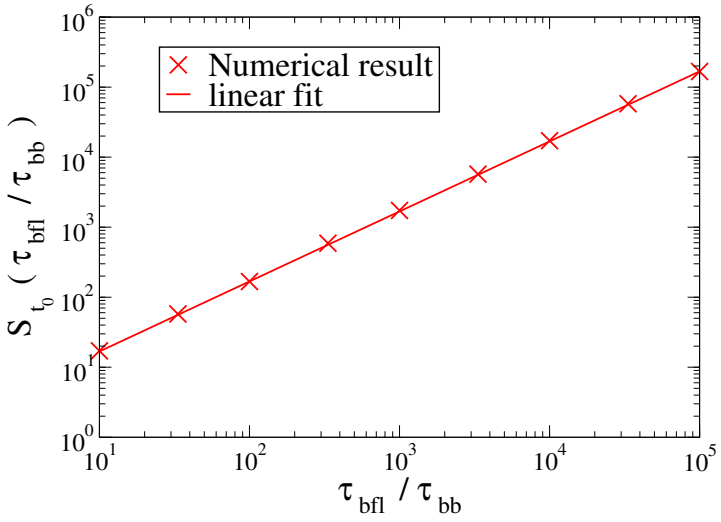

Figure 2.31: The suppression factor $\mathcal{S}_{t_0}(\tau_{\mathrm{bfl}}/\tau_{\mathrm{bb}}) = \frac{\Delta\vec{\sigma}^{\mathrm{bfl}}_{\mathrm{rms}}(t_0)}{\Delta\vec{\sigma}^{\mathrm{bb}}_{\mathrm{rms}}(t_0)}$ evaluated for $t_0 = \tau_{\mathrm{Sys}}$ as a function of the ratio $\tau_{\mathrm{bfl}}/\tau_{\mathrm{bb}}$ of the mean fluctuator time and the bang-bang pulse separation
.

We now systematically study the dependence of $\mathcal{S}_{t_0}$ on $\tau_{\mathrm{bfl}}/\tau_{\mathrm{bb}}$ for a constant mean bfl switching rate $\tau_{\mathrm{bfl}} = 10^{-2}\tau_{\mathrm{sys}}$ at a fixed evolution time $t_0 = \tau_{\mathrm{sys}}$. The numerical data in Fig. 2.31 show that the suppression efficiency is linear in the bang-bang repetition rate, $S_{\tau_{\mathrm{sys}}} = \mu\tau_{\mathrm{bfl}}/\tau_{\mathrm{bb}}$. The numerically derived value of the coefficient, $\mu_{\mathrm{numerical}} \approx 1.679$, shows good agreement with our analytical result $\mu_{\mathrm{analytical}} = \sqrt{5/2} \simeq 1.581$ from the saddle point approximation, eq. (2.31) and (2.76).

This small discrepancy between the numerical and analytical results is due to the fact that our analytical calculations neglect correlations between the parallel (dephasing) and perpendicular (relaxating/exciting) components of the random walk. This leads to an underestimate of the rms-deviation $\Delta\vec{\sigma}^{\mathrm{bfl}}_{\mathrm{rms}}$ in the case without bang-bang control (compare also to Fig. 2.30). Therefore, we have quantitatively proven our qualitative intuition: bang-bang control affects the bfl noise signal working like a high-pass filter, an effect which was generally predicted for dynamical decoupling techniques [37].

2.5.6 Bang-bang refocusing of finite temperature bfl-noise

After having examined the high-pass filter behaviour of the refocusing of an idealized, symmetric bistable fluctuator we want to expand our investigations of bang-bang efficiency on the mere realistic case of temperature dependent bfl-noise. Thereby we apply our former model of temperature dependence, expressed concisely in eq. (2.37).

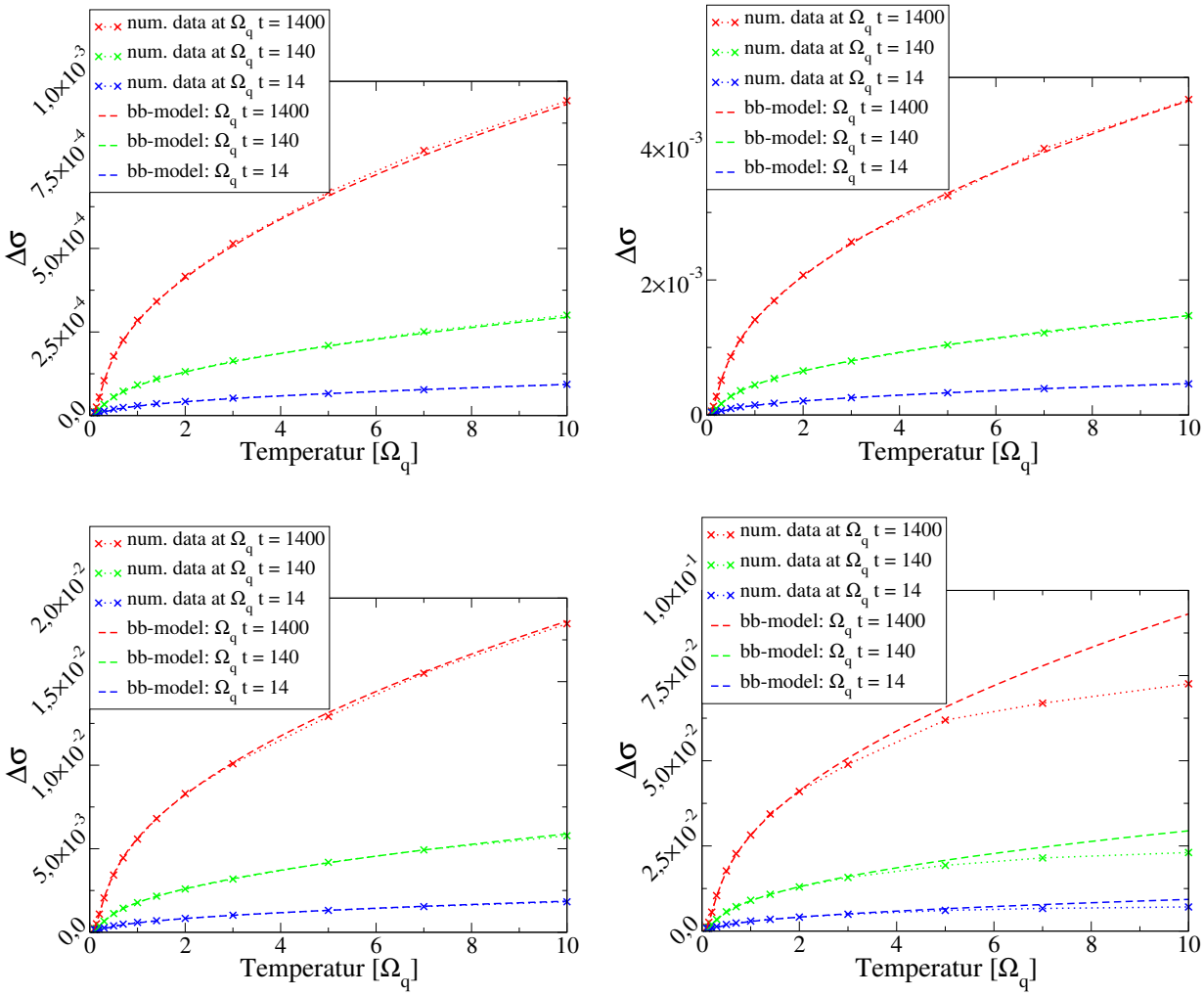

Figure 2.32: Temperature dependences of dynamically refocused bfl-noise deviations at different bang-bang time scales $\tau_{\mathrm{bb}} = 10^{-13}\mathrm{s} \simeq 7 \cdot 10^{-4}/\Omega_q$ (plot left top), $\tau_{\mathrm{bb}} = 5 \cdot 10^{-13}\mathrm{s} \simeq 3.5 \cdot 10^{-3}/\Omega_q$ (right top), $\tau_{\mathrm{bb}} = 2 \cdot 10^{-12}\mathrm{s} \simeq 1.4 \cdot 10^{-2}/\Omega_q$ (left bottom) and $\tau_{\mathrm{bb}} = 10^{-11}\mathrm{s} \simeq 7 \cdot 10^{-2}/\Omega_q$ (right bottom). The coupling constant between qubit and bfl is chosen as $\alpha = 0.01\Omega_q$, the bfl-Bath coupling parameter accounts $\lambda = 10^2$. Its bfl flipping rates are given by eq. 2.37 with parameters $\Delta_{\mathrm{bfl}} = 1/\sqrt{1.01} \cdot 10^9$ Hz and $\epsilon_{\mathrm{bfl}} = 1/\sqrt{1.01} \cdot 10^{10}$ Hz.

Under the assumption, that the bang-bang pulse sequence period is much faster than the

typical bfl flipping times we expect an analogous one-step deviation of the corresponding refocused random walk as described in the symmetric bfl-noise case (eq. (2.73)). Applying the corresponding temperature dependent time distribution of (double) steps we receive an effective refocused random walk deviation of

$$\begin{aligned}\Delta\sigma_{\mathrm{bb}}^{\mathrm{asymm}}(t) &= \sqrt{\frac{t}{\tau_{\mathrm{bfl}}^{\mathrm{mean}}}}\sqrt{2}\alpha\tau_{\mathrm{bb}} = \sqrt{\frac{2t}{(\tau_{\mathrm{bfl}}^{\uparrow}+\tau_{\mathrm{bfl}}^{\downarrow})}}\sqrt{2}\alpha\tau_{\mathrm{bb}} \\ &= \sqrt{\frac{4t}{2(e^{-\Omega_{\mathrm{bfl}}\beta/2}+e^{\Omega_{\mathrm{bfl}}\beta/2})\sinh(\Omega_{\mathrm{bfl}}\beta/2)\frac{\Omega_{\mathrm{bfl}}}{\lambda\Delta_{\mathrm{bfl}}^2}}}\alpha\tau_{\mathrm{bb}} \\ &= \sqrt{\frac{t\lambda\Delta_{\mathrm{bfl}}^2}{\cosh(\Omega_{\mathrm{bfl}}\beta/2)\sinh(\Omega_{\mathrm{bfl}}\beta/2)\Omega_{\mathrm{bfl}}}}\alpha\tau_{\mathrm{bb}} = \sqrt{\frac{2t}{\sinh(\Omega_{\mathrm{bfl}}\beta)}}\sqrt{\frac{\lambda\Delta_{\mathrm{bfl}}^2}{\Omega_{\mathrm{bfl}}}}\alpha\tau_{\mathrm{bb}}.\end{aligned} \tag{2.80}$$

One clearly recognizes in Fig. 2.32 the approximative $\sqrt{T}$-like behaviour (for small temperatures, *i.e.* $\Omega_{\mathrm{bfl}}\beta < 1$), which agrees perfectly with the analytically predicted standard deviations. Only small disagreements between analytical and numerical datas were visible in the case of low-frequently bang-bang pulses ($\tau_{\mathrm{bb}} = 10^{-11}$ s).

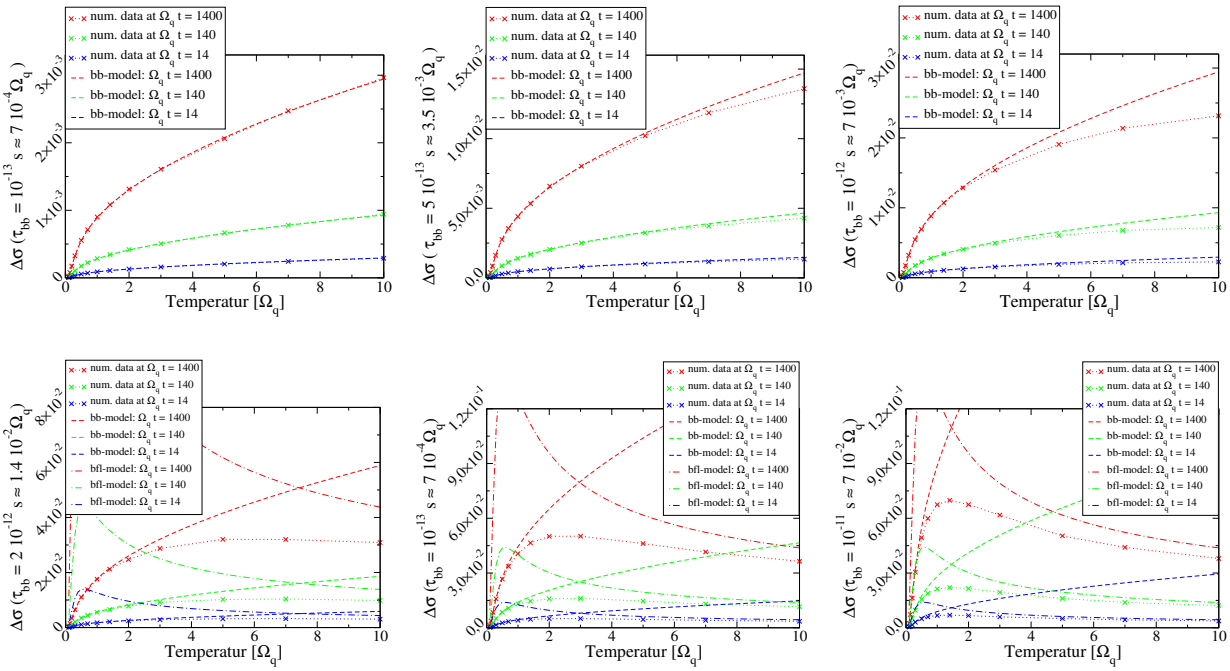

Figure 2.33: Temperature dependence of dynamical refocused bfl-noise deviations at various bang-bang time scales (see corresponding specifications at the y-axis). The τ_{bfl}-rates are given by eq. (2.37) with bfl parameters $\Delta_{\mathrm{bfl}} = 10^9/\sqrt{1.01}$ Hz, $\epsilon_{\mathrm{bfl}} = 10^{10}/\sqrt{1.01}$ Hz and $\lambda = 10^2$. The qubit-bfl coupling accounts $\alpha = 0.01\Omega_q$.

In contrast to plot 2.32 the agreement between numerical data and refocused random walk analysis is much worse for to faster bfl flipping times (see Fig. 2.33); for longer bang-bang periods and higher temperatures it almost reaches the form of the uncompensated bfl random walk. This is not surprising, as with increasing bang-bang periods for decreasing bfl flipping times the basic assumption of constant single-step distributions (eq. 2.29) crosses over to the original bfl random walk distributions (eq. C.9). As consequence we receive qualitatively pure bfl noise like behaviour, with slightly reduced amplitude due to the remaining refocusing effects.

If we now plot the suppression factor $\mathcal{S}_{t_0}(\tau_{\mathrm{bb}})$ (2.79) for given qubit and bfl parameters ($\Delta_{\mathrm{q}} = \epsilon_{\mathrm{q}} = 10^{10}$ Hz, $\Delta_{\mathrm{bfl}} = 0.1\epsilon_{\mathrm{bfl}} = \frac{10^9}{\sqrt{1.01}}$ Hz, $\alpha = 0.01$) at low and high frequently bfl-noise (*i.e.* $\lambda = 100$, respectively $\lambda = 1000$) we observe the following behaviour.

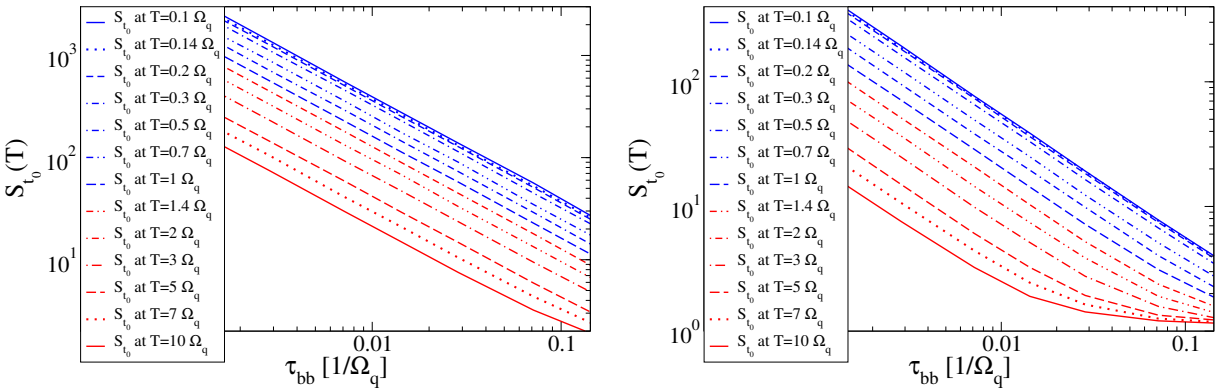

Figure 2.34: Suppression factors of bang-bang refocusing, applied on bfl-noise of various temperatures (between $T_{\mathrm{min}} = 0.0014\Omega_q$ and $T_{\mathrm{max}} = 0.14\Omega_q$), evaluated at time $t_0 = 10^{-7}$ s. Besides usual qubit and bfl properties ($\Delta_{\mathrm{q}} = \epsilon_{\mathrm{q}} = 10^{10}$ Hz, $\Delta_{\mathrm{bfl}} = \frac{10^9}{\sqrt{1.01}}$ Hz, $\epsilon_{\mathrm{bfl}} = \frac{10^{10}}{\sqrt{1.01}}$ Hz and $\alpha = 0.01 \cdot 10^{10}$ Hz), we consider compareably low and high frequency bfl-noise given by $\lambda = 100$ (left plot), respectively $\lambda = 1000$ (right plot).

Obviously for the low-frequent bfl case we receive in good accuracy the expected linear dependence of the suppression factor on the time scale ratio $\tau_{\mathrm{bfl}}/\tau_{\mathrm{bb}}$ (*i.e.* antilinear in τ_{bb}). In the high-frequent bfl situation we recognize for higher temperatures and lower τ_{bb}, that comparable bfl and bang-bang time scales lead to vanishing compensation efficiency and to a saturation effect of $\mathcal{S}_{t_0}(\tau_{\mathrm{bfl}}/\tau_{\mathrm{bb}}) \overset{\tau_{\mathrm{bfl}}/\tau_{\mathrm{bb}} \to 1}{\longrightarrow} 1$. If one consider the temperature dependence of the suppression ratio for given bang-bang periods (Fig. 2.35), one can see similarily how the bfl-noise compensation saturates for higher temperatures and lower bang-bang pulse frequencies converging to almost no positive effect.

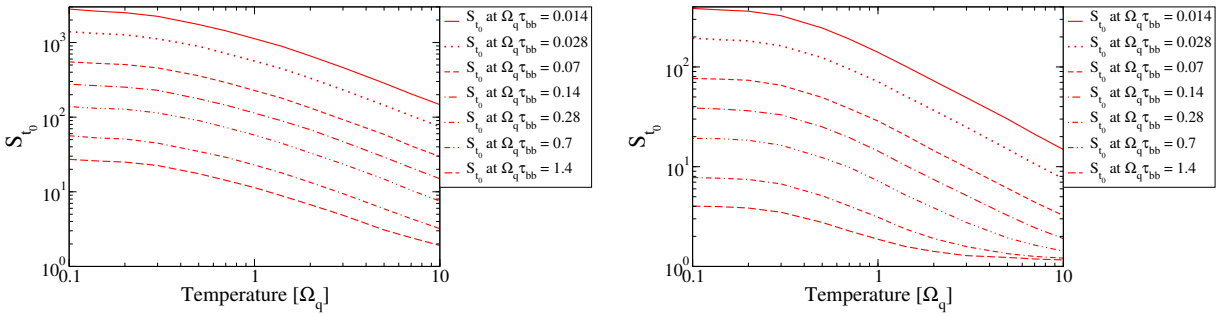

Figure 2.35: Suppression factors of various bang-bang pulse periods (τ_{bb} from 10^{-13}s to 10^{-11}s), applied on bfl-noise as function of temperatures (between $T_{\mathrm{min}} = 0.01$ K and $T_{\mathrm{max}} = 1$ K), evaluated at time $t_0 = 10^{-7}$ s. Given usual qubit and bfl properties ($\Delta_{\mathrm{q}} = \epsilon_{\mathrm{q}} = 10^{10}$ Hz, $\Delta_{\mathrm{bfl}} = \frac{10^9}{\sqrt{1.01}}$ Hz, $\epsilon_{\mathrm{bfl}} = \frac{10^{10}}{\sqrt{1.01}}$ Hz and $\alpha = 0.01 \cdot 10^{10}$ Hz), we considered compareably low (left) and high (right) frequent bfl-noise (corresponding to $\lambda = 100$, respectively $\lambda = 1000$).

2.5.7 Applicability of imperfect bang-bang pulses

Thus far, we have tacitly assumed that one is capable to produce perfect, zero-width π-pulses exactly along the $\hat{\sigma}_{\mathrm{x}}$-axis of the Bloch sphere. We now take into account, that the control pulses themselves can have slight fluctuations in regard of their duration or direction. This would interfere with the desired refocusing. As already shown at the end of section2.5.2, the restriction of pulses to infinitesimal duration can be significantly relaxed. Now we investigate to what extent the restriction to perfectly applied pulses can be relaxed.

We essentially analyze two generic types of errors that could occur in the control apparatus when trying to apply π-pulses in $\hat{\sigma}_{\mathrm{x}}$-direction. At first, the duration of each pulse could exhibit fluctuations, preoducing fluctuations in the resulting rotation-angle around the desired value of π. Secondly, the polarization axis could suffer from directional deviations around the desired direction (*i.e.* of $\hat{\sigma}_{\mathrm{x}}$). Assuming the statistical independence of each pulse error, we expect for both types of imperfections a random-walk-like behaviour of cumulating deviations compared to evolutions with perfect pulses.

One-dimensional pulse error (dephasing)

We make the quite general assumption that we may model the one-dimensional phase fluctuation of the imperfect bang-bang pulses $\phi_j(x)$ as a Gaussian distribution of the pulse durations and therefore of the rotation angles around their intended value π. This is no crucial restriction, as we expect that any roughly symmetric and smooth distribution of fluctuations will produce Gaussian formed total distributions after several inaccurate bang-bang steps, satisfying the central limit theorem. The Gaussian distribution is parameterized by its standard deviation $\delta\phi_0$ (see Fig. 2.36). Thus, the corresponding pulse angle

aberration of the jth step is given by

$$\phi_j^{1\mathrm{d}}(x) \;=\; \frac{1}{\sqrt{2\pi}\delta\phi_0} e^{-\frac{x^2}{2\delta\phi_0{}^2}} \quad . \tag{2.81}$$

Having assumed a Gaussian distribution, we can exactly evaluate the distributions of the N-step deviation $\Delta\Phi_N$ (which are usually given as N-fold time-convoluted integrals) by use of the convolution theorem as follows

$$\begin{aligned} \Phi_N^{1\mathrm{d}} &= \mathscr{F}^{-1}\left[\Pi_{j=1}^N \tilde{\phi}_j\right] \\ &= \frac{1}{\sqrt{2\pi N}\delta\phi_0} e^{-\frac{x^2}{2N\delta\phi_0{}^2}} \end{aligned} \tag{2.82}$$

with $\tilde{\phi}_j^{1\mathrm{d}} = \mathscr{F}[\phi_j]$ denoting the Fourier transformed of $\phi_j^{1\mathrm{d}}$ and $\mathscr{F}^{-1}$ the inverse Fourier transformation.

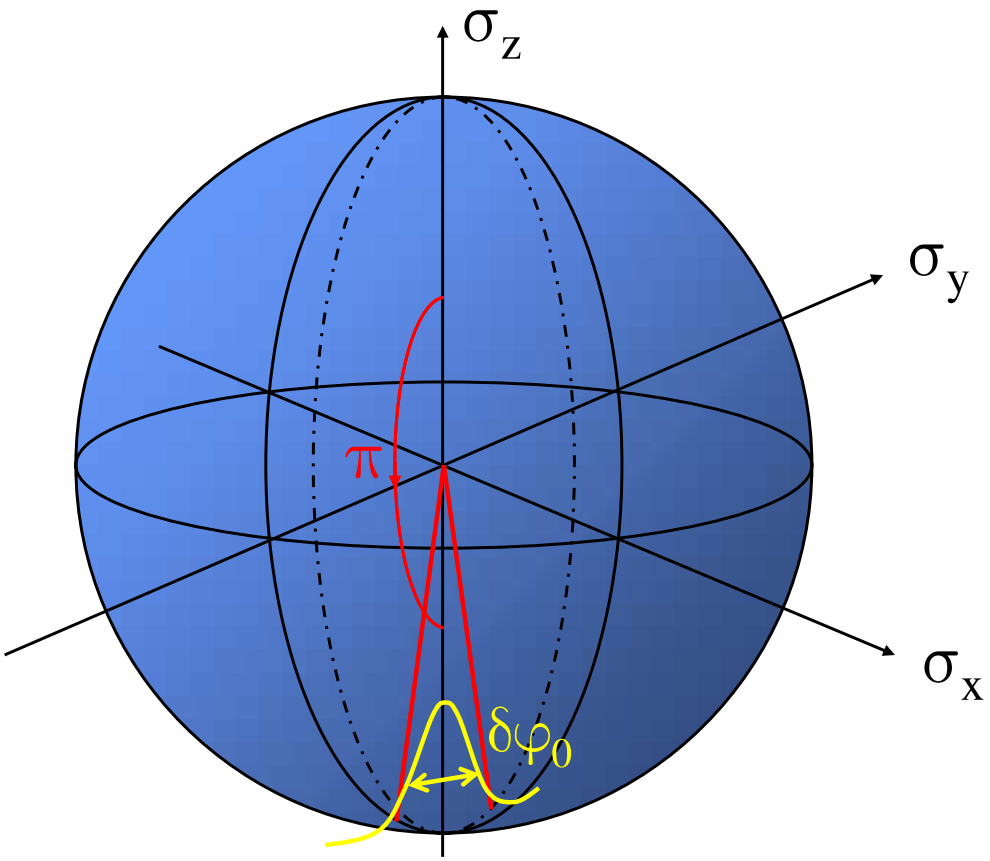

Figure 2.36: Sketch of one-dimensional bang-bang aberration. The variations $\delta\phi_0$ of the rotation angle around the desired value of π leads to slight deviations in parallel to the permitted dynamical direction, thus generating dephasing.

Consequently the rms displacement in the random walk increases as square-root of the number N of bang-bang pulses: $\delta\phi_N = \sqrt{N}\delta\phi_0$. Equivalently, the dephasing grows as square-root in time

$$\delta\phi(t) = \sqrt{t/\tau_{\rm bb}}\delta\phi_0 \tag{2.83}$$

on the time scale of our coarse-graining (which is here given as $\tau_{\rm bb}$).

Two-dimensional pulse error (dephasing as well as relaxation/excitation)

A similar argument works when there appear fluctuations around the desired $\hat{\sigma}_{\rm x}$ rotation axis. Each individual variation of the axis can be split into two components: (1) $\delta\phi_{\rm perp}$, which is perpendicular to the connecting vector between the $\hat{\sigma}_{\rm x}$-axis and the qubit state $\vec{\sigma}(t)$ on the Bloch sphere, and (2) $\delta\phi_{\rm tan}$, which is transverse to it (see Fig. 2.37). To first order, the perpendicular part does not disturb the intended spin-flip [2]. However, the transverse part does cause a deviation from the ideal spin-flip in a direction toward or away from the previous qubit state. Therefore, it produces relaxation or excitation, as its effect is orthogonal to the free $\hat{\sigma}_{\rm x}$-evolution. In a statistical average we only have to consider a fraction of $1/\sqrt{2}$ of the typical total mean $\delta\phi_0$ of the aberration. The effect of a π-rotation around an axis tilted by an angle $\delta\phi_{\rm tan}$ is a deviation $2\delta\phi_{\rm tan}$ from the trajectory of the perfect evolutions; thus we receive altogether a deviation on the order of $\sqrt{2}\delta\phi_0$.

From there we obtain analogously to Equ. (2.81) for each single step distribution

$$\phi_j^{\rm 2d}(x) \;=\; \frac{1}{\sqrt{2\pi}\sqrt{2}\delta\phi_0} e^{-\frac{x^2}{4{\delta\phi_0}^2}} \;; \tag{2.84}$$

and analogously to Equ. 2.82 for the deviation after N steps

$$\Phi_N^{\rm 2d} \;=\; \frac{1}{\sqrt{2\pi}\sqrt{2N}\delta\phi_0} e^{-\frac{x^2}{4N{\delta\phi_0}^2}} \;. \tag{2.85}$$

Equivalently, in terms of the time t

$$\delta\phi(t) = \sqrt{2t/\tau_{\rm bb}} \cdot \delta\phi_0 \;. \tag{2.86}$$

2.5.8 Numerical and analytical results

In the same manner as our previous integrations of a stochastic Schrödinger equation, we numerically simulate qubit dynamics under inaccurate pulses. In the first instance, we work without bfl-noise to verify our analytical random walk model. Later, we add the bfl-noise in order to study the competition between the two sources of error.

[2] The attentive reader might object here, that a spin-flip around a different axis on the xy-equator does not commute with pure $\hat{\sigma}_{\rm x}$-dynamics, but rather with something nearby. As we do not consider any $\hat{\sigma}_{\rm y}$-components yet, we do not bother about the minimal distortion of pure $\hat{\sigma}_{\rm x}$-operations, which can be estimated to be on the 2^{nd} order of the aberration parameter $\delta\phi_0$, which we assume to be very small anyway.

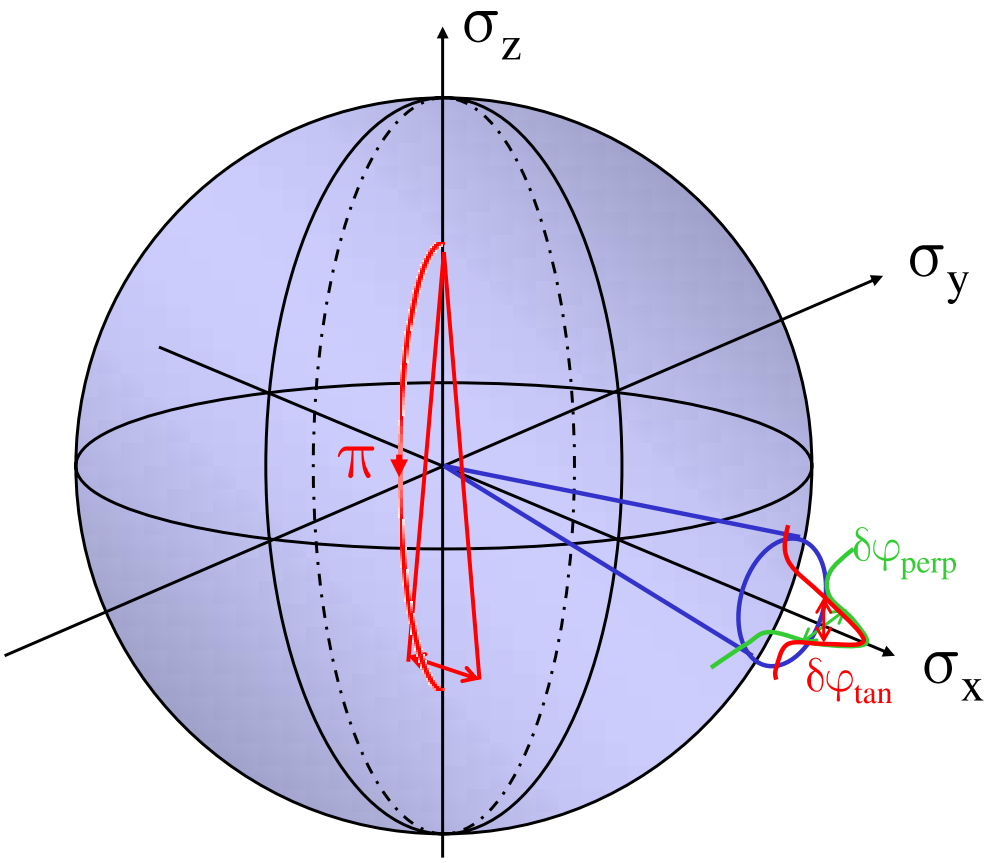

Figure 2.37: Sketch of two-dimensional bang-bang aberration. To first order, variations $\delta\phi_{\mathrm{perp}}$ of the rotation axis perpendicular to the connection vector between σ_{x} and the qubit state (here for simplicity: $\sigma_{\mathrm{z}} = +1$) do not influence the intended spin-flip, whereas the variations $\delta\phi_{\mathrm{tan}}$ along this line causes deviations on the Bloch sphere perpendicular to the permitted evolution trajectories (therefore producing relaxation or excitation).

Random walk due to inaccurate bang-bang pulses only

We analyze deviations on the Bloch sphere between the noiseless case trajectories that occur when the bang-bang pulses are perfect and those when they are not. As described in eq. (2.33), we calculate the rms-deviation over ensembles of $N = 10^3$ realizations. As a representative time point we take $t_0 = \tau_{\mathrm{Sys}}$. This is an appropriate choice, as explained in the discussion of Fig. 2.13, this time scale should exhibit neither short-time effects nor near-total decoherence. From eq. (2.83) and (2.86) it immediately follows, that for the mean deviations at t_0 results if there are phase errors

$$\Delta\sigma_{\mathrm{bb}}^{\mathrm{1d}}(t_0) \;=\; \sqrt{N_{\mathrm{bb}}}\delta\phi_0 \;=\; \sqrt{\frac{t_0}{\tau_{\mathrm{bb}}}}\delta\phi_0 \;, \tag{2.87}$$

and if there are axis errors

$$\Delta\sigma_{\rm bb}^{\rm 2d}(t_0) \;=\; \sqrt{2N_{\rm bb}}\delta\phi_0 \;=\; \sqrt{2\frac{t_0}{\tau_{\rm bb}}}\delta\phi_0 \;. \tag{2.88}$$

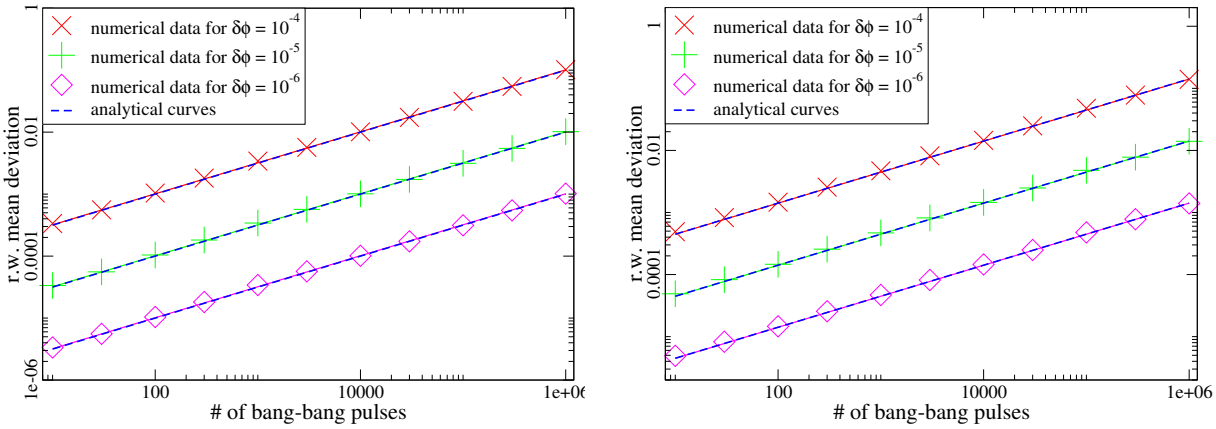

Figure 2.38: Plot of the one- respectively two-dimensional imperfectly bang-bang pulsed evolution. Dashed lines are square-root fits of the numerical data, while the solid lines denotes the analytical calculations.

As characteristic values for the mean accuracy of single pulses, we choose $\delta\phi_0$ in the range of 10^{-6} to 10^{-4}, which should be technologically feasible. As one can see in the double logarithmic plots of Fig. 2.38, the numerically determined evolutions follow the analytically expected square-root type random walk behavior.

Random walk due to inaccurate bb-pulses and bfl-noise

We now combine our imperfect bang-bang pulse operations with our former bfl-noise signal to discuss the applicability of our control scheme when realistic pulse generators are used. As before, we calculate the rms deviations at $t_0 = \tau_{\rm Sys}$ by averaging over 10^3 realizations. The bfl-parameters are the same used previously: a coupling strength $\alpha = 0.1$ and an average switching time $\tau_{\rm bfl} = 0.01\tau_{\rm Sys}$. However, with the aim of determining the optimal bang-bang protocol in the presence of pulse imperfections, we now consider different pulse separation times $\tau_{\rm bb}/\tau_{\rm Sys}$ ranging from 10^{-5} to 10^{-2}.

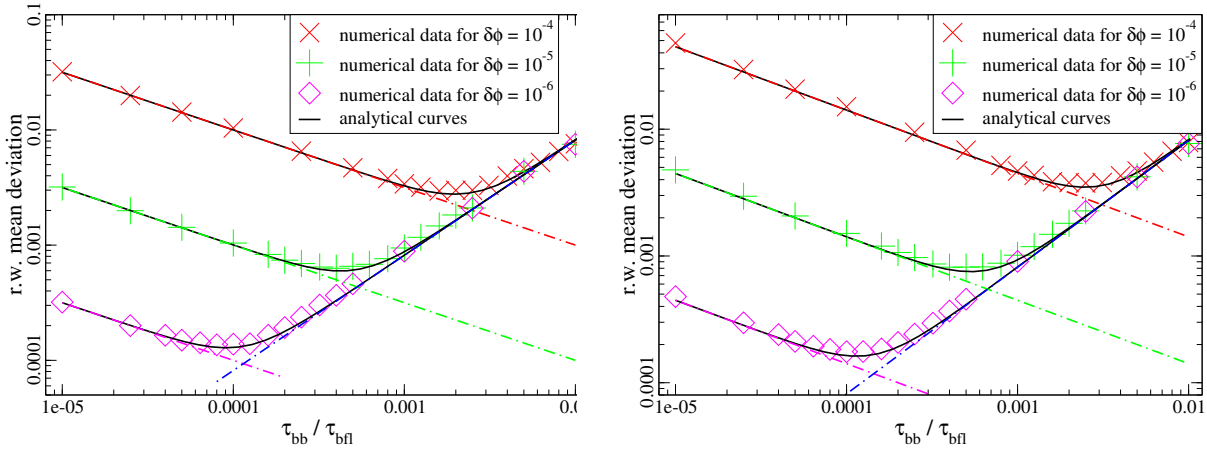

Figure 2.39: Plot of the Bloch sphere rms deviations received by one-/two-dimensional inaccurately pulsed bang-bang compensation of the typical bfl-perturbation. Dashed lines describe the aberrances for pure faulty bang-bang (*i.e.* without bfl-noise), respectively the exactly compensated bfl-case (see Fig. 2.13), while solid lines denotes the deviations calculated by random walk analysis.

We assume that the errors induced by the bfl and those induced by the pulse generator are statistically independent, and thus we can add them in the usual rms-fashion. In comparison to the case of ideal bang-bang pulses, eq. (2.76), we find here the average total deviations induced by both bfl telegraph noise and imperfect bang-bang pulses to be

$$\begin{aligned} \Delta\sigma_{\rm tot}^{1d} &= \sqrt{\Delta\sigma_{\rm bfl}^2 + \Delta\sigma_{\rm bb}^{1d\,2}} \\ &= \sqrt{\frac{1}{2}N_{\rm bfl}\alpha^2\tau_{\rm bb}^2 + N_{\rm bb}\delta\phi_0^2} \\ &= \sqrt{\frac{1}{2}\alpha^2\tau_{\rm bb}^2\frac{t_0}{\tau_{\rm bfl}} + \delta\phi_0^2\frac{t_0}{\tau_{\rm bb}}} \end{aligned} \tag{2.89}$$

in the one-dimensional case where imperfect pulses only impart phase errors (due to imprecise pulse duration), and

$$\begin{aligned} \Delta\sigma_{\rm tot}^{2d} &= \sqrt{\Delta\sigma_{\rm bfl}^2 + \Delta\sigma_{\rm bb}^{2d\,2}} \\ &= \sqrt{\frac{1}{2}N_{\rm bfl}\alpha^2\tau_{\rm bb}^2 + 2N_{\rm bb}\delta\phi_0^2} \\ &= \sqrt{\frac{1}{2}\alpha^2\tau_{\rm bb}^2\frac{t_0}{\tau_{\rm bfl}} + 2\delta\phi_0^2\frac{t_0}{\tau_{\rm bb}}} \end{aligned} \tag{2.90}$$

in the two-dimensional case when imperfect pulses impart both phase and relaxation/excitation errors (due to imprecision in the pulses' polarization axis).

As Fig. 2.39 demonstrates, we observe a very good agreement between our numerical and analytical results. Such data make it possible to determine an optimal bang-bang separation time $\tau_{\mathrm{bb}}^{\mathrm{opt}}$. Specifically, this optimum can be derived by calculating the zero value of the derivative of eq. (2.89) and (2.90) with respect to τ_{bb}. We therefore conclude that the optimal period between bang-bang pulses is

$$\tau_{\mathrm{bb}}^{1d} = \sqrt[3]{\tau_{\mathrm{bfl}}\frac{\delta\phi_0^2}{\alpha^2}} \tag{2.91}$$

for the one-dimensional case and

$$\tau_{\mathrm{bb}}^{2d} = \sqrt[3]{2\tau_{\mathrm{bfl}}\frac{\delta\phi_0^2}{\alpha^2}} \tag{2.92}$$

for the two-dimensional case. These optimal times respectively correspond to minimized variances at $t_0 = \tau_{\mathrm{Sys}}$ of

$$\Delta\sigma_{\mathrm{opt}}^{1d} = \sqrt{\frac{1}{2}+1}\frac{\alpha^{1/3}\delta\phi_0^{2/3}}{\tau_{\mathrm{bfl}}^{1/6}}\sqrt{t_0} \tag{2.93}$$

for the one-dimensional case of only imprecise pulse durations and

$$\Delta\sigma_{\mathrm{opt}}^{2d} = \sqrt{2^{-1/3}+2^{2/3}}\frac{\alpha^{1/3}\delta\phi_0^{2/3}}{\tau_{\mathrm{bfl}}^{1/6}}\sqrt{t_0} \tag{2.94}$$

for the two-dimensional case of both imprecise pulse durations and polarization axis.

Chapter 3

Quantum phase diagram of a coupled qubit system

In this chapter we investigate the disappearance of coherence as well as entanglement of a coupled two spin system attached to two different sorts of bosonic Baths, which represents localized and collective error sources. In contrast to our former decoherence analysis, we do not to focus on time evolutions, generated by appropriate master equations. We are rather interested in the occurrence, respectively suppression of coherence and entanglement of the two-spin system as a function of the dissipative coupling strengths to both kinds of baths. Thus we will mainly discuss static features of the dressed double spin system, technically after having derived an effective pure spin Hamiltonian, that only implicitly depends on the bath couplings. These dynamical and entanglement properties hereby were derived by considering the corresponding *fixed point Hamiltonian*, derived by means of an appropriate scaling analysis of the effective spin-operators couplings.

3.1 The 2-spins-3-bosonic-baths model

The theoretical model is constituted as follows; two spins with local coherent dynamics given by $\Delta_0\hat{\sigma}_j^x$ were coupled to each other by a $\hat{\sigma}_1^y \otimes \hat{\sigma}_2^y$ type interaction of the strength $\Delta_{\rm I}$. This quantum system itself is attached to one common Bosonic bath via a $(\hat{\sigma}_1^z + \hat{\sigma}_2^z)$-term, as well as to two local baths, whose interaction is also of $\hat{\sigma}_j^z$-form. This pareticular choice of coupling offers maximal mutual interactions of the coupling, as none of them commute with the others.

The total 2-spin-3-baths Hamiltonian reads as follows

$$\hat{H}_{\rm 2s3b} = \hat{H}_{\rm S_1} + \hat{H}_{\rm S_2} + \hat{H}_{\rm S_{12}} + \hat{H}_{\rm S_1,B_{local}} + \hat{H}_{\rm S_2,B_{local}} + \hat{H}_{\rm S,B_{coll}} + \hat{H}_{\rm B} \ , \tag{3.1}$$

with intra-spin dynamics on the j^{th} spin

$$\hat{H}_{\rm S_j} = \frac{\Delta_0}{a}\hat{\sigma}_j^x \tag{3.2}$$

and spin-spin coupling of Ising type

$$\hat{H}_{\mathrm{S}_{12}} = \frac{\Delta_I}{a}\left(\hat{\sigma}_1^y \otimes \hat{\sigma}_2^y\right) \quad . \tag{3.3}$$

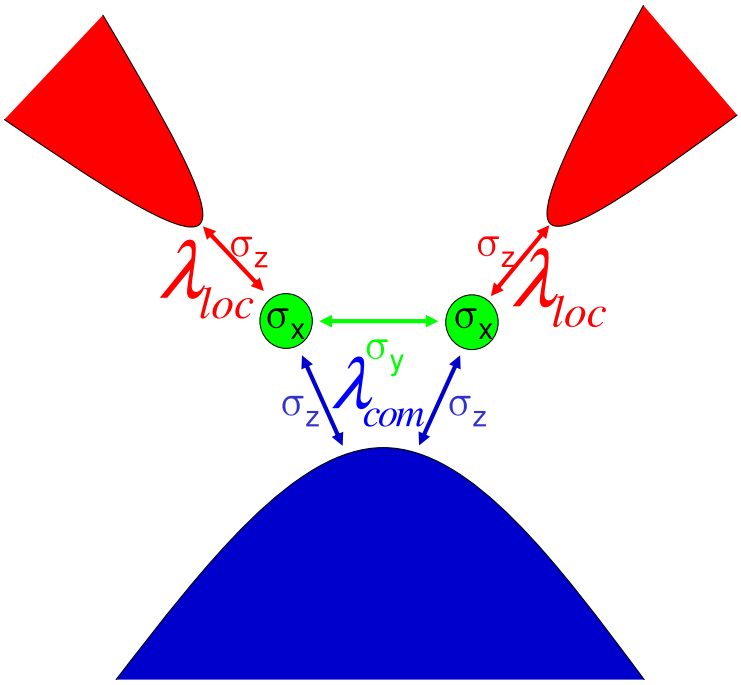

Figure 3.1: Schematic plot of a 2-spin-3-Bosonic-baths model. In order to receive a maximal degree of mutual influences of the different interactions, non-commutativity for the single-spin, the double-spin, as well as the bath-spin couplings is chosen.

The normalization factor $1/a$ corresponds to the band-width of the Bosonic bath. The coupling to the dissipative baths is distinguished into the localized parts

$$\hat{H}_{\mathrm{S_j,B_{local}}} = \frac{1}{2}\lambda_{\mathrm{local}}\hat{\sigma}_j^z\frac{\partial\Phi_j}{\partial x} \tag{3.4}$$

and the collective one

$$\hat{H}_{\mathrm{SB_{coll}}} = \frac{1}{2}\lambda_{\mathrm{coll}}\left(\hat{\sigma}_1^z + \hat{\sigma}_2^z\right)\frac{\partial\Phi_3}{\partial x} \quad , \tag{3.5}$$

while dynamics of the bosonic baths are given in field theoretical notation [68] by

$$\hat{H}_{\mathrm{B}} = \sum_{\mu\in\{1,2,3\}}\int_{-L/2}^{L/2}\frac{1}{2}{}^{*}_{*}\left[\partial_x\Phi_\mu(x)\right]^2{}^{*}_{*}\frac{dx}{2\pi} + \frac{2\pi}{2L}\hat{N}_\mu\left(\hat{N}_\mu + 1 - \delta_{\mathrm{boundary}}\right) \quad , \tag{3.6}$$

which is equivalent to the harmonic oscillator bath representation used in chapter 1.

L denotes the (usually spatial) size of the Bosonic system(s), $\partial_x \Phi$ ist abbreviated for $\frac{\partial \Phi(x)}{\partial x}$, $\hat{N}_\mu$ were the corresponding Bosonic excitation number operators. δ_{boundary} takes into account boundary conditions (*e.g.* periodic or anti-periodic ones), for details [68] and references therein are recommended.

Note also, that this description of the origin of decoherence as bosonic baths does not necessarily disqualify fermionic noise sources (*e.g.* as one encounters with fluctuation of electronic leads), as in particular fermi sea environments can formally be interpreted bosonically by use of appropriate bosonization rules (see [68]).

A possible experimental realization of this setup would appear as suggested in Fig. 3.2. Here the $\hat{\sigma}_x^j$ type dynamics on the spins would be driven by the embraced magnetic flux of two Josephson flux qubit. The spin-spin interaction $\hat{\sigma}_1^y \otimes \hat{\sigma}_2^y$ could be implemented by an electro-magnetic coil, while the collective, as well as localized noise sources would be given by the impedances of the common, respectively individual supply lines.

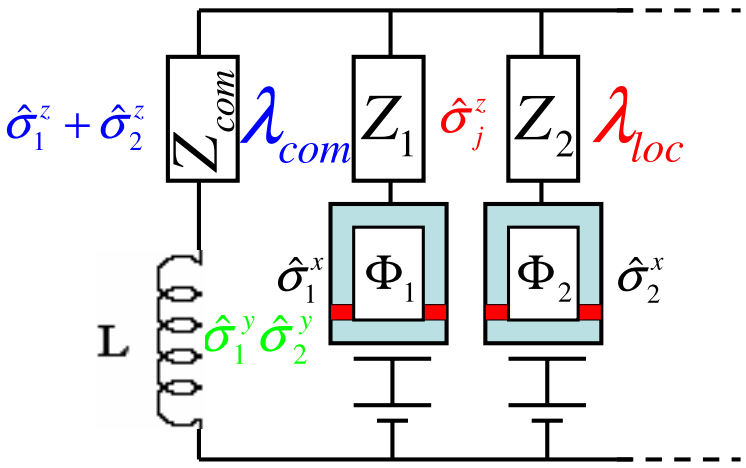

Figure 3.2: Schematic plot of the electric circuit realization of the 2-spin-3-Bosonic-baths model by means of Josephson flux qubits. The $\hat{\sigma}_j^x$ coupling on each spin is controlled by the enclosed magnetic field, while the spin-spin interaction is given by an external coil. The localized, as well as common bath coupling is generated by the dissipative impedances in the single, respectively common supply lines.

3.2 The dressed double-spin Hamiltonian

In the following we want to apply an appropriate unitary transformation (the Emery-Kivelson transformation [69, 70]) on the 2-spins-3-Bosonic-baths Hamiltonian. This is in order to receive an expression, which explicitly only depends on effective (so-called dressed) spin degrees of freedom. At first we therefor have to reorder some terms, for technical reasons as well as for making the symmetry effects of our transformation more visible.

For the spin-bath Hamiltonian we combine the collective and the localized terms to a symmetric and an antisymmetric part of spin-bath interaction

$$\begin{aligned}\hat{H}_{\mathrm{SB}} &= \hat{H}_{\mathrm{S,B_{coll}}} + \hat{H}_{\mathrm{S_1,B_{local}}} + \hat{H}_{\mathrm{S_2,B_{local}}} \\ &= \frac{1}{2}\left(\hat{\sigma}_1^z + \hat{\sigma}_2^z\right)\left(\lambda_{\mathrm{coll}}\partial_x\Phi_3 + 1/\sqrt{2}\lambda_{\mathrm{local}}\partial_x\Phi_S\right) + \\ &\quad + \frac{1}{2}\left(\hat{\sigma}_1^z - \hat{\sigma}_2^z\right)1/\sqrt{2}\lambda_{\mathrm{local}}\partial_x\Phi_A \\ &= \frac{1}{2}\left(\hat{\sigma}_1^z + \hat{\sigma}_2^z\right)\lambda_S\partial_x\Phi_S + \frac{1}{2}\left(\hat{\sigma}_1^z - \hat{\sigma}_2^z\right)\lambda_{\mathrm{A}}\partial_x\Phi_A \ , \end{aligned} \tag{3.7}$$

here we introduced for the sake of clarity as new coupling constants and Bosonic fields

$$\lambda_S = \sqrt{\lambda_{\mathrm{coll}}^2 + \frac{\lambda_{\mathrm{local}}^2}{2}} \tag{3.8}$$

$$\partial_x\Phi_S = \frac{1}{\tilde{\lambda}}\left(\lambda_{\mathrm{coll}}\partial_x\Phi_3 + 1/\sqrt{2}\lambda_{\mathrm{local}}\left(\partial_x\Phi_1 + \partial_x\Phi_2\right)\right) \tag{3.9}$$

for the symmetric case and

$$\lambda_A = \frac{\lambda_{\mathrm{local}}}{\sqrt{2}} \tag{3.10}$$

$$\partial_x\Phi_A = \frac{1}{\sqrt{2}}\left(\partial_x\Phi_1 - \partial_x\Phi_2\right) \tag{3.11}$$

for the antisymmetric one.

For the single as well as double-spin interactions we replace the former Pauli-spin matrix terms $\hat{\sigma}_j^x$, $\hat{\sigma}_j^y$ and $\hat{\sigma}_j^z$ by corresponding combinations of $\hat{\sigma}_j^{\pm}$ operators defined by

$$\hat{\sigma}_j^{\pm} = \frac{1}{2}\left(\hat{\sigma}_j^x \pm i\hat{\sigma}_j^y\right) \ , \tag{3.12}$$

such that

$$\hat{H}_{\mathrm{S_j}} = \frac{\Delta_0}{a}\hat{\sigma}_j^x = \frac{\Delta_0}{a}\left(\hat{\sigma}_j^+ + \hat{\sigma}_j^-\right) \ , \tag{3.13}$$

and

$$\hat{H}_{\mathrm{S}_{12}} = \frac{\Delta_I}{a}\left(\hat{\sigma}_1^y\hat{\sigma}_2^y\right) = \frac{\Delta_I}{a}\left[-\left(\hat{\sigma}_1^+\hat{\sigma}_2^+ + h.c.\right) + \left(\hat{\sigma}_1^+\hat{\sigma}_2^- + h.c.\right)\right] \quad . \tag{3.14}$$

This is useful, as the latter transformation relations for the $\hat{\sigma}_j^{\pm}$-terms are more easy to calculate. Anyway, as $\hat{\sigma}_j^{\pm}$ represents spin-up respectively spin-down flips, the mathematical results later on obtain easy to recognize physical interpretations.

As we furthermore will encounter different scaling behaviour for the $\hat{\sigma}_1^{\pm}\hat{\sigma}_2^{\pm}$ terms as for to the $\hat{\sigma}_1^{\pm}\hat{\sigma}_2^{\mp}$ ones, we will introduce here distinct coupling constants for both terms

$$\hat{H}_{\mathrm{S}_{12}} = \frac{\Delta_{++}}{a}\left(\hat{\sigma}_1^+\hat{\sigma}_2^+ + h.c.\right) + \frac{\Delta_{+-}}{a}\left(\hat{\sigma}_1^+\hat{\sigma}_2^- + h.c.\right) \quad . \tag{3.15}$$

3.2.1 The Emery-Kivelson-transformation

The Emery-Kivelson-transformation [69, 70] for our two different bath terms (symmetric and antisymmetric)is given as

$$U(\alpha,\beta) = \exp\left[i\left(\alpha\frac{1}{2}\left(\hat{\sigma}_1^z + \hat{\sigma}_2^z\right)\Phi_S + \beta\frac{1}{2}\left(\hat{\sigma}_1^z - \hat{\sigma}_2^z\right)\Phi_{\mathrm{A}}\right)\right] \quad . \tag{3.16}$$

If we apply this unitary transformation on our total Hamiltonian

$$\hat{H}_{\mathrm{2s3b}}^{\mathrm{dressed}} := U(\alpha,\beta)\hat{H}_{\mathrm{2s3b}}U^{\dagger}(\alpha,\beta) \tag{3.17}$$

some algebra following the Bosonic commutation relation

$$[\Phi, \partial_x\Phi] = i\mathbb{1} \tag{3.18}$$

via the Baker-Hausdorff-formula (appendix C in [68])

$$\exp\left(i\gamma\Phi\right)\left[\partial_x\Phi\right]^2\exp\left(-i\gamma\Phi\right) = \left[\partial_x\Phi - \gamma\mathbb{1}\right]^2 \tag{3.19}$$

leads from $\hat{H}_B$ to prefactor changes of the explicit bath-spin interactions of

$$\begin{aligned}\hat{H}_{\mathrm{B}}^{\mathrm{dressed}} + \hat{H}_{\mathrm{SB}}^{\mathrm{dressed}} = & \sum_{\mu\in\{1,2,3\}}\int_{-L/2}^{L/2}\frac{1}{2}{}^*_*\left[\partial_x\Phi_\mu(x)\right]^2{}^*_*\frac{dx}{2\pi} + \frac{2\pi}{2L}\hat{N}_\mu\left(\hat{N}_\mu + 1 - \delta_{\mathrm{boundary}}\right) + \\ & + \frac{1}{2}\left(\hat{\sigma}_1^z + \hat{\sigma}_2^z\right)\left(\lambda_S - \alpha\right)\partial_x\Phi_S + \frac{1}{2}\left(\hat{\sigma}_1^z - \hat{\sigma}_2^z\right)\left(\lambda_A - \beta\right)\partial_x\Phi_A + \\ & + \text{ constant terms} \quad ,\end{aligned} \tag{3.20}$$

such that the explicit spin-bath term $\hat{H}_{\rm SB}$ of the 2s3B-Hamiltonian disappears for the choice

$$\alpha = \lambda_S \qquad \beta = \lambda_A. \tag{3.21}$$

Here we disregard any constant offsets, we receive from $\hat{H}_B^{\rm dressed}$ and $\hat{H}_{SB}^{\rm dressed}$. A more detailed discussion can be found [71].

According the spin-operator commutation rules

$$\left[\hat{\sigma}_j^z, \hat{\sigma}_k^{\pm}\right] = \pm\delta_{j,k}\hat{\sigma}_k^{\mp} \tag{3.22}$$

and Baker-Hausdorff

$$\exp\left(i\delta\left(\hat{\sigma}_1^z + \hat{\sigma}_2^z\right)\right)\hat{\sigma}_j^{\pm}\exp\left(-i\delta\left(\hat{\sigma}_1^z + \hat{\sigma}_2^z\right)\right) = \hat{\sigma}_j^{\pm}\exp\left(\mp i\delta\right) \ , \tag{3.23}$$

respectively

$$\exp\left(i\delta\left(\hat{\sigma}_1^z - \hat{\sigma}_2^z\right)\right)\hat{\sigma}_j^{\pm}\exp\left(-i\delta\left(\hat{\sigma}_1^z - \hat{\sigma}_2^z\right)\right) = \hat{\sigma}_j^{\pm}\exp\left(\pm(-1)^j i\delta\right) \ , \tag{3.24}$$

the $\hat{\sigma}_j^{\pm}$ and $\hat{\sigma}_1^+\hat{\sigma}_2^{\pm}$ terms transform as follows

$$\hat{\sigma}_1^{\pm} \mapsto \hat{\sigma}_1^{\pm}e^{\mp i(\lambda_S\Phi_S + \lambda_A\Phi_A)} \tag{3.25}$$
$$\hat{\sigma}_2^{\pm} \mapsto \hat{\sigma}_2^{\pm}e^{\mp i(\lambda_S\Phi_S - \lambda_A\Phi_A)} \tag{3.26}$$
$$\hat{\sigma}_1^+\hat{\sigma}_2^+ \mapsto \hat{\sigma}_1^+\hat{\sigma}_2^+e^{-2i\lambda_S\Phi_S} \tag{3.27}$$
$$\hat{\sigma}_1^+\hat{\sigma}_2^- \mapsto \hat{\sigma}_1^+\hat{\sigma}_2^-e^{-2i\lambda_A\Phi_A} \ . \tag{3.28}$$

With the following definition of vertex operators of the (anti)-symmetric Boson fields

$$\hat{V}_{\gamma}^S = a^{-\gamma^2/2}e^{i\gamma\Phi_S} \tag{3.29}$$
$$\hat{V}_{\delta}^A = a^{-\delta^2/2}e^{i\delta\Phi_A} \tag{3.30}$$

we can concisely rewrite the effective, dressed spin Hamiltonian parts to

$$\begin{aligned}\hat{H}_{\rm S_{local}}^{\rm dressed} &= \hat{H}_{\rm S_1}^{\rm dressed} + \hat{H}_{\rm S_2}^{\rm dressed} \\ &= a^{-y_0}\Delta_0\left[\hat{\sigma}_1^+\hat{V}_{-\lambda_S}^S\hat{V}_{-\lambda_A}^A + \hat{\sigma}_2^+\hat{V}_{-\lambda_S}^S\hat{V}_{\lambda_A}^A + h.c.\right] = a^{-y_0}\Delta_0\sqrt{2}\mathscr{O}_0\end{aligned} \tag{3.31}$$

for the local spin-couplings and to

$$\hat{H}_{\rm S_{12}}^{\rm dressed} = \hat{H}_{\rm S++}^{\rm dressed} + \hat{H}_{\rm S+-}^{\rm dressed} \tag{3.32}$$

with

$$\hat{H}_{\rm S++}^{\rm dressed} = a^{-y_{++}}\Delta_{++}\left[\hat{\sigma}_1^+\hat{\sigma}_2^+\hat{V}_{-2\lambda_S}^S + h.c.\right] = a^{-y_{++}}\Delta_{++}\sqrt{2}\mathscr{O}_{++} \tag{3.33}$$

and

$$\hat{H}^{\text{dressed}}_{\text{S}+-} = a^{-y_{+-}}\Delta_{+-}\left[\hat{\sigma}_1^+\hat{\sigma}_2^-\hat{V}^A_{-2\lambda_A} + h.c.\right] = a^{-y_{+-}}\Delta_{+-}\sqrt{2}\mathscr{O}_{+-} \tag{3.34}$$

for the spin-spin interactions. Note the exponents of the renormalization prefactors, which were depending on the original spin-bath couplings in the following way

$$y_0 = 1 - \frac{\lambda_S^2}{2} - \frac{\lambda_A^2}{2} = 1 - \frac{\lambda^2_{\text{local}} + \lambda^2_{\text{coll}}}{2} \tag{3.35}$$

$$y_{++} = 1 - 2\lambda_A^2 = 1 - \lambda^2_{\text{local}} \tag{3.36}$$

$$y_{++} = 1 - 2\lambda_S^2 = 1 - \lambda^2_{\text{local}} - 2\lambda^2_{\text{coll}} \tag{3.37}$$

due to the corresponding normalization factors of the respective vertex operators.

3.3 Scaling analysis and quantum phase diagram

3.3.1 Scaling equations 1^{st} order

The dressed-spin Hamiltonian $\hat{H}_{\mathrm{2s3b}}^{\mathrm{dressed}}$, derived in the previous section, turns out to be only implicitly depending on the Bosonic bath degrees of freedom. Firstly via the corresponding vertex operators and in consequence on the hereby received renormalization prefactors. If we now take into account, that these prefactors, respectively their according coupling factors Δ_0, Δ_{++} and Δ_{+-} do rescale in a certain way with respect to the band width a of the Bose fields, respectively the corresponding UV-cutoff, then we are able to formulate scaling equations of these couplings. In first order scaling theory they appear as follows (for detailed calculations see Appendix D.1)

$$\begin{aligned} \frac{\partial \Delta_0}{\partial a} &= y_0 \Delta_0 \\ \frac{\partial \Delta_{++}}{\partial a} &= y_{++} \Delta_{++} \\ \frac{\partial \Delta_{+-}}{\partial a} &= y_{+-} \Delta_{+-} \ . \end{aligned} \tag{3.38}$$

First order means here, that the exact scaling behaviour would involve also expressions of arbitrary powers of Δ_0, Δ_{++} and Δ_{+-}, but that we disregard all higher powers restricting ourselves on the regime of appropriately small coupling values.

If we now take a closer look on eq. (3.38), we evidently recognize exponential functions as solutions

$$\begin{aligned} \Delta_0(l) &\simeq \Delta_0(0) e^{y_0 l} \\ \Delta_{++}(l) &\simeq \Delta_{++}(0) e^{y_{++} l} \\ \Delta_{+-}(l) &\simeq \Delta_{+-}(0) e^{y_{+-} l} \ . \end{aligned} \tag{3.39}$$

Therefore we expect the solutions to scale to zero or infinity depending on the algebraic sign of the corresponding exponential factors y_0, y_{++} and y_{+-}. In the limit of diverging exponential solutions (if $y_j > 0$) we are obviously leaving the regime of first order scaling equations and higher order terms would guarantee limiting values. As consequence, we can draw (at least qualitatively) a diagram of the convergence regimes of the couplings in dependence of the local and collective coupling strength to the respective types of baths.

If one consider this first order scaling phase diagram (see Fig. 3.3), one recognizes the transition lines, where the corresponding exponential factors changes their sign. These represents the boundaries between phases with finite and vanishing values for the according dressed-spin couplings, which in consequence leads to different fixed point Hamiltonian (*i.e.* the effective dressed-spin Hamiltonian, received in the scaling limit $a \to \infty$). Phase number **1** denotes the *full quantum dynamical phase*, where each kind of interaction in

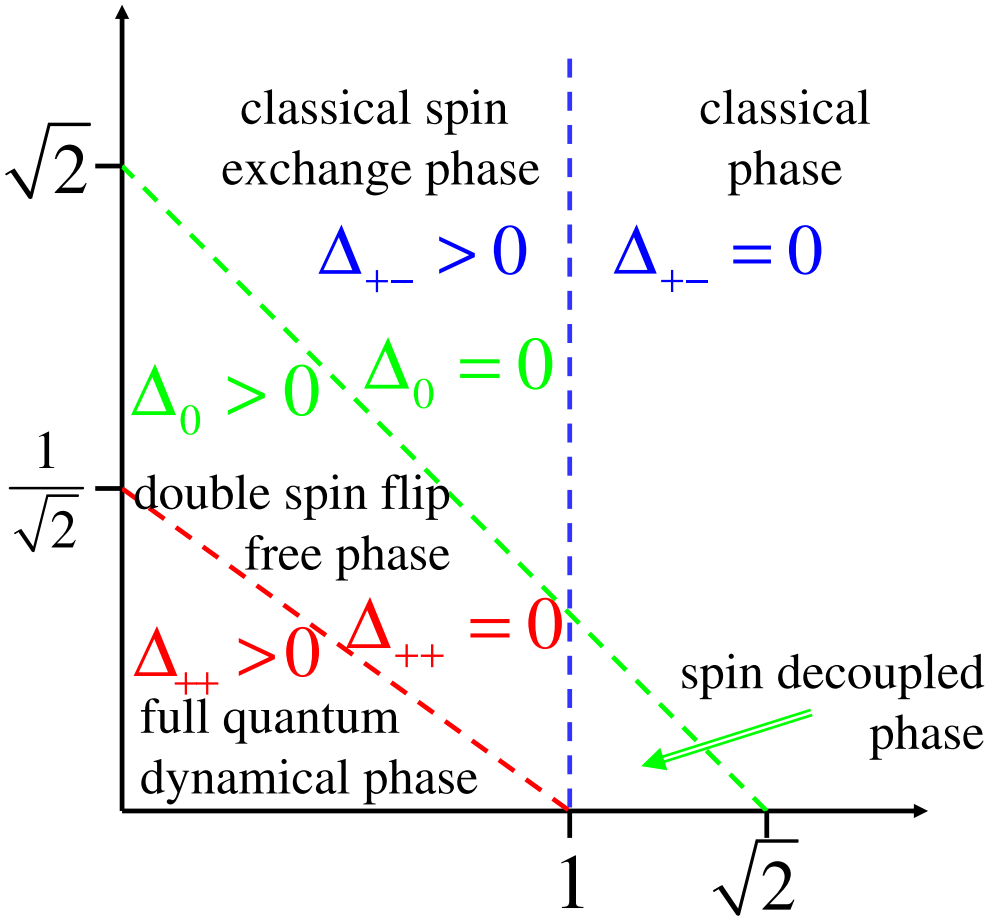

Figure 3.3: Schematic quantum phase diagram of the scaling convergence of the various terms of the dressed-spin Hamiltonian $\hat{H}_{\mathrm{2s3b}}^{\mathrm{dressed}}$. The different transition lines indicate, where the according coupling factors disappear in the $l \to 0$ limit. The numeration $1-5$ denotes the various parameter regimes with different effective dynamics of the dressed spins.

general is present. At the crossover to the *double-spin flip free phase* (number **2**) the coupling constant Δ_{++} of the double-spin flip terms $\mathscr{O}_{++}$ vanishes, as the compareably strong couplings to the local as well as common baths prevent this type of spin-spin process. If the localized bath coupling is even stronger, we obtain the *spin-decoupled phase* (number **3**), where even no spin-exchange of both qubits is possible. Less localized bath coupling ($\lambda_{\mathrm{loc}} < 1$), but larger collective bath interaction, generate the *classical spin-exchange phase* (number **4**), where still spin-exchange processes ($\Delta_{+-} > 0$) are admitted, although any quantum dynamics on each qubit is switched off. Finally we reach the *classical phase* (number **5**), where any kind of quantum dynamics is frozen, as both spins, together and individually, are too strongly observed by the two types of bath coupling. The corresponding Hamiltonian disappears.

3.3.2 Entanglement capability of the fixed point Hamiltonian

Besides the suppression of various effective spin-interactions, we also consider by means of the corresponding fixed point Hamiltonian [72], the entanglement capability of the two-qubit system in the different phase regimes. For these representatives of the different phase regimes we assumes the corresponding eigenstates to be the preferred, respectively permitted two spin states in regard of the environmental influences. For the sake of simplicity we restrict ourselves on simplified versions of the various fixed point Hamiltonian. Thereby we assume the non-vanishing coupling constants to be exactly one. This should be a sufficient choice to receive at least qualitative insights in the entanglement capability of the corresponding two spin regimes. In principle, a more detailed and quantitative analysis of the higher order scaling equations could be used to evaluate an appropriate entanglement measure (*e.g.* concurrence) for any initial spin-coupling values. But as any choice of initial coupling strengths is somehow arbitrary and could be realized by an appropriate physical setup, we are contented here with a bare structural discussion.

The different representatives for fixed point Hamiltonian were composed as follows. Considering the usual two-spin $\hat{\sigma}_z$ basis (where *e.g.* $|\uparrow,\uparrow\rangle$ denotes the product state, where both spins were up in the z-basis we obtain for the simplified fixed point Hamiltonian in the various quantum phase regimes

$$\begin{aligned}
\hat{H}_{\mathbf{1}}^{\text{fixed point}} &= \begin{pmatrix} 0 & 1 & 1 & 1 \\ 1 & 0 & 1 & 1 \\ 1 & 1 & 0 & 1 \\ 1 & 1 & 1 & 0 \end{pmatrix} \qquad \hat{H}_{\mathbf{2}}^{\text{fixed point}} = \begin{pmatrix} 0 & 1 & 1 & 0 \\ 1 & 0 & 1 & 1 \\ 1 & 1 & 0 & 1 \\ 0 & 1 & 1 & 0 \end{pmatrix} \\
\hat{H}_{\mathbf{3}}^{\text{fixed point}} &= \begin{pmatrix} 0 & 1 & 1 & 0 \\ 1 & 0 & 0 & 1 \\ 1 & 0 & 0 & 1 \\ 0 & 1 & 1 & 0 \end{pmatrix} \qquad \hat{H}_{\mathbf{4}}^{\text{fixed point}} = \begin{pmatrix} 0 & 0 & 0 & 0 \\ 0 & 0 & 1 & 0 \\ 0 & 1 & 0 & 0 \\ 0 & 0 & 0 & 0 \end{pmatrix} \\
\hat{H}_{\mathbf{5}}^{\text{fixed point}} &= \begin{pmatrix} 0 & 0 & 0 & 0 \\ 0 & 0 & 0 & 0 \\ 0 & 0 & 0 & 0 \\ 0 & 0 & 0 & 0 \end{pmatrix} .
\end{aligned} \tag{3.40}$$

Evidently we can derive for these fixed point Hamiltonian the following eigenvectors. For the *full quantum dynamical phase* (number **1**) we receive separable eigenstates

$$EV_{1/2}^{\mathbf{1}} = (|\uparrow\rangle + |\downarrow\rangle)(|\uparrow\rangle \pm |\downarrow\rangle) \ , \tag{3.41}$$

as well as maximally entangled (Bell) states

$$\begin{aligned}
EV_3^{\mathbf{1}} &= |\uparrow,\uparrow\rangle - |\downarrow,\downarrow\rangle \ , \\
EV_4^{\mathbf{1}} &= |\uparrow,\downarrow\rangle - |\downarrow,\uparrow\rangle \ .
\end{aligned} \tag{3.42}$$

For the *double-spin flip free phase* we receive partially entangled eigenstates

$$EV_{1/2}^{\mathbf{2}} = |\uparrow,\uparrow\rangle + \mu_{\pm}|\uparrow,\downarrow\rangle + \mu_{\pm}|\downarrow,\uparrow\rangle + |\downarrow,\downarrow\rangle \ , \tag{3.43}$$

with $\mu_{\pm} = \frac{1}{4}\left(1 \pm \sqrt{17}\right)$ and Bell type eigenstates

$$\begin{aligned} EV_3^{\mathbf{2}} &= |\uparrow,\uparrow\rangle - |\downarrow,\downarrow\rangle \ , \\ EV_4^{\mathbf{2}} &= |\uparrow,\downarrow\rangle - |\downarrow,\uparrow\rangle \ . \end{aligned} \tag{3.44}$$

The *spin decoupled phase* exhibits separable eigenstates

$$EV_{1/2}^{\mathbf{3}} = (|\uparrow\rangle + |\downarrow\rangle)(\uparrow\rangle \pm \downarrow\rangle) \ , \tag{3.45}$$

and fully entangled eigenstates

$$\begin{aligned} EV_3^{\mathbf{3}} &= |\uparrow,\uparrow\rangle - |\downarrow,\downarrow\rangle \ , \\ EV_4^{\mathbf{3}} &= |\uparrow,\downarrow\rangle - |\downarrow,\uparrow\rangle \ . \end{aligned} \tag{3.46}$$

The *classical spin-exchange phase* possesses separable eigenstates

$$\begin{aligned} EV_1^{\mathbf{4}} &= |\uparrow,\uparrow\rangle \ , \\ EV_2^{\mathbf{4}} &= |\downarrow,\downarrow\rangle \ , \end{aligned} \tag{3.47}$$

and Bell eigenstates

$$EV_3/4^{\mathbf{4}} = |\uparrow,\downarrow\rangle \pm |\downarrow,\uparrow\rangle \ . \tag{3.48}$$

We disregard the trivial fixed point Hamiltonian $\hat{H}_{\mathbf{2}}^{\text{fixed point}}$, where appearantly no more spin dynamics is permitted by the overwhelming bath influences.

Obviously, we encounter in each of the quantum regimes at least two maximally entangled eigenstates of the corresponding fixed point Hamiltonian. As the fixed point Hamiltonian represents the effectively accessible dynamics, evidently entanglement will be conserved even in the stronger bath controlled regimes of the double spin system. In particular, the basis of these eigenvectors constitutes the states, which were preferred, if not enforced by the environmental influences. As consequence we expect, that separable initial states, which were not eigenstates of the fixed point Hamiltonian from the very beginning, will become entangled states as consequence of the dissipative evolution into the eigenbasis of the fixed point Hamiltonian.

Evidently, in the regimes (**1** - **3**), where local quantum dynamics is still possible, we receive the same Bell type eigenstates, while int the *classical spin-exchange phase* with compareably less freedom of quantum dynamics, just the two Bell states $|\uparrow,\downarrow\rangle \pm |\downarrow,\uparrow\rangle$, which only differ in the relative phase of the second term.

The overall result is, that apparently, although quantum dynamics on and between the two spins will be diminished with increasing coupling to the external baths, there is still entanglement between both spins preserved. Beyond its preservation, we also expect, that entanglement, if not Bell type states, will be produced, if starting from separable initial states, as these belong to the preferred dressed-spin eigenbasis.

3.4 Scaling equations 2^{nd} order

Now we want to demonstrate, how our initial approach to scaling analysis in first order can be expanded to higher order differential equations of the according dressed-spin couplings. This serves also to obtain at least qualitatively more reliable results. Therefor we intend to apply an extended technique, also called *operator product expansion* [72], which takes into account higher order processes in the spin operators. This works similarily by use of a scaling invariance argument.

3.4.1 Operator product expansion

The idea behind the *operator product expansion* is, analogously to the first order scaling analysis, that infinitesimal changings of the basic length scale δl of the baths should lead to variations in the renormalized spin-coupling constants, but which still leave the physical effects of the dressed-spin Hamiltonian invariant. As representation of the general physical state of the dressed-two-spin system its partition function Z is chosen. This in regard of a fixed point Hamiltonian $\hat{H}^*$ is depending on the scaling effective spin-couplings as follows (see also [72] chapter 5)

$$Z(\Delta_0, \Delta_{++}, \Delta_{+-}) \;=\; \mathrm{tr}\left\{\exp\left(-\hat{H}^* - \sum_j \Delta_j \int a^{-y_j}\mathscr{O}_j(z)\,dz\right)\right\}. \tag{3.49}$$

This expression for Z now can be expanded in a power series of the effective spin operators $\mathcal{O}_j$ (respectively its expectation values)

$$\begin{aligned} Z \;=\; Z^*\Big[1 &- \sum_j \Delta_j \int a^{-y_j}\big\langle\mathscr{O}_j(z_1)\big\rangle\,dz_1 + \\ &+\frac{1}{2!}\sum_{j,k}\Delta_j\Delta_k\int\int a^{-y_j-y_k}\big\langle\mathscr{O}_j(z_1)\mathscr{O}_k(z_2)\big\rangle\,dz_1\,dz_2 - \\ &-\frac{1}{3!}\sum_{j,k,l}\Delta_j\Delta_k\Delta_l\int\int\int a^{-y_j-y_k-y_l}\big\langle\mathscr{O}_j(z_1)\mathscr{O}_k(z_2)\mathscr{O}_l(z_3)\big\rangle\,dz_1\,dz_2\,dz_3 + ...\Big], \end{aligned} \tag{3.50}$$

where

$$Z^* \;=\; \mathrm{tr}_{\mathrm{total}}\left\{-\hat{H}^*\right\} \tag{3.51}$$

denotes the partition function of the unperturbed fixed point Hamiltonian and

$$\big\langle\mathscr{O}_j...\big\rangle \;=\; \mathrm{tr}_{\mathrm{total}}\left\{\rho_{\mathrm{total}}(\beta)\mathscr{O}_j...\right\} \tag{3.52}$$

represents the thermal expectation values of the corresponding spin-operator products (with $\beta = \frac{1}{k_B T}$ and $\rho_{\mathrm{total}} = \frac{e^{-\beta\hat{H}_{\mathrm{total}}}}{\mathrm{tr}\{e^{-\beta\hat{H}_{\mathrm{total}}}\}}$).

The assumption of scaling invariance of the partition function Z can be expressed by the relation $Z[a(1+\delta l)] = Z[a]$ (where $a(1+\delta l)$ denotes an infinitesimal rescaling), *i.e.*

$$\left[\sum_j \Delta_j \int a^{-y_j} \left\langle \mathscr{O}_j \right\rangle dz_1 + \frac{1}{2}\sum_{j,k} \Delta_j \Delta_k \int\int d^{-y_j-y_k} \left\langle \mathscr{O}_j \mathscr{O}_k \right\rangle dz_1\, dz_2 + ...\right]_{a\to a(1+\delta l)} = 0 \ . \tag{3.53}$$

This means, that all the rescaled spin-operator factors should mutually compensate. For writing down these self-compensating terms, we restrict ourself on spin operator product terms up to second order. But principally the corresponding calculations could be applied on arbitrary orders, to the price of more complicated equations.

At this point the *operator product expansion* comes into account; it denotes the possibility of expanding operator product terms, *e.g.* $\mathscr{O}_j(z_1)\mathscr{O}_k(z_2)$, into the basis of effective spin-operators

$$\mathscr{O}_j(z_1)\mathscr{O}_k(z_2) = \sum_l C_{jkl}(z_1 - z_2)\mathscr{O}_l\left(\frac{z_1+z_2}{2}\right) \tag{3.54}$$

with according expansion functions $C_{jkl}(z)$. Due to scaling properties ([72], chapter 5.1), these are uniquely defined by so-called operator product expansion coefficients c_{jkl}

$$C_{jkl}(z_1 - z_2) = \frac{c_{jkl}}{|z_1 - z_2|^{x_j + x_k - x_l}}, \tag{3.55}$$

which were combinatorically derived constants (for details see Appendix D.2.1). The z-variable exponents x_μ hereby were given by the corresponding first order scaling exponents

$$x_\mu = d - y_\mu \tag{3.56}$$

with d the dimension of the bosonic fields.

If we apply some calculus on eq. 3.53 (Appendix D.2.1, respectively [72]) we receive generally as second order scaling equations for the coupling constants Δ_l

$$\frac{\partial \Delta_l}{\partial a} = y_l \Delta_l - \frac{S_d}{2}\sum_{jk} c_{jkl}\Delta_j\Delta_k \tag{3.57}$$

with $S_d = \frac{2\pi^{d/2}}{\Gamma(d/2)}$ the area of a d-dimensional hypersphere (Γ Euler's Gamma-function); d denotes here the dimension of the Bosonic fields.

But there is a price, one has to pay for that algebraic expansion, as the effective dressed-spin operations $\{\mathscr{O}_0, \mathscr{O}_{++}, \mathscr{O}_{+-}\}$ does not form a closed algebra. One also has to take into

account further composite spin operators terms, which emerges from second order products of the first three objects, which were

$$\begin{aligned}
\mathscr{O}_{\mathbf{1}} &= \mathbb{1}, && (3.58)\\
\mathscr{O}_z &= \hat{\sigma}_1^z \hat{\sigma}_2^z, && (3.59)\\
\mathscr{O}_S &= \frac{1}{\sqrt{2}} \left(\hat{\sigma}_1^z + \hat{\sigma}_2^z\right) \partial_x \Phi_S, && (3.60)\\
\mathscr{O}_A &= \frac{1}{\sqrt{2}} \left(\hat{\sigma}_1^z - \hat{\sigma}_2^z\right) \partial_x \Phi_A. && (3.61)
\end{aligned}$$

After some tedious, but straightforward calculations (Appendix D.2.1) one receives from eq. (3.57) the second order scaling equations in explicit form

$$\begin{aligned}
\frac{\partial \Delta_0}{\partial l} &= y_0 \Delta_0 - \frac{S_d}{2} \left[\sqrt{2} \left(\Delta_0 \Delta_{++} + \Delta_0 \Delta_{+-} \right) + \frac{\lambda_S}{2} \Delta_0 \Delta_S + \frac{\lambda_A}{2} \Delta_0 \Delta_A \right]\\
\frac{\partial \Delta_{++}}{\partial l} &= y_{++} \Delta_{++} - \frac{S_d}{2} \left[\frac{1}{\sqrt{2}} \Delta_0^2 + 2 \Delta_{++} \Delta_z - \sqrt{8} \lambda_S \Delta_{++} \Delta_S \right]\\
\frac{\partial \Delta_{+-}}{\partial l} &= y_{+-} \Delta_{+-} - \frac{S_d}{2} \left[\frac{1}{\sqrt{2}} \Delta_0^2 + 2 \Delta_{+-} \Delta_z - \sqrt{8} \lambda_A \Delta_{+-} \Delta_A \right]\\
\frac{\partial \Delta_{\mathbf{1}}}{\partial l} &= y_{\mathbf{1}} \Delta_{\mathbf{1}} - \frac{S_d}{2} \left[\Delta_0^2 + \Delta_{++}^2 + \Delta_{+-}^2 + \Delta_z^2 \right] && (3.62)\\
\frac{\partial \Delta_z}{\partial l} &= y_z \Delta_z - \frac{S_d}{2} \left[\Delta_{++}^2 - \Delta_{+-}^2 \right]\\
\frac{\partial \Delta_S}{\partial l} &= y_S \Delta_S - \frac{S_d}{2} \left[\frac{\lambda_S}{\sqrt{2}} \Delta_0^2 + \sqrt{8} \Delta_{++}^2 + 2 \Delta_z \Delta_S \right]\\
\frac{\partial \Delta_A}{\partial l} &= y_A \Delta_A - \frac{S_d}{2} \left[\frac{\lambda_A}{\sqrt{2}} \Delta_0^2 - 2 \Delta_z \Delta_A \right] \quad ;
\end{aligned}$$

hereby we considered always symmetrized sums of the operator products (*i.e.* of the form $\langle \mathscr{O}_j \mathscr{O}_k \rangle + \langle \mathscr{O}_j \mathscr{O}_k \rangle$), such as they appear in our second order analysis.

Appendix A

Born master equation of the spin-Boson model

In this chapter we will derive the time dependent memory kernel for the non-Markovian Born master equation of the considered spin-Boson model 1.4. Using this formal expression we will be able to evaluate corresponding density matrix evolutions by numerical means for arbitrary parameters.

A.1 Derivation of the Born approximation correlation functions

Starting with the Born approximation master equation 1.74

$$\begin{aligned}\frac{\partial \rho_{\mathrm{S}}(t)}{\partial t} &= -\frac{i}{\hbar}\left[\hat{H}_{\mathrm{S}}, \rho_{\mathrm{S}}(t)\right] - \\ &\quad -\frac{\lambda^2}{\hbar^2}\int_0^t ds \int_0^\infty d\omega \Bigg(\mathcal{R}_\omega(t-s)\left[\hat{\sigma}_z, e^{-i/\hbar \hat{H}_{\mathrm{S}}(t-s)}\left[\hat{\sigma}_z, \rho_{\mathrm{Sys}}(s)\right] e^{i/\hbar \hat{H}_{\mathrm{S}}(t-s)}\right] + \\ &\qquad +\mathcal{I}_\omega(t-s)\left[\hat{\sigma}_z, e^{-i/\hbar \hat{H}_{\mathrm{S}}(t-s)}\left[\hat{\sigma}_z, \rho_{\mathrm{Sys}}(s)\right]_+ e^{i/\hbar \hat{H}_{\mathrm{S}}(t-s)}\right]\Bigg) \ ,\end{aligned} \tag{A.1}$$

with corresponding correlation functions of the ohmic bath spectral density eq. (1.68)

$$\begin{aligned}\mathcal{R}_\omega(t-s) &= \frac{J(\omega)}{\pi}\coth(\hbar\omega\beta/2)\cos(\omega(t-s)) \\ \mathcal{I}_\omega(t-s) &= -i\frac{J(\omega)}{\pi}\sin(\omega(t-s)) \ .\end{aligned} \tag{A.2}$$

In order to receive the correct time (delay) dependence of the non-Markovian memory kernel, we have to integrate these correlation functions in regard of their frequency parameter. Applying the residual theorem we obtain

$$\begin{aligned}\int_0^\infty \mathcal{R}_\omega(\tau)\,d\omega &= \int_0^\infty \frac{J(\omega)}{\pi}\coth(\hbar\omega\beta/2)\cos(\omega\tau)\,d\omega \\ &= \frac{1}{\pi}\int_0^\infty \alpha\omega\frac{\omega_c^2}{\omega^2+\omega_c^2}\coth(\hbar\omega\beta/2)\cos(\omega\tau)\,d\omega \\ &= \frac{\alpha}{2\pi}\mathscr{R}\left\{\int_{-\infty}^\infty \omega\frac{\omega_c^2}{\omega^2+\omega_c^2}\coth(\hbar\omega\beta/2)e^{i\omega\tau}\,d\omega\right\} \qquad \text{(A.3)} \\ &= \frac{\alpha}{2\pi}\mathscr{R}\left\{2\pi i\left[i\omega_c\frac{\omega_c^2}{2i\omega_c}\frac{1}{i}\cot(\hbar\omega_c\beta/2)e^{-\omega_c\tau}+\sum_j \omega_j\frac{\omega_c^2}{\omega_j^2+\omega_c^2}\frac{\hbar\beta}{2}e^{i\omega_j\tau}\right]\right\}\ ,\end{aligned}$$

with $\omega_j := i\frac{2\pi}{\hbar\beta}j$ the corresponding Matsubara frequencies (corresponding to the $\coth(\hbar\omega_j\beta/2)$ poles in the upper complex half plane) [31]. Hereby we encounter a series of the type

$$\sum_j \frac{j}{j^2-\kappa^2}e^{-\mu j} = \frac{1}{2}\left[\text{LerchPhi}(e^{-\mu},1,\kappa)+\text{LerchPhi}(e^{-\mu},1,-\kappa)\right]\ , \qquad \text{(A.4)}$$

with LerchΦ the Lerch-Phi-function [73].

Such that

$$\begin{aligned}\int_0^\infty \mathcal{R}_\omega(\tau)\,d\omega &= \int_0^\infty \frac{J(\omega)}{\pi}\coth(\hbar\omega\beta/2)\cos(\omega\tau)\,d\omega \\ &= \frac{\alpha\omega_c^2}{4}\cot(\hbar\omega_c\beta/2)e^{-\omega_c\tau}+ \qquad \text{(A.5)} \\ &\quad +\frac{\alpha\omega_c^2\hbar^2\beta^2}{16\pi}\left[\text{LerchPhi}(e^{-\frac{2\pi}{\hbar\beta}\tau},1,\frac{2\pi}{\hbar\beta}\omega_c)+\text{LerchPhi}(e^{-\frac{2\pi}{\hbar\beta}\tau},1,-\frac{2\pi}{\hbar\beta}\omega_c)\right]\ .\end{aligned}$$

The same calculation for the imaginary part of the correlation functions leads to

$$\int_0^\infty \mathcal{I}_\omega(\tau)\,d\omega = \int_0^\infty -i\frac{J(\omega)}{\pi}\sin(\omega\tau)\,d\omega = -i\frac{\alpha\omega_c^2}{2}e^{-\omega_c\tau}\ . \qquad \text{(A.6)}$$

If we now take a closer look on these time depending memory amplitudes, we will perceive from its pictorial evaluation (Fig. A.1), that these correlation functions behaves in very good accuracy like $e^{-\omega_c t}$. This decay proceed on a timescale, which is ruled by the environmental energy cutoff ω_c, which we quite arbitrarily have set to $\omega_c = 100\Omega$, *i.e.* one hundred times the spin energy. This deliver the convenient effect, that our numerical integrations, in order to receive the infinitesimal changings of the density matrices, does not

have to grow to arbitrary long expressions. For instance, in very good accuracy (up to errors in the order of 10^{-4}) we can disregard any feedback terms, which were given over time separations longer than ten times $1/\omega_c$ (see Fig. 1.5).

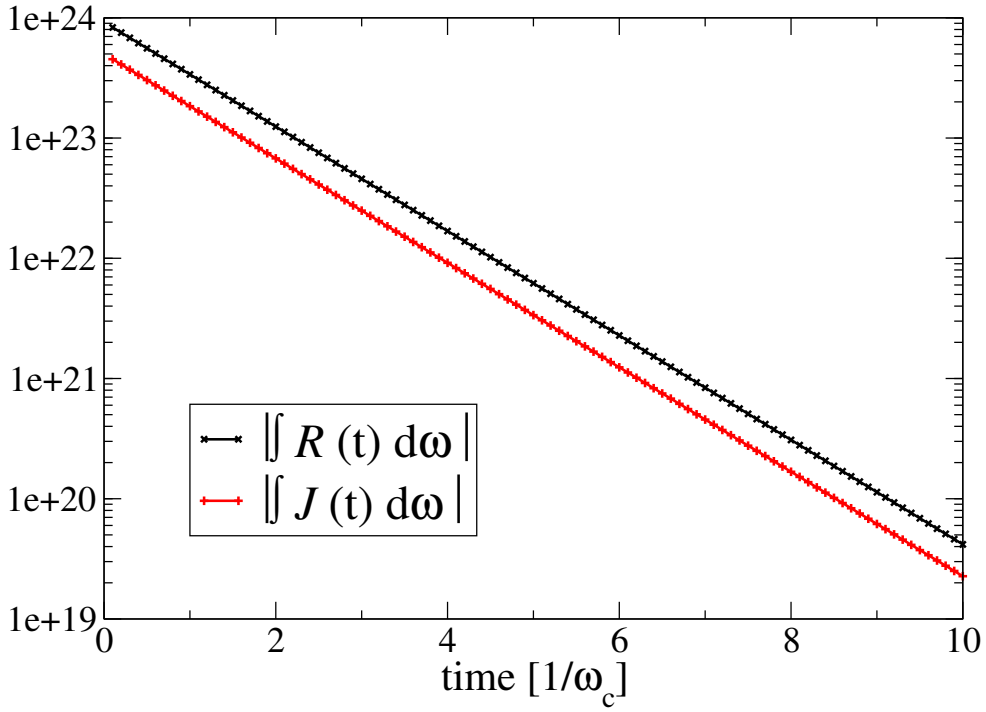

Figure A.1: Temporal decay of the Born correlation functions (distinguished between real and imaginary parts). Evidently both terms decrease in excellent accuracy like $e^{-\omega_c t}$, where $\omega_c = 10^{12}$ Hz.

By means of this finite memory-time we can easily numerically integrate the corresponding time-nonlocal differential equation by use of standard time-discretization techniques, as from a compareably short initial time delay on ($10/\omega_c = 0.1/\Omega$ with $1/\Omega$ the typical evolution time scale of the free system) the increase of memory and computational requirements grows only linearly with the upper integration variable.

Appendix B

Born-Markovian approximations of the Spin-Boson model

Now we evaluate the former described Markovian approximations.

B.1 Naïve Markov approximation

Firstly, for the naïve choice (1.41) we receive as Markovian master equation from eq. 1.74

$$\begin{aligned}\frac{\partial \rho_{\mathrm{S}}(t)}{\partial t} &= -i/\hbar \left[\hat{H}_{\mathrm{S}}, \rho_{\mathrm{S}}(t)\right] - \\ &\quad -\frac{\lambda^2}{\hbar^2}\iint_0^\infty \Big(\mathcal{R}_\omega(t-s)\left[\hat{\sigma}_z, e^{-i/\hbar\hat{H}_{\mathrm{S}}(t-s)}\left[\hat{\sigma}_z, \rho_{\mathrm{S}}(t)\right] e^{i/\hbar\hat{H}_{\mathrm{S}}(t-s)}\right] + \\ &\qquad +\mathcal{I}_\omega(t-s)\left[\hat{\sigma}_z, e^{-i/\hbar\hat{H}_{\mathrm{S}}(t-s)}\left[\hat{\sigma}_z, \rho_{\mathrm{S}}(t)\right]_+ e^{i/\hbar\hat{H}_{\mathrm{S}}(t-s)}\right]\Big) d\omega\, ds \ .\end{aligned} \tag{B.1}$$

For concrete calculations it exposes to be convenient to change into the Bloch sphere representation

$$\rho(t) = \sigma_x(t)\hat{\sigma}_x + \sigma_y(t)\hat{\sigma}_y + \sigma_z(t)\hat{\sigma}_z + \frac{\mathbb{1}}{2} \ , \tag{B.2}$$

such that ordinary Pauli spin-matrix algebra can be used.

From that we obtain

$$\begin{aligned}
\frac{\partial \rho_{\mathrm{S}}(t)}{\partial t} &= -i/\hbar \left[\hat{H}_{\mathrm{S}}, \rho_{\mathrm{S}}(t)\right] - \\
&\quad -\frac{\lambda^2}{\hbar^2}\iint_0^\infty \Bigg(\mathcal{R}_\omega(t-s)\left[\hat{\sigma}_z, e^{-i/\hbar\hat{H}_{\mathrm{S}}(t-s)}\left[i\sigma_x(t)\hat{\sigma}_y - i\sigma_y(t)\hat{\sigma}_x\right]e^{i/\hbar\hat{H}_{\mathrm{S}}(t-s)}\right] + \\
&\qquad +\mathcal{I}_\omega(t-s)\left[\hat{\sigma}_z, e^{-i/\hbar\hat{H}_{\mathrm{S}}(t-s)}\left[\sigma_z(t)\mathbb{1}_{\mathrm{S}} + \hat{\sigma}_z\right]e^{i/\hbar\hat{H}_{\mathrm{S}}(t-s)}\right]\Bigg)\, d\omega\, ds \\
&= -i/\hbar \left[\hat{H}_{\mathrm{S}}, \rho_{\mathrm{S}}(t)\right] - \\
&\quad -\frac{\lambda^2}{\hbar^2}\iint_0^\infty \Bigg(\mathcal{R}_\omega(t-s)\left\{i\sigma_x(t)\left[\hat{\sigma}_z, \tilde{\hat{\sigma}}_y(s-t)\right] - i\sigma_y(t)\left[\hat{\sigma}_z, \tilde{\hat{\sigma}}_x(s-t)\right]\right\} + \\
&\qquad +\mathcal{I}_\omega(t-s)\left[\hat{\sigma}_z, \tilde{\hat{\sigma}}_z(s-t)\right]\Bigg)\, d\omega\, ds \ . \qquad \text{(B.3)}
\end{aligned}$$

The Heisenberg/interaction picture $\tilde{\hat{\sigma}}_z(t)$ operators are most easy to evaluate by considering the corresponding rotating frame

$$\begin{aligned}
\hat{\sigma}'_z &:= \frac{\Delta\hat{\sigma}_x + \epsilon\hat{\sigma}_z}{\Omega} \quad \Longleftrightarrow \quad \hat{\sigma}_z = \frac{-\Delta\hat{\sigma}'_x + \epsilon\hat{\sigma}'_z}{\Omega} \\
&\qquad\qquad \hat{\sigma}'_y := \hat{\sigma}_y \qquad\qquad \text{(B.4)} \\
\hat{\sigma}'_x &:= \frac{\epsilon\hat{\sigma}_x - \Delta\hat{\sigma}_z}{\Omega} \quad \Longleftrightarrow \quad \hat{\sigma}_x = \frac{\epsilon\hat{\sigma}'_x + \Delta\hat{\sigma}'_z}{\Omega}
\end{aligned}$$

with $\Omega = \sqrt{\epsilon^2 + \Delta^2}$; such that

$$\begin{aligned}
\tilde{\hat{\sigma}}_z(t) &= e^{+i/\hbar\hat{H}_{\mathrm{S}}t}\hat{\sigma}_z e^{-i/\hbar\hat{H}_{\mathrm{S}}t} \\
&= e^{+i\hat{\sigma}'_z\Omega t}\hat{\sigma}_z e^{-i\hat{\sigma}'_z\Omega t} \\
&= e^{+i\hat{\sigma}'_z\Omega t}\frac{\epsilon\hat{\sigma}'_z - \Delta\hat{\sigma}'_x}{\Omega}e^{-i\hat{\sigma}'_z\Omega t} \\
&= \frac{\epsilon}{\Omega}\hat{\sigma}'_z - \frac{\Delta}{\Omega}\left(\cos(\Omega t)\hat{\sigma}'_x - \sin(\Omega t)\hat{\sigma}'_y\right) \\
&= \frac{\epsilon\Delta}{\Omega^2}\left(1 - \cos(\Omega t)\right)\hat{\sigma}_x + \frac{\Delta}{\Omega}\sin(\Omega t)\hat{\sigma}_y + \frac{\epsilon^2 + \Delta^2\cos(\Omega t)}{\Omega^2}\hat{\sigma}_z \\
&=: \mu_{zx}(t)\hat{\sigma}_x + \mu_{zy}(t)\hat{\sigma}_y + \mu_{zz}(t)\hat{\sigma}_z \ . \qquad \text{(B.5)}
\end{aligned}$$

Analogously

$$\begin{aligned}
\tilde{\hat{\sigma}}_x(t) &= e^{+i\hat{\sigma}'_z\Omega t}\frac{\epsilon\hat{\sigma}'_x + \Delta\hat{\sigma}'_z}{\Omega}e^{-i\hat{\sigma}'_z\Omega t} \\
&= \frac{\epsilon}{\Omega}\left(\cos(\Omega t)\hat{\sigma}'_x - \sin(\Omega t)\hat{\sigma}'_y\right) + \frac{\Delta}{\Omega}\hat{\sigma}'_z \\
&= \frac{\epsilon^2\cos(\Omega t) + \Delta^2}{\Omega^2}\hat{\sigma}_x - \frac{\epsilon}{\Omega}\sin(\Omega t)\hat{\sigma}_y + \frac{\epsilon\Delta}{\Omega^2}\left(1 - \cos(\Omega t)\right)\hat{\sigma}_z \\
&=: \mu_{xx}(t)\hat{\sigma}_x + \mu_{xy}(t)\hat{\sigma}_y + \mu_{xz}(t)\hat{\sigma}_z \ , \qquad \text{(B.6)}
\end{aligned}$$

and

$$\begin{aligned}\tilde{\hat{\sigma}}_y(t) &= e^{+i\hat{\sigma}'_z\Omega t}\hat{\sigma}'_y e^{-i\hat{\sigma}'_z\Omega t} \\ &= \left(\cos(\Omega t)\hat{\sigma}'_y + \sin(\Omega t)\hat{\sigma}'_x\right) \\ &= \frac{\epsilon\sin(\Omega t)}{\Omega}\hat{\sigma}_x + \cos(\Omega t)\hat{\sigma}_y - \frac{\Delta\sin(\Omega t)}{\Omega}\hat{\sigma}_z \\ &=: \mu_{yx}(t)\hat{\sigma}_x + \mu_{yy}(t)\hat{\sigma}_y + \mu_{yz}(t)\hat{\sigma}_z \ . \end{aligned} \tag{B.7}$$

By using that concise description we receive for the Pauli spin commutator terms from eq. B.3

$$\begin{aligned}\left[\hat{\sigma}_z, \tilde{\hat{\sigma}}_x(s-t)\right] &= [\hat{\sigma}_z, \mu_{xx}(s-t)\hat{\sigma}_x + \mu_{xy}(s-t)\hat{\sigma}_y + \mu_{xz}(s-t)\hat{\sigma}_z] \\ &= i\left(\mu_{xx}(s-t)\hat{\sigma}_y - \mu_{xy}(s-t)\hat{\sigma}_x\right) \ , \end{aligned} \tag{B.8}$$

$$\left[\hat{\sigma}_z, \tilde{\hat{\sigma}}_y(s-t)\right] = i\left(\mu_{yx}(s-t)\hat{\sigma}_y - \mu_{yy}(s-t)\hat{\sigma}_x\right) \ , \tag{B.9}$$

$$\left[\hat{\sigma}_z, \tilde{\hat{\sigma}}_z(s-t)\right] = i\left(\mu_{zx}(s-t)\hat{\sigma}_y - \mu_{zy}(s-t)\hat{\sigma}_x\right) \ . \tag{B.10}$$

Therewith we receive for equation B.3

$$\begin{aligned}\frac{\partial\rho_{\mathrm{S}}(t)}{\partial t} &= -i/\hbar\left[\hat{H}_{\mathrm{S}}, \rho_{\mathrm{S}}(t)\right] - \\ &\quad -\frac{\lambda^2}{\hbar^2}\iint_0^\infty \Big(i^2\mathcal{R}_\omega(t-s)\big\{\sigma_x(t)\big(\mu_{yx}(s-t)\hat{\sigma}_y - \mu_{yy}(s-t)\hat{\sigma}_x\big) - \\ &\qquad -\sigma_y(t)\big(\mu_{xx}(s-t)\hat{\sigma}_y - \mu_{xy}(s-t)\hat{\sigma}_x\big)\big\} + \\ &\qquad +i\mathcal{I}_\omega(t-s)\big\{\mu_{zx}(s-t)\hat{\sigma}_y - \mu_{zy}(s-t)\hat{\sigma}_x\big\}\Big)\, d\omega\, ds \ . \end{aligned} \tag{B.11}$$

From equation B.12 we can easily derive the corresponding matrix form regarding description 1.13

$$\frac{\partial\vec{\sigma}(t)}{\partial t} = \hat{M}_0\vec{\sigma}(t) + \vec{I}_0 \ , \tag{B.12}$$

with $\hat{M}_0$ the linear and $\vec{I}_0$ the inhomogenous term. $\hat{M}_0$ is composed by the Hamiltonian part $\hat{M}^0_{\mathrm{H_S}}$ and the integro-differential one $\hat{M}^0_{\mathrm{diss}}$. The first one is given as

$$\hat{M}_{\mathrm{unitary}} = 2\begin{pmatrix} 0 & -\epsilon & 0 \\ \epsilon & 0 & -\Delta \\ 0 & \Delta & 0 \end{pmatrix} \ , \tag{B.13}$$

the latter one as

$$\hat{M}^0_{\text{diss}} = -\lambda^2/\hbar^2 \begin{pmatrix} M^0_{xx} & M^0_{xy} & 0 \\ M^0_{yx} & M^0_{yy} & 0 \\ 0 & 0 & 0 \end{pmatrix} , \tag{B.14}$$

with

$$\begin{aligned} M^0_{xx} &= -\iint_0^\infty \mathcal{R}_\omega(t-s)\mu_{yy}(s-t)\,d\omega\,ds \\ &= -\iint_0^\infty \frac{J(\omega)}{\pi}\coth(\hbar\beta\omega/2)\cos(\omega(t-s))\cos(\Omega(s-t)) \\ &= -\iint_0^\infty \frac{J(\omega)}{\pi}\coth(\hbar\beta\omega/2)\cos(\omega\tau)\cos(\Omega\tau))\,d\tau\,d\omega \\ &= -\int_0^\infty \frac{J(\omega)}{\pi}\coth(\hbar\beta\omega/2)\frac{1}{4}\int_0^\infty e^{i(\Omega+\omega)\tau}+e^{i(\Omega-\omega)\tau}+e^{-i(\Omega+\omega)\tau}+e^{-i(\Omega-\omega)\tau}\,d\tau\,d\omega \\ &= -\frac{1}{4}\int_0^\infty \frac{J(\omega)}{\pi}\coth(\hbar\beta\omega/2)\Big\{\frac{i}{\Omega+\omega+i\eta}+\frac{i}{\Omega-\omega+i\eta}+ \\ &\qquad +\frac{-i}{\Omega-\omega-i\eta}+\frac{-i}{\Omega+\omega-i\eta}\Big\}\,d\omega\ , \end{aligned}$$

where we have introduced the infinitesimal convergence factor η, which according to Mattuck [74] leads to

$$\frac{1}{x+i\eta} = \mathcal{P}\left(\frac{1}{x}\right) - i\pi\delta(x) \tag{B.15}$$

with $\mathcal{P}$ the principal value (briefly: omitting the poles of the inserted function during applications of residual theory) and $\delta(x)$ the usual delta-distribution.

In order to perform the ω-integration, one has to notice, that the integrand is an even function of ω, such that residual theory can be applied

$$M^0_{xx} = \int_0^\infty \frac{J(\omega)}{\pi}\coth(\hbar\beta\omega/2)\ldots\,d\omega = \frac{1}{2}\int_{-\infty}^\infty \frac{J(\omega)}{\pi}\coth(\hbar\beta\omega/2)\ldots\,d\omega\ .$$

Expanding the integration onto a closed contour in $\mathbb{C}$ one receives from relation B.15

and by use of the residual theorem

$$\begin{aligned} M^0_{xx} &= \frac{1}{2}\int_{-\infty}^{\infty}\frac{J(\omega)}{\pi}\coth(\hbar\beta\omega/2)\ldots\, d\omega \\ &= -\frac{1}{2}J(\Omega)\coth(\hbar\beta\Omega/2)+\frac{1}{2}\sum_{j>0}J(\omega_j)\underbrace{\left(\frac{1}{\Omega+\omega_j}+\frac{1}{\Omega-\omega_j}-\frac{1}{\Omega-\omega_j}-\frac{1}{\Omega+\omega_j}\right)}_{=0}+ \\ &\qquad +\alpha\omega_c^2/2\underbrace{\left(\frac{1}{\Omega+i\omega_c}+\frac{1}{\Omega-i\omega_c}-\frac{1}{\Omega-i\omega_c}-\frac{1}{\Omega+i\omega_c}\right)}_{=0} \\ &= -\frac{1}{2}J(\Omega)\coth(\hbar\beta\Omega/2) \end{aligned} \tag{B.16}$$

with

$$\omega_j := i\frac{2\pi}{\hbar\beta}j\ , \tag{B.17}$$

the corresponding Matsubara frequencies [31].

Similar calculations (compare also with B.32,B.33,B.34,B.35) leads to

$$\begin{aligned} M^0_{xy} &= -\iint_0^\infty \mathcal{R}_\omega(t-s)\mu_{yx}(s-t)\,d\omega\,ds \\ &= -\frac{\epsilon}{\pi\Omega}\iint_0^\infty J(\omega)\coth(\hbar\beta\omega/2)\cos(\omega\tau)\sin(-\Omega\tau)\,d\tau\,d\omega \\ &= -\frac{\epsilon}{2\Omega}\left(i\sum_j J(\omega_j)\frac{2}{\hbar\beta}\left(\frac{1}{\Omega+\omega_j}+\frac{1}{\Omega-\omega_j}\right)+J(\Omega)\cot(\hbar\beta\omega_c/2)\right)\ , \end{aligned} \tag{B.18}$$

$$\begin{aligned} M^0_{yx} &= -\iint_0^\infty \mathcal{R}_\omega(t-s)\mu_{xy}(s-t)\,d\omega\,ds \\ &= \frac{\epsilon}{\pi\Omega}\iint_0^\infty J(\omega)\coth(\hbar\beta\omega/2)\cos(\omega\tau)\sin(-\Omega\tau)\,d\tau\,d\omega \\ &= \frac{\epsilon}{2\Omega}\left(i\sum_j J(\omega_j)\frac{2}{\hbar\beta}\left(\frac{1}{\Omega+\omega_j}+\frac{1}{\Omega-\omega_j}\right)+J(\Omega)\cot(\hbar\beta\omega_c/2)\right)\ , \end{aligned} \tag{B.19}$$

$$\begin{aligned} M^0_{yy} &= \iint_0^\infty \mathcal{R}_\omega(t-s)\mu_{xx}(s-t)\,d\omega\,ds \\ &= \frac{1}{\pi}\iint_0^\infty J(\omega)\coth(\hbar\beta\omega/2)\cos(\omega\tau)\frac{\epsilon^2\cos(\Omega\tau)+\Delta^2}{\Omega^2}\,d\tau\,d\omega \\ &= \frac{\epsilon^2}{2\Omega^2}J(\Omega)\coth(\hbar\beta\Omega/2)+\frac{\Delta^2}{2\Omega^2}\left(J(x)\coth(\hbar\beta x/2)\right)_{x\to 0} \\ &= \frac{\epsilon^2}{2\Omega^2}J(\Omega)\coth(\hbar\beta\Omega/2)+\frac{\Delta^2}{2\Omega^2}\frac{2\alpha}{\hbar\beta}\ . \end{aligned} \tag{B.20}$$

Thereby (in eq. B.18 and B.19) we encountered the following term

$$\begin{aligned} i\sum_j J(\omega_j)\frac{2}{\hbar\beta}\frac{2\Omega}{\Omega^2-\omega_j^2} &= i\alpha\frac{2}{\hbar\beta}\sum_j \omega_j \frac{\omega_c^2}{\omega_c^2+\omega_j^2}\frac{2\Omega}{\Omega^2-\omega_j^2} \\ &= 2\alpha\omega_c^2\Omega\frac{2}{\hbar\beta}\left(\frac{\hbar\beta}{2\pi}\right)^3\sum_j \frac{j}{(j^2+c_1^2)(j^2-c_2^2)} \end{aligned} \tag{B.21}$$

with

$$c_1 = \frac{\Omega\hbar\beta}{2\pi} \quad \text{and} \quad c_2 = \frac{\omega_c\hbar\beta}{2\pi} \ , \tag{B.22}$$

which can be translated into appropriate combinations of Digamma functions Ψ, cotangents and hyperbolic cotangents (for details see M. Storcz [58], appendix D and references therein) as follows

$$\begin{aligned} i\sum_j J(\omega_j)\frac{2}{\hbar\beta}\frac{2\Omega}{\Omega^2-\omega_j^2} &= \frac{\alpha\omega_c^2\Omega}{\pi}\left(\frac{\hbar\beta}{2\pi}\right)^2\frac{1}{c_1^2+c_2^2}\big[\Psi(ic_1)+\Psi(1+ic_1)-i\pi\coth(\pi c_1)- \\ &\qquad -\Psi(1+c_2)-\pi\cot(\pi c_2)-\Psi(c_2)\big] \\ &=: \mathscr{M}(\Omega,\omega_c,\beta) \ . \end{aligned} \tag{B.23}$$

For the sake of clarity, we will furthermore abbreviate this cumbersome expression by $\mathscr{M}(\Omega,\omega_c,\beta)$ as function of (inverse) temperature, cutoff and systems frequency.

Analogously we derive the inhomogenous part of B.12

$$\vec{I}_0 = -\frac{\lambda^2}{\hbar^2}\begin{pmatrix} I_x^0 \\ I_y^0 \\ 0 \end{pmatrix} \ , \tag{B.24}$$

with

$$\begin{aligned} I_x^0 &= i\iint_0^\infty \mathcal{I}_\omega(t-s)\mu_{zy}(s-t)\,d\omega\,ds \\ &= i\frac{\Delta}{\Omega}\iint_0^\infty -i\frac{J(\omega)}{\pi}\sin(\omega\tau)\sin(-\Omega\tau)\,d\tau\,d\omega \\ &= -\frac{\Delta}{\Omega}\int_{-\infty}^\infty \frac{J(\omega)}{4\pi}\left(\frac{i}{-\Omega+\omega+i\eta}-\frac{i}{\Omega+\omega+i\eta}-\frac{i}{-\Omega-\omega+i\eta}+\frac{i}{\Omega-\omega+i\eta}\right)d\omega \\ &= -\frac{\Delta}{\Omega}J(\Omega) \end{aligned} \tag{B.25}$$

and

$$\begin{aligned} I_y^0 &= -i \iint_0^\infty \mathcal{I}_\omega(t-s)\mu_{zx}(s-t)\, d\omega\, ds \\ &= -i\frac{\epsilon\Delta}{\Omega^2} \iint_0^\infty -i\frac{J(\omega)}{\pi} \sin(\omega\tau)(1-\cos(-\Omega\tau))\, d\tau\, d\omega \\ &= i\frac{\epsilon\Delta}{2\Omega^2} \int_{-\infty}^\infty \frac{J(\omega)}{4\pi} \Bigg\{ 2\left(\frac{i}{\omega+i\eta} - \frac{i}{-\omega+i\eta}\right) - \left(\frac{i}{\Omega+\omega+i\eta} + \right. \\ &\qquad \left. + \frac{i}{-\Omega+\omega+i\eta} - \frac{i}{\Omega-\omega+i\eta} - \frac{i}{-\Omega-\omega+i\eta}\right)\Bigg\} d\omega \\ &= \frac{\epsilon\Delta}{2\Omega^2}\alpha\left(\frac{\omega_c^3}{\Omega^2+\omega_c^2} - \omega_c\right) = -\alpha\frac{\epsilon\Delta}{2\Omega^2}\omega_c\frac{\Omega^2}{\Omega^2+\omega_c^2}\ , \end{aligned} \tag{B.26}$$

with ω_c the Drude-cutoff given as in eq. 1.68.

B.2 Bloch-Redfield approximation

We start analogous to the naïve Markov approximation

$$\begin{aligned}\frac{\partial\rho_{\rm S}(t)}{\partial t} &= -i/\hbar\left[\hat{H}_{\rm S},\rho_{\rm S}(t)\right]- \\ &\quad -\frac{\lambda^2}{\hbar^2}\iint_0^\infty\Big(\mathcal{R}_\omega(t-s)\left[\hat{\sigma}_z,e^{-i/\hbar\hat{H}_{\rm S}(t-s)}\left[\hat{\sigma}_z,\rho_{\rm S}(s)\right]e^{i/\hbar\hat{H}_{\rm S}(t-s)}\right]+ \\ &\qquad +\mathcal{I}_\omega(t-s)\left[\hat{\sigma}_z,e^{-i/\hbar\hat{H}_{\rm S}(t-s)}\left[\hat{\sigma}_z,\rho_{\rm S}(s)\right]_+e^{i/\hbar\hat{H}_{\rm S}(t-s)}\right]\Big)\,d\omega\,ds\end{aligned} \tag{B.27}$$

and replace in second order perturbation theory $\rho_{\rm S}(s)$ by

$$\rho_{\rm S}(s) = e^{-\mathcal{L}_{\rm S}(t-s)}\rho_{\rm S}(t)+\mathcal{O}\left(\lambda^2\right) = e^{+i/\hbar\hat{H}_{\rm S}(t-s)}\rho_{\rm S}(t)e^{-i/\hbar\hat{H}_{\rm S}(t-s)}+\mathcal{O}\left(\lambda^2\right) \tag{B.28}$$

such that

$$\begin{aligned}\frac{\partial\rho_{\rm S}(t)}{\partial t} &\simeq -i/\hbar\left[\hat{H}_{\rm S},\rho_{\rm S}(t)\right]- \\ &\quad -\frac{\lambda^2}{\hbar^2}\iint_0^\infty\mathcal{R}_\omega(t-s)\left[\hat{\sigma}_z,e^{-i/\hbar\hat{H}_{\rm S}(t-s)}\left[\hat{\sigma}_z,e^{+i/\hbar\hat{H}_{\rm S}(t-s)}\rho_{\rm S}(t)e^{-i/\hbar\hat{H}_{\rm S}(t-s)}\right]e^{i/\hbar\hat{H}_{\rm S}(t-s)}\right]+ \\ &\qquad +\mathcal{I}_\omega(t-s)\left[\hat{\sigma}_z,e^{-i/\hbar\hat{H}_{\rm S}(t-s)}\left[\hat{\sigma}_z,e^{+i/\hbar\hat{H}_{\rm S}(t-s)}\rho_{\rm S}(t)e^{-i/\hbar\hat{H}_{\rm S}(t-s)}\right]_+e^{i/\hbar\hat{H}_{\rm S}(t-s)}\right]d\omega\,ds \\ &= -i/\hbar\left[\hat{H}_{\rm S},\rho_{\rm S}(t)\right]- \\ &\quad -\frac{\lambda^2}{\hbar^2}\iint_0^\infty\mathcal{R}_\omega(\tau)\left[\hat{\sigma}_z,\left[\tilde{\hat{\sigma}}_z(\tau),\rho_{\rm S}(t)\right]\right]+\mathcal{I}_\omega(\tau)\left[\hat{\sigma}_z,\left[\tilde{\hat{\sigma}}_z(\tau),\rho_{\rm S}(t)\right]_+\right]d\omega\,d\tau\ .\end{aligned} \tag{B.29}$$

Here we use the Bloch-sphere representation and equation B.5 to obtain

$$\begin{aligned}\frac{\partial\rho_{\rm S}(t)}{\partial t} &= -i/\hbar\left[\hat{H}_{\rm S},\rho_{\rm S}(t)\right]- \\ &\quad -\frac{\lambda^2}{\hbar^2}\iint_0^\infty\mathcal{R}_\omega(\tau)\Big\{\sigma_x(t)\left[\hat{\sigma}_z,\left[\frac{\epsilon^2+\Delta^2\cos(\Omega\tau)}{\Omega^2}\hat{\sigma}_z,\hat{\sigma}_x\right]\right]+ \\ &\qquad +\sigma_y(t)\left[\hat{\sigma}_z,\left[\frac{\epsilon^2+\Delta^2\cos(\Omega\tau)}{\Omega^2}\hat{\sigma}_z,\hat{\sigma}_y\right]\right]+ \\ &\qquad +\sigma_z(t)\left[\hat{\sigma}_z,\left[\frac{\epsilon\Delta}{\Omega^2}(1-\cos(\Omega\tau))\hat{\sigma}_x+\frac{\Delta}{\Omega}\sin(\Omega\tau)\hat{\sigma}_y,\hat{\sigma}_z\right]\right]\Big\}+ \\ &\quad +\mathcal{I}_\omega(\tau)\left[\hat{\sigma}_z,\frac{\epsilon\Delta}{\Omega^2}(1-\cos(\Omega\tau))\hat{\sigma}_x+\frac{\Delta}{\Omega}\sin(\Omega\tau)\hat{\sigma}_y\right]d\omega\,d\tau\ ;\end{aligned} \tag{B.30}$$

thereby we have tacitly omitted those $\hat{\sigma}_j$ as well as $\frac{\mathbb{1}_{\rm S}}{2}$-terms in the (anti)-commutators, which evidently disappears during these operations.

After some Pauli-spin matrix commutator algebra we receive

$$\begin{aligned}\frac{\partial\rho_{\rm S}(t)}{\partial t} &= -i/\hbar\left[\hat{H}_{\rm S},\rho_{\rm S}(t)\right]- \\ &\quad -\frac{\lambda^2}{\hbar^2}\iint_0^\infty \mathcal{R}_\omega(\tau)\Big\{\sigma_x(t)\frac{\epsilon^2+\Delta^2\cos(\Omega\tau)}{\Omega^2}\hat{\sigma}_x+\sigma_y(t)\frac{\epsilon^2+\Delta^2\cos(\Omega\tau)}{\Omega^2}\hat{\sigma}_y+ \\ &\qquad +\sigma_z(t)\left(-\frac{\epsilon\Delta}{\Omega^2}(1-\cos(\Omega\tau))\hat{\sigma}_x-\frac{\Delta}{\Omega}\sin(\Omega\tau)\hat{\sigma}_y\right)\Big\}+ \\ &\quad +i\mathcal{I}_\omega(\tau)\left\{\frac{\epsilon\Delta}{\Omega^2}(1-\cos(\Omega\tau))\hat{\sigma}_y-\frac{\Delta}{\Omega}\sin(\Omega\tau)\hat{\sigma}_x\right\}d\omega\,d\tau\ . \qquad \text{(B.31)}\end{aligned}$$

At this point we evaluate the following integration relations

$$\begin{aligned}\iint_0^\infty \mathcal{R}_\omega(\tau)\sin(k\Omega\tau)\,d\tau\,d\omega &= \iint_0^\infty \frac{J(\omega)}{\pi}\coth(\hbar\beta\omega/2)\cos(\omega\tau)\sin(k\Omega\tau)\,d\tau\,d\omega \\ &= \iint_0^\infty \frac{J(\omega)}{\pi}\coth(\hbar\beta\omega/2)\frac{1}{4i}\left[e^{i(k\Omega+\omega)\tau}+e^{i(k\Omega-\omega)\tau}-e^{-i(k\Omega+\omega)\tau}-e^{-i(k\Omega-\omega)\tau}\right]d\tau\,d\omega \\ &= \frac{1}{2}\int_{-\infty}^\infty \frac{J(\omega)}{\pi}\coth(\hbar\beta\omega/2)\frac{1}{4}\Big[\frac{1}{k\Omega+\omega+i\eta}+\frac{1}{k\Omega-\omega+i\eta}+ \\ &\qquad +\frac{1}{k\Omega+\omega-i\eta}+\frac{1}{k\Omega-\omega-i\eta}\Big]d\omega \\ &= \frac{2\pi i}{2}\Big\{\frac{1}{\pi}\sum_j J(\omega_j)\frac{2}{\hbar\beta}\frac{1}{2}\left[\frac{1}{k\Omega+\omega_j}+\frac{1}{k\Omega-\omega_j}\right]+ \\ &\qquad +\frac{1}{\pi}\alpha i\omega_c\frac{\omega_c^2}{2i\omega_c}\coth(i\omega_c\hbar\beta/2)\frac{1}{2}\left[\frac{1}{k\Omega+i\omega_c}+\frac{1}{k\Omega-i\omega_c}\right]\Big\} \\ &= i\sum_j J(\omega_j)\frac{2}{\hbar\beta}\left[\frac{k\Omega}{k^2\Omega^2-\omega_j^2}\right]+\frac{1}{2}J(k\Omega)\cot(\omega_c\hbar\beta/2) \\ &= \frac{1}{2}\big(\mathscr{M}(k\Omega,\omega_c,\beta)+J(k\Omega)\cot(\omega_c\hbar\beta/2)\big)\ , \qquad \text{(B.32)}\end{aligned}$$

with $\mathscr{M}(\dots)$ the Matsubara series as defined in eq. B.23;

$$\begin{aligned}
\iint_0^\infty \mathcal{R}_\omega(\tau)\cos(k\Omega\tau)\,d\tau\,d\omega &= \iint_0^\infty \frac{J(\omega)}{\pi}\coth(\hbar\beta\omega/2)\cos(\omega\tau)\cos(k\Omega\tau)\,d\tau\,d\omega \\
&= \iint_0^\infty \frac{J(\omega)}{\pi}\coth(\hbar\beta\omega/2)\frac{1}{4}\left[e^{i(k\Omega+\omega)\tau}+e^{i(k\Omega-\omega)\tau}+e^{-i(k\Omega+\omega)\tau}+e^{-i(k\Omega-\omega)\tau}\right]d\tau\,d\omega \\
&= \frac{1}{2}\int_{-\infty}^\infty \frac{J(\omega)}{\pi}\coth(\hbar\beta\omega/2)\frac{i}{4}\Bigg[\frac{1}{k\Omega+\omega+i\eta}+\frac{1}{k\Omega-\omega+i\eta}- \\
&\qquad -\frac{1}{k\Omega+\omega-i\eta}-\frac{1}{k\Omega-\omega-i\eta}\Bigg]d\omega \\
&= \frac{1}{2}J(k\Omega)\coth(k\Omega\hbar\beta/2)\ , \qquad \text{(B.33)}
\end{aligned}$$

for the real part correlation functions, as well as

$$\begin{aligned}
\iint_0^\infty \mathcal{I}_\omega(\tau)\sin(k\Omega\tau)\,d\tau\,d\omega &= -i\iint_0^\infty \frac{J(\omega)}{\pi}\sin(\omega\tau)\sin(k\Omega\tau)\,d\tau\,d\omega \\
&= -i\iint_0^\infty \frac{J(\omega)}{\pi}\frac{-1}{4}\left[e^{i(k\Omega+\omega)\tau}-e^{i(k\Omega-\omega)\tau}-e^{-i(k\Omega+\omega)\tau}+e^{-i(k\Omega-\omega)\tau}\right]d\tau\,d\omega \\
&= \frac{1}{2}\int_{-\infty}^\infty \frac{J(\omega)}{\pi}\frac{-1}{4}\left[\frac{1}{k\Omega+\omega+i\eta}-\frac{1}{k\Omega-\omega+i\eta}+\frac{1}{k\Omega+\omega-i\eta}-\frac{1}{k\Omega-\omega-i\eta}\right]d\omega \\
&= \frac{-i}{2}J(k\Omega)\ , \qquad \text{(B.34)}
\end{aligned}$$

and

$$\begin{aligned}
\iint_0^\infty \mathcal{I}_\omega(\tau)\cos(k\Omega\tau)\,d\tau\,d\omega &= -i\iint_0^\infty \frac{J(\omega)}{\pi}\sin(\omega\tau)\cos(k\Omega\tau)\,d\tau\,d\omega \\
&= -i\iint_0^\infty \frac{J(\omega)}{\pi}\frac{1}{4i}\left[e^{i(k\Omega+\omega)\tau}-e^{i(k\Omega-\omega)\tau}-e^{-i(k\Omega+\omega)\tau}+e^{-i(k\Omega-\omega)\tau}\right]d\tau\,d\omega \\
&= \frac{1}{2}\int_{-\infty}^\infty \frac{J(\omega)}{\pi}\frac{-i}{4}\left[\frac{1}{k\Omega+\omega+i\eta}-\frac{1}{k\Omega-\omega+i\eta}+\frac{1}{k\Omega+\omega-i\eta}-\frac{1}{k\Omega-\omega-i\eta}\right]d\omega \\
&= \pi i\frac{1}{\pi}\alpha i\omega_c\frac{\omega_c^2}{2i\omega_c}\frac{-i}{4}2\left[\frac{1}{k\Omega+i\omega_c}-\frac{1}{k\Omega-i\omega_c}\right] \\
&= \frac{1}{2}\frac{-i\alpha\omega_c^3}{k^2\Omega^2+\omega_c^2}\ , \qquad \text{(B.35)}
\end{aligned}$$

for the imaginary parts.

By means of these intermediate results we receive for the Bloch-Redfield master equation in Bloch-sphere matrix formulation

$$\frac{\partial\vec{\sigma}(t)}{\partial t} = \hat{M}_{\mathrm{BR}}\vec{\sigma}(t)+\vec{I}_{\mathrm{BR}}\ , \qquad \text{(B.36)}$$

with the usual free Hamiltonian part B.13 and the second order perturbation term

$$\hat{M}^{\mathrm{BR}}_{\mathrm{diss}} = -\lambda^2/\hbar^2 \begin{pmatrix} M^{\mathrm{BR}}_{xx} & 0 & 0 \\ 0 & M^{\mathrm{BR}}_{yy} & 0 \\ M^{\mathrm{BR}}_{zx} & M^{\mathrm{BR}}_{zy} & 0 \end{pmatrix} \quad , \tag{B.37}$$

as well as for the inhomogenous term

$$\vec{I}_{\mathrm{BR}} = -\lambda^2/\hbar^2 \begin{pmatrix} I^{\mathrm{BR}}_{x} \\ I^{\mathrm{BR}}_{y} \\ 0 \end{pmatrix} \quad . \tag{B.38}$$

Using the formerly calculated integration relations B.32, B.33,B.34,B.35 we obtain from eq. B.31 for the individual entries of $\hat{M}^{\mathrm{BR}}_{\mathrm{diss}}$

$$\begin{aligned} M^{\mathrm{BR}}_{xx} &= \iint_0^\infty \mathcal{R}_\omega(\tau) \left(\frac{\epsilon^2}{\Omega^2} + \frac{\Delta^2}{\Omega^2} \cos(\Omega\tau) \right) d\omega \, d\tau \\ &= \frac{\epsilon^2}{2\Omega^2} \frac{2\alpha}{\hbar\beta} + \frac{\Delta^2}{2\Omega^2} J(\Omega) \coth(\Omega\hbar\beta/2) \;=\; M^{\mathrm{BR}}_{yy} \quad , \end{aligned} \tag{B.39}$$

$$\begin{aligned} M^{\mathrm{BR}}_{zx} &= \iint_0^\infty \mathcal{R}_\omega(\tau) \frac{\Delta\epsilon}{\Omega^2} (\cos(\Omega\tau) - 1) \, d\omega \, d\tau \\ &= \frac{\Delta\epsilon}{2\Omega^2} J(\Omega) \coth(\Omega\hbar\beta/2) - \frac{\Delta\epsilon}{2\Omega^2} \frac{2\alpha}{\hbar\beta} \quad , \end{aligned} \tag{B.40}$$

$$\begin{aligned} M^{\mathrm{BR}}_{zy} &= \iint_0^\infty \mathcal{R}_\omega(\tau) \frac{-\Delta}{\Omega} \sin(\Omega\tau) \, d\omega \, d\tau \\ &= -\frac{\Delta}{\Omega} \big(\mathscr{M}(\Omega, \omega_c, \beta) + J(\Omega) \cot(\omega_c \hbar\beta/2) \big) \quad , \end{aligned} \tag{B.41}$$

as well as for $\vec{I}_{\mathrm{BR}}$

$$\begin{aligned} I^{\mathrm{BR}}_{x} &= -i \iint_0^\infty \mathcal{I}_\omega(\tau) \frac{\Delta}{\Omega} \sin(\Omega\tau) \, d\omega \, d\tau \\ &= -\frac{\Delta}{2\Omega} J(\Omega) \quad , \end{aligned} \tag{B.42}$$

$$\begin{aligned} I^{\mathrm{BR}}_{y} &= i \iint_0^\infty \mathcal{I}_\omega(\tau) \frac{\Delta\epsilon}{\Omega^2} (1 - \cos(\Omega\tau)) \, d\omega \, d\tau \\ &= \frac{\Delta\epsilon}{2\Omega^2} \left(\alpha\omega_c - \frac{\alpha\omega_c^3}{\Omega^2 + \omega_c^2} \right) \;=\; \frac{\Delta\epsilon}{2\Omega^2} \frac{\alpha\Omega^2\omega_c}{\Omega^2 + \omega_c^2} \quad . \end{aligned} \tag{B.43}$$

B.3 Davies-Łuczka approximation

Now we calculate the matrix form of the Davies-Łuczka Markov approximation 1.58

$$\mathcal{M}_{\mathrm{DL}} \;:=\; \bar{\mathscr{K}} \;=\; \sum_n \mathbb{P}_n \left(\int_0^\infty e^{-\mathcal{L}_0 \tau} \mathcal{K}(\tau)\, d\tau \right) \mathbb{P}_n \;. \tag{B.44}$$

for the spin-boson memory kernel 1.74

$$\begin{aligned} \mathcal{K}(\tau)\rho_{\mathrm{S}}(t) \;=\; -\frac{\lambda^2}{\hbar^2} \int_0^\infty & \mathcal{R}_\omega(\tau) \left[\hat{\sigma}_z, e^{-i/\hbar \hat{H}_{\mathrm{S}} \tau} \left[\hat{\sigma}_z, \rho_{\mathrm{S}}(t) \right] e^{i/\hbar \hat{H}_{\mathrm{S}} \tau} \right] + \\ & + \mathcal{I}_\omega(\tau) \left[\hat{\sigma}_z, e^{-i/\hbar \hat{H}_{\mathrm{S}} \tau} \left[\hat{\sigma}_z, \rho_{\mathrm{S}}(t) \right]_+ e^{i/\hbar \hat{H}_{\mathrm{S}} \tau} \right] d\omega \;. \end{aligned} \tag{B.45}$$

The corresponding projection operators 1.54 can be derived by means of the rotating frame spin operators B.4

$$\mathcal{L}_0 \;=\; -i/\hbar \left[\hat{H}_{\mathrm{S}}, .. \right] \;=\; -i\Omega \left[\hat{\sigma}'_z, .. \right] \tag{B.46}$$

such that the corresponding "eigenstates" were given by

$$\begin{aligned} \mathcal{L}_0 \hat{\sigma}'_z \;&=\; -i\Omega \left[\hat{\sigma}'_z, \hat{\sigma}'_z \right] \;=\; 0 \\ \mathcal{L}_0 \hat{\sigma}'_\pm \;&=\; -i\Omega \left[\hat{\sigma}'_z, \hat{\sigma}'_\pm \right] \;=\; \mp i\Omega \hat{\sigma}'_\pm \\ \mathcal{L}_0 \mathbb{1}_{\mathrm{S}} \;&=\; -i\Omega \left[\hat{\sigma}'_z, \mathbb{1}_{\mathrm{S}} \right] \;=\; 0 \end{aligned} \tag{B.47}$$

with

$$\hat{\sigma}'_\pm \;=\; \frac{1}{2} \left(\hat{\sigma}'_x \pm i \hat{\sigma}'_y \right) \;, \tag{B.48}$$

such that

$$\begin{aligned} \mathbb{P}_0 \;&:=\; |\hat{\sigma}'_z >< \hat{\sigma}'_z| \\ \mathbb{P}_\pm \;&:=\; |\hat{\sigma}'_\pm >< \hat{\sigma}'_\pm| \\ \mathbb{P}_{\mathbf{1}_{\mathrm{S}}} \;&:=\; |\mathbb{1}_{\mathrm{S}} >< \mathbb{1}_{\mathrm{S}}| \;. \end{aligned} \tag{B.49}$$

Here we have to take care, as the precondition of a non-degenerated spectrum of $\mathcal{L}_0$ for a dissolution of the time/weak-coupling averaged memory kernel in projectional parts is violated for $\hat{\sigma}'_z$ and $\mathbb{1}_{\mathrm{S}}$ B.47; this means, that we furthermore have to take into account for both operational terms effects in regard of each other. This does not make the calculations

much more extensive, as terms in $\mathbb{1}_{\mathrm{S}}$ as usual disappears during the second commutator.

Anyway it is most easy to calculate the Davies-Łuczka master equation inside the rotating frame and back-translating the results into the ordinary spin-picture afterwards. We obtain for eq. B.44

$$\begin{aligned}\mathcal{M}_{\mathrm{DL}} \;:=\; -\frac{\lambda^2}{\hbar^2}\iint_0^\infty \mathcal{R}_\omega(\tau)\Big\{ &\Big(\sigma'_z(t)\left[\tilde{\hat{\sigma}}_z(\tau),[\hat{\sigma}_z,\hat{\sigma}'_z]\right]\Big)_{\sigma'_z\oplus\mathbb{1}_{\mathrm{S}}} + \Big(\sigma'_+(t)\left[\tilde{\hat{\sigma}}_z(\tau),[\hat{\sigma}_z,\hat{\sigma}'_+]\right]\Big)_{\sigma'_+} \\ &+ \Big(\sigma'_-(t)\left[\tilde{\hat{\sigma}}_z(\tau),[\hat{\sigma}_z,\hat{\sigma}'_-]\right]\Big)_{\sigma'_-}\Big\} + \\ +\mathcal{I}_\omega(\tau)\Big\{ &\Big(\sigma'_z(t)\left[\tilde{\hat{\sigma}}_z(\tau),[\hat{\sigma}_z,\hat{\sigma}'_z]_+\right]\Big)_{\sigma'_z\oplus\mathbb{1}_{\mathrm{S}}} + \Big(\sigma'_+(t)\left[\tilde{\hat{\sigma}}_z(\tau),[\hat{\sigma}_z,\hat{\sigma}'_+]_+\right]\Big)_{\sigma'_+} \\ &+ \Big(\sigma'_-(t)\left[\tilde{\hat{\sigma}}_z(\tau),[\hat{\sigma}_z,\hat{\sigma}'_-]_+\right]\Big)_{\sigma'_-} + \Big(1/2\left[\tilde{\hat{\sigma}}_z(\tau),[\hat{\sigma}_z,\mathbb{1}_{\mathrm{S}}]_+\right]\Big)_{\sigma'_z\oplus\mathbb{1}_{\mathrm{S}}}\Big\}\, d\omega\, d\tau \;,\end{aligned}$$

where $\sigma'_{z,\pm}(t)$ denotes the Bloch sphere representation terms of the actual density matrix in the rotating frame

$$\rho_{\mathrm{S}}(t) \;=\; \sigma'_z(t)\hat{\sigma}'_z + \sigma'_+(t)\hat{\sigma}'_+ + \sigma'_-(t)\hat{\sigma}'_- + \mathbb{1}_{\mathrm{S}}/2 \;, \tag{B.50}$$

with $\sigma'_\pm$ replacing the usual $\sigma'_{x,y}$. $\left(\hat{X}\right)_{\sigma'_{x/y}}$ designates the $\sigma'_{x/y}$-part of the spin operator $\hat{X}$, paying tribute to the second (left) projection operation of eq. B.44. $\left(\hat{X}\right)_{\sigma'_z\oplus\mathbb{1}_{\mathrm{S}}}$ were the corresponding $\hat{\sigma}'_z$ and $\mathbb{1}_{\mathrm{S}}$ terms following its degenerated free Liouvillian eigenvalues. Evidently all terms in $\mathbb{1}_{\mathrm{S}}$ vanishes due to the external commutator.

Considering the rotating frame expansion B.4

$$\hat{\sigma}_z \;=\; \frac{1}{\Omega}\left(\epsilon\hat{\sigma}'_z - \Delta\hat{\sigma}'_x\right) \;=\; \frac{1}{\Omega}\left(\epsilon\hat{\sigma}'_z - \Delta\hat{\sigma}'_+ - \Delta\hat{\sigma}'_-\right) \tag{B.51}$$

we get

$$\begin{aligned}\left[\hat{\sigma}_z,\hat{\sigma}'_z\right] &= \frac{1}{\Omega}\left[\epsilon\hat{\sigma}'_z - \Delta\hat{\sigma}'_+ - \Delta\hat{\sigma}'_-,\hat{\sigma}'_z\right] \\ &= \frac{\Delta}{\Omega}\left(\hat{\sigma}'_+ - \hat{\sigma}'_-\right) \\ \left[\hat{\sigma}_z,\hat{\sigma}'_\pm\right] &= \pm\frac{\epsilon}{\Omega}\hat{\sigma}'_\pm \pm \frac{\Delta}{2\Omega}\hat{\sigma}'_z \;,\end{aligned} \tag{B.52}$$

and

$$\begin{aligned}\left[\hat{\sigma}_z,\hat{\sigma}'_z\right]_+ &= \frac{\epsilon}{2\Omega}\mathbb{1}_{\mathrm{S}} \\ \left[\hat{\sigma}_z,\hat{\sigma}'_\pm\right]_+ &= -\frac{\Delta}{4\Omega}\mathbb{1}_{\mathrm{S}} \\ \frac{1}{2}\left[\hat{\sigma}_z,\mathbb{1}_{\mathrm{S}}\right]_+ = \hat{\sigma}_z &= \frac{\epsilon}{\Omega}\hat{\sigma}'_z - \frac{\Delta}{\Omega}\hat{\sigma}'_x = \frac{\epsilon}{\Omega}\hat{\sigma}'_z - \frac{\Delta}{\Omega}\left(\hat{\sigma}'_+ + \hat{\sigma}'_-\right) \;,\end{aligned} \tag{B.53}$$

we receive

$$\begin{aligned}\mathcal{M}_{\rm DL} \;:=\; & -\frac{\lambda^2}{\hbar^2}\iint_0^\infty \mathcal{R}_\omega(\tau)\Bigg\{ \left(\sigma_z'(t)\frac{\Delta}{\Omega}\left[\tilde{\hat\sigma}_z(\tau),\hat\sigma_+'-\hat\sigma_-'\right]\right)_{\sigma_z'\oplus\mathbb{1}_{\rm S}} + \\ & + \left(\sigma_+'(t)\left[\tilde{\hat\sigma}_z(\tau),\frac{\epsilon}{\Omega}\hat\sigma_+'+\frac{\Delta}{2\Omega}\hat\sigma_z'\right]\right)_{\sigma_+'} + \left(\sigma_-'(t)\left[\tilde{\hat\sigma}_z(\tau),-\frac{\epsilon}{\Omega}\hat\sigma_-'-\frac{\Delta}{2\Omega}\hat\sigma_z'\right]\right)_{\sigma_-'}\Bigg\} + \\ & +\mathcal{I}_\omega(\tau)\Bigg\{ \left(\sigma_z'(t)\left[\tilde{\hat\sigma}_z(\tau),\frac{\epsilon}{2\Omega}\mathbb{1}_{\rm S}\right]\right)_{\sigma_z'\oplus\mathbb{1}_{\rm S}} - \left(\sigma_+'(t)\left[\tilde{\hat\sigma}_z(\tau),\frac{\Delta}{4\Omega}\mathbb{1}_{\rm S}\right]\right)_{\sigma_+'} - \\ & - \left(\sigma_-'(t)\left[\tilde{\hat\sigma}_z(\tau),\frac{\Delta}{4\Omega}\mathbb{1}_{\rm S}\right]\right)_{\sigma_-'} + \left(\left[\tilde{\hat\sigma}_z(\tau),\frac{\epsilon}{\Omega}\hat\sigma_z'-\frac{\Delta}{\Omega}\hat\sigma_+'-\frac{\Delta}{\Omega}\hat\sigma_-'\right]\right)_{\sigma_z'\oplus\mathbb{1}_{\rm S}}\Bigg\}\, d\omega\, d\tau \;.\end{aligned}$$

By using the relation

$$\tilde{\hat\sigma}_z(\tau) \;=\; \frac{1}{\Omega}\left(\epsilon\tilde{\hat\sigma}_z'(\tau)-\Delta\tilde{\hat\sigma}_+'(\tau)-\Delta\tilde{\hat\sigma}_+'(\tau)\right) \;=\; \frac{1}{\Omega}\left(\epsilon\hat\sigma_z'-\Delta e^{-i\Omega\tau}\hat\sigma_+'-\Delta e^{+i\Omega\tau}\hat\sigma_+'\right) \;, \tag{B.54}$$

follows

$$\begin{aligned}\mathcal{M}_{\rm DL} \;:=\; & -\frac{\lambda^2}{\hbar^2}\iint_0^\infty \mathcal{R}_\omega(\tau)\frac{1}{\Omega^2}\Bigg\{ \left(\sigma_z'(t)\Delta\left[\epsilon\hat\sigma_z'-\Delta e^{-i\Omega\tau}\hat\sigma_+'-\Delta e^{+i\Omega\tau}\hat\sigma_-',\hat\sigma_+'-\hat\sigma_-'\right]\right)_{\sigma_z'\oplus\mathbb{1}_{\rm S}} + \\ & + \left(\sigma_+'(t)\left[\epsilon\hat\sigma_z'-\Delta e^{-i\Omega\tau}\hat\sigma_+'-\Delta e^{+i\Omega\tau}\hat\sigma_-',\epsilon\hat\sigma_+'+\frac{\Delta}{2}\hat\sigma_z'\right]\right)_{\sigma_+'} + \\ & + \left(\sigma_-'(t)\left[\epsilon\hat\sigma_z'-\Delta e^{-i\Omega\tau}\hat\sigma_+'-\Delta e^{+i\Omega\tau}\hat\sigma_-',-\epsilon\hat\sigma_-'-\frac{\Delta}{2}\hat\sigma_z'\right]\right)_{\sigma_-'}\Bigg\} + \\ & +\mathcal{I}_\omega(\tau)\frac{1}{\Omega^2}\Bigg\{ \left(\left[\epsilon\hat\sigma_z'-\Delta e^{-i\Omega\tau}\hat\sigma_+'-\Delta e^{+i\Omega\tau}\hat\sigma_-',\epsilon\hat\sigma_z'-\Delta\hat\sigma_+'-\Delta\hat\sigma_-'\right]\right)_{\sigma_z'\oplus\mathbb{1}_{\rm S}}\Bigg\}\, d\omega\, d\tau \\ = \; & -\frac{\lambda^2}{\hbar^2}\iint_0^\infty \mathcal{R}_\omega(\tau)\Bigg\{\sigma_z'(t)\frac{\Delta^2}{\Omega^2}\cos(\Omega\tau)\hat\sigma_z' + \sigma_+'(t)\left[\frac{\epsilon^2}{\Omega^2}+\frac{\Delta^2}{2\Omega^2}e^{-i\Omega\tau}\right]\hat\sigma_+' + \\ & +\sigma_-'(t)\left[\frac{\epsilon^2}{\Omega^2}+\frac{\Delta^2}{2\Omega^2}e^{i\Omega\tau}\right]\hat\sigma_-'\Bigg\} + \mathcal{I}_\omega(\tau)\left[\frac{\Delta^2}{2\Omega^2}\left(e^{-i\Omega\tau}-e^{i\Omega\tau}\right)\right]\hat\sigma_z'\, d\omega\, d\tau \\ = \; & -\frac{\lambda^2}{\hbar^2}\iint_0^\infty \mathcal{R}_\omega(\tau)\Bigg\{\sigma_z'(t)\frac{\Delta^2}{\Omega^2}\cos(\Omega\tau)\hat\sigma_z' + \sigma_x'(t)\Bigg(\left[2\frac{\epsilon^2}{\Omega^2}+\frac{\Delta^2}{\Omega^2}\cos(\Omega\tau)\right]\hat\sigma_x' + \\ & + \left[\frac{\Delta^2}{\Omega^2}\sin(\Omega\tau)\right]\hat\sigma_y'\Bigg) + \sigma_y'(t)\left(\left[\frac{\Delta^2}{\Omega^2}\sin(\Omega\tau)\right]\hat\sigma_x' + \left[-2\frac{\epsilon^2}{\Omega^2}-\frac{\Delta^2}{\Omega^2}\cos(\Omega\tau)\right]\hat\sigma_y'\right)\Bigg\} \\ & -i\mathcal{I}_\omega(\tau)\left[\frac{\Delta^2}{\Omega^2}\sin(\Omega\tau)\right]\hat\sigma_z'\, d\omega\, d\tau \;,\end{aligned} \tag{B.55}$$

where we have retranslated $\hat\sigma_\pm' = 1/2(\hat\sigma_x' \pm i\hat\sigma_y')$. Now, we just have to change back into the non-rotating frame by use of relations B.4. In order to keep equations compact, we just

list here the effects of the non-rotating "coordinates" $\sigma_j(t)$ in regard of the non-rotating spin operators $\hat{\sigma}_j$.

$$\begin{aligned}
\sigma_x(t) \quad \cdot \quad & \left\{ \left(\frac{\epsilon^2}{\Omega^2} \left[2\frac{\epsilon^2}{\Omega^2} + \frac{\Delta^2}{\Omega^2}\cos(\Omega\tau) \right] + \frac{\Delta^2}{\Omega^2} \left[\frac{\Delta^2}{\Omega^2}\cos(\Omega\tau) \right] \right) \hat{\sigma}_x + \frac{\epsilon}{\Omega} \left[\frac{\Delta^2}{\Omega^2}\sin(\Omega\tau) \right] \hat{\sigma}_y + \right. \\
& \left. + \left(-\frac{\epsilon\Delta}{\Omega^2} \left[2\frac{\epsilon^2}{\Omega^2} + \frac{\Delta^2}{\Omega^2}\cos(\Omega\tau) \right] + \frac{\epsilon\Delta}{\Omega^2} \left[\frac{\Delta^2}{\Omega^2}\cos(\Omega\tau) \right] \right) \hat{\sigma}_z \right\} \\
= \quad & \sigma_x(t) \left\{ \left(2\frac{\epsilon^4}{\Omega^4} + \frac{\Delta^2}{\Omega^2}\cos(\Omega\tau) \right) \hat{\sigma}_x + \frac{\epsilon\Delta^2}{\Omega^3}\sin(\Omega\tau)\hat{\sigma}_y - 2\frac{\epsilon^3\Delta}{\Omega^4}\hat{\sigma}_z \right\} \ , \qquad \text{(B.56)} \\
\sigma_y(t) \quad \cdot \quad & \left\{ \frac{\epsilon}{\Omega} \left[\frac{\Delta^2}{\Omega^2}\sin(\Omega\tau) \right] \hat{\sigma}_x + \left[-2\frac{\epsilon^2}{\Omega^2} - \frac{\Delta^2}{\Omega^2}\cos(\Omega\tau) \right] \hat{\sigma}_y - \frac{\Delta^3}{\Omega^3}\sin(\Omega\tau)\hat{\sigma}_z \right\} \\
= \quad & \sigma_y(t) \left\{ \frac{\epsilon\Delta^2}{\Omega^3}\sin(\Omega\tau)\hat{\sigma}_x - \left(2\frac{\epsilon^2}{\Omega^2} + \frac{\Delta^2}{\Omega^2}\cos(\Omega\tau) \right) \hat{\sigma}_y - \frac{\Delta^3}{\Omega^3}\sin(\Omega\tau)\hat{\sigma}_z \right\} \ , \qquad \text{(B.57)} \\
\sigma_z(t) \quad \cdot \quad & \left\{ \left(\frac{\epsilon\Delta}{\Omega^2} \left[\frac{\Delta^2}{\Omega^2}\cos(\Omega\tau) \right] - \frac{\epsilon\Delta}{\Omega^2} \left[2\frac{\epsilon^2}{\Omega^2} + \frac{\Delta^2}{\Omega^2}\cos(\Omega\tau) \right] \right) \hat{\sigma}_x - \frac{\Delta}{\Omega} \left[\frac{\Delta^2}{\Omega^2}\sin(\Omega\tau) \right] \hat{\sigma}_y + \right. \\
& \left. + \left(\frac{\epsilon^2}{\Omega^2} \left[\frac{\Delta^2}{\Omega^2}\cos(\Omega\tau) \right] + \frac{\Delta^2}{\Omega^2} \left[2\frac{\epsilon^2}{\Omega^2} + \frac{\Delta^2}{\Omega^2}\cos(\Omega\tau) \right] \right) \hat{\sigma}_z \right\} \\
= \quad & \sigma_z(t) \left\{ -2\frac{\epsilon^3\Delta}{\Omega^4}\hat{\sigma}_x - \frac{\Delta^3}{\Omega^3}\sin(\Omega\tau)\hat{\sigma}_y + \left(2\frac{\epsilon^2\Delta^2}{\Omega^4} + \frac{\Delta^2}{\Omega^2}\cos(\Omega\tau) \right) \hat{\sigma}_z \right\} \ . \qquad \text{(B.58)}
\end{aligned}$$

For the inhomogenous term (so to say generated by the constant part $\mathbb{1}_{\mathrm{S}}$ of $\rho_{\mathrm{S}}(t)$) we obtain

$$-i \quad \cdot \quad \left\{ \frac{\Delta^3}{\Omega^3}\sin(\Omega\tau)\hat{\sigma}_x + \frac{\epsilon\Delta^2}{\Omega^3}\sin(\Omega\tau)\hat{\sigma}_z \right\} \ . \qquad \text{(B.59)}$$

Altogether we receive for the Bloch sphere matrix representation of the Davies-Łuczka Markov approximation

$$\frac{\partial\vec{\sigma}(t)}{\partial t} = \hat{M}_{\mathrm{DL}}\vec{\sigma}(t) + \vec{I}_{\mathrm{DL}} \ , \qquad \text{(B.60)}$$

by use of eqs. B.32 and B.33 the as matrix entries of the dissipative part

$$\begin{aligned}
M_{xx}^{\mathrm{DL}} &= \frac{\epsilon^4}{\Omega^4}\frac{2\alpha}{\hbar\beta} + \frac{\Delta^2}{2\Omega^2}J(\Omega)\coth(\Omega\hbar\beta/2) \ , \\
M_{xy}^{\mathrm{DL}} &= \frac{\epsilon\Delta^2}{2\Omega^3}\left[\mathscr{M}(\Omega,\omega_c,\beta) + J(\Omega)\cot(\omega_c\hbar\beta/2)\right] \ , \\
M_{xz}^{\mathrm{DL}} &= -\frac{\epsilon^3\Delta}{\Omega^4}\frac{2\alpha}{\hbar\beta} \ ,
\end{aligned}$$

$$
\begin{aligned}
M_{yx}^{\mathrm{DL}} &= \frac{\epsilon\Delta^2}{2\Omega^3}\left[\mathscr{M}(\Omega,\omega_c,\beta)+J(\Omega)\cot(\omega_c\hbar\beta/2)\right] \ , \\
M_{yy}^{\mathrm{DL}} &= -\frac{\epsilon^2}{\Omega^2}\frac{2\alpha}{\hbar\beta}-\frac{\Delta^2}{2\Omega^2}J(\Omega)\coth(\Omega\hbar\beta/2) \ , \\
M_{yz}^{\mathrm{DL}} &= -\frac{\Delta^3}{2\Omega^3}\left[\mathscr{M}(\Omega,\omega_c,\beta)+J(\Omega)\cot(\omega_c\hbar\beta/2)\right] \ , \\
M_{zx}^{\mathrm{DL}} &= -\frac{\epsilon^3\Delta}{\Omega^4}\frac{2\alpha}{\hbar\beta} \ , \\
M_{zy}^{\mathrm{DL}} &= -\frac{\Delta^3}{2\Omega^3}\left[\mathscr{M}(\Omega,\omega_c,\beta)+J(\Omega)\cot(\omega_c\hbar\beta/2)\right] \ , \\
M_{zz}^{\mathrm{DL}} &= \frac{\epsilon^2\Delta^2}{\Omega^4}\frac{2\alpha}{\hbar\beta}+\frac{\Delta^2}{2\Omega^2}J(\Omega)\coth(\Omega\hbar\beta/2) \ . \qquad \text{(B.61)}
\end{aligned}
$$

The inhomogenous vector $\vec{I}_{\mathrm{DL}}$ is evaluated with eq. B.34 as follows

$$
\begin{aligned}
I_x^{\mathrm{DL}} &= -\frac{\Delta^3}{2\Omega^3}J(\Omega) \\
I_z^{\mathrm{DL}} &= -\frac{\epsilon\Delta^2}{2\Omega^3}J(\Omega) \ . \qquad \text{(B.62)}
\end{aligned}
$$

B.4 Lindblad approximation according Celio and Loss

As mentioned in chapter 1.3.2 the Markov approximation according Celio and Loss [42] is composed as arithmetic average of the former discussed Bloch-Redfield formula

$$\mathcal{M}_{\mathrm{CL},1} \;=\; -\lambda^2/\hbar^2 \int_0^\infty \langle \mathcal{L}_\mathrm{I} e^{-\mathcal{L}_0\tau} \mathcal{L}_\mathrm{I} \rangle_\beta e^{\mathcal{L}_S\tau}\, d\tau \;, \tag{B.63}$$

plus an approach with inverse symmetry

$$\mathcal{M}_{\mathrm{CL},2} \;=\; -\lambda^2/\hbar^2 \int_0^\infty e^{-\mathcal{L}_S\tau} \langle \mathcal{L}_\mathrm{I} e^{-\mathcal{L}_0\tau} \mathcal{L}_\mathrm{I} \rangle_\beta \, d\tau \;, \tag{B.64}$$

such that

$$\mathcal{M}_\mathrm{CL} \;=\; \frac{1}{2}\left(\mathcal{M}_{\mathrm{CL},1} + \mathcal{M}_{\mathrm{CL},2}\right) \;=\; -\frac{\lambda^2}{2\hbar^2} \int_0^\infty \left(e^{-\mathcal{L}_S\tau} \langle \mathcal{L}_\mathrm{I} e^{-\mathcal{L}_0\tau} \mathcal{L}_\mathrm{I} \rangle_\beta + \langle \mathcal{L}_\mathrm{I} e^{-\mathcal{L}_0\tau} \mathcal{L}_\mathrm{I} \rangle_\beta e^{-\mathcal{L}_S\tau} \right) d\tau \;. \tag{B.65}$$

As the first case is evaluated in chapter B.2, we focus on expression B.64 at first. From eq. B.45 we obtain

$$\begin{aligned}
\mathcal{M}_{\mathrm{CL},2}\rho_\mathrm{S}(t) \;&=\; -\frac{\lambda^2}{\hbar^2} \iint_0^\infty \mathcal{R}_\omega(\tau) e^{i/\hbar \hat{H}_\mathrm{S}\tau} \left[\hat{\sigma}_z, e^{-i/\hbar\hat{H}_\mathrm{S}\tau}\left[\hat{\sigma}_z, \rho_\mathrm{S}(t)\right] e^{i/\hbar\hat{H}_\mathrm{S}\tau}\right] e^{-i/\hbar\hat{H}_\mathrm{S}\tau} + \\
&\qquad + \mathcal{I}_\omega(\tau) e^{i/\hbar\hat{H}_\mathrm{S}\tau} \left[\hat{\sigma}_z, e^{-i/\hbar\hat{H}_\mathrm{S}\tau}\left[\hat{\sigma}_z, \rho_\mathrm{S}(t)\right]_+ e^{i/\hbar\hat{H}_\mathrm{S}\tau}\right] e^{-i/\hbar\hat{H}_\mathrm{S}\tau}\, d\tau\, d\omega \;. \\
&=\; -\frac{\lambda^2}{\hbar^2} \iint_0^\infty \mathcal{R}_\omega(\tau) \left[\tilde{\hat{\sigma}}_z(\tau), \left[\hat{\sigma}_z, \rho_\mathrm{S}(t)\right]\right] + \mathcal{I}_\omega(\tau) \left[\tilde{\hat{\sigma}}_z(\tau), \left[\hat{\sigma}_z, \rho_\mathrm{S}(t)\right]_+\right] d\omega \\
&=\; -\frac{\lambda^2}{\hbar^2} \iint_0^\infty i\mathcal{R}_\omega(\tau) \left[\tilde{\hat{\sigma}}_z(\tau), \left(\sigma_x(t)\hat{\sigma}_y - \sigma_y(t)\hat{\sigma}_x\right)\right] + \\
&\qquad + \mathcal{I}_\omega(\tau) \left[\tilde{\hat{\sigma}}_z(\tau), \left(2\sigma_z(t)\mathbb{1}_\mathrm{S} + \hat{\sigma}_z\right)\right] d\tau\, d\omega \\
&=\; -\frac{\lambda^2}{\hbar^2} \iint_0^\infty i^2\mathcal{R}_\omega(\tau) \Bigg\{ \sigma_x(t) \left(-\frac{\epsilon^2 + \Delta^2\cos(\Omega\tau)}{\Omega^2}\hat{\sigma}_x + \frac{\epsilon\Delta}{\Omega^2}(1-\cos(\Omega\tau))\hat{\sigma}_z \right) + \\
&\qquad + \sigma_y(t) \left(-\frac{\epsilon^2 + \Delta^2\cos(\Omega\tau)}{\Omega^2}\hat{\sigma}_y + \frac{\Delta}{\Omega}\sin(\Omega\tau)\hat{\sigma}_z \right) \Bigg\} + \\
&\qquad + i\mathcal{I}_\omega(\tau) \left(-\frac{\epsilon\Delta}{\Omega^2}(1-\cos(\Omega\tau))\hat{\sigma}_y + \frac{\Delta}{\Omega}\sin(\Omega\tau)\hat{\sigma}_x \right) d\tau\, d\omega \;,
\end{aligned} \tag{B.66}$$

which evidently has almost the same results as the Bloch-Redfield calculation B.31.

In order to derive the corresponding Bloch-sphere matrix form 1.13

$$\frac{\partial\vec{\sigma}(t)}{\partial t} \;=\; \left(\hat{M}_\mathrm{unitary} - \lambda^2/\hbar^2\hat{M}_{\mathrm{CL},2}\right)\vec{\sigma}(t) - \lambda^2/\hbar^2\vec{I}_{\mathrm{CL},2} \;, \tag{B.67}$$

with $\hat{M}_{\text{untary}}$ as given in B.13, we apply formula B.33 and B.35, such that

$$\begin{aligned} M_{xx}^{\text{CL},2} &= \iint_0^\infty \mathcal{R}_\omega(\tau)\frac{\epsilon^2+\Delta^2\cos(\Omega\tau)}{\Omega^2}\,d\tau\,d\omega \\ &= \frac{\epsilon^2}{2\Omega^2}\left[J(x)\coth(x\hbar\beta/2)\right]_{x\leftarrow 0} + \frac{\Delta^2}{2\Omega^2}J(\Omega)\coth(\Omega\hbar\beta/2) \\ &= \frac{\epsilon^2}{2\Omega^2}\frac{2\alpha}{\hbar\beta} + \frac{\Delta^2}{2\Omega^2}J(\Omega)\coth(\Omega\hbar\beta/2) \;=\; M_{yy}^{\text{CL},2}\ , \end{aligned} \tag{B.68}$$

$$\begin{aligned} M_{xz}^{\text{CL},2} &= \iint_0^\infty \mathcal{R}_\omega(\tau)\frac{\epsilon\Delta}{\Omega^2}(\cos(\Omega\tau)-1)\,d\tau\,d\omega \\ &= \frac{\epsilon\Delta}{2\Omega^2}\left(J(\Omega)\coth(\Omega\hbar\beta/2) - \frac{2\alpha}{\hbar\beta}\right)\ , \end{aligned} \tag{B.69}$$

$$\begin{aligned} M_{yz}^{\text{CL},2} &= -\iint_0^\infty \mathcal{R}_\omega(\tau)\frac{\Delta}{\Omega}\sin(\Omega\tau)\,d\tau\,d\omega \\ &= \frac{-\Delta}{2\Omega}\big(\mathscr{M}(\Omega,\omega_c,\beta) + J(\Omega)\cot(\omega_c\hbar\beta/2)\big)\ , \end{aligned} \tag{B.70}$$

as well as for the inhomogenous term

$$\begin{aligned} I_x^{\text{CL},2} &= i\iint_0^\infty \mathcal{I}_\omega(\tau)\frac{\Delta}{\Omega}\,d\tau\,d\omega \\ &= \frac{\Delta}{2\Omega}J(\Omega)\ , \end{aligned} \tag{B.71}$$

$$\begin{aligned} I_y^{\text{CL},2} &= i\iint_0^\infty \mathcal{I}_\omega(\tau)\frac{\Delta\epsilon}{\Omega^2}(\cos(\Omega\tau)-1)\,d\tau\,d\omega \\ &= \frac{\Delta\epsilon}{2\Omega^2}\alpha\left(\frac{\omega_c^3}{\Omega^2+\omega_c^2} - \omega_c\right) \;=\; -\alpha\frac{\Delta\epsilon}{2\Omega}\omega_c\frac{\Omega^2}{\Omega^2+\omega_c^2}\ . \end{aligned} \tag{B.72}$$

Apparently, $\hat{M}_{\text{CL},2}$ is just the Hermitian transposed form of $\hat{M}_{\text{BR}}$, while the inhomogenous terms have only different signs of their entries (such that $\vec{I}_{\text{CL}} = \vec{0}$). If we now regard the Bloch-Redfield terms 1.46-B.43 we get altogether for the dissipative Celio-Loss matrix

$$\hat{M}_{\text{CL}} \;=\; \begin{pmatrix} M_{xx}^{\text{CL}} & 0 & M_{xz}^{\text{CL}} \\ 0 & M_{yy}^{\text{CL}} & M_{yz}^{\text{CL}} \\ M_{zx}^{\text{CL}} & M_{zy}^{\text{CL}} & 0 \end{pmatrix}\ , \tag{B.73}$$

with

$$\begin{aligned} M_{xx}^{\text{CL}} &= \frac{\epsilon^2}{2\Omega^2}\frac{2\alpha}{\hbar\beta} + \frac{\Delta^2}{2\Omega^2}J(\Omega)\coth(\Omega\hbar\beta/2) \;=\; M_{yy}^{\text{CL}}\ , \\ M_{xz}^{\text{CL}} &= \frac{\epsilon\Delta}{2\Omega^2}\left(J(\Omega)\coth(\Omega\hbar\beta/2) - \frac{2\alpha}{\hbar\beta}\right) \;=\; M_{zx}^{\text{CL}}\ , \\ M_{yz}^{\text{CL}} &= \frac{-\Delta}{2\Omega}\big(\mathscr{M}(\Omega,\omega_c,\beta) + J(\Omega)\cot(\omega_c\hbar\beta/2)\big) \;=\; M_{zy}^{\text{CL}}\ . \end{aligned} \tag{B.74}$$

Appendix C

Random walk analysis

In chapter 2.3.1 we derived different random walk models to evaluate analytically the decoherence impact of a bfl-noise source applied on a single qubit; thereby was chosen a stochastical Hamiltonian approach, where the dissipative evolution of the qubit was represented by the corresponding set of (quantum) trajectories, a spin performs on its Bloch sphere. The usual description of using density matrices following adequate master equations, which leads to according observable expectation values, was replaced by statistical averages respectively distributions of pure spin state sets on the Bloch sphere .

C.1 Symmetrical random walk (driftless)

C.1.1 Pure bfl-noise

In 2.5.2 we derived the one-step random walk distributions $\Phi^{\text{bfl}}_{\text{odd/even}}$ of the pure and symmetrical bfl noise

$$\Phi^{\text{bfl}}_{\text{odd/even}}(x) = \frac{e^{\mp x/\gamma}\theta(\pm x)}{\gamma} \tag{C.1}$$

with $\gamma = \frac{\sqrt{5}}{2}\alpha\tau_{\text{bfl}}$ the typical one-step deviation as calculated in Equ. 2.28.

For the following two- and several-step random walk analysis it proves to be helpful to change into the Fourier-transformed k-space, where deriving N-step distributions just corresponds to according products of one- (or here for symmetry reasons two-)step distributions (in accordance to the convolution theorem [47]). With $\tilde{\Phi}(k) = \mathscr{F}[\Phi(x)]$ denoting the Fourier transformed of $\Phi(x)$ one receives for our one-step distributions

$$\begin{aligned}\tilde{\Phi}^{\text{bfl}}_{\text{odd/even}} &= \int_{-\infty}^{\infty} dx e^{-ikx}\Phi^{\text{bfl}}_{\text{odd/even}} = \int_{-\infty}^{\infty} dx e^{-ikx}\frac{e^{\mp x/\gamma}\theta(\pm x)}{\gamma} \\ &= \frac{1}{\gamma}\int_{0}^{\infty} dx e^{-x(1/\gamma\pm ik)} = \frac{-1}{1\pm i\gamma k}\left[e^{-x(1/\gamma\pm ik)}\right]_0^{\infty} = \frac{1}{1\pm i\gamma k},\end{aligned} \tag{C.2}$$

and therefore for our two-step distributions

$$\tilde{\Phi}_2^{\text{bfl}} = \tilde{\Phi}_{\text{odd}}^{\text{bfl}} \cdot \tilde{\Phi}_{\text{even}}^{\text{bfl}} = \frac{1}{(1+i\gamma k)(1-i\gamma k)} = \frac{1}{1+\gamma^2 k^2}. \quad \text{(C.3)}$$

To receive the corresponding (and drift-less) $2N$-step distribution, one has only to apply the Fourier-analysis convolution theorem iteratively

$$\tilde{\Phi}_{2N}^{\text{bfl}} = \left(\tilde{\Phi}_2^{\text{bfl}}\right)^N = \frac{1}{(1+\gamma^2 k^2)^N}. \quad \text{(C.4)}$$

As generally known from stochastical analysis [61], one can easily derives drift-effects ($\langle x\rangle$, with $\langle ...\rangle$ the expectation value in regard of the distribution Φ) and σ-deviations ($\Delta\sigma = \sqrt{\langle x^2\rangle - \langle x\rangle^2}$), if the Fourier-transformed $\tilde{\Phi}(k)$ were well-known functions by following equivalence(s)

$$\langle x\rangle = \int_{-\infty}^{\infty} dx x\Phi(x) = i\left[\frac{d}{dk}\tilde{\Phi}(k)\right]_{k=0}, \quad \text{(C.5)}$$

respectively

$$\langle x^2\rangle = \int_{-\infty}^{\infty} dx x^2\Phi(x) = -\left[\frac{d^2}{dk^2}\tilde{\Phi}(k)\right]_{k=0}. \quad \text{(C.6)}$$

First derivation from expression C.4 leads to

$$\frac{d}{dk}\tilde{\Phi}(k) = -2N\gamma^2 k\left(\frac{1}{1+\gamma^2 k^2}\right)^{N+1} \quad \text{(C.7)}$$

i.e. drift disappeares for that symmetric distribution (as expected); the σ-deviation can easily be calculated to

$$\Delta\sigma_{2N}^{\text{bfl}} = \sqrt{-\frac{d^2}{dk^2}\tilde{\Phi}_{2N}^{\text{bfl}}(k)} = \sqrt{2N\gamma^2\left[\left(\frac{1}{1+\gamma^2 k^2}\right)^{N+1}\right]_{k=0}} = \sqrt{2N}\gamma, \quad \text{(C.8)}$$

thus follows equation 2.31.

C.1.2 Bang-bang refocused random walk

For the spin-echo refocused random walk we have derived flat distributions for the one-step deviations

$$\Phi^{\mathrm{bb}}_{\mathrm{odd/even}}(x) \;=\; \frac{\theta(\pm x)\theta\left(\gamma_{\mathrm{bb}} \mp x\right)}{\gamma_{\mathrm{bb}}}, \tag{C.9}$$

from which we analogously to eq. C.2 receive

$$\begin{aligned}\tilde{\Phi}^{\mathrm{bb}}_{\mathrm{odd/even}} &= \int_{-\infty}^{\infty} dx e^{-ikx}\frac{\theta(\pm x)\theta\left(\gamma_{\mathrm{bb}} \mp x\right)}{\gamma_{\mathrm{bb}}} = \frac{1}{\gamma_{\mathrm{bb}}}\int_0^{\gamma_{\mathrm{bb}}} dx e^{\mp ikx} \\ &= \frac{\pm i}{\gamma_{\mathrm{bb}}k}\left[e^{\mp ikx}\right]_0^{\gamma_{\mathrm{bb}}} = \frac{\mp i(1-e^{\mp i\gamma_{\mathrm{bb}}k})}{\gamma_{\mathrm{bb}}k}.\end{aligned} \tag{C.10}$$

For the two-step distribution follows

$$\tilde{\Phi}^{\mathrm{bb}}_{2} \;=\; \tilde{\Phi}^{\mathrm{bb}}_{\mathrm{odd}}\cdot\tilde{\Phi}^{\mathrm{bb}}_{\mathrm{even}} \;=\; \frac{-i(1-e^{-i\gamma_{\mathrm{bb}}k})}{\gamma_{\mathrm{bb}}k}\cdot\frac{i(1-e^{i\gamma_{\mathrm{bb}}k})}{\gamma_{\mathrm{bb}}k} \;=\; 2\frac{1-\cos(\gamma_{\mathrm{bb}}k)}{\gamma_{\mathrm{bb}}^2k^2}. \tag{C.11}$$

As one apparently sees, the two-step and thus the $2N$-step distributions were symmetric around $k=0$ as well (therefore the drift $\langle x\rangle = 0$); in order to derive the corresponding σ-deviation $\Delta\sigma_{2N}$ we calculate at first the first derivation of $\tilde{\Phi}^{\mathrm{bb}}_{2N}(k)$

$$\frac{d}{dk}\tilde{\Phi}^{\mathrm{bb}}_{2N}(k) \;=\; N\left(2\frac{1-\cos(\gamma_{\mathrm{bb}}k)}{\gamma_{\mathrm{bb}}^2k^2}\right)^{N-1}\left[2\frac{\gamma_{\mathrm{bb}}\sin(\gamma_{\mathrm{bb}}k)\gamma_{\mathrm{bb}}^2k^2-(1-\cos(\gamma_{\mathrm{bb}}k))2\gamma_{\mathrm{bb}}^2k}{\gamma_{\mathrm{bb}}^4k^4}\right]\xrightarrow{k\to 0}0 \tag{C.12}$$

which follows *e.g.* from expansion of the sine- and cosine-terms in [...] in the first orders of k.

Second derivation at $k=0$ leads to

$$\begin{aligned}\Delta\sigma^{\mathrm{bb}}_{2N} &= \sqrt{-\frac{d^2}{dk^2}\tilde{\Phi}^{\mathrm{bb}}_{2N}(k)} \\ &= \sqrt{-\frac{d}{dk}N\left(2\frac{1-\cos(\gamma_{\mathrm{bb}}k)}{\gamma_{\mathrm{bb}}^2k^2}\right)^{N-1}\left[2\frac{\gamma_{\mathrm{bb}}\sin(\gamma_{\mathrm{bb}}k)\gamma_{\mathrm{bb}}^2k^2-(1-\cos(\gamma_{\mathrm{bb}}k))2\gamma_{\mathrm{bb}}^2k}{\gamma_{\mathrm{bb}}^4k^4}\right]} \\ &\overset{k\to 0}{=} \sqrt{-N\frac{d}{dk}\left[2\frac{\gamma_{\mathrm{bb}}\sin(\gamma_{\mathrm{bb}}k)\gamma_{\mathrm{bb}}^2k^2-(1-\cos(\gamma_{\mathrm{bb}}k))2\gamma_{\mathrm{bb}}^2k}{\gamma_{\mathrm{bb}}^4k^4}\right]_{k=0}} = \ldots \\ &= \sqrt{2N\left[\frac{4\gamma_{\mathrm{bb}}^3k\sin(\gamma_{\mathrm{bb}}k)-\gamma_{\mathrm{bb}}^4k^2\cos(\gamma_{\mathrm{bb}}k)-6\gamma_{\mathrm{bb}}^2(1-\cos(\gamma_{\mathrm{bb}}k))}{\gamma_{\mathrm{bb}}^4k^4}\right]_{k=0}} \\ &= \sqrt{\frac{2N}{\gamma_{\mathrm{bb}}^4k^4}\left[4\gamma_{\mathrm{bb}}^4k^2-\frac{4}{3!}\gamma_{\mathrm{bb}}^6k^4-\gamma_{\mathrm{bb}}^4k^2+\frac{1}{2!}\gamma_{\mathrm{bb}}^6k^4-\frac{6}{2!}\gamma_{\mathrm{bb}}^4k^2+\frac{6}{4!}\gamma_{\mathrm{bb}}^6k^4+\mathcal{O}(k^6)\right]_{k=0}} \\ &= \sqrt{\frac{N}{6}}\gamma_{\mathrm{bb}},\end{aligned} \tag{C.13}$$

from which equation 2.76 follows.

Appendix D

Bosonic fields scaling formalism

D.1 Derivation of the first order scaling equations

In order to apply *operator product expansions* on the arising second order terms of the dressed-spin couplings we firstly have to understand, how the argument of scaling invariance of the corresponding partition function Z (3.51) takes into account. For receiving second order expressions we content ourselfes here with the second order approximation of Z

$$Z \simeq Z^* \left[1 - \sum_j \Delta_j \int a^{-y_j} \left\langle \mathscr{O}_j \right\rangle dx_1 + \frac{1}{2!} \sum_{j,k} \Delta_j \Delta_k \int \int a^{-y_j - y_k} \left\langle \mathcal{O}_j \mathcal{O}_k \right\rangle d^d x_1 \, d^d x_2 \right]. \tag{D.1}$$

Thereby the integrations has to be performed on the bath degrees of freedom, which here is assumed to be a bosonic lattice field with a given lattice size L, an appropriate microscopic energy band-width a, as well as a specified bath systems dimension d (*e.g.* $d \in \{1, 2, 3\}$ depending on the physical nature of the bath).

In accordance with J. Cardy ([72]) there are two different contributions to the scaling behaviour of the dressed-spin couplings at an infinitesimal changing of the band-with $a \mapsto a(1 + \delta l)$. First, explicitly by direct changing of the prefactors a^{-y_j}; second, implicitly via the shifting of the lower boundaries of the integrals, which were given by the varied low-energy cut-off a.

The first one will lead to a linearly rescaling of the coupling factors as follows

$$a^{-y_j} \Delta_j(l) \mapsto a^{-y_j} \left(1 + \delta l\right)^{-y_j} \Delta_j(a(1 + \delta l)) = a^{-y_j} \left(1 - y_j \delta l + \mathcal{O}(|\delta l|^2)\right) \Delta_j(a(1 + \delta l)) \tag{D.2}$$

which in order to compensate first order effects results in

$$\Delta_j(a(1 + \delta l)) = \frac{\Delta_j(a)}{(1 - y_j \delta l + \mathcal{O}(|\delta l|^2)} = \Delta_j(a)(1 + y_j \delta l + \mathcal{O}(|\delta l|^2)) \tag{D.3}$$

such that

$$\frac{\partial \Delta_j}{\partial l} = \lim_{\delta l \to 0} \frac{\Delta_j(a(1+\delta l)) - \Delta_j(a)}{\delta l} = y_j \Delta_j(a) \tag{D.4}$$

delivers the scaling equations first order.

D.2 Derivation of the second order scaling equations

To receive further, higher order terms, we have to take into account how the integral expression in eq. D.1 changes with varying low-energy cut-off a; therefor we notice, that when the lower integration limit a will be enlarged to $a(1+\delta l)$, the rescaled integration will provide a difference of

$$\int_{|x_1-x_2|>a(1+\delta l)} = \int_{|x_1-x_2|>a} - \int_{a(1+\delta l)>|x_1-x_2|>a}, \tag{D.5}$$

which by use of the *operation product expansion* (weak) identity (see eq. 3.54)

$$\mathscr{O}_j(x_1)\mathscr{O}_k(x_2) = \sum_l C_{jkl}(x_1-x_2)\mathscr{O}_l\left(\frac{x_1+x_2}{2}\right) \tag{D.6}$$

and the corresponding constant expansion coefficients

$$C_{jkl}(x_1-x_2) = \frac{c_{jkl}}{|x_1-x_2|^{z_j+z_k-z_l}}\ , \tag{D.7}$$

with

$$z_\mu = d - y_\mu$$

will in total lead to a second order variation of

$$\frac{1}{2}\sum_{jkl} c_{jkl} a^{z_l-z_j-z_k} \int_{a(1+\delta l)>|x_1-x_2|>a} \left\langle \mathscr{O}_l\left(\frac{x_1-x_2}{2}\right)\right\rangle \frac{d^d x_1\, d^d x_2}{a^{2d-z_j-z_k}}\ ; \tag{D.8}$$

such that the scaling compensation of the couplings Δ_l has to be fulfilled by

$$\Delta_l(a(1+\delta l)) \simeq \Delta_l(a) + y_l\Delta_l(a) - \frac{1}{2}S_d \sum_{jk} c_{jkl}\Delta_j\Delta_k \delta l\ . \tag{D.9}$$

This leads to a second order differential term of $-\frac{1}{2}S_d\sum_{jk} c_{jkl}\Delta_j\Delta_k$ and as total second order scaling equations we receive

$$\frac{\partial \Delta_l}{\partial l} = y_l\Delta_l - \frac{1}{2}S_d\sum_{jk} c_{jkl}\Delta_j\Delta_k\ , \tag{D.10}$$

where it remains to evaluate the combinatorical *operator product expansion* coefficients c_{jkl} by appropriate application mainly of vertex operator calculus.

D.2.1 Calculation of the *operator product expansions*

First of all we review the list of effective spin operators, which arise during second order processes from the elementary couplings

$$\mathscr{O}_0 = \frac{1}{\sqrt{2}}\left[\hat{\sigma}_1^+ \hat{V}^S_{-\lambda_S}\hat{V}^A_{-\lambda_A} + \hat{\sigma}_2^+ \hat{V}^S_{-\lambda_S}\hat{V}^A_{\lambda_A} + h.c.\right] \tag{D.11}$$

$$\mathscr{O}_{++} = \sqrt{2}\left[\hat{\sigma}_1^+\hat{\sigma}_2^+ \hat{V}^S_{-2\lambda_S} + h.c.\right] \tag{D.12}$$

$$\mathscr{O}_{+-} = \sqrt{2}\left[\hat{\sigma}_1^+\hat{\sigma}_2^- \hat{V}^A_{-2\lambda_A} + h.c.\right], \tag{D.13}$$

with the formerly defined vertex operators

$$\hat{V}^S_\gamma = d^{-\gamma^2/2} e^{i\gamma\tilde{\Phi}} \tag{D.14}$$

$$\hat{V}^A_\delta = d^{-\delta^2/2} e^{i\delta\Phi_A}, \tag{D.15}$$

which there are

$$\mathscr{O}_{\mathbf{1}} = \mathbb{1}, \tag{D.16}$$

$$\mathscr{O}_z = \hat{\sigma}_1^z\hat{\sigma}_2^z, \tag{D.17}$$

$$\mathscr{O}_S = \frac{1}{\sqrt{2}}\left(\hat{\sigma}_1^z + \hat{\sigma}_2^z\right)\partial_x\Phi_S, \tag{D.18}$$

$$\mathscr{O}_A = \frac{1}{\sqrt{2}}\left(\hat{\sigma}_1^z - \hat{\sigma}_2^z\right)\partial_x\Phi_A. \tag{D.19}$$

To evaluate the various second order products of the effective spin operators one first has to remember, how the vertex operators of the different bosonic fields (symmetric Φ_S and antisymmetric Φ_A) does behave, when being multiplied with each other. Evidently, products of vertex operators from different fields do not mutually affect, as they commute. But if vertex operators of the same sort of fields encounter, they accumulate (in increasing order of the rescaling parameter a) as follows

$$\hat{V}^j_\gamma(x)\hat{V}^j_\delta(x') = \hat{V}^j_{\gamma+\delta}(x')\left(ix - ix' + a\right)^{\gamma\delta} + \gamma^*_* \hat{V}^j_{\gamma+\delta}(x')\partial_{x'}\Phi_j(x')\left(ix - ix' + a\right)^{\gamma\delta+1}{}^*_* + ...,$$

where one has to consider the typical normal-ordering calculation procedures (for details see J. von Delft and H. Schoeller [68], chapter 9.C); ${}^*_*\mathscr{F}(\Phi, \partial_x\Phi)^*_*$ denotes the appropriate normal ordered form of a function $\mathscr{F}(\Phi, \partial_x\Phi)$ of fields operators Φ and its derivatives $\partial_x\Phi$. For $x \to x'$ this goes to

$$\left[\hat{V}^j_\gamma(x)\hat{V}^j_\delta(x')\right]_{x\to x'} = \hat{V}^j_{\gamma+\delta}(x')a^{\gamma\delta} + \gamma^*_*\hat{V}^j_{\gamma+\delta}(x')\partial_{x'}\Phi_j(x')a^{\gamma\delta+1}{}^*_* + ... \quad . \tag{D.20}$$

Now we have to distinguish between two particular cases. First, if the vertex operator coefficients were of equal absolute value, but different sign $\delta = -\gamma$, than the product according eq. (D.20) can be written concisely as

$$\hat{V}^j_\gamma \hat{V}^j_{-\gamma} \;=\; a^{-\gamma^2}\mathbb{1} + \gamma a^{-\gamma^2+1}\partial_x \Phi_j + \mathcal{O}(a^{-\gamma^2+2}), \tag{D.21}$$

where we neglect terms of the class $\mathcal{O}\left(|\partial_z \Phi^j_z|^2\right)$ in consideration of dimensional analysis. Otherwise (*i.e.* if $\delta \neq -\gamma$) we receive

$$\hat{V}^j_\gamma \hat{V}^j_\delta \;=\; a^{-\gamma\delta}\hat{V}^j_{\gamma+\delta} + \gamma a^{-\gamma\delta+1}\hat{V}^j_{\gamma+\delta}\partial_x \Phi_j + \mathcal{O}(a^{-\gamma^2+2}). \tag{D.22}$$

In consistence with the operator product expansion (weak) identity (eq. (3.54)), we furthermore will neglect terms of non-fitting exponential dependence in a.

The products of $\hat{\sigma}^\pm_j$ and $\hat{\sigma}^z_j$ operators behave as follows

$$\begin{aligned}
\hat{\sigma}^\pm_j \hat{\sigma}^\pm_j &= \frac{1}{4}\left(\hat{\sigma}^x_j \pm i\hat{\sigma}^y_j\right)^2 \\
&= \frac{1}{4}\left(\hat{\sigma}^x_j\hat{\sigma}^x_j \pm i\left(\hat{\sigma}^x_j\hat{\sigma}^y_j + \hat{\sigma}^y_j\hat{\sigma}^x_j\right) - \hat{\sigma}^y_j\hat{\sigma}^y_j\right) \\
&= \frac{1}{4}\left(\mathbb{1} \pm i\left(\hat{\sigma}^x_j\hat{\sigma}^y_j - \hat{\sigma}^x_j\hat{\sigma}^y_j\right) - \mathbb{1}\right) \;=\; 0 \quad ,
\end{aligned} \tag{D.23}$$

$$\begin{aligned}
\hat{\sigma}^\pm_j \hat{\sigma}^\mp_j &= \frac{1}{4}\left(\hat{\sigma}^x_j\hat{\sigma}^x_j \mp i\left(\hat{\sigma}^x_j\hat{\sigma}^y_j - \hat{\sigma}^y_j\hat{\sigma}^x_j\right) + \hat{\sigma}^y_j\hat{\sigma}^y_j\right) \\
&= \frac{1}{2}\left(\mathbb{1} \mp \hat{\sigma}^z_j\right) \quad ,
\end{aligned} \tag{D.24}$$

$$\begin{aligned}
\hat{\sigma}^\pm_j \hat{\sigma}^z_j &= \frac{1}{2}\left(\hat{\sigma}^x_j\hat{\sigma}^z_j \pm i\hat{\sigma}^y_j\hat{\sigma}^z_j\right) \\
&= \frac{1}{2}\left(i\hat{\sigma}^y_j \pm \hat{\sigma}^x_j\right) \;=\; \pm\hat{\sigma}^\pm_j \;=\; -\hat{\sigma}^z_j\hat{\sigma}^\pm_j \quad .
\end{aligned} \tag{D.25}$$

By use of these spin and vertex operator product rules, we can evaluate the numerous dressed-spin operator product expansions as follows

$$\begin{aligned}
\mathscr{O}_0\mathscr{O}_0 &= \frac{1}{2}\left[\hat{\sigma}^+_1\hat{V}^S_{-\lambda_S}\hat{V}^A_{-\lambda_A} + \hat{\sigma}^+_2\hat{V}^S_{-\lambda_S}\hat{V}^A_{\lambda_A} + \hat{\sigma}^-_1\hat{V}^S_{\lambda_S}\hat{V}^A_{\lambda_A} + \hat{\sigma}^-_2\hat{V}^S_{\lambda_S}\hat{V}^A_{-\lambda_A}\right]^2 \\
&= \frac{1}{2}\Big[\hat{\sigma}^+_1\hat{\sigma}^+_2\hat{V}^S_{-\lambda_S}\hat{V}^S_{-\lambda_S}(\hat{V}^A_{-\lambda_A}\hat{V}^A_{\lambda_A} + \hat{V}^A_{\lambda_A}\hat{V}^A_{-\lambda_A}) + \hat{\sigma}^+_1\hat{\sigma}^-_1\hat{V}^S_{-\lambda_S}\hat{V}^S_{\lambda_S}\hat{V}^A_{-\lambda_A}\hat{V}^A_{\lambda_A} + \\
&\quad + \hat{\sigma}^-_1\hat{\sigma}^+_1\hat{V}^S_{\lambda_S}\hat{V}^S_{-\lambda_S}\hat{V}^A_{\lambda_A}\hat{V}^A_{-\lambda_A} + \hat{\sigma}^+_1\hat{\sigma}^-_2(\hat{V}^S_{-\lambda_S}\hat{V}^S_{\lambda_S} + \hat{V}^S_{\lambda_S}\hat{V}^S_{-\lambda_S})\hat{V}^A_{-\lambda_A}\hat{V}^A_{-\lambda_A} + \\
&\quad + \hat{\sigma}^-_1\hat{\sigma}^+_2(\hat{V}^S_{\lambda_S}\hat{V}^S_{-\lambda_S} + \hat{V}^S_{-\lambda_S}\hat{V}^S_{\lambda_S})\hat{V}^A_{\lambda_A}\hat{V}^A_{\lambda_A} + \hat{\sigma}^+_2\hat{\sigma}^-_2\hat{V}^S_{-\lambda_S}\hat{V}^S_{\lambda_S}\hat{V}^A_{\lambda_A}\hat{V}^A_{-\lambda_A} + \\
&\quad + \hat{\sigma}^-_2\hat{\sigma}^+_2\hat{V}^S_{\lambda_S}\hat{V}^S_{-\lambda_S}\hat{V}^A_{-\lambda_A}\hat{V}^A_{\lambda_A} + \hat{\sigma}^-_1\hat{\sigma}^-_2\hat{V}^S_{\lambda_S}\hat{V}^S_{\lambda_S}(\hat{V}^A_{\lambda_A}\hat{V}^A_{-\lambda_A} + \hat{V}^A_{-\lambda_A}\hat{V}^A_{\lambda_A})\Big]
\end{aligned} \tag{D.26}$$

which by appropriate disregarding of prefactors of the art $a^{-\lambda_S^2-\lambda_A^2+j}$ with $j \leq 1$ leads to

$$\begin{aligned}
\mathscr{O}_0\mathscr{O}_0 &= \frac{1}{2}\Big[\hat{\sigma}_1^+\hat{\sigma}_2^+ a^{-\lambda_S^2}\hat{V}^S_{-2\lambda_S}(2a^{-\lambda_A^2}\mathbb{1}) + \\
&\quad + \frac{1}{2}\left(\mathbb{1}-\hat{\sigma}_1^z\right)\left(a^{-\lambda_S^2}\mathbb{1}-\lambda_S a^{-\lambda_S^2+1}\partial_x\Phi_S\right)\cdot\left(a^{-\lambda_A^2}\mathbb{1}-\lambda_A a^{-\lambda_A^2+1}\partial_x\Phi_A\right) + \\
&\quad + \frac{1}{2}\left(\mathbb{1}+\hat{\sigma}_1^z\right)\left(a^{-\lambda_S^2}\mathbb{1}+\lambda_S a^{-\lambda_S^2+1}\partial_x\Phi_S\right)\cdot\left(a^{-\lambda_A^2}\mathbb{1}+\lambda_A a^{-\lambda_A^2+1}\partial_x\Phi_A\right) + \\
&\quad + \hat{\sigma}_1^+\hat{\sigma}_2^-(2a^{-\lambda_S^2}\mathbb{1})\hat{V}^A_{-2\lambda_A} + \hat{\sigma}_1^-\hat{\sigma}_2^+(2a^{-\lambda_S^2}\mathbb{1})\hat{V}^A_{2\lambda_A} + \\
&\quad + \frac{1}{2}\left(\mathbb{1}-\hat{\sigma}_2^z\right)\left(a^{-\lambda_S^2}\mathbb{1}-\lambda_S a^{-\lambda_S^2+1}\partial_x\Phi_S\right)\cdot\left(a^{-\lambda_A^2}\mathbb{1}+\lambda_A a^{-\lambda_A^2+1}\partial_x\Phi_A\right) + \\
&\quad + \frac{1}{2}\left(\mathbb{1}+\hat{\sigma}_2^z\right)\left(a^{-\lambda_S^2}\mathbb{1}+\lambda_S a^{-\lambda_S^2+1}\partial_x\Phi_S\right)\cdot\left(a^{-\lambda_A^2}\mathbb{1}-\lambda_A a^{-\lambda_A^2+1}\partial_x\Phi_A\right) + \\
&\quad + \hat{\sigma}_1^-\hat{\sigma}_2^- a^{-\lambda_S^2}\hat{V}^S_{2\lambda_S}(2a^{-\lambda_A^2}\mathbb{1})\Big] \qquad \text{(D.27)} \\
&= \frac{a^{-\lambda_S^2-\lambda_A^2}}{\sqrt{2}}\mathscr{O}_{++} + \frac{a^{-\lambda_S^2-\lambda_A^2}}{\sqrt{2}}\mathscr{O}_{+-} + a^{-\lambda_S^2-\lambda_A^2}\mathscr{O}_{\mathbb{1}} + \\
&\quad + \frac{\lambda_S a^{-\lambda_S^2-\lambda_A^2+1}}{\sqrt{2}}\mathscr{O}_S + \frac{\lambda_A a^{-\lambda_S^2-\lambda_A^2+1}}{\sqrt{2}}\mathscr{O}_A + \mathcal{O}\left(|\partial_x\Phi|^2\right) \quad . \qquad \text{(D.28)}
\end{aligned}$$

Therefor considering the weak sense relation (D.6 and D.7) we can write

$$\left\langle \mathscr{O}_0\mathscr{O}_0 \right\rangle \simeq \frac{\langle\mathscr{O}_{++}\rangle}{\sqrt{2}} + \frac{\langle\mathscr{O}_{+-}\rangle}{\sqrt{2}} + \langle\mathscr{O}_{\mathbb{1}}\rangle + \lambda_S\frac{\langle\mathscr{O}_S\rangle}{\sqrt{2}} + \lambda_A\frac{\langle\mathscr{O}_A\rangle}{\sqrt{2}} + \mathcal{O}\left(|\partial_x\Phi|^2\right) \quad , \qquad \text{(D.29)}$$

respectively

$$c_{0,0,++} = \tfrac{1}{\sqrt{2}} \ , \ c_{0,0,+-} = \tfrac{1}{\sqrt{2}} \ , \ c_{0,0,\mathbb{1}} = 1 \ , \ c_{0,0,S} = \tfrac{\lambda_S}{\sqrt{2}} \ , \ c_{0,0,A} = \tfrac{\lambda_A}{\sqrt{2}} \ . \qquad \text{(D.30)}$$

The further mixed products will we evaluate in symmetric sums $(\mathscr{O}_j\mathscr{O}_k + \mathscr{O}_k\mathscr{O}_j)$ as they appear in these combinations in our double sums in D.1

$$\begin{aligned}
\mathscr{O}_0\mathscr{O}_{++} + \mathscr{O}_{++}\mathscr{O}_0 &= \left[\hat{\sigma}_1^+\hat{V}^S_{-\lambda_S}\hat{V}^A_{-\lambda_A} + \hat{\sigma}_2^+\hat{V}^S_{-\lambda_S}\hat{V}^A_{\lambda_A} + h.c.\right]\cdot\left[\hat{\sigma}_1^+\hat{\sigma}_2^+\hat{V}^S_{-2\lambda_S} + h.c.\right] + \\
&\quad + \left[\hat{\sigma}_1^+\hat{\sigma}_2^+\hat{V}^S_{-2\lambda_S} + h.c.\right]\cdot\left[\hat{\sigma}_1^+\hat{V}^S_{-\lambda_S}\hat{V}^A_{-\lambda_A} + \hat{\sigma}_2^+\hat{V}^S_{-\lambda_S}\hat{V}^A_{\lambda_A} + h.c.\right] \\
&= \big[\hat{\sigma}_1^+\hat{\sigma}_1^-\hat{\sigma}_2^-\hat{V}^S_{-\lambda_S}\hat{V}^S_{2\lambda_S}\hat{V}^A_{-\lambda_A} + \hat{\sigma}_2^+\hat{\sigma}_2^-\hat{\sigma}_1^-\hat{V}^S_{-\lambda_S}\hat{V}^S_{2\lambda_S}\hat{V}^A_{\lambda_A} + \\
&\quad + \hat{\sigma}_1^-\hat{\sigma}_1^+\hat{\sigma}_2^+\hat{V}^S_{\lambda_S}\hat{V}^S_{-2\lambda_S}\hat{V}^A_{\lambda_A} + \hat{\sigma}_2^-\hat{\sigma}_2^+\hat{\sigma}_1^+\hat{V}^S_{\lambda_S}\hat{V}^S_{-2\lambda_S}\hat{V}^A_{-\lambda_A}\big] + \\
&\quad + \big[\hat{\sigma}_1^-\hat{\sigma}_1^+\hat{\sigma}_2^-\hat{V}^S_{2\lambda_S}\hat{V}^S_{-\lambda_S}\hat{V}^A_{-\lambda_A} + \hat{\sigma}_2^-\hat{\sigma}_2^+\hat{\sigma}_1^-\hat{V}^S_{2\lambda_S}\hat{V}^S_{-\lambda_S}\hat{V}^A_{\lambda_A} + \\
&\quad + \hat{\sigma}_1^+\hat{\sigma}_1^-\hat{\sigma}_2^+\hat{V}^S_{-2\lambda_S}\hat{V}^S_{\lambda_S}\hat{V}^A_{\lambda_A} + \hat{\sigma}_2^+\hat{\sigma}_2^-\hat{\sigma}_1^+\hat{V}^S_{-2\lambda_S}\hat{V}^S_{\lambda_S}\hat{V}^A_{-\lambda_A}\big] \qquad \text{(D.31)}
\end{aligned}$$

due eq. D.24 we have $\hat{\sigma}_j^+\hat{\sigma}_j^- + \hat{\sigma}_j^-\hat{\sigma}_j^+ = \mathbb{1}$ and $\hat{\sigma}_j^+\hat{\sigma}_j^- - \hat{\sigma}_j^-\hat{\sigma}_j^+ = -\hat{\sigma}_j^z$, such that we receive

$$\begin{aligned}
\mathscr{O}_0\mathscr{O}_{++} + \mathscr{O}_{++}\mathscr{O}_0 &= a^{-2\lambda_S^2}\hat{\sigma}_2^-\hat{V}_{\lambda_S}^S\hat{V}_{-\lambda_A}^A + a^{-2\lambda_S^2}\hat{\sigma}_1^-\hat{V}_{\lambda_S}^S\hat{V}_{\lambda_A}^A + \\
&\quad + a^{-2\lambda_S^2}\hat{\sigma}_2^+\hat{V}_{-\lambda_S}^S\hat{V}_{\lambda_A}^A + a^{-2\lambda_S^2}\hat{\sigma}_1^+\hat{V}_{-\lambda_S}^S\hat{V}_{-\lambda_A}^A - \\
&\quad - \frac{3}{2}\lambda_S a^{-2\lambda_S^2+1}\cdot\left(\hat{\sigma}_1^z\hat{\sigma}_{2\,*}^{-\,*}\hat{V}_{\lambda_S}^S\hat{V}_{-\lambda_A}^A\partial_x\Phi_{S*}^* + \hat{\sigma}_2^z\hat{\sigma}_{1\,*}^{-\,*}\hat{V}_{\lambda_S}^S\hat{V}_{\lambda_A}^A\partial_x\Phi_{S*}^* + \right. \\
&\quad \left. + \hat{\sigma}_1^z\hat{\sigma}_{2\,*}^{+\,*}\hat{V}_{-\lambda_S}^S\hat{V}_{\lambda_A}^A\partial_x\Phi_{S*}^* + \hat{\sigma}_2^z\hat{\sigma}_{1\,*}^{+\,*}\hat{V}_{-\lambda_S}^S\hat{V}_{-\lambda_A}^A\partial_x\Phi_{S*}^*\right) \\
&= \sqrt{2}a^{-2\lambda_S^2}\mathscr{O}_0 + \mathcal{O}\left(a^{-2\lambda_S^2+1}\right) \ , \qquad \text{(D.32)}
\end{aligned}$$

providing

$$c_{0,++,0} + c_{++,0,0} = \sqrt{2} \ . \qquad \text{(D.33)}$$

Similarily

$$\begin{aligned}
\mathscr{O}_0\mathscr{O}_{+-} + \mathscr{O}_{+-}\mathscr{O}_0 &= \left[\hat{\sigma}_1^+\hat{V}_{-\lambda_S}^S\hat{V}_{-\lambda_A}^A + \hat{\sigma}_2^+\hat{V}_{-\lambda_S}^S\hat{V}_{\lambda_A}^A + h.c.\right]\cdot\left[\hat{\sigma}_1^+\hat{\sigma}_2^-\hat{V}_{-2\lambda_A}^A + h.c.\right] + \\
&\quad + \left[\hat{\sigma}_1^+\hat{\sigma}_2^-\hat{V}_{-2\lambda_A}^A + h.c.\right]\cdot\left[\hat{\sigma}_1^+\hat{V}_{-\lambda_S}^S\hat{V}_{-\lambda_A}^A + \hat{\sigma}_2^+\hat{V}_{-\lambda_S}^S\hat{V}_{\lambda_A}^A + h.c.\right] \\
&= \hat{\sigma}_1^+\hat{\sigma}_1^-\hat{\sigma}_2^+\hat{V}_{-\lambda_S}^S\hat{V}_{-\lambda_A}^A\hat{V}_{2\lambda_A}^A + \hat{\sigma}_2^+\hat{\sigma}_2^-\hat{\sigma}_1^+\hat{V}_{-\lambda_S}^S\hat{V}_{\lambda_A}^A\hat{V}_{-2\lambda_A}^A + \\
&\quad + \hat{\sigma}_1^-\hat{\sigma}_1^+\hat{\sigma}_2^-\hat{V}_{\lambda_S}^S\hat{V}_{\lambda_A}^A\hat{V}_{-2\lambda_A}^A + \hat{\sigma}_2^-\hat{\sigma}_2^+\hat{\sigma}_1^-\hat{V}_{\lambda_S}^S\hat{V}_{-\lambda_A}^A\hat{V}_{2\lambda_A}^A + \\
&\quad + \hat{\sigma}_1^-\hat{\sigma}_1^+\hat{\sigma}_2^+\hat{V}_{-\lambda_S}^S\hat{V}_{2\lambda_A}^A\hat{V}_{-\lambda_A}^A + \hat{\sigma}_2^-\hat{\sigma}_2^+\hat{\sigma}_1^+\hat{V}_{-\lambda_S}^S\hat{V}_{-2\lambda_A}^A\hat{V}_{\lambda_A}^A + \\
&\quad + \hat{\sigma}_1^+\hat{\sigma}_1^-\hat{\sigma}_2^-\hat{V}_{\lambda_S}^S\hat{V}_{-2\lambda_A}^A\hat{V}_{\lambda_A}^A + \hat{\sigma}_2^+\hat{\sigma}_2^-\hat{\sigma}_1^-\hat{V}_{\lambda_S}^S\hat{V}_{2\lambda_A}^A\hat{V}_{-\lambda_A}^A \\
&= a^{-2\lambda_A^2}\left[\hat{\sigma}_2^+\hat{V}_{-\lambda_S}^S\hat{V}_{\lambda_A}^A + \hat{\sigma}_1^+\hat{V}_{-\lambda_S}^S\hat{V}_{-\lambda_A}^A + \right. \\
&\quad \left. + \hat{\sigma}_2^-\hat{V}_{\lambda_S}^S\hat{V}_{-\lambda_A}^A + \hat{\sigma}_1^-\hat{V}_{\lambda_S}^S\hat{V}_{\lambda_A}^A\right] + \mathcal{O}\left(a^{-2\lambda_A^2+1}\right) \\
&= \sqrt{2}a^{-2\lambda_A^2}\mathscr{O}_0 + \mathcal{O}\left(a^{-2\lambda_A^2+1}\right) \ , \qquad \text{(D.34)}
\end{aligned}$$

gives

$$c_{0,+-,0} + c_{+-,0,0} = \sqrt{2} \ . \qquad \text{(D.35)}$$

Continuing expanding products with $\mathscr{O}_0$, we have to consider combinations with the furthermore arising operators $\mathscr{O}_z$, $\mathscr{O}_S$ and $\mathscr{O}_A$ ($\mathscr{O}_{\mathbf{1}}$ is trivially, as $\mathscr{O}_j\mathscr{O}_{\mathbf{1}} = \mathscr{O}_{\mathbf{1}}\mathscr{O}_j = \mathscr{O}_j$ for all j). We receive

$$\begin{aligned}
\mathscr{O}_0\mathscr{O}_z + \mathscr{O}_z\mathscr{O}_0 &= \frac{1}{\sqrt{2}}\left[\hat{\sigma}_1^+\hat{V}_{-\lambda_S}^S\hat{V}_{-\lambda_A}^A + \hat{\sigma}_2^+\hat{V}_{-\lambda_S}^S\hat{V}_{\lambda_A}^A + h.c.\right]\hat{\sigma}_1^z\hat{\sigma}_2^z + \\
&\quad + \frac{1}{\sqrt{2}}\hat{\sigma}_1^z\hat{\sigma}_2^z\left[\hat{\sigma}_1^+\hat{V}_{-\lambda_S}^S\hat{V}_{-\lambda_A}^A + \hat{\sigma}_2^+\hat{V}_{-\lambda_S}^S\hat{V}_{\lambda_A}^A + h.c.\right] = 0 \ , \qquad \text{(D.36)}
\end{aligned}$$

where we have regarded eq. D.25.

$$\begin{aligned}
\mathscr{O}_0\mathscr{O}_S + \mathscr{O}_S\mathscr{O}_0 &= \frac{1}{2}\left[\hat{\sigma}_1^+\hat{V}^S_{-\lambda_S}\hat{V}^A_{-\lambda_A} + \hat{\sigma}_2^+\hat{V}^S_{-\lambda_S}\hat{V}^A_{\lambda_A} + h.c.\right](\hat{\sigma}_1^z + \hat{\sigma}_2^z)\,\partial_x\Phi_S + \\
&\quad \frac{1}{2}(\hat{\sigma}_1^z + \hat{\sigma}_2^z)\,\partial_x\Phi_S\left[\hat{\sigma}_1^+\hat{V}^S_{-\lambda_S}\hat{V}^A_{-\lambda_A} + \hat{\sigma}_2^+\hat{V}^S_{-\lambda_S}\hat{V}^A_{\lambda_A} + h.c.\right] \\
&= \frac{1}{2}\Big\{\left[\hat{\sigma}_1^+\hat{V}^S_{-\lambda_S}\hat{V}^A_{-\lambda_A}, \partial_x\Phi_S\right]_- + \left[\hat{\sigma}_2^+\hat{V}^S_{-\lambda_S}\hat{V}^A_{\lambda_A}, \partial_x\Phi_S\right]_- - \\
&\quad - \left[\hat{\sigma}_1^-\hat{V}^S_{\lambda_S}\hat{V}^A_{\lambda_A}, \partial_x\Phi_S\right]_- - \left[\hat{\sigma}_2^-\hat{V}^S_{\lambda_S}\hat{V}^A_{-\lambda_A}, \partial_x\Phi_S\right]_- + \\
&\quad + \left[\hat{\sigma}_1^+\hat{\sigma}_2^z\hat{V}^S_{-\lambda_S}\hat{V}^A_{-\lambda_A}, \partial_x\Phi_S\right]_+ + \left[\hat{\sigma}_1^z\hat{\sigma}_2^+\hat{V}^S_{-\lambda_S}\hat{V}^A_{\lambda_A}, \partial_x\Phi_S\right]_+ + \\
&\quad + \left[\hat{\sigma}_1^-\hat{\sigma}_2^z\hat{V}^S_{\lambda_S}\hat{V}^A_{\lambda_A}, \partial_x\Phi_S\right]_+ + \left[\hat{\sigma}_1^z\hat{\sigma}_2^-\hat{V}^S_{\lambda_S}\hat{V}^A_{-\lambda_A}, \partial_x\Phi_S\right]_+\Big\} \qquad \text{(D.37)}
\end{aligned}$$

where $\left[\hat{A},\hat{B}\right]_- = \hat{A}\hat{B} - \hat{A}\hat{B}$ denotes the commutator, $\left[\hat{A},\hat{B}\right]_+ = \hat{A}\hat{B} + \hat{A}\hat{B}$ the anti-commutator. By applying Baker-Haussdorff

$$e^{i\gamma\Phi}\partial_x\Phi e^{-i\gamma\Phi} = \partial_x\Phi - \gamma\mathbb{1} \qquad \text{(D.38)}$$

we can rewrite

$$\left[e^{i\gamma\Phi}, \partial_x\Phi\right]_- = -\gamma e^{i\gamma\Phi} \qquad \text{(D.39)}$$

and

$$\left[e^{i\gamma\Phi}, \partial_x\Phi\right]_+ = 2\partial_x\Phi e^{i\gamma\Phi} - \gamma e^{i\gamma\Phi}\ . \qquad \text{(D.40)}$$

Which results in

$$\begin{aligned}
\mathscr{O}_0\mathscr{O}_S + \mathscr{O}_S\mathscr{O}_0 &= \frac{1}{2}\lambda_S\left[\hat{\sigma}_1^+\hat{V}^S_{-\lambda_S}\hat{V}^A_{-\lambda_A} + \hat{\sigma}_2^+\hat{V}^S_{-\lambda_S}\hat{V}^A_{\lambda_A} + h.c.\right] + \\
&\quad + \big[\hat{\sigma}_1^+\hat{\sigma}_2^z\,(2\partial_x\Phi_S + \lambda_S)\,\hat{V}^S_{-\lambda_S}\hat{V}^A_{-\lambda_A} + \hat{\sigma}_1^z\hat{\sigma}_2^+\,(2\partial_x\Phi_S + \lambda_S)\,\hat{V}^S_{-\lambda_S}\hat{V}^A_{\lambda_A} + \\
&\quad + \hat{\sigma}_1^-\hat{\sigma}_2^z\,(2\partial_x\Phi_S - \lambda_S)\,\hat{V}^S_{\lambda_S}\hat{V}^A_{\lambda_A} + \hat{\sigma}_1^z\hat{\sigma}_2^-\,(2\partial_x\Phi_S - \lambda_S)\,\hat{V}^S_{\lambda_S}\hat{V}^A_{-\lambda_A}\big]\ .
\end{aligned}$$

Applying the normal-ordering commutation rule from J. von Delft et al. [68] (ch. 9.C)

$$\partial_x\Phi\cdot\hat{V}_\lambda = \frac{\lambda}{a}\hat{V}_\lambda + {}^*_*\hat{V}_\lambda\partial_x\Phi^*_* \qquad \text{(D.41)}$$

we find

$$\begin{aligned}
\mathscr{O}_0\mathscr{O}_S + \mathscr{O}_S\mathscr{O}_0 &= \frac{\lambda_S}{2}\mathscr{O}_0 + \lambda_S\Big[(-2/a+1)\left(\hat{\sigma}_1^+\hat{\sigma}_2^z\hat{V}^S_{-\lambda_S}\hat{V}^A_{-\lambda_A} + \hat{\sigma}_1^z\hat{\sigma}_2^+\hat{V}^S_{-\lambda_S}\hat{V}^A_{\lambda_A}\right) + \\
&\quad + (2/a-1)\left(\hat{\sigma}_1^-\hat{\sigma}_2^z\hat{V}^S_{\lambda_S}\hat{V}^A_{\lambda_A} + \hat{\sigma}_1^z\hat{\sigma}_2^-\hat{V}^S_{\lambda_S}\hat{V}^A_{-\lambda_A}\right)\Big] + \\
&\quad + 2\big[\hat{\sigma}_1^+\hat{\sigma}_{2*}^{z*}\hat{V}^S_{-\lambda_S}\partial_x\Phi_S\hat{V}^{A\,*}_{-\lambda_A{}*} + \hat{\sigma}_1^z\hat{\sigma}_2^{+\,*}_*\hat{V}^S_{-\lambda_S}\partial_x\Phi_S\hat{V}^{A\,*}_{\lambda_A{}*} + \\
&\quad + \hat{\sigma}_1^-\hat{\sigma}_{2*}^{z*}\hat{V}^S_{\lambda_S}\partial_x\Phi_S\hat{V}^{A\,*}_{\lambda_A{}*} + \hat{\sigma}_1^z\hat{\sigma}_2^{-\,*}_*\hat{V}^S_{\lambda_S}\partial_x\Phi_S\hat{V}^{A\,*}_{-\lambda_A{}*}\big]\ .
\end{aligned} \qquad \text{(D.42)}$$

Therefor

$$c_{0,S,0} + c_{S,0,0} = \frac{\lambda_S}{2} \ . \tag{D.43}$$

We analogously proceed with

$$\begin{aligned}
\mathscr{O}_0\mathscr{O}_A + \mathscr{O}_A\mathscr{O}_0 &= \frac{1}{2}\left[\hat{\sigma}_1^+\hat{V}^S_{-\lambda_S}\hat{V}^A_{-\lambda_A} + \hat{\sigma}_2^+\hat{V}^S_{-\lambda_S}\hat{V}^A_{\lambda_A} + h.c.\right](\hat{\sigma}_1^z - \hat{\sigma}_2^z)\,\partial_x\Phi_A + \\
&\quad \frac{1}{2}(\hat{\sigma}_1^z - \hat{\sigma}_2^z)\,\partial_x\Phi_A\left[\hat{\sigma}_1^+\hat{V}^S_{-\lambda_S}\hat{V}^A_{-\lambda_A} + \hat{\sigma}_2^+\hat{V}^S_{-\lambda_S}\hat{V}^A_{\lambda_A} + h.c.\right] \\
&= \frac{1}{2}\Big\{\left[\hat{\sigma}_1^+\hat{V}^S_{-\lambda_S}\hat{V}^A_{-\lambda_A}, \partial_x\Phi_A\right]_- - \left[\hat{\sigma}_2^+\hat{V}^S_{-\lambda_S}\hat{V}^A_{\lambda_A}, \partial_x\Phi_A\right]_- - \\
&\quad - \left[\hat{\sigma}_1^-\hat{V}^S_{\lambda_S}\hat{V}^A_{\lambda_A}, \partial_x\Phi_A\right]_- + \left[\hat{\sigma}_2^-\hat{V}^S_{\lambda_S}\hat{V}^A_{-\lambda_A}, \partial_x\Phi_A\right]_- - \\
&\quad - \left[\hat{\sigma}_1^+\hat{\sigma}_2^z\hat{V}^S_{-\lambda_S}\hat{V}^A_{-\lambda_A}, \partial_x\Phi_A\right]_+ + \left[\hat{\sigma}_1^z\hat{\sigma}_2^+\hat{V}^S_{-\lambda_S}\hat{V}^A_{\lambda_A}, \partial_x\Phi_A\right]_+ - \\
&\quad - \left[\hat{\sigma}_1^-\hat{\sigma}_2^z\hat{V}^S_{\lambda_S}\hat{V}^A_{\lambda_A}, \partial_x\Phi_A\right]_+ + \left[\hat{\sigma}_1^z\hat{\sigma}_2^-\hat{V}^S_{\lambda_S}\hat{V}^A_{-\lambda_A}, \partial_x\Phi_A\right]_+\Big\} \\
&= \frac{1}{2}\lambda_A\left[\hat{\sigma}_1^+\hat{V}^S_{-\lambda_S}\hat{V}^A_{-\lambda_A} + \hat{\sigma}_2^+\hat{V}^S_{-\lambda_S}\hat{V}^A_{\lambda_A} + h.c.\right] + \\
&\quad + \big[\hat{\sigma}_1^+\hat{\sigma}_2^z\,(2\partial_x\Phi_A - \lambda_A)\,\hat{V}^S_{-\lambda_S}\hat{V}^A_{-\lambda_A} + \hat{\sigma}_1^z\hat{\sigma}_2^+\,(2\partial_x\Phi_A - \lambda_A)\,\hat{V}^S_{-\lambda_S}\hat{V}^A_{\lambda_A} + \\
&\qquad + \hat{\sigma}_1^-\hat{\sigma}_2^z\,(2\partial_x\Phi_A + \lambda_A)\,\hat{V}^S_{\lambda_S}\hat{V}^A_{\lambda_A} + \hat{\sigma}_1^z\hat{\sigma}_2^-\,(2\partial_x\Phi_A + \lambda_A)\,\hat{V}^S_{\lambda_S}\hat{V}^A_{-\lambda_A}\big] \\
&= \frac{\lambda_A}{2}\mathscr{O}_0 + \lambda_A\Big[(2/a+1)\left(-\hat{\sigma}_1^+\hat{\sigma}_2^z\hat{V}^S_{-\lambda_S}\hat{V}^A_{-\lambda_A} + \hat{\sigma}_1^-\hat{\sigma}_2^z\hat{V}^S_{\lambda_S}\hat{V}^A_{\lambda_A}\right) + \\
&\qquad + (2/a-1)\left(\hat{\sigma}_1^z\hat{\sigma}_2^+\hat{V}^S_{-\lambda_S}\hat{V}^A_{\lambda_A} + \hat{\sigma}_1^z\hat{\sigma}_2^-\hat{V}^S_{\lambda_S}\hat{V}^A_{-\lambda_A}\right)\Big] + \\
&\quad + 2\big[\hat{\sigma}_1^+\hat{\sigma}_{2*}^{z*}\hat{V}^S_{-\lambda_S}\hat{V}^A_{-\lambda_A}\partial_x\Phi_{A*}^* + \hat{\sigma}_1^z\hat{\sigma}_{2\ *}^{+*}\hat{V}^S_{-\lambda_S}\hat{V}^A_{\lambda_A}\partial_x\Phi_{A*}^* + \\
&\qquad + \hat{\sigma}_1^-\hat{\sigma}_{2*}^{z*}\hat{V}^S_{\lambda_S}\hat{V}^A_{\lambda_A}\partial_x\Phi_{A*}^* + \hat{\sigma}_1^z\hat{\sigma}_{2\ *}^{-*}\hat{V}^S_{\lambda_S}\hat{V}^A_{-\lambda_A}\partial_x\Phi_{A*}^*\big] \ .
\end{aligned} \tag{D.44}$$

Thus

$$c_{0,A,0} + c_{A,0,0} = \frac{\lambda_A}{2} \ . \tag{D.45}$$

Furthermore

$$\begin{aligned}
\mathscr{O}_{++}\mathscr{O}_{++} &= 2\left[\hat{\sigma}_1^+\hat{\sigma}_2^+\hat{V}^S_{-2\lambda_S} + \hat{\sigma}_1^-\hat{\sigma}_2^-\hat{V}^S_{2\lambda_S}\right]^2 \\
&= 2\left(\hat{\sigma}_1^+\hat{\sigma}_1^-\hat{\sigma}_2^+\hat{\sigma}_2^-\hat{V}^S_{-2\lambda_S}\hat{V}^S_{2\lambda_S} + \hat{\sigma}_1^-\hat{\sigma}_1^+\hat{\sigma}_2^-\hat{\sigma}_2^+\hat{V}^S_{2\lambda_S}\hat{V}^S_{-2\lambda_S}\right) \\
&= \frac{1}{2}\Big[\left(\mathbb{1}-\hat{\sigma}_1^z\right)\left(\mathbb{1}-\hat{\sigma}_2^z\right)\left(a^{-4\lambda_S^2}\mathbb{1} - 2\lambda_S a^{-4\lambda_S^2+1}\partial_x\Phi_S\right) + \\
&\qquad + \left(\mathbb{1}+\hat{\sigma}_1^z\right)\left(\mathbb{1}+\hat{\sigma}_2^z\right)\left(a^{-4\lambda_S^2}\mathbb{1} + 2\lambda_S a^{-4\lambda_S^2+1}\partial_x\Phi_S\right)\Big] \\
&= a^{-4\lambda_S^2}\left(\mathbb{1}+\hat{\sigma}_1^z\hat{\sigma}_2^z\right) + 2a^{-4\lambda_S^2+1}\left(\hat{\sigma}_1^z+\hat{\sigma}_2^z\right)\partial_x\Phi_S \\
&= a^{-4\lambda_S^2}\mathscr{O}_{\mathbf{1}} + a^{-4\lambda_S^2}\mathscr{O}_z + \sqrt{8}a^{-4\lambda_S^2+1}\mathscr{O}_S
\end{aligned} \tag{D.46}$$

providing

$$c_{++,++,\mathbf{1}} = 1 \ , \quad c_{++,++,z} = 1 \ , \quad c_{++,++,S} = \sqrt{8} \ . \tag{D.47}$$

And now for something completely different

$$\begin{aligned}
\mathscr{O}_{++}\mathscr{O}_{+-} + \mathscr{O}_{+-}\mathscr{O}_{++} &= 2\Big[\left(\hat{\sigma}_1^+\hat{\sigma}_2^+\hat{V}^S_{-2\lambda_S} + \hat{\sigma}_1^-\hat{\sigma}_2^-\hat{V}^S_{2\lambda_S}\right)\left(\hat{\sigma}_1^+\hat{\sigma}_2^-\hat{V}^A_{-2\lambda_A} + \hat{\sigma}_1^-\hat{\sigma}_2^+\hat{V}^A_{2\lambda_A}\right) + \\
&\qquad + \left(\hat{\sigma}_1^+\hat{\sigma}_2^-\hat{V}^A_{-2\lambda_A} + \hat{\sigma}_1^-\hat{\sigma}_2^+\hat{V}^A_{2\lambda_A}\right)\left(\hat{\sigma}_1^+\hat{\sigma}_2^+\hat{V}^S_{-2\lambda_S} + \hat{\sigma}_1^-\hat{\sigma}_2^-\hat{V}^S_{2\lambda_S}\right)\Big] = 0
\end{aligned} \tag{D.48}$$

as always terms of the form $\left(\hat{\sigma}_j^\pm\right)^2 = 0$ occurs.

Next

$$\begin{aligned}
\mathscr{O}_{++}\mathscr{O}_z + \mathscr{O}_z\mathscr{O}_{++} &= \sqrt{2}\Big[\left(\hat{\sigma}_1^+\hat{\sigma}_2^+\hat{V}^S_{-2\lambda_S} + \hat{\sigma}_1^-\hat{\sigma}_2^-\hat{V}^S_{2\lambda_S}\right)\hat{\sigma}_1^z\hat{\sigma}_2^z + \\
&\qquad \hat{\sigma}_1^z\hat{\sigma}_2^z\left(\hat{\sigma}_1^+\hat{\sigma}_2^+\hat{V}^S_{-2\lambda_S} + \hat{\sigma}_1^-\hat{\sigma}_2^-\hat{V}^S_{2\lambda_S}\right)\Big] = 2\mathscr{O}_{++}
\end{aligned} \tag{D.49}$$

as each change of sign due to $\hat{\sigma}_j^-\hat{\sigma}_j^z = -\hat{\sigma}_j^-$ or $\hat{\sigma}_j^z\hat{\sigma}_j^+ = -\hat{\sigma}_j^+$ appears twice and therefor cancels, ergo

$$c_{++,z,++} + c_{z,++,++} = 2 \ . \tag{D.50}$$

Now

$$\begin{aligned}
\mathscr{O}_{++}\mathscr{O}_S + \mathscr{O}_S\mathscr{O}_{++} &= \Big[\left(\hat{\sigma}_1^+\hat{\sigma}_2^+\hat{V}^S_{-2\lambda_S} + \hat{\sigma}_1^-\hat{\sigma}_2^-\hat{V}^S_{2\lambda_S}\right)(\hat{\sigma}_1^z + \hat{\sigma}_2^z)\,\partial_x\Phi_S + \\
&\qquad (\hat{\sigma}_1^z + \hat{\sigma}_2^z)\,\partial_x\Phi_S\left(\hat{\sigma}_1^+\hat{\sigma}_2^+\hat{V}^S_{-2\lambda_S} + \hat{\sigma}_1^-\hat{\sigma}_2^-\hat{V}^S_{2\lambda_S}\right)\Big] \\
&= 2\hat{\sigma}_1^+\hat{\sigma}_2^+\left[\hat{V}^S_{-2\lambda_S}, \partial_x\Phi_S\right]_- - 2\hat{\sigma}_1^-\hat{\sigma}_2^-\left[\hat{V}^S_{2\lambda_S}, \partial_x\Phi_S\right]_- \\
&= -4\lambda_S\left(\hat{\sigma}_1^+\hat{\sigma}_2^+\hat{V}^S_{-2\lambda_S} + \hat{\sigma}_1^-\hat{\sigma}_2^-\hat{V}^S_{2\lambda_S}\right) \\
&= -\sqrt{8}\lambda_S\mathscr{O}_{++} \qquad \text{(D.51)}
\end{aligned}$$

following eq. D.39 and receiving

$$c_{++,S,++} + c_{S,++,++} = -\sqrt{8}\lambda_S\ . \qquad \text{(D.52)}$$

Otherwise

$$\begin{aligned}
\mathscr{O}_{++}\mathscr{O}_A + \mathscr{O}_A\mathscr{O}_{++} &= \Big[\left(\hat{\sigma}_1^+\hat{\sigma}_2^+\hat{V}^S_{-2\lambda_S} + \hat{\sigma}_1^-\hat{\sigma}_2^-\hat{V}^S_{2\lambda_S}\right)(\hat{\sigma}_1^z - \hat{\sigma}_2^z)\,\partial_x\Phi_A + \\
&\qquad (\hat{\sigma}_1^z - \hat{\sigma}_2^z)\,\partial_x\Phi_A\left(\hat{\sigma}_1^+\hat{\sigma}_2^+\hat{V}^S_{-2\lambda_S} + \hat{\sigma}_1^-\hat{\sigma}_2^-\hat{V}^S_{2\lambda_S}\right)\Big] = 0
\end{aligned} \qquad \text{(D.53)}$$

as for every $\hat{\sigma}_j^\pm\hat{\sigma}_j^z = \pm\hat{\sigma}_j^\pm$ and $\hat{\sigma}_j^z\hat{\sigma}_j^\pm = \mp\hat{\sigma}_j^\pm$ there exist an equal term with opposite sign.

Also

$$\begin{aligned}
\mathscr{O}_{+-}\mathscr{O}_{+-} &= 2\left[\hat{\sigma}_1^+\hat{\sigma}_2^-\hat{V}^A_{-2\lambda_A} + \hat{\sigma}_1^-\hat{\sigma}_2^+\hat{V}^A_{2\lambda_A}\right]^2 \\
&= 2\left(\hat{\sigma}_1^+\hat{\sigma}_1^-\hat{\sigma}_2^-\hat{\sigma}_2^+\hat{V}^A_{-2\lambda_A}\hat{V}^A_{2\lambda_A} + \hat{\sigma}_1^-\hat{\sigma}_1^+\hat{\sigma}_2^+\hat{\sigma}_2^-\hat{V}^A_{2\lambda_A}\hat{V}^A_{-2\lambda_A}\right) \\
&= \frac{1}{2}\Big[(\mathbb{1} - \hat{\sigma}_1^z)(\mathbb{1} + \hat{\sigma}_2^z)\left(a^{-4\lambda_A^2}\mathbb{1} - 2\lambda_A a^{-4\lambda_A^2+1}\partial_x\Phi_A\right) + \\
&\qquad + (\mathbb{1} + \hat{\sigma}_1^z)(\mathbb{1} - \hat{\sigma}_2^z)\left(a^{-4\lambda_A^2}\mathbb{1} + 2\lambda_A a^{-4\lambda_A^2+1}\partial_x\Phi_A\right)\Big] \\
&= a^{-4\lambda_S^2}(\mathbb{1} - \hat{\sigma}_1^z\hat{\sigma}_2^z) = a^{-4\lambda_S^2}\mathscr{O}_{\mathbf{1}} - a^{-4\lambda_S^2}\mathscr{O}_z\ , \qquad \text{(D.54)}
\end{aligned}$$

such that

$$c_{+-,+-,\mathbf{1}} = 1\ , \quad c_{+-,+-,z} = -1\ . \qquad \text{(D.55)}$$

Anyway

$$\begin{aligned}\mathscr{O}_{+-}\mathscr{O}_z + \mathscr{O}_z\mathscr{O}_{+-} &= \sqrt{2}\Big[\left(\hat{\sigma}_1^+\hat{\sigma}_2^-\hat{V}^A_{-2\lambda_A} + \hat{\sigma}_1^-\hat{\sigma}_2^+\hat{V}^A_{2\lambda_A}\right)\hat{\sigma}_1^z\hat{\sigma}_2^z + \\ &\qquad \hat{\sigma}_1^z\hat{\sigma}_2^z\left(\hat{\sigma}_1^+\hat{\sigma}_2^-\hat{V}^A_{-2\lambda_A} + \hat{\sigma}_1^+\hat{\sigma}_2^-\hat{V}^A_{2\lambda_A}\right)\Big] \\ &= -2\mathscr{O}_{+-} \end{aligned} \tag{D.56}$$

giving

$$c_{+-,z,+-} + c_{z,+-,+-} = -2 \ . \tag{D.57}$$

Moreover

$$\begin{aligned}\mathscr{O}_{+-}\mathscr{O}_S + \mathscr{O}_S\mathscr{O}_{+-} &= \Big[\left(\hat{\sigma}_1^+\hat{\sigma}_2^-\hat{V}^A_{-2\lambda_A} + \hat{\sigma}_1^-\hat{\sigma}_2^+\hat{V}^A_{2\lambda_A}\right)(\hat{\sigma}_1^z + \hat{\sigma}_2^z)\,\partial_x\Phi_S + \\ &\qquad (\hat{\sigma}_1^z + \hat{\sigma}_2^z)\,\partial_x\Phi_S\left(\hat{\sigma}_1^+\hat{\sigma}_2^-\hat{V}^A_{-2\lambda_A} + \hat{\sigma}_1^-\hat{\sigma}_2^+\hat{V}^A_{2\lambda_A}\right)\Big] = 0 \end{aligned} \tag{D.58}$$

analogously to expression D.53.

While

$$\begin{aligned}\mathscr{O}_{+-}\mathscr{O}_A + \mathscr{O}_A\mathscr{O}_{+-} &= \Big[\left(\hat{\sigma}_1^+\hat{\sigma}_2^-\hat{V}^A_{-2\lambda_A} + \hat{\sigma}_1^-\hat{\sigma}_2^+\hat{V}^A_{2\lambda_A}\right)(\hat{\sigma}_1^z - \hat{\sigma}_2^z)\,\partial_x\Phi_A + \\ &\qquad (\hat{\sigma}_1^z - \hat{\sigma}_2^z)\,\partial_x\Phi_A\left(\hat{\sigma}_1^+\hat{\sigma}_2^-\hat{V}^A_{-2\lambda_A} + \hat{\sigma}_1^-\hat{\sigma}_2^+\hat{V}^A_{2\lambda_A}\right)\Big] \\ &= 2\hat{\sigma}_1^+\hat{\sigma}_2^-\left[\hat{V}^A_{-2\lambda_A}, \partial_x\Phi_A\right]_- - 2\hat{\sigma}_1^-\hat{\sigma}_2^+\left[\hat{V}^A_{2\lambda_A}, \partial_x\Phi_A\right]_- \\ &= -4\lambda_A\left(\hat{\sigma}_1^+\hat{\sigma}_2^-\hat{V}^A_{-2\lambda_A} + \hat{\sigma}_1^-\hat{\sigma}_2^+\hat{V}^A_{2\lambda_A}\right) \\ &= -\sqrt{8}\lambda_A\mathscr{O}_{+-} \ , \end{aligned} \tag{D.59}$$

such that

$$c_{+-,A,+-} + c_{A,+-,+-} = -\sqrt{8}\lambda_A \ . \tag{D.60}$$

Now we come to the products between the additional terms

$$\mathscr{O}_z\mathscr{O}_z = (\hat{\sigma}_1^z\hat{\sigma}_2^z)^2 = \mathbb{1} = \mathscr{O}_{\mathbf{1}} \ , \tag{D.61}$$

so

$$c_{z,z,\mathbb{1}} \;=\; 1 \;. \tag{D.62}$$

Item

$$\begin{aligned} \mathscr{O}_z\mathscr{O}_S + \mathscr{O}_S\mathscr{O}_z &= \frac{1}{\sqrt{2}}\left[\hat{\sigma}_1^z\hat{\sigma}_2^z\left(\hat{\sigma}_1^z+\hat{\sigma}_2^z\right)\partial_x\Phi_S + \left(\hat{\sigma}_1^z+\hat{\sigma}_2^z\right)\hat{\sigma}_1^z\hat{\sigma}_2^z\partial_x\Phi_S\right] \\ &= \frac{1}{\sqrt{2}}2\left(\hat{\sigma}_2^z+\hat{\sigma}_1^z\right)\partial_x\Phi_S \;=\; 2\mathscr{O}_S \;, \end{aligned} \tag{D.63}$$

ergo

$$c_{z,S,S} + c_{S,z,S} \;=\; 2 \;. \tag{D.64}$$

Likewise

$$\begin{aligned} \mathscr{O}_z\mathscr{O}_A + \mathscr{O}_A\mathscr{O}_z &= \frac{1}{\sqrt{2}}\left[\hat{\sigma}_1^z\hat{\sigma}_2^z\left(\hat{\sigma}_1^z-\hat{\sigma}_2^z\right)\partial_x\Phi_A + \left(\hat{\sigma}_1^z-\hat{\sigma}_2^z\right)\hat{\sigma}_1^z\hat{\sigma}_2^z\partial_x\Phi_A\right] \\ &= \frac{1}{\sqrt{2}}2\left(\hat{\sigma}_2^z-\hat{\sigma}_1^z\right)\partial_x\Phi_A \;=\; -2\mathscr{O}_A \;, \end{aligned} \tag{D.65}$$

resulting in

$$c_{z,A,A} + c_{A,z,A} \;=\; -2 \;. \tag{D.66}$$

Otherwise

$$\mathscr{O}_S\mathscr{O}_S \;=\; \frac{1}{2}\left[\left(\hat{\sigma}_1^z+\hat{\sigma}_2^z\right)\partial_x\Phi_S\right]^2 \;=\; \left(\mathbb{1}+\hat{\sigma}_1^z\hat{\sigma}_2^z\right)\left(\partial_x\Phi_S\right)^2 \;=\; \mathcal{O}\left(|\partial_x\Phi_S|^2\right) \;. \tag{D.67}$$

$$\mathscr{O}_S\mathscr{O}_A + \mathscr{O}_A\mathscr{O}_S \;=\; \frac{1}{2}\left[\left(\hat{\sigma}_1^z+\hat{\sigma}_2^z\right)\partial_x\Phi_S\left(\hat{\sigma}_1^z-\hat{\sigma}_2^z\right)\partial_x\Phi_A + \left(\hat{\sigma}_1^z-\hat{\sigma}_2^z\right)\partial_x\Phi_A\left(\hat{\sigma}_1^z+\hat{\sigma}_2^z\right)\partial_x\Phi_S\right] = 0 \tag{D.68}$$

as $\left(\hat{\sigma}_1^z+\hat{\sigma}_2^z\right)\left(\hat{\sigma}_1^z-\hat{\sigma}_2^z\right)=0$.

$$\mathscr{O}_A\mathscr{O}_A \;=\; \frac{1}{2}\left[\left(\hat{\sigma}_1^z-\hat{\sigma}_2^z\right)\partial_x\Phi_A\right]^2 \;=\; \left(\mathbb{1}-\hat{\sigma}_1^z\hat{\sigma}_2^z\right)\left(\partial_x\Phi_A\right)^2 \;=\; \mathcal{O}\left(|\partial_x\Phi_A|^2\right) \;. \tag{D.69}$$

Altogether we receive as non-trivial *operation product expansion* coefficients for the coupling Δ_0

$$c_{0,++,0}+c_{++,0,0}=\sqrt{2}\ ,\ \ c_{0,+-,0}+c_{+-,0,0}=\sqrt{2}\ ,\ \ c_{0,S,0}+c_{S,0,0}=\tfrac{\lambda_S}{2}\ ,\ \ c_{0,A,0}+c_{A,0,0}=\tfrac{\lambda_A}{2}\ , \tag{D.70}$$

for Δ_{++}

$$c_{0,0,++}=\tfrac{1}{\sqrt{2}}\ ,\ \ c_{++,z,++}+c_{z,++,++}=2\ ,\ \ c_{++,S,++}+c_{S,++,++}=-\sqrt{8}\lambda_S\ , \tag{D.71}$$

for Δ_{+-}

$$c_{0,0,+-}=\tfrac{1}{\sqrt{2}}\ ,\ \ c_{+-,z,+-}+c_{z,+-,+-}=-2\ ,\ \ c_{+-,A,+-}+c_{A,+-,+-}=-\sqrt{8}\lambda_A\ , \tag{D.72}$$

for $\Delta_{\mathbb{1}}$

$$c_{0,0,\mathbb{1}}=1\ ,\ \ c_{++,++,\mathbb{1}}=1\ ,\ \ c_{+-,+-,\mathbb{1}}=1\ ,\ \ c_{z,z,\mathbb{1}}=1\ , \tag{D.73}$$

for Δ_z

$$c_{++,++,z}=1\ ,\ \ c_{+-,+-,z}=-1\ , \tag{D.74}$$

for Δ_S

$$c_{0,0,S}=\tfrac{\lambda_S}{\sqrt{2}}\ ,\ \ c_{++,++,S}=\sqrt{8}\ ,\ \ c_{z,S,S}+c_{S,z,S}=2\ , \tag{D.75}$$

and for Δ_A

$$c_{0,0,A}=\tfrac{\lambda_A}{\sqrt{2}}\ ,\ \ c_{z,A,A}+c_{A,z,A}=-2\ . \tag{D.76}$$

Such that in total the second order scaling equations can be written as

$$\begin{aligned}
\frac{\partial\Delta_0}{\partial l} &= y_0\Delta_0-\frac{S_d}{2}\left[\sqrt{2}\left(\Delta_0\Delta_{++}+\Delta_0\Delta_{+-}\right)+\frac{\lambda_S}{2}\Delta_0\Delta_S+\frac{\lambda_A}{2}\Delta_0\Delta_A\right]\\
\frac{\partial\Delta_{++}}{\partial l} &= y_{++}\Delta_{++}-\frac{S_d}{2}\left[\frac{1}{\sqrt{2}}\Delta_0^2+2\Delta_{++}\Delta_z-\sqrt{8}\lambda_S\Delta_{++}\Delta_S\right]\\
\frac{\partial\Delta_{+-}}{\partial l} &= y_{+-}\Delta_{+-}-\frac{S_d}{2}\left[\frac{1}{\sqrt{2}}\Delta_0^2+2\Delta_{+-}\Delta_z-\sqrt{8}\lambda_A\Delta_{+-}\Delta_A\right]\\
\frac{\partial\Delta_{\mathbb{1}}}{\partial l} &= y_{\mathbb{1}}\Delta_{\mathbb{1}}-\frac{S_d}{2}\left[\Delta_0^2+\Delta_{++}^2+\Delta_{+-}^2+\Delta_z^2\right]\\
\frac{\partial\Delta_z}{\partial l} &= y_z\Delta_z-\frac{S_d}{2}\left[\Delta_{++}^2-\Delta_{+-}^2\right]\\
\frac{\partial\Delta_S}{\partial l} &= y_S\Delta_S-\frac{S_d}{2}\left[\frac{\lambda_S}{\sqrt{2}}\Delta_0^2+\sqrt{8}\Delta_{++}^2+2\Delta_z\Delta_S\right]\\
\frac{\partial\Delta_A}{\partial l} &= y_A\Delta_A-\frac{S_d}{2}\left[\frac{\lambda_A}{\sqrt{2}}\Delta_0^2-2\Delta_z\Delta_A\right]\quad .
\end{aligned} \tag{D.77}$$

Bibliography

[1] D. Esteve, J.-M. Raimond, and J. Dalibard. *Les Houches 2003 - quantum entanglement and information processing*. Elsevier, Amsterdam, 2003.

[2] M.A. Nielsen and I.L. Chuang. *Quantum Computation and Quantum Information*. Cambridge University Press, Cambridge, 2000.

[3] L.M.K. Vandersypen, R. Hanson, L.H. Willems van Beveren, J.M. Elzerman, J.S. Greidanus, S. De Franceschi, and L.P. Kouwenhoven. *Quantum Computing and Quantum bits in Mesoscopic Systems*. Kluwer, 2002.

[4] D. Giulini, E. Joos, C. Kiefer, J. Kupsch andI. O. Stamatescu, and H.D. Zeh. *Decoherence and the Appearance of a Classical World in Quantum Theory*. Springer, Berlin, 1996.

[5] R.P. Feynman. Simulating physics with computers. *International Journal of Theoretical Physics*, 21:467, 1982.

[6] I. Chiorescu, Y. Nakamura, C.J.P.M. Harmans, and J.E. Mooij. Coherent quantum dynamics of a superconducting flux qubit. *Science*, 299:1869–1871, 2003.

[7] M. Brune, P. Nussenzweig, F. Schmidt-Kaler, F. Bernardot, A. Maali, J.M. Raimond, and S. Haroche. From lamb shift to light shifts: Vacuum and subphoton cavity fields measured by atomic phase sensitive detection. *Physical Review Letters*, 72:3339, 1994.

[8] T. Yamamoto, Yu.A. Pashkin, O. Astafiev, Y. Nakamura, and J.S. Tsai. Demonstration of conditional gate operation using superconducting charge qubits. *Nature*, 425:941, 2003.

[9] E. Knill, R. Laflamme, and L. Viola. Theory of quantum error correction for general noise. *Physical Review Letters*, 84:2525, 2000.

[10] D.A. Lidar, I.L. Chuang, and K.B. Whaley. Decoherence free subspaces for quantum computation. *Physical Reviw Letters*, 81:2594, 1998.

[11] J. Kempe, D. Bacon, D.A. Lidar, and K.B. Whaley. Theory of decoherence-free fault-tolerant universal quantum computation. *Physical Review A*, 63:042307, 2001.

[12] E. Farhi, J. Goldstone, S. Gutmann, J. Lapan, A. Lundgren, and D. Preda. A quantum adiabatic evolution algorithm applied to random instances of an np-complete problem. *Science*, 292:472–475, 2001.

[13] D.P. Divincenzo. Quantum computation. *Science*, 270:255, 1995.

[14] R. Hughes, the ARDA Quantum Information Science, and Technology Panel. A quantum information science and technology roadmap. available at http://qist.lanl.gov.

[15] C.P. Slichter. *Principles of magnetic resonance*. Springer Series in Solid-State Sciences, Berlin, 1996.

[16] L.M.K. Vandersypen, M. Steffen, G. Breyta, C.S. Yannoni, M.H. Sherwood, and I.L. Chuang. Experimental realization of shor's quantum factoring algorithm using nuclear magnetiy resonance. *Nature*, 414:883, 2001.

[17] E. Knill, R. Laflamme, and G.J. Milburn. A scheme of efficient quantum computing with linear optics. *Nature*, 409:46, 2001.

[18] H.-J. Briegel, T. Calarco, D. Jaksch, J.I. Cirac, and P. Zoller. Quantum computing with neutral atoms. *Journal of modern optics*, 47:415, 2000.

[19] J.I Cirac and P. Zoller. Quantum computations with cold trapped ions. *Physical Review Letters*, 74:4091, 1995.

[20] D. Kielpinski, C. Monroe, and D.J. Wineland. Architecture for a large-scale ion-trap quantum computer. *Nature*, 417:709, 2002.

[21] D. Loss and D.P. DiVincenzo. Quantum computation with quantum dots. *Physical Review A*, 57:120, 1998.

[22] R.H. Blick and H. Lorenz. Possible definition of quantum bits in coupled quantum dots. *Proceedings IEEE International Symposium on Circuits and Systems*, II:245, 2000.

[23] Y. Makhlin, G. Schön, and A. Shnirman. Quantum-state engineering with josephson-junction devices. *Review of Modern Physics*, 73:357–400, 2001.

[24] D. Vion, A. Aassime, A. Cottet, P. Joyez, H. Pothier, C. Urbina, D. Esteve, and M.H. Devoret. Manipulating the quantum state of an electrical circuit. *Science*, 296:286, 2002.

[25] J.E. Mooij, T.P. Orlando, L. Levitov, L. Tian, C.H. van der Wal, and S. Lloyd. Josephson persistent current qubit. *Science*, 285:1036, 1999.

[26] T.P. Orlando, J.E. Mooij, L. Tian, C.H. van der Wal, L. Levitov, S. Lloyd, and J.J. Mazo. Superconducting persistent-current qubit. *Physical Review B*, 60:15398, 1999.

[27] C.H. van der Wal, A.C.J. ter Haar, F.K. Wilhelm, R.N. Schouten, C.J.P.M. Harmans, T.P. Orlando, S. Lloyd, and J.E. Mooij. Quantum superposition of macroscopic persistent-current states. *Science*, 290:773, 2000.

[28] H.P.G. Gutmann. Methoden zur beschreibung offener quantenmechanischer systeme. diploma thesis at the university of Bonn, 2001.

[29] N. Metropolis and S. Ulam. The monte carlo method. *Journal of the AMerican Statistical Association*, 44:335–341, 1949.

[30] U. Schollwöck. The density-matrix renormalization group. *Review of Modern Physics*, 77:259, 2005.

[31] U. Weiss. *Quantum dissipative systems*. World Scientific, Singapore, 2001.

[32] H. Carmichael. *An Open Systems Approach to Quantum Optics*. Springer, Berlin, 1993.

[33] G. Lindblad. On the generators of quantum dynamical semigroups. *Communications in Mathematical Physics*, 48:119–130, 1976.

[34] V. Gorini, A. Kossakowski, and E.C.G. Sudarshan. Completely positive dynamical semigroups of n-level systems. *Journal of Mathematical Physics*, 17:821–825, 1976.

[35] E.B. Davies. *Quantum theory of open systems*. Academic Press, London, 1976.

[36] S. Lloyd and L. Viola. Dynamical suppression of decoherence in two-state quantum systems. *Physical Review A*, 58:2733–2744, 1998.

[37] S. Lloyd, E. Knill, and L. Viola. Dynamical decoupling of open quantum systems. *Physical Review Letters*, 82:2417–2421, 1999.

[38] S. Lloyd, E. Knill, and L. Viola. Universal control of decoupled quantum systems. *Physical Review Letters*, 83:4888–4891, 1999.

[39] A. J. Leggett, S. Chakravarty, A.T. Dorsey, M. P. A. Fisher, A. Garg, and W. Zwerger. Dynamics of the dissipative two-state system. *Review of modern physics*, 59:1, 1987.

[40] C.H. van der Wal, F.K. Wilhelm, C.J.P.M. Harmans, and J.E. Mooij. Engineering decoherence in josephson persistent-current qubits. *European Physical Journal B*, 31:111–124, 2003.

[41] R. Dümcke and H. Spohn. The proper form of the generator in the weak coupling limit. *Zeitschrift für Physik B*, 34:419–422, 1979.

[42] M. Celio and D. Loss. Comparison between different markov approximations for open spin systems. *Physica A*, 158:769–783, 1989.

[43] J. Łuczka. On markovian kinetic equations: Zubarev's nonequilibrium statistical operator approach. *Physica*, 149A:245–266, 1989.

[44] E.B. Davies. Markovian master equations i. *Communications in mathematical Physics*, 39:91–110, 1974.

[45] E.B. Davies. Markovian master equations ii. *Mathematical Annales*, 219:147–158, 1976.

[46] M.J. Storcz and F.K. Wilhelm. Decoherence and gate performance of coupled solid-state qubits. *Physical Review A*, 67:042319, 2003.

[47] I.N. Bronstein and K.A. Semendjajew. *Teubner - Taschenbuch der Mathematik*. B.G. Teubner, Stuttgart, 1996.

[48] R. Wakai and D. van Harlingen. Direct lifetime measurements and interactions of charged defect states in submicron josephson junctions. *Physical Review Letters*, 58:1687–1690, 1987.

[49] Y. Nakamura, Yu.A. Pashkin, T. Yamamoto, and J.S. Tsai. Charge echo in a cooper-pair box. *Physical Review Letters*, 88:047901, 2002.

[50] O. Astafiev, Yu.A. Pashkin, Y. Nakamura, and J.S. Tsai. Quantum noise in the josephson charge qubit. *Physical Review Letters*, 93:267007, 2004.

[51] P. Dutta and P.M. Horn. Low-frequency fluctuations in solids: 1/f noise. *Review of Modern Physics*, 53:497–516, 1981.

[52] G. Falci, E. Paladino, and R. Fazio. *Quantum Phenomena of Mesoscopic Systems*. IOS Press, Amsterdam, 2004.

[53] E. Paladino, L. Faoro, and G. Falci. Decoherence due to discrete noise in josephson qubits. *Advanced Solid State Physics*, 43:747, 2003.

[54] E. Paladino, A. Mastellone, A. D'Arrigo, and G. Falci. Decoherence due to telegraph and 1/f noise in josephson qubits. *cond-mat/0407484*, 2004.

[55] E. Paladino, L. Faoro, G. Falci, and R. Fazio. Decoherence and 1/f noise in josephson qubits. *Physical Review Letters*, 88:228304, 2002.

[56] H. Gassmann, F. Marquardt, and C. Bruder. Non-markoffian effects of a simple nonlinear bath. *Physical Review E*, 66:041111, 2002.

[57] M.B. Weissmann. $1/f$ noise and other slow, nonexponential kinetics in condensed matter. *Review of Modern Physics*, 60:537, 1988.

[58] Markus J. Storcz. Decoherence of coupled solid state qubits. diploma thesis at the university of Bonn, 2002.

[59] L. Arnold. *Stochastische Differentialgleichungen*. Oldenbourg, München, 1973.

[60] N.G. van Kampen. *Stochastic processes in physics and chemistry*. Elsevier, Amsterdam, 1997.

[61] G.H. Weiss. *Aspects and applications of the random walk*. North-Holland, Amsterdam, 1994.

[62] Cohen-Tannoudji. *Quantum Mechanics Vol. 2*. John Wiley & Sons, New York, 1978.

[63] T. Dittrich, P. Hänggi, and G.L. Ingold. *Quantum Transport and Dissipation*. VCH Verlag, 1997.

[64] Göran Johansson, Andreas Käck, and Göran Wendin. Full frequency back-action spectrum of a single-electron transistor during qubit readout. *Physical Review Letters*, 88:046802, 2002.

[65] Göran Johansson, Andreas Käck, and Göran Wendin. Full-frequency voltage noise spectral density of a single-electron transistor. *Physical Review B*, 67:035301, 2003.

[66] R.J. Schoelkopf, A.A. Clerk, S.M. Girvin, K.W. Lehnert, and M.H. Devoret. Qubits as spectrometers of quantum noise. *cond-mat/0210247*, 2002.

[67] H. Carr and E. Purcell. Effects of diffusion on free precession in nuclear magnetic resonance experiments. *Physical Review*, 94:630, 1954.

[68] Jan von Delft and Herbert Schoeller. Bosonization for beginners - refermionization for experts. *Annalen der Physik*, 7:225–306, 1998.

[69] T. A. Costi and G. Zarand. Thermodynamics of the dissipative two-state system: A bethe-ansatz study. *Phys. Rev. B*, 59:12398, 1999.

[70] M. Garst, S. Kehrein, T. Pruschke, A. Rosch, and M. Vojta. Quantum phase transition of ising-coupled kondo impurities. *Physical Review B*, 69, 2004.

[71] Gergely Zarand and Jan von Delft. Analytical calculation of the finite-size crossover spectrum of the anisotropic 2-channel kondo model. *Physical Review B*, 61:6918, 2000.

[72] John Cardy. *Scaling and Renormalization in Statistical Physics*. Cambridge University Press, Cambridge, 2002.

[73] A. Erdelyi. *Higher Transcendental Functions Vol. 1*. McGraw-Hill, New York, 1953.

[74] R.D. Mattuck. *A Guide to Feynman Diagrams in the Many-Body Problem*. Dover Publications, New York, 1992.

Acknowledgements

First of all I really have to thank all my colleagues and collaborators, who have made it possible for me to work on such exciting fields and with so much intense and enthusiasm. In order not to waste too much energy in deciding, who should be mentioned earlier than others, I'll try to express my gratitude in chronological order (as far as possible).

I would never have met such an interesting field of research, if not my former advisor of my Diploma thesis, Prof. Klaus Dietz, would have introduced me in the fascinating and still up-to-date world of open quantum systems. I am greatly in his debt for that.

Not any less gratitude I want to express to Prof. Jan von Delft, who started his first support of my development, when I was still accomplishing my Diploma thesis in Bonn. I am in particular really grateful for his confidence in advance when he accept me as Ph.D. student long before I finished my own Diploma thesis.

Surely the most merits for having been able to complete my dissertation in the extent and on the level as it is, should be adressed to my supervisor Frank Wilhelm. Without his visionary power combined with his indefatigable patience, when encountering my most stupid questions, the achievements we have done would not have received the results and the form it has. Evidently only me, not he, should be blamed for any errors, mistypes and deficiencies, which might have survived his maximum efforts of advising my work.

At this point, I wish to thank Prof. Axel Schenzle for refereeing this thesis, as well as Prof. Wagner and Prof. Weinfurter for participating on my rigorosum.

Also big appreciation I have to dedicate our collaboration partner Professor Seth Lloyd from the department of mechanical engineering at the MIT, Massachusetts. It was a big pleasure to have had the privilege (thanks to Frank) to cooperate with such an impressive mathematical physicist. Not to forget to thank his Ph.D. student Bill Kaminsky, who gave me the necessary support and assistance during my research visits in 2002 and 2004. Referring to this I also want appreciate the unique and wonderful hospitality, Terry Orlando and his group manifested that time. In particular, Scott Burris, Dave Berns, Dan Nakada, Janice Lee, and in memoriam Bhuwan Singh gave me the feeling of being hosted in a big family!

For financial contributions I am very grateful to the DAAD-NSF travel grant for submitting my research visits at the MIT, for general fundings to the National Security Agency (NSA) and to the Advanced Research and Development Activity (ARDA) under Army Research Office (ARO) contract no. P-43385-PH-QC, as well as to the Deutsche Forschungs-Gemeinschaft (DFG) via SFB 631.

Most numerical parts of my work would not have reached its upper level of results without the brave contributions, our intern Andreas Holzner have performed. I hope, he will find an academic career, in which he can successfully develop his numerous and impressive skills.

For technical support I am very thankful to Ralph Simmler, Sigmund Stintzing and not to forget Jens Schmalzing. Thanks a lot also to Stéphane Schoonover for all the help with bureaucracy.

Here in Munich I want to express my gratitude to all the group members, guests and former colleagues of the Lehrstuhl von Delft, who made work and living here so comfortable and exciting. In particular, I want to thank Udo Hartmann and Markus Storcz, formerly colleagues from Bonn, who inspired in me the idea of quantum computation and going to Jans group. As special friends I will always remember Konstanze Jähne and Andreas Käck, who made staying with them in my office a special time. Thanks also to Svetla Käck (?) for the great hospitality at Gøteborg. All my thankfulness goes also to Silvia Kleff, Corinna Kollath, Dominique Gobert, Andreas Friedrich, Robert Dahlke, Michael Sindel, László Borda, Igor Gazuz, Rolf Helmes, Benjamin Abel, Hamed Saberi, Uli Schollwöck, Achim Rosch, Sascha Khaetskii, Mikhail Kiselev, Lloyd Hollenberg, Birgitta Whaley and all the other short term guests, I have not have the place here to mention. I certainly should not forget the attendants of our last Mauterndorf workshop, as there are Theresa Hecht, Ioana Serban, Johannes Ferber (thanks for the cookies), Andreas Weichselbaum, Eva-Maria Jahn and almost Michael Möckel (thanks for the transcendental discussions).

I should not finish the official line of gratitude without considering all the valuable partners of discussions, I had the delightness to meet. Although most probably not a complete list I want to thank Wolfgang Dür, Hans Briegel, Herbert Spohn, Herbert Wagner, Ivo Sachs, Axel Schenzle, Prof. Peter Hänggi, Igor Goychuk, Sigmund Kohler and in particular (as especially precious) Andreas Käck again.

Last but not least I am deeply in debt to my family, who supported me so absolutely, in particular my mother Dagmar Gutmann and in memoriam my father Manfred Hülsewig, who gave me the suitable example of studying physics. I should also mention my grandparents Ingeborg and Hasso Schwabe, who gave me the feelings to be always supported. Not to forget my so-called godfather Friedrich Hetzer, for giving me the moral guidelines.

At the end I really want to thank all my friends from Bonn, who did not forget me having moved “abroad”. Ladies first I should be grateful to Veronika Orlovius and Mayra Irion, formerly known as Fornet-Ponse, for still treating me as a very good friend. As begin of an almost neverending list I can only mention (chronologically ordered): Robert Oeckl, Daniel Fischer, Dirk Merten, Christian Herwig, Olaf Köhnken, Alexander Irion, Thomas Kuhn (wherever he is...), last but not least Luitgard Meyer. Thanks to the Bavarian side goes to Sabrina Herkt for having found a good shooting friend, as well as to Caro & Geli for making it really hard for me to leave Munich again.

The probably most patience during the last three years (even more than from my advisors and office colleagues) I have requested from my girl friend Maya Ibbeken, who reminded me, that there are is also a reality without physical formulas.

Curriculum Vitae

Henryk Peter Gregor Gutmann

born	08.08.1972 in Bonn-Bad Godesberg
School	1979–1983 Primary school in Bonn 1983–1992 Clara-Schumann Gymnasium in Bonn
Civilian service	Theatre and stage technician at the "Brotfabrik" theatre in Bonn-Beuel
Studies	10/1993–11/2001 Study of physics at the Rheinische Friedrich-Wilhelms-University of Bonn 11/2001–2005 Ph.D. studies in physics at the Lehrstuhl für theoretische Festkörperphysik, Ludwigs-Maximilians-University, München 08/1995 Vordiplom in physics (university of Bonn) 08/1995 Vordiplom in mathematics (university of Bonn) 11/2001 Diplom in physics (university of Bonn)
Diplomarbeit	"Methoden zur Beschreibung offener quantenmechanischer Systeme" supervised by Prof. Klaus Dietz at the Physikalisches Institut, university of Bonn

Deutsche Zusammenfassung

Die Dekohärenz mesoskopischer Quantensysteme, sowie die Entwicklung von Methoden diese zu überwinden, hat während des letzten Jahrzehnts erheblich an Bedeutung gewonnen. Dies begründet sich in den enormen experimentellen Erfolgen, solche Systeme für quanteninformationstechnische Anwendungen einzusetzen, wie *z.B.* der festkörperbasierten Realisierung von Quanten-Bits. In dieser Arbeit werden verschieden Ansätze zur Beschreibung unterschiedlicher Rauscheinflüsse behandelt. Um die verschiedenartigen Dekohärenzphänomene einer detaillierten analytischen und numerischen Untersuchung zu unterziehen, verwenden wir dabei sowohl etablierte, als auch neuartige, speziell konzeptionierte Methoden. Desweiteren präsentieren wir im zentralen Teil der Arbeit (Kapitel 2) eine dynamische Entkopplungsmethode zur Kontrolle von speziellen Dekohärenzquellen, die die Grundlage von $1/f$-Rauschen bilden. Dieses stellt in festkörperbasierten Quantensystemen eine weit verbreitete und besonders relevante Störquelle dar.

Die Dissertation besteht aus drei unterschiedlichen, einander ergänzenden Teilen: Das erste Kapitel beschäftigt sich mit der qualitativen und quantitativen Analyse verschiedene Formen der Born-Markov Näherung des Spin-Boson Modells unter Annahme Ohm'scher Spektraldichte des Bades, d.h. linearer Abhängigkeit in der Frequenz. Dies stellt ein typisches mikroskopisches Modell *z.B.* eines Qubits unter dem Einfluss von Dissipation dar. Dabei wird qualitativ untersucht, welche Näherung in welchem Temperaturbereich zur vollständigen Positivität der Dynamik führt. Dies stellt ein wesentliches Kriterium dar, ob eine gegebene Markov'sche Mastergleichung physikalisch sinnvolle, weil nur positive Wahrscheinlichkeiten aufweisende Lösungen hervorbringt. Im Anschluss an die recht unterschiedlichen Ergebnisse von verschiedenen Näherungen (jeweils in zweiter Ordnung Störungstheorie in der Spin-Bad Kopplung) führen wir quantitative Vergleiche verschiedener Ergebnisse mittels eines auf gemischte Zustände erweiterten Qualitätsmaßes, der sogenannten "mixed-state fidelity", durch. Dabei stellt sich heraus, dass nur ein Teil der Born-Markov Näherungen vollständige Positivität der Mastergleichungen liefern und dies auch nur oberhalb gewisser Grenzwerttemperaturen.

Im zweiten Teil wird eine weitere spezifische, aber weit verbreitete Form von Rauscheinfluss auf ein einzelnes Qubits mit verschiedenen Methoden untersucht. Das "bistabile Fluktuator" Modell dient dazu, den Ursprung von Telegraphen-Rauschen, sowie des $1/f$-Rauschens näher zu verstehen. Dieses stellt ein allgegenwärtiges Phänomen der Dekohärenz

in zahlreichen festkörperbasierten Quantensystemen dar und wird zurückgeführt auf langsame Fluktuationen von Defekten, die unvermeidlich in verspannten, bzw. ungeordneten Oxidgrenzen und Substraten auftreten. Zunächst findet eine detaillierte mikroskopische Untersuchung des Dekohärenzverlaufs des Qubits unter variierenden Fluktuatorparameter und insbesondere in Abhängigkeit der Umgebungstemperatur statt. Es ergibt sich ein Resonanzmuster der Dekohärenzraten in Abhängigkeit des Verhältnisses von Qubit zu Fluktuator-Energie. Dieses weist eine Hybridisierung auf, *d.h.* man erhält zwei benachbarte Maxima der Resonanzkurve, bei denen der Energie- und Phasen-Verlust des Qubits and den Fluktuator besonders groß ist. Der Verlauf der Peak-Positionen, sowie der Resonanzbreiten ist stark temperaturabhängig. Eine Aufsummierung der Dekohärenzraten des Qubits über alle Fluktuator-Energien (als Abschätzung der Gesamtdekohärenz verursacht durch ein Ensemble energetisch gleichverteilter Fluktuatoren) ergibt im Bereich niedriger Temperaturen eine $1/f$-artige Abhängigkeit (mit f der Qubitfrequenz), für höhere Temperaturbereiche, *d.h.* im Verhältnis geringerer Qubitenergien ergibt sich ein Übergang zu einem $1/f^2$-ähnlichen Verhalten. Dieses Ergebnis spiegelt experimentelle Erfahrungen wider.

Für weitere Untersuchungen wird eine effektive Beschreibung des Qubit-Fluktuator Modells eingeführt, in der der Fluktuator als semi-klassische Rauschquelle mit Poissonverteiltem Spektrum dargestellt wird. Dabei werden auch starke Ankopplungen an ein externes Wärmebad berücksichtigt, ein Parameterbereich, der mit den vorherigen perturbativen Standardtechniken des ersten Kapitels nicht beschrieben werden kann. Neben Abhängigkeiten der Dekohärenz von endlichen Temperaturen des Fluktuators, wird insbesondere auch ein konkreter physikalischer Aufbau eines Einzel-Elektron-Transistors (SET) als Meßapparat für eine Realisierung eines Qubits als Einzel-Elektron-Box (SCB) untersucht. Hierbei resultieren die bistabilen Fluktuationen aus den Fluktuationen der Besetzungswahrscheinlichkeit der den SET definierenden Insel. Wir können mittels eines geeigneten analytischen Random Walk Modells in sehr guter Übereinstimmung die zeitliche Entwicklung der bistabilen Fluktuator Dekohärenz eines Qubits beschreiben. Aus der exzellenten Übereinstimmung zwischen den numerischen und analytischen Ergebnissen leitet sich ab, dass die dekohärente Entwicklung eines Qubits unter dem Einfluss bistabilen Fluktuator Rauschens einen Random Walk auf der Blochkugel darstellt. Dessen Ausmaß ist eindeutig durch die Parameter des Fluktuators definiert.

Diese Erkenntnis ermöglicht die Konzeption eines geeignetes Gegenmittel für diese Form der Dissipation in Form der dynamischen Entkopplung. Dabei werden die überwiegend niederfrequenten Rauscheinflüsse des Fluktuators durch eine hoch-frequente Puls-Sequenz angewendet auf das Qubit herausgemittelt. Dies stellt eine Erweiterung des aus der NMR hinlänglich bekannten Spin-Echo Verfahrens dar. Dieses Methode wirkt wie ein Hoch-Paß-Filter, bei dem hauptsächlich die niederfrequenten Einflüsse der Rauschquelle herausgefiltert werden. Da diese niederfrequenten Rauschterme den überwiegend schädlichsten Anteil am $1/f$ Rauschen darstellen, liefert dieses Konzept eine vielversprechendes Mittel gegen diese besonders destruktive Form der Dekohärenz.

Im letzten Abschnitt untersuchen wir ein gekoppeltes Doppel-Spin System, welches an zwei individuelle Störquellen, sowie ein gemeinsames Wärmebad gekoppelt ist. Dabei interessieren wir uns hauptsächlich für das Auftreten unterschiedlicher Quanten-Phasen und der entsprechenden effektiven Eigenzustände als Folge starker Ankopplungen an die Bäder. In Abhängigkeit von den Bad-Kopplungsstärken leiten wir die effektive Doppel-Spin Dynamik in einem "dressed-spin" Modell her. Hierbei treten die ursprünglichen Bad-Spin Kopplungen nur noch implizit in den effektiven Spin-Operator Termen auf. Wir erhalten dabei Skalierungs-Gleichungen, deren nähere Analyse in erster Ordnung der effektiven Spin-Kopplungen ein Phasen-Diagramm liefert, Aus diesem geht hervor, welche effektive Quantendynamik aus den Badeinflüssen bei gegebenen Kopplungsstärken resultiert. Diese effektiv-zulässige Spin-Dynamik erhalten wir anhand der Fixpunkt-Hamilton der einzelnen Phasen und stellt ein wensentliches Ergebnis der Skalierungsanalyse dar. Zudem läßt sich von den Eigenzuständen der Fixpunkt-Hamilton ableiten, dass in allen Quantenphasen stark bis maximal verschränkte stabile Zustände auftreten, selbst in den Regimen starker Bad-Ankopplungen (der klassischen Spin-Austausch Phase, sowie der Spin-entkoppelten Phase), bei denen die kohärente Spin-Dynamik größtenteils unterdrückt wird. Dies stellt auf den ersten Blick einen intuitiven Widerspruch dar, da offenbar quantenmechanische Nicht-Lokalität in Phasen stark reduzierten Quantendynamik überlebt, wenn nicht sogar gebildet wird. Dieser scheinbare Widerspruch ist aber darin begründet, dass gerade die starke Ankopplung an externe Freiheitsgrade zu einem effektiven Doppel-Spin System führt, dessen klassische Pointer-Zustände gerade nicht mit der Basis des Tensorproduktes der Einzel-Spins übereinstimmt.

Zum Abschluss dieses Kapitels führen wir noch eine systematische Fortentwicklung der Skalierungsgleichungen zu beliebigen Ordnungen in den effektiven Spin-Kopplungen an. Exemplarisch berechnen wir mittels sogenannter *Operator Produkt Entwicklung* die explizite Form der Skalierungsgleichungen in zweiter Ordnung. Diese weisen gegenüber den ursprünglich drei verschiedenen Spin-Operator Termen der Gleichungen erster Ordnung bereits sieben verschiedene effektive Spinkopplungen auf, die in den entsprechenden Spin-Operator Produkten entstehen.